Advances
in Clinical and Experimental Medicine

MONTHLY ISSN 1899-5276 (PRINT) ISSN 2451-2680 (ONLINE) advances.umw.edu.pl

2025, Vol. 34, No. 3 (March)

Impact Factor (IF) – 2.1
Ministry of Science and Higher Education – 70 pts
Index Copernicus (ICV) – 171.00 pts

Wroclaw Medical University

Advances
in Clinical and Experimental
Medicine

Advances
in Clinical and Experimental Medicine

ISSN 1899-5276 (PRINT) ISSN 2451-2680 (ONLINE) advances.umw.edu.pl

MONTHLY 2025
Vol. 34, No. 3
(March)

Advances in Clinical and Experimental Medicine (*Adv Clin Exp Med*) publishes high-quality original articles, research-in-progress, research letters and systematic reviews and meta-analyses of recognized scientists that deal with all clinical and experimental medicine.

Editorial Office
ul. Marcinkowskiego 2–6
50-368 Wrocław, Poland
Tel.: +48 71 784 12 05
E-mail: redakcja@umw.edu.pl

Publisher
Wroclaw Medical University
Wybrzeże L. Pasteura 1
50-367 Wrocław, Poland

Online edition is the original version of the journal

Editorial Policy

Advances in Clinical and Experimental Medicine (Adv Clin Exp Med) is an independent multidisciplinary forum for exchange of scientific and clinical information, publishing original research and news encompassing all aspects of medicine, including molecular biology, biochemistry, genetics, biotechnology and other areas. During the review process, the Editorial Board conforms to the "Uniform Requirements for Manuscripts Submitted to Biomedical Journals: Writing and Editing for Biomedical Publication" approved by the International Committee of Medical Journal Editors (www.ICMJE.org). The journal publishes (in English only) original papers and reviews. Short works considered original, novel and significant are given priority. Experimental studies must include a statement that the experimental protocol and informed consent procedure were in compliance with the Helsinki Convention and were approved by an ethics committee.

For all subscription-related queries please contact our Editorial Office: redakcja@umw.edu.pl
For more information visit the journal's website: advances.umw.edu.pl

Pursuant to the ordinance of the Rector of Wroclaw Medical University No. 37/XVI R/2024, from March 1, 2024, authors are required to pay a fee for each manuscript accepted for publication in the journal Advances in Clinical and Experimental Medicine. The fee amounts to 1600 EUR for all types of papers.

Indexed in: MEDLINE, Science Citation Index Expanded, Journal Citation Reports/Science Edition, Scopus, EMBASE/Excerpta Medica, Ulrich's™ International Periodicals Directory, Index Copernicus

Typographic design: Piotr Gil, Monika Kolęda
DTP: Wydawnictwo UMW
Cover: Monika Kolęda
Printing and binding: Drukarnia I-BiS Bierońscy Sp.k.

Advances
in Clinical and Experimental Medicine

MONTHLY 2025, Vol. 34, No. 3 (March)

ISSN 1899-5276 (PRINT)
ISSN 2451-2680 (ONLINE)
advances.umw.edu.pl

Contents

Editorials

Meta-analysis

Original papers

Reviews

Non-pharmacological approaches for stress-related neuropsychiatric disorders: Focus on physical activity and natural compounds

Nasrollah Moradikor[D–F]

International Center for Neuroscience Research, Institute for Intelligent Research, Tbilisi, Georgia

A – research concept and design; B – collection and/or assembly of data; C – data analysis and interpretation;
D – writing the article; E – critical revision of the article; F – final approval of the article

Advances in Clinical and Experimental Medicine, ISSN 1899–5276 (print), ISSN 2451–2680 (online) *Adv Clin Exp Med*. 2025;34(3):309–313

Address for correspondence
Nasrollah Moradikor
E-mail:moradikor@neuroscience.edu.ge

Funding sources
None declared

Conflict of interest
None declared

Received on January 22, 2025
Reviewed on February 14, 2025
Accepted on March 6, 2025

Published online on March 13, 2025

Abstract

This editorial emphasizes on non-pharmacological approaches for stress-related neuropsychiatric disorders due to side effects of pharmacological approaches. It highlights various exercises, specific natural compounds and their mechanisms for stress reduction. A combination of both can be a good strategy for the stress management. There are some challenges for these approaches. One major limitation is the standardization of these interventions. Natural compounds often have different quality and potency depending on their source and preparation, which can impact their efficiency. Additionally, determining the optimal dosage for different compounds remains a significant challenge, as individual responses can vary considerably. Interdisciplinary collaboration between researchers, clinicians and policymakers must be established to address the challenges. By conducting large-scale, well-designed clinical trials researchers gain a deeper understanding of the mechanisms underlying these approaches and can prepare clear guidelines for their integration into mainstream healthcare, ultimately improving patient outcomes and reducing dependence on pharmacological treatments.

Key words: inflammation, physical activity, antioxidants, natural compounds, stress-related disorders

Cite as
Moradikor N. Non-pharmacological approaches for stress-related neuropsychiatric disorders: Focus on physical activity and natural compounds. *Adv Clin Exp Med*. 2025;34(3):309–313. doi:10.17219/acem/202674

DOI
10.17219/acem/202674

Introduction

Stress is one of the primary risk factors for a range of neuropsychiatric conditions. It is typically defined as an organism's response to environmental challenges aimed at maintaining bodily equilibrium. Prolonged stress activates the hypothalamic–pituitary–adrenal (HPA) axis, triggering significant inflammatory responses.[1] Stress not only affects HPA, but it also impacts neuronal structure, such as hippocampus, amygdala and prefrontal cortex.[2] The brain is profoundly affected by adverse environmental conditions, as seen in numerous structural and functional maladaptive changes observed in both preclinical models and clinical studies of depression.[3] Oxidative stress contributes to neuronal damage, including lipid peroxidation and protein oxidation.[4] Prolonged exposure to stress can negatively impact cognitive abilities and alter the dendritic architecture of pyramidal neurons in the CA3 region of the rat hippocampus. Furthermore, stress can impair brain development, leading to deficits in adult learning and memory.[5] Oxidative stress has been implicated in a variety of neurodegenerative disorders, such as Parkinson's disease and Alzheimer's disease, and neuropsychiatric conditions like schizophrenia, bipolar disorder, anxiety, and depression.[6] While antidepressants and antipsychotics are widely used to treat neuropsychiatric disorders, they come with significant limitations. Many medications cause side effects, including weight gain, sedation, gastrointestinal issues, and metabolic disturbances, which can reduce patient compliance.[7] As a result, non-pharmacological approaches offer a promising alternative for treating stress-related disorders. These approaches are gaining attention as effective options for managing and treating stress-related neuropsychiatric conditions.[4,8] This editorial examines physical activity and natural compounds as potential non-pharmacological treatments for stress-related neuropsychiatric disorders, drawing on the authors' expertise and experience.

Physical activity as a non-pharmacological approach for stress-related neuropsychiatric disorders

A key strategy for reducing the adverse effects of stress is physical activity. Studies have demonstrated that exercise mitigates cognitive impairments and increases brain-derived neurotrophic factor (BDNF) levels, ultimately lowering the risk of neuropsychiatric disorders. The beneficial effects of exercise on brain function are, at least in part, mediated by BDNF.[9,10] Moradikor et al. investigated the effects of wheel running exercise on adolescent stress-induced anxiety and depressive-like symptoms. Their study demonstrated positive effects in reducing stress and enhancing behavioral responses, primarily by increasing antioxidant capacity and upregulating BDNF expression.[11] In another study, the effects of voluntary exercise on stress in female rats were investigated, revealing that exercise reduced corticosterone levels and increased BDNF expression.[5] There is also evidence supporting the effects of treadmill exercise in reducing inflammation and enhancing antioxidant status in stressed rats.[4] A human study examining the effects of various types of physical exercise on stress coping in 9 university students reported that physical exercise alleviates stress by eliciting positive emotions, which, in turn, regulate health behaviors and enhance overall wellbeing.[12] Another study on women reported that physical exercise can decrease psychosocial stress.[13] This paper mentioned some cases of the positive effects of exercise in decreasing stress. Exercise is not limited only to treadmills; other exercises, such as yoga and walking, can decrease the negative effects of stress. Exercise not only mitigates the negative effects of stress by enhancing antioxidant capacity and reducing inflammation, but it also regulates the HPA axis, lowers cortisol levels and strengthens stress resilience. Additionally, it boosts BDNF levels, promotes neuroplasticity and improves cognitive function. Exercise strengthened the mitochondria in the hippocampus by boosting brain plasticity, lowering cell death and improving stress symptoms.[14] An increase in BDNF levels due to exercise can enhance mitochondrial function, promote neuroplasticity and regulate apoptosis signaling in the hippocampus, contributing to stress reduction. Physical activity, when combined with medication, can improve outcomes in key brain regions such as the amygdala and hippocampus, contributing to better stress management and overall mental health.[14] Exercise may enhance antioxidant levels by activating cellular pathways such as Nrf2, which regulates antioxidant responses. Additionally, physical activity modulates inflammatory factors by decreasing pro-inflammatory cytokines such as tumor necrosis factor alpha (TNF-α) while increasing anti-inflammatory cytokines like interleukin 10 (IL-10). In human models, these mechanisms primarily contribute to improved emotional regulation and stress resilience.

Natural compounds as a non-pharmacological approach for stress-related neuropsychiatric disorders

Natural compounds and their derivatives have been utilized for stress management due to their strong antioxidant properties.[15] These compounds, including medicinal plants, their derivatives and active compounds, help alleviate stress by reducing inflammation, regulating cortisol levels and promoting neuroprotection. Additionally, L-theanine, magnesium and probiotics support mood regulation and improve brain function, offering potential benefits for stress-related neuropsychiatric disorders.[16,17] Moradikor et al. investigated the effects of *Spirulina platensis* in the treatment of stress and reported its beneficial effects through the upregulation of BDNF and tropomyosin receptor kinase B (TrkB) expression.[8] In another study, *Spirulina platensis* was shown to improve scopolamine-induced memory deficits by reducing malondialdehyde (MDA) levels

in stressed rats.[18] Coating antioxidants is an effective strategy to enhance their efficiency and bioavailability. Curcumin nano-phytosomes decreased stress by increasing the BDNF and improving antioxidant status.[19] Natural compounds can increase neuroplasticity in the hippocampus, decrease hyperactivity in the amygdala and support emotional regulation in the prefrontal cortex.[20] As mentioned, natural antioxidants can have abilities for the management of stress. However, a combination of exercise and natural compounds shows greater efficiency than single approach.[5,8]

It has been reported that physical exercise increases the release of BDNF and TrkB, which are ultimately delivered to the brain.[21] There is also evidence showing that physical activity increases hippocampal BDNF expression to a desired level.[22] Additionally, BDNF-induced TrkB activation promotes the mitogen-activated protein kinase (MAPK) and phosphatidylinositol-3 kinase (PI3K)/Akt signaling pathways, which play essential roles in encouraging neuronal survival and synaptic plasticity.[23] Studies have reported the stimulatory effects of exercise on BDNF-induced TrkB activation.[24] It has been reported that low-intensity physical exercise increases the mRNA expression of BDNF and neuronal activation in stressed rats.[25] The exercise-induced increase in BDNF may result from an increased release of serotonin and/or norepinephrine.[26] The effects of exercise might be mediated by an increase in 5-HT/NE neurotransmission, which promotes cyclic adenosine monophosphate (cAMP)/protein kinase A (PKA) signaling and the transcription factor cAMP response element-binding protein (CREB). The protein activation enhances the expression and secretion of BDNF, which acts via TrkB receptors. Similary, *Spirulina platensis* extract, as a natural compound, boosted the activation of both p-ERK (extracellular signal–related protein kinase) and p-CREB proteins, which in turn increased BDNF levels in the hippocampus and improved memory in mice.[27] Additionally, non-protein parts of *Spirulina platensis* have been shown to promote *BDNF* gene activity by activating heme oxygenase-1 in glial cells.[28] These results emphasize the importance of BDNF in the positive effects of *Spirulina platensis* on brain function. There are evidences for the effects of other natural compounds on BDNF/TrkB, such as phenols.[29] Thus, exercises and natural compounds can work in similar pathways for affecting BDNF/TrkB. On the other hand, acute exercise boosts Nrf2 signaling by reactive oxygen species (ROS) production. Nrf2 is a regulator of antioxidant defenses and regulates expression of more than 200 cytoprotective genes.[30] Different compounds can activate the Nrf2-antioxidant responsive element (ARE) pathway, which is responsible for triggering antioxidant responses in cells.[31,32] This pathway helps decrease the damage caused by free radicals and inflammation, which are key contributors to neurodegenerative diseases and aging. The increase of expression of these molecular pathways, both physical activity and certain compounds can work together to improve brain health and mitigate the negative effects of oxidative stress.

In summary, physical exercise and natural compounds exert anti-stress effects through similar mechanisms, and their combination may serve as an effective strategy for stress management. The synergistic effect of exercise and compounds targeting BDNF-TrkB and Nrf2-ARE pathways can protect against stressful factors and decrease the risk of age-related cognitive decline or neurological disorders. The ability of exercise to enhance BDNF levels can complement the antioxidant effects mediated by Nrf2 activation. However, the effectiveness of these natural compounds may be constrained by challenges such as limited bioavailability, variability in potency and potential adverse effects. These factors can influence their clinical applicability and should be carefully considered when assessing their potential for stress alleviation.

Challenges and future directions

Although studies have highlighted the promising potential of non-pharmacological approaches, such as physical activity and natural compounds, in the treatment of stress-related neuropsychiatric disorders, several challenges remain. One major limitation is the standardization of these interventions. Natural compounds often exhibit variations in quality and potency depending on their source and preparation, which can impact their efficacy. Additionally, determining the optimal dosage for different compounds remains a significant challenge, as individual responses can vary considerably. The long-term effects of these approaches are also not fully elucidated, and further research is essential to investigate their safety and effectiveness over extended periods of use. It is essential to note that most studies have been conducted on rodents, and their results cannot be directly generalized to humans. To address these challenges, further research and clinical validation are essential to ensure the efficacy, safety and standardization of these non-pharmacological approaches. Controlled clinical trials and systematic studies can significantly elucidate the mechanisms by which these interventions exert their effects and provide evidence for their use in clinical practice. The need for large-scale, well-designed studies is essential to ensure that these approaches can be safely integrated into mainstream healthcare. Additionally, further studies must identify and elucidate the possible mechanisms underlying the effects of physical activity and natural compounds on stress-related neuropsychiatric disorders. By building an extensive body of literature, these approaches can be effectively integrated into existing treatment frameworks, with the goal of improving patient outcomes and reducing reliance on pharmacological treatments. Finally, while rodent studies provide valuable insights, their direct applicability to humans is limited. Additionally, challenges remain in designing large-scale clinical trials and addressing regulatory concerns to facilitate the integration of these approaches into mainstream healthcare.

Conclusion

In summary, both physical activity and natural compounds offer promising non-pharmacological strategies for managing stress-related neuropsychiatric disorders. Physical activity, through various forms such as treadmill exercise, yoga and walking, can reduce stress by regulating the HPA axis, decreasing inflammation, improving antioxidant status, and boosting BDNF. These effects enhance stress resilience, cognitive function and overall brain health. Similarly, natural compounds like *Spirulina platensis* and curcumin play significant roles in reducing inflammation, regulating cortisol levels and promoting neuroprotection, further supporting stress management. When combined, physical exercise and natural compounds appear to be more effective than either approach alone, suggesting a synergistic potential for stress management. However, despite their promising effects, several challenges remain unresolved. The standardization of these approaches, including the quality and potency of natural compounds, is a major obstacle. Additionally, determining optimal dosages for individual responses and understanding the long-term effects of these strategies require further research. While most studies have been conducted in animal models, more human-based clinical trials are essential to validate these findings and better understand their clinical relevance. Animal studies provide base information and open a way for future studies on humans. Future research should focus on overcoming these challenges, with interdisciplinary collaboration between researchers, clinicians and policymakers being crucial for advancing these approaches. Large-scale, well-designed clinical trials will be key to providing deeper insights into the underlying mechanisms and establishing clear guidelines for integrating these strategies into mainstream healthcare, ultimately improving patient outcomes and reducing reliance on pharmacological treatments.

ORCID iDs

Nasrollah Moradikor https://orcid.org/0000-0001-9905-6845

References

1. Azarfarin M, Moradikor N, Matin S, Dadkhah M. Association between stress, neuroinflammation, and irritable bowel syndrome: The positive effects of probiotic therapy. *Cell Biochem Funct*. 2024;42(8):e70009. doi:10.1002/cbf.70009
2. McEwen BS, Nasca C, Gray JD. Stress effects on neuronal structure: Hippocampus, amygdala, and prefrontal cortex. *Neuropsychopharmacology*. 2016;41(1):3–23. doi:10.1038/npp.2015.171
3. Sanacora G, Yan Z, Popoli M. The stressed synapse 2.0: Pathophysiological mechanisms in stress-related neuropsychiatric disorders. *Nat Rev Neurosci*. 2022;23(2):86–103. doi:10.1038/s41583-021-00540-x
4. Safakhah HA, Moradikor N, Bazargani A, et al. Forced exercise attenuates neuropathic pain in chronic constriction injury of male rat: An investigation of oxidative stress and inflammation. *J Pain Res*. 2017;10:1457–1466. doi:10.2147/JPR.S135081
5. Moradikor N, Ghanbari A, Rashidipour H, Yousefi B, Bandegi AR, Rashidy-Pour A. Beneficial effects of *Spirulina platensis*, voluntary exercise and environmental enrichment against adolescent stress induced deficits in cognitive functions, hippocampal BDNF and morphological remolding in adult female rats. *Horm Behav*. 2019;112:20–31. doi:10.1016/j.yhbeh.2019.03.004
6. Wadhwa R, Gupta R, Maurya PK. Oxidative stress and accelerated aging in neurodegenerative and neuropsychiatric disorder. *Curr Pharm Des*. 2018;24(40):4711–4725. doi:10.2174/1381612825666190115121018
7. Lehrer PM, Woolfolk RL, eds. *Principles and Practice of Stress Management*. 2nd ed. New York, USA: Guilford Press; 1993. ISBN: 978-0-89862-162-4, 978-0-89862-766-4.
8. Moradikor N, Ghanbari A, Rashidipour H, et al. Therapeutic effects of *Spirulina platensis* against adolescent stress-induced oxidative stress, brain-derived neurotrophic factor alterations and morphological remodeling in the amygdala of adult female rats. *J Exp Pharmacol*. 2020;12:75–85. doi:10.2147/JEP.S237378
9. Vaynman S, Ying Z, Gomez-Pinilla F. Hippocampal BDNF mediates the efficacy of exercise on synaptic plasticity and cognition. *Eur J Neurosci*. 2004;20(10):2580–2590. doi:10.1111/j.1460-9568.2004.03720.x
10. Lapmanee S, Charoenphandhu J, Teerapornpuntakit J, Krishnamra N, Charoenphandhu N. Agomelatine, venlafaxine, and running exercise effectively prevent anxiety- and depression-like behaviors and memory impairment in restraint stressed rats. *PLoS One*. 2017;12(11):e0187671. doi:10.1371/journal.pone.0187671
11. Moradikor N, Dadkhah M, Ghanbari A, et al. Protective effects of *Spirulina platensis*, voluntary exercise and environmental interventions against adolescent stress-induced anxiety and depressive-like symptoms, oxidative stress and alterations of BDNF and 5HT-3 receptors of the prefrontal cortex in female rats. *Neuropsychiatr Dis Treat*. 2020;16:1777–1794. doi:10.2147/NDT.S247599
12. Kim JH, McKenzie LA. The impacts of physical exercise on stress coping and well-being in university students in the context of leisure. *Health*. 2014;6(19):2570–2580. doi:10.4236/health.2014.619296
13. Klaperski S, Von Dawans B, Heinrichs M, Fuchs R. Does the level of physical exercise affect physiological and psychological responses to psychosocial stress in women? *Psychol Sport Exerc*. 2013;14(2):266–274. doi:10.1016/j.psychsport.2012.11.003
14. Seo JH, Park HS, Park SS, Kim CJ, Kim DH, Kim TW. Physical exercise ameliorates psychiatric disorders and cognitive dysfunctions by hippocampal mitochondrial function and neuroplasticity in post-traumatic stress disorder. *Exp Neurol*. 2019;322:113043. doi:10.1016/j.expneurol.2019.113043
15. Mehta J, Rayalam S, Wang X. Cytoprotective effects of natural compounds against oxidative stress. *Antioxidants (Basel)*. 2018;7(10):147. doi:10.3390/antiox7100147
16. Noah L, Morel V, Bertin C, et al. Effect of a combination of magnesium, B vitamins, rhodiola, and green tea (L-theanine) on chronically stressed healthy individuals: A randomized, placebo-controlled study. *Nutrients*. 2022;14(9):1863. doi:10.3390/nu14091863
17. Ma X, Shin YJ, Park HS, et al. *Lactobacillus casei* and its supplement alleviate stress-induced depression and anxiety in mice by the regulation of BDNF expression and NF-κB activation. *Nutrients*. 2023;15(11):2488. doi:10.3390/nu15112488
18. Ghanbari A, Vafaei AA, Naghibi Nasab FS, Attarmoghaddam M, Bandegi AR, Moradi-Kor N. Spirulina microalgae improves memory deficit induced by scopolamine in male pup rats: Role of oxidative stress. *S Afr J Botany*. 2019;127:220–225. doi:10.1016/j.sajb.2019.08.045
19. Baradaran S, Hajizadeh Moghaddam A, Khanjani Jelodar S, Moradikor N. Protective effects of curcumin and its nano-phytosome on carrageenan-induced inflammation in mice model: Behavioral and biochemical responses. *J Inflamm Res*. 2020;13:45–51. doi:10.2147/JIR.S232462
20. Cichon N, Saluk-Bijak J, Gorniak L, Przyslo L, Bijak M. Flavonoids as a natural enhancer of neuroplasticity: An overview of the mechanism of neurorestorative action. *Antioxidants (Basel)*. 2020;9(11):1035. doi:10.3390/antiox9111035
21. Aguiar AS, Tuon T, Pinho CA, et al. Intense exercise induces mitochondrial dysfunction in mice brain. *Neurochem Res*. 2008;33(1):51–58. doi:10.1007/s11064-007-9406-x
22. Adlard PA, Cotman CW. Voluntary exercise protects against stress-induced decreases in brain-derived neurotrophic factor protein expression. *Neuroscience*. 2004;124(4):985–992. doi:10.1016/j.neuroscience.2003.12.039
23. Pizzorusso T, Ratto GM, Putignano E, Maffei L. Brain-derived neurotrophic factor causes cAMP response element-binding protein phosphorylation in absence of calcium increases in slices and cultured neurons from rat visual cortex. *J Neurosci*. 2000;20(8):2809–2816. doi:10.1523/JNEUROSCI.20-08-02809.2000

24. Lista I, Sorrentino G. Biological mechanisms of physical activity in preventing cognitive decline. *Cell Mol Neurobiol*. 2010;30(4):493–503. doi:10.1007/s10571-009-9488-x
25. Fang ZH, Lee CH, Seo MK, et al. Effect of treadmill exercise on the BDNF-mediated pathway in the hippocampus of stressed rats. *Neurosci Res*. 2013;76(4):187–194. doi:10.1016/j.neures.2013.04.005
26. Samorajski T, Rolsten C, Przykorska A, Davis CM. Voluntary wheel running exercise and monoamine levels in brain, heart and adrenal glands of aging mice. *Exp Gerontol*. 1987;22(6):421–431. doi:10.1016/0531-5565(87)90022-2
27. Choi WY, Kang DH, Lee HY. Effect of fermented *Spirulina maxima* extract on cognitive-enhancing activities in mice with scopolamine-induced dementia. *Evid Based Complement Alternat Med*. 2018;2018:7218504. doi:10.1155/2018/7218504
28. Morita K, Itoh M, Nishibori N, Her S, Lee MS. Spirulina non-protein components induce *BDNF* gene transcription via HO-1 activity in C6 glioma cells. *Appl Biochem Biotechnol*. 2015;175(2):892–901. doi:10.1007/s12010-014-1300-9
29. Qi G, Mi Y, Wang Y, et al. Neuroprotective action of tea polyphenols on oxidative stress-induced apoptosis through the activation of the TrkB/CREB/BDNF pathway and Keap1/Nrf2 signaling pathway in SH-SY5Y cells and mice brain. *Food Funct*. 2017;8(12):4421–4432. doi:10.1039/c7fo00991g
30. Done AJ, Traustadóttir T. Nrf2 mediates redox adaptations to exercise. *Redox Biol*. 2016;10:191–199. doi:10.1016/j.redox.2016.10.003
31. Chen B, Zhao J, Zhang R, et al. Neuroprotective effects of natural compounds on neurotoxin-induced oxidative stress and cell apoptosis. *Nutr Neurosci*. 2022;25(5):1078–1099. doi:10.1080/1028415X.2020.1840035
32. Hannan MA, Dash R, Sohag AAM, Haque MN, Moon IS. Neuroprotection against oxidative stress: Phytochemicals targeting TrkB signaling and the Nrf2-ARE antioxidant system. *Front Mol Neurosci*. 2020;13:116. doi:10.3389/fnmol.2020.00116

Diagnostic accuracy of digital breast tomosynthesis and digital mammography in women with dense or non-dense breast tissue: A systematic review and meta-analysis

*Hao Lin[1,A], *Yimeng Zhang[2,B], Lixia Wu[3,C], Ceng Li[4,D–F]

[1] Department of Radiology, General Hospital of the Yangtze River Shipping-Wuhan Brain Hospital, China
[2] Department of General Surgery, The Third Affiliated Hospital of Zhejiang Chinese Medical University, Hangzhou, China
[3] Department of Pulmonary and Critical Care Medicine, The Third Affiliated Hospital of Zhejiang Chinese Medicine University, Hangzhou, China
[4] Department of Radiology, Xuzhou Cancer Hospital, China

A – research concept and design; B – collection and/or assembly of data; C – data analysis and interpretation;
D – writing the article; E – critical revision of the article; F – final approval of the article

Advances in Clinical and Experimental Medicine, ISSN 1899–5276 (print), ISSN 2451–2680 (online) *Adv Clin Exp Med*. 2025;34(3):315–326

Address for correspondence
Ceng Li
E-mail: licengxz@sina.com

Funding sources
None declared

Conflict of interest
None declared

*Hao Lin and Yimeng Zhang contributed equally to this work.

Received on November 3, 2023
Reviewed on November 20, 2023
Accepted on February 29, 2024

Published online on August 1, 2024

Cite as
Lin H, Zhang Y, Wu L, Li C. Diagnostic accuracy of digital breast tomosynthesis and digital mammography in women with dense or non-dense breast tissue: A systematic review and meta-analysis. *Adv Clin Exp Med*. 2025;34(3):315–326. doi:10.17219/acem/185522

DOI
10.17219/acem/185522

Abstract

Background. Despite its excellent screening effectiveness and sensitivity for breast cancer (BC), digital breast tomosynthesis (DBT) is controversial due to its high radiation exposure and long reading time. This study examines the diagnostic accuracy of DBT and digital mammography (DM) for BC screening and diagnosis in women with dense or non-dense breast tissue.

Materials and methods. PRISMA-compliant searches were performed on Medline, Embase, PubMed, Web of Science, and the Cochrane databases for articles comparing DBT and DM for BC screening until March 2023. Meta-analysis was performed using RevMan sofware, and the Cochrane Risk of Bias Assessment Tool was employed to assess study quality.

Results. This meta-analysis included 11 trials with a total of 2,124,018 individuals. Screening with DBT resulted in a greater cancer detection rate, as demonstrated by a risk ratio (RR) of 1.27 (95% confidence interval (95% CI): 1.14–1.41). Digital breast tomosynthesis also had a reduced recall rate, with a RR of 0.88 (95% CI: 0.78–0.99), higher sensitivity and specificity values (pooled sensitivity of 0.91 (95% CI: 0.59–0.99)) and pooled specificity of 0.90 (95% CI: 0.42–1.0)) than DM (pooled sensitivity of 0.86 (95% CI: 0.52–1.0) and pooled specificity of 0.81 (95% CI: 0.12–1.0)). All acquired data exhibited reliability, lack of bias and statistical significance ($p < 0.05$).

Conclusions. Digital breast tomosynthesis is a more effective screening and diagnostic assessment tool for women with dense or non-dense breasts than DM in terms of incremental cancer detection, sensitivity and recall rate.

Key words: breast cancer, digital mammography, digital breast tomosynthesis, cancer detection rate, overall recall rate

Background

Breast cancer (BC) is widely prevalent among women and is the primary cause of cancer-associated mortality in the global female population.[1] Numerous countries have implemented population-wide BC screening, originally with X-ray-based film-screen technology, before transitioning to digital mammography (DM), with the objective of reducing BC mortality through early detection.[2] Mammography, also known as screen-film mammography (SFM), is the most common breast imaging modality and is widely regarded as the gold standard for verifying or ruling out the existence of breast cancer. Compression of the breast is an essential component of mammography that employs X-ray technology to investigate the breast. Nevertheless, DM exhibits considerable sensitivity, with estimates ranging from 67.3% to 93.3%.[3]

Mammography findings are summarized and classified into separate categories using the standardized Breast Imaging Reporting and Data System (BI-RADS). Mammographic breast tissue densities greater than 50% fall into BI-RADS categories 3 or 4, or C or D, in the 4th and 5th editions, respectively. Such high density may have a masking effect, reducing the sensitivity of mammography. As dense parenchyma overlaps fibro glandular tissue, it may affect the mammographic identification of lesions and it may increases false-positive outcomes..[4,5]

Breast density is a distinct risk factor for BC, and approx. 50% of women participating in screening are believed to have dense breast tissue. However, the proportion of dense breast tissue varies across different age groups. There is a positive correlation between high mammographic density, characterized by heterogeneously or excessively dense breast tissue and elevated susceptibility to BC, an association that extends to interstitial BC.[6,7]

Digital breast tomosynthesis (DBT) is a medical imaging technique that generates reconstructed, nearly 3-dimensional (3D) mammographic images of the breast and is thought to enhance cancer detection during screening by offering improved visualization of lesions that may be difficult to identify on traditional 2-dimensional (2D) DM. This is particularly relevant in cases where dense or overlapping breast tissue may obscure the presence of such lesions.[8,9] Furthermore, DBT has the potential to decrease the occurrence of cancer-simulating artifacts caused by overlapping breast tissue, which may reduce the initial high rates of recalling patients for additional examination.[10] Digital breast tomosynthesis allows for the acquisition of pseudo-3D images of the breast, leading to enhanced differentiation of tissue features and, perhaps, enhanced visualization of cancerous lesions. Therefore, it can be argued that DBT has the capacity to enhance the sensitivity and specificity of imaging in BC screening, resulting in a higher number of accurately identified tumors while minimizing false positive results.[11]

Several prospective and retrospective studies have investigated different screening populations and have consistently shown improved screening accuracy when DBT is employed.[12–14] However, some studies have indicated that the combined use of DM and DBT leads to increased radiation exposure to the breast.[15,16]

Objectives

Since there has been limited research comparing the diagnostic accuracy and reliability of DBT and DM for BC screening in women with dense or non-dense breast tissue, the primary aim of this study was to systematically evaluate and meta-analyze selected studies.[17–27]

Materials and methods

The current investigation followed the Preferred Reporting Items for Systematic Reviews and Meta-analyses (PRISMA) guidelines.[28]

Eligibility criteria

This study analyzed the comparative outcomes of relevant publications between 2015 and 2023, with priority given to incorporating full-text articles into the investigation. The inclusion criteria were studies: 1) reporting the screening of BC using DBT or DM, 2) involving dense and non-dense breast tissues, 3) including patients older than 18 years, and 4) published in English. In the meta-analysis, only abstracts with sufficient information were included. The analysis excluded studies with insufficient data, those extraneous to BC screening, and published before 2015.

Information sources

The researchers conducted an extensive examination of the academic literature using PubMed, Embase, Web of Science, Scopus, and Cochrane Library databases. The search methodology combined Medical Subject Headings (MeSH) and textual keywords using the Boolean operator "AND".

Search strategy

A comprehensive and systematic review of relevant studies on the diagnostic accuracy and reliability of DBT compared to DM was conducted using PubMed and the Cochrane Library databases, following the PRISMA guidelines. To find relevant studies, we searched the medical literature for the following terms: breast cancer, digital mammography, mammography, DBT, cancer detection rate (CDR), overall recall rate, sensitivity, specificity, dense

breast tissue, non-dense breast tissue, systematic review, and meta-analysis.

Selection process

Two authors, H.L. and Y.Z., thoroughly examined the pertinent literature to identify relevant articles. The researchers used inclusion criteria to exclude outdated references and incorporate relevant studies of importance.

Data collection process

Two researchers (H.L. and Y.Z.) carried out a thorough bibliographic search to find pertinent and significant works. A methodical selection approach was used to find and incorporate all relevant studies published between 2015 and 2023.

Data items

Two other authors, Y.W. and C.Y., summarized brief characteristics of the participants in the included studies and event data separately from the studies included in the analysis. The 4 key metrics discussed were: 1) CDR – the proportion of cancer cases correctly identified by a diagnostic test; 2) "overall recall rates" – the percentage of individuals called back for further testing after an initial screening; 3) "sensitivity" – the ability of a test to correctly identify individuals with BC; and 4) "specificity" – the ability of a test to correctly identify individuals without BC.

Risk of bias assessment

The assessment of potential bias in the research included in the study was undertaken using a previously established standardized questionnaire (Supplementary Table 1). A summary and graphical representation of the risk of bias was generated using the Cochrane Risk of Bias (Robvis) tool.[31]

Effect measures

H.L. and Y.Z. conducted independent evaluations of the methodological validity of the studies included in the analysis. L.W. assumed the responsibility of resolving any problems that emerged between H.L. and Y.Z. The determination was made based on the heterogeneity of the included trials. The Cochran's Q statistic and the I^2 index were employed in a random bivariate mode[29] as part of the investigation of heterogeneity. The research was conducted using the RevMan v. 5 software (Cochrane Collaboration, Copenhagen, Denmark).[30] Various other factors contributing to variability were examined, including the employment of full-text articles instead of abstracts, discrepancies in age groups and sample sizes, variations in the techniques used, and differences in the study outcomes.

Statistical analyses

The meta-analysis employed RevMan software v. 5. Since the studies were conducted under different conditions, a random effect model was used. The primary methodology employed in this research was the Mantel–Haenszel process, incorporating random bivariate effects. Statistical metrics, including odds ratio (OR), risk ratio (RR), sensitivity, and specificity, together with a 95% confidence interval (95% CI), were mostly computed using the Mantel–Haenszel method. Assessing the number of standard deviations by which a value deviated from the mean used z-test statistics, and $p < 0.05$ was considered statistically significant. Moreover, forest plots were made to visually represent the results, and tau^2, χ^2, I^2, and z-values measured heterogeneity in the publications evaluated. The diagnostic OR was calculated using a 2×2 contingency table and the DerSimonian and Laird method.[32]

The assessment of publication bias used Begg's test,[33] Egger's test[34] and Deek's funnel plots.[35] Deek's funnel plot was generated by plotting the natural logarithm of the OR for each publication against its corresponding standard error using MedCalc software (MedCalc Software, Ostend, Belgium).[36] The development of Youden plots[37] and hierarchical summary receiver operating characteristic curves (HSROCs)[38] aimed to evaluate the degree of inter-study variability.

Results

Literature search results

The application of the PRISMA flowchart for selecting research studies is illustrated in Fig. 1. After conducting a thorough analysis of online sources, a collection of 347 academic papers was identified. Following the removal of duplicate submissions, 241 studies were screened based on their abstracts and titles. A total of 136 papers that satisfied the predetermined inclusion criteria were comprehensively evaluated. The current meta-analysis comprised 11 publications selected based on predetermined inclusion and exclusion criteria. The studies incorporated in the analysis investigated and assessed the diagnostic precision and dependability of DBT and DM in the context of screening for BC in women with dense and non-dense breast tissue. Table 1 presents a comprehensive overview of the pertinent characteristics of the research being examined. This study encompasses various attributes, such as the identification of studies, publication years, journals of publication, countries where the studies were conducted, interventions employed, screening intervals for mammographic density, total number of participants, patient age, sample size, and the instruments used for DBT and DM.

Table 1. Characteristics of the included studies for comparing the diagnostic accuracy of DBT vs DM in women with dense or non-dense breast tissue

Study ID	Year of publication	Journal of publication	Country of study	Screening intervals	Total number of participants	Age of patients [years]	Sample size for DBT	Sample size for DM	Instrument used for DBT	Instrument used for DM
Aase et al.[17]	2018	*European Radiology*	Norway	annual	14,274	50–71	7,155	7119	GE (Seno Claire 3D Breast Tomosynthesis™)	GE Healthcare Mammo Workstation v. 4.7.0 Image Diagnostic
Bernardi et al.[18]	2016	*The Lancet Oncology*	Italy	biennial	19,259	53–63	9,587	9,672	Selenia® Dimension® Hologic, Marlborough, (USA)	Omnipaque®, GE Healthcare, Chalfont St. Giles (UK)
Chudgar et al.[19]	2017	*Clinical Radiology*	USA	annual	35,314	49–77	24,563	10,751	Dimension, Hologic, Bedford, (USA)	Dimension, Hologic, Bedford, (USA)
Conant et al.[20]	2016	*Breast Cancer Research and Treatment*	USA	annual	198,881	40–74	55,998	142,883	Hologic 3Dimensions™ Mammography System units	Hologic 3Dimensions™ Mammography System units
Ha et al.[21]	2022	*Korean Journal of Radiology*	South Korea	annual	2,589	40–78	863	1,726	Selenia Dimensions, Hologic Inc.	Selenia Dimensions, Hologic Inc.; Senographe 2000D, GE Medical Systems
Kerlikowske et al.[22]	2022	*JAMA Oncology*	USA	biennial	365,080	40–79	56,939	308,141	Hologic 3Dimensions™ Mammography System units	Hologic 3Dimensions™ Mammography System units
McDonald et al.[23]	2016	*JAMA Oncology*	USA	biennial	21,735	40–70	10,728	11,007	Dimensions; Hologic Inc.	Dimensions; Hologic Inc.
Nicosia et al.[24]	2023	*Cancers*	Italy	annual	98	40–80	49	49	GE® Healthcare, Senographe Pristina®, Chalfont St. Giles (UK)	Omnipaque®, GE Healthcare, Chalfont St. Giles (UK)
Rafferty et al.[25]	2016	*Research Letter JAMA*	USA	annual	452,320	40–80	173,414	278,906	Hologic 3Dimensions™ Mammography System units	Hologic 3Dimensions™ Mammography System units
Siminiak et al.[26]	2022	*Frontiers in Oncology*	Italy	annual	402	50–69	202	200	Mammomat Fusion, Siemens Healthcare, Erlangen (Germany)	Mammomat Inspiration Prime and Mammomat Revelation, Siemens Healthcare, Erlangen (Germany)
Sudhir et al.[27]	2021	*British Institute of Radiology*	India	annual	242	24–72	108	134	GE Healthcare, Inc. Cork (Ireland)	GE Healthcare, Inc. Cork (Ireland)

DBT – digital breast tomosynthesis, DM – digital mammography.

Table 2. Assessment of bias for included studies

Signaling questions	Aase et al.[17]	Bernardi et al. [18]	Chudgar et al.[19]	Conant et al.[20]	Ha et al. [21]	Kerlikowske et al.[22]	McDonald et al.[23]	Nicosia et al.[24]	Rafferty et al.[25]	Siminiak et al.[26]	Sudhir et al.[27]
Did the study avoid inappropriate exclusions?	Y	Y	Y	Y	Y	Y	Y	Y	Y	Y	Y
Did all patients receive the same reference standard?	Y	Y	Y	Y	Y	Y	Y	Y	Y	Y	Y
Were all patients included in the analysis?	N	N	N	N	N	N	N	N	N	N	N
Was the sample frame appropriate to address the target population?	Y	Y	Y	Y	Y	Y	Y	Y	Y	Y	Y
Were study participants sampled in an appropriate way?	Y	Y	Y	Y	Y	Y	Y	Y	Y	Y	Y
Were the study participants and the setting described in detail?	Y	Y	Y	Y	Y	Y	Y	Y	Y	Y	Y
Were valid methods used for the identification of the condition?	Y	Y	Y	Y	Y	Y	Y	Y	Y	Y	Y
Was the condition measured in a standard reliable way for all participants?	Y	Y	Y	Y	Y	Y	Y	Y	Y	Y	Y

Y = yes; N = no.

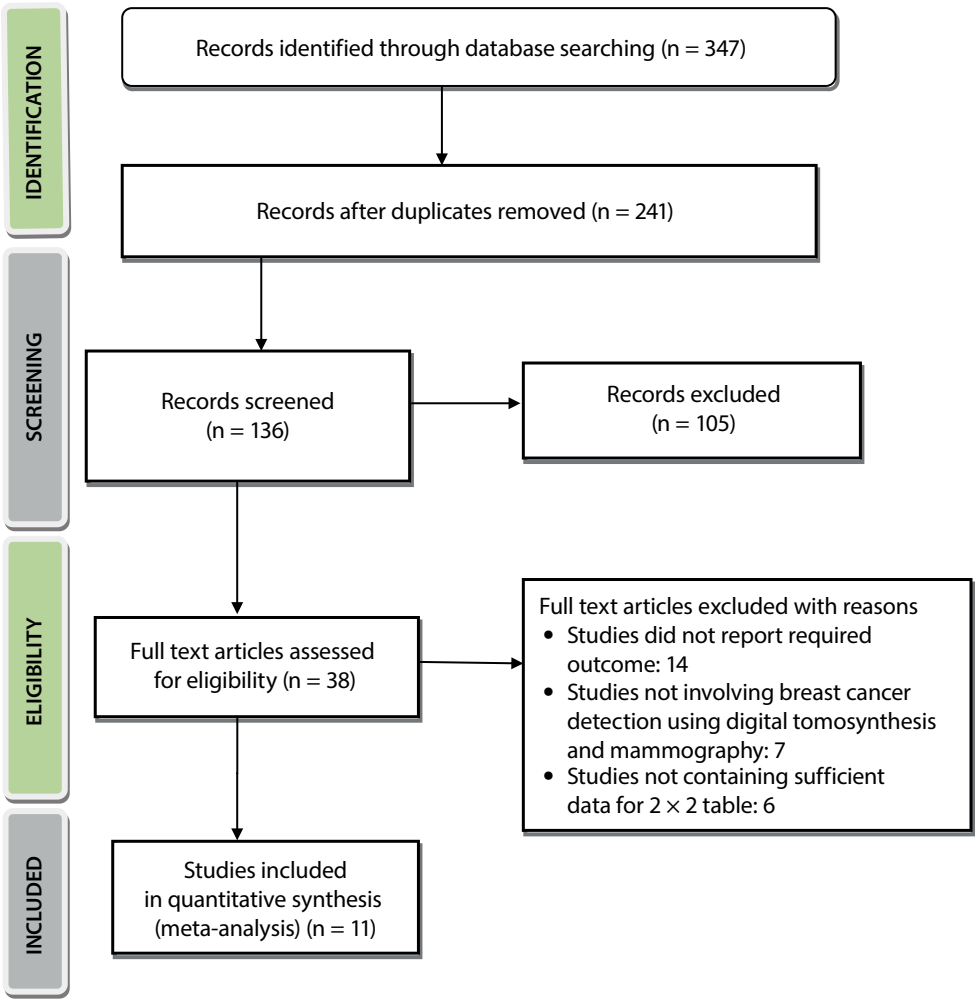

Fig. 1. Preferred Reporting Items for Systematic Reviews and Meta-analyses (PRISMA) flowchart of study selection

Evaluating overall study quality

Table 2 presents a comprehensive assessment of the methodological rigor and overall quality of the studies incorporated in the meta-analysis. Figure 2 gives a succinct overview of the potential for bias, and Fig. 3 visually represents the danger of bias. Out of the 11 studies, 6 had a low risk of bias as they employed valid methodology for patient allocation to alternative treatments, maintained a low attrition rate, and implemented suitable measures to prevent bias, assess outcomes, analyze data, and report findings. As a consequence, the reported results are valid, and there was no selection bias, performance bias, detection bias, attrition bias, or reporting bias. However, 4 studies displayed a moderate risk of bias as a result of concerns regarding random sequence creation, allocation concealment and blinding of participants and staff. The remaining study carried a high risk of bias and allocation concealment. As indicated by the symmetrical funnel plot[39] and the lack of statistical significance ($p > 0.05$) in Begg's ($p = 0.354$) and Egger's tests ($p = 0.224$),[40] the results presented in Fig. 4 indicate a low probability of publication bias.

Primary outcome statistical analysis

The current meta-analysis comprised a sample of 11 studies, either prospective or retrospective in nature, with a total of 1,110,194 participants. A total of 339,606 people underwent screening using the DBT method, while 770,588 received DM screening. The key outcomes of the studies were statistically analyzed to compare DBT and DM for BC screening in women with dense or non-dense breast tissue.

Cancer detection rate of DBT vs DM

Figure 5 illustrates 11 studies that reported CDRs, with a combined total of 1,286,449 people screened with DBT and 837,569 participants assessed through DM. The DBT group exhibited higher accuracy in detecting cancer (RR = 1.27, 95% CI: 1.14–1.41). The findings exhibited heterogeneity, as shown by the values of $tau^2 = 0.02$, $\chi^2 = 205.63$, degrees of freedom (df) = 10, $z = 4.36$, $I^2 = 95$ %, and $p < 0.001$ (Fig. 5A). Similarly, DBT had a higher chance of detecting BC than DM (OR = 2.29, 95% CI: 1.49–3.51). The findings exhibited heterogeneity, as shown by the $tau^2 = 0.38$, $\chi^2 = 35.48$, df = 11, $z = 3.78$, $I^2 = 69$ %, and $p < 0.001$ values (Fig. 5B).

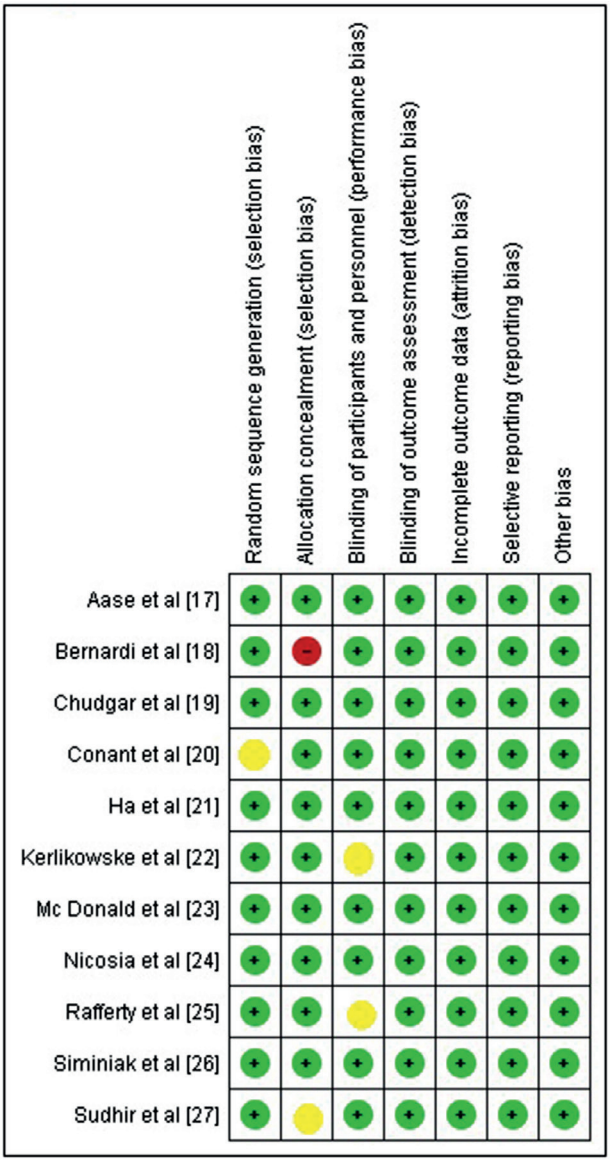

Fig. 2. Risk of bias summary

Overall recall rate of DBT vs DM

Figure 6 illustrates the results of 11 studies that reported an overall recall rate. The sample consisted of 1,286,449 participants tested using DBT, and 837,569 people screened using DM. The study revealed that the DM group had a greater recall rate than the DBT group (RR = 0.88, 95% CI: 0.78–0.99). The findings exhibited heterogeneity, as indicated by the tau^2 (0.02), χ^2 (67.89), df (10), z (2.16), I^2 (85%), and p (< 0.001) values (Fig. 6A). Similarly, the OR of 1.24 (95% CI: 1.01–1.5; tau^2 = 0.08, χ^2 = 28.06, df = 11, z = 2.01, I^2 = 61%, and p < 0.001) showed that the DM group had a greater recall rate than the DBT group (Fig. 6B).

Sensitivity and specificity of DBT and DM

Imaging instruments used for BC screening must have high sensitivity and specificity[41] to accurately detect the presence or absence of BC. Using the dataset extracted from the 11 included studies, we determined the sensitivity and specificity of DBT and DM. In Fig. 7A, the data

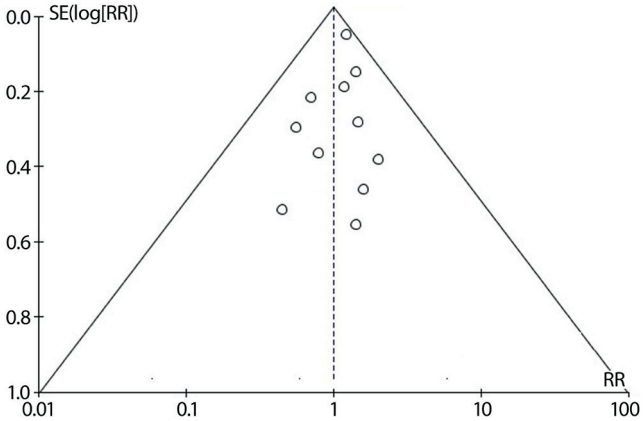

Fig. 4. Funnel plot for publication bias

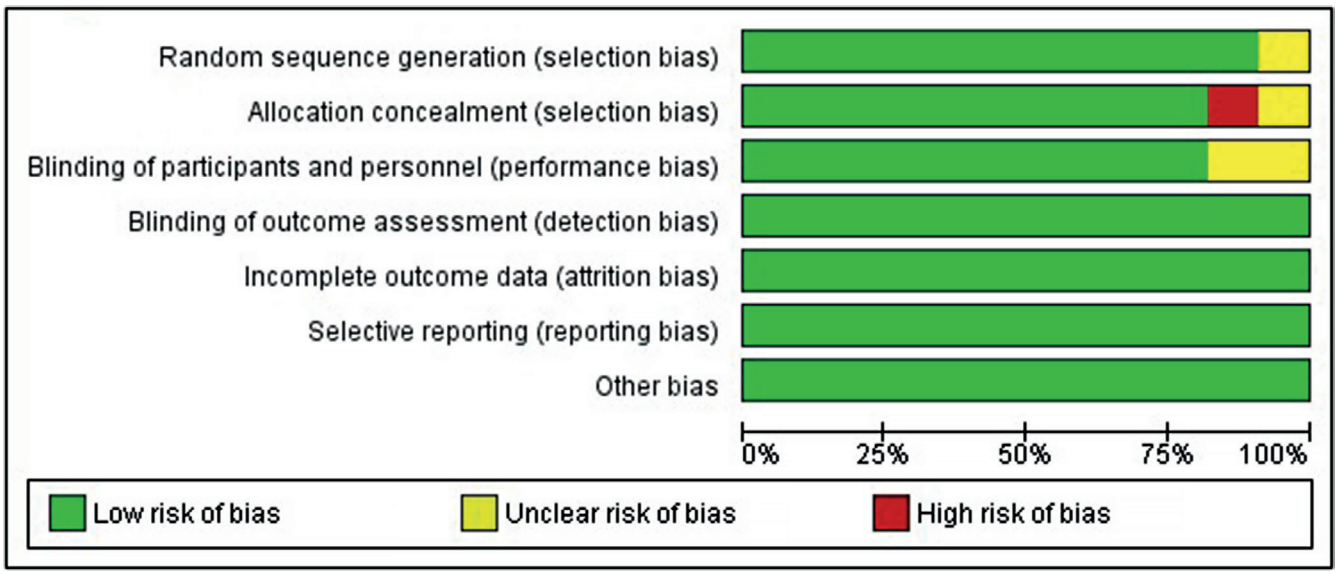

Fig. 3. Risk of bias graph

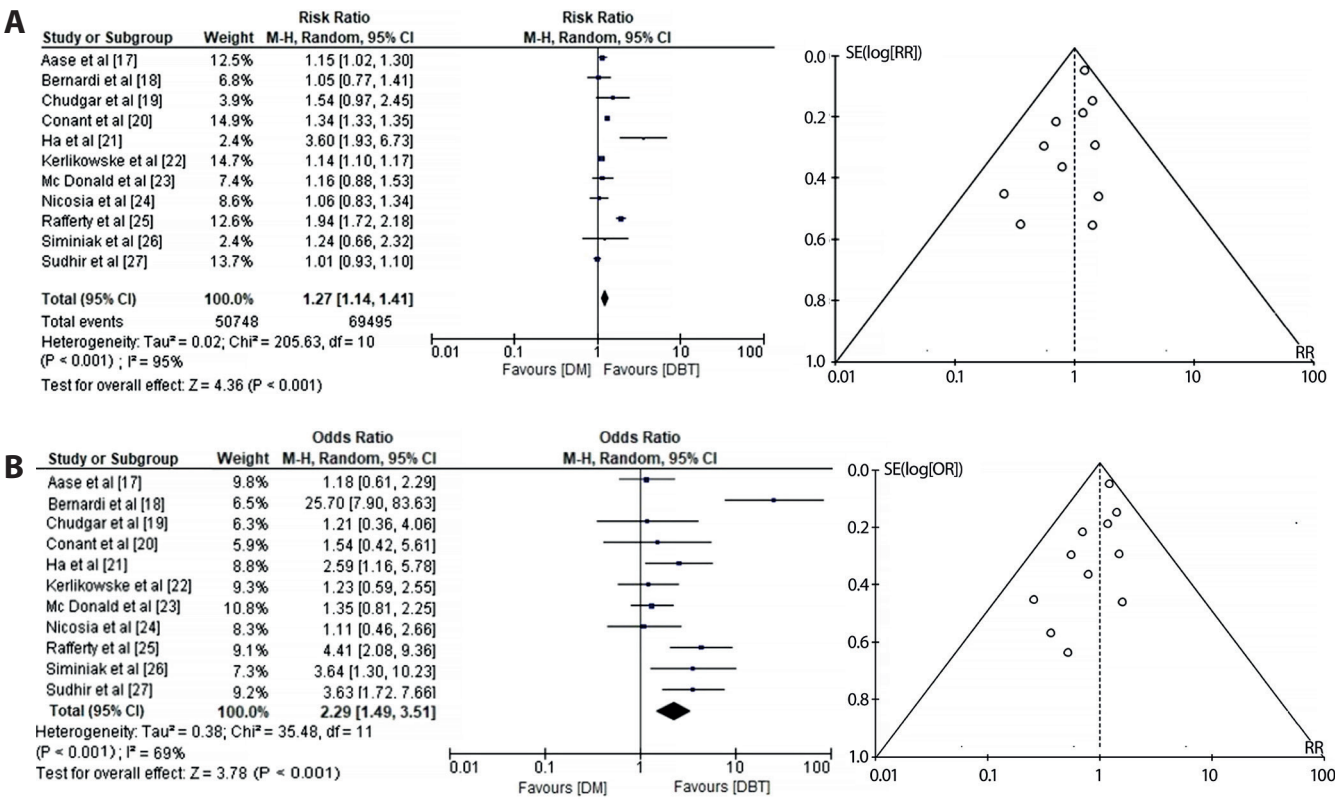

Fig. 5. Forest plot for primary outcomes and funnel plot for cancer detection rate for digital breast tomosynthesis (DBT) and digital mammography (DM). A. Risk ratio (Rr); B. Odds ratio (OR)

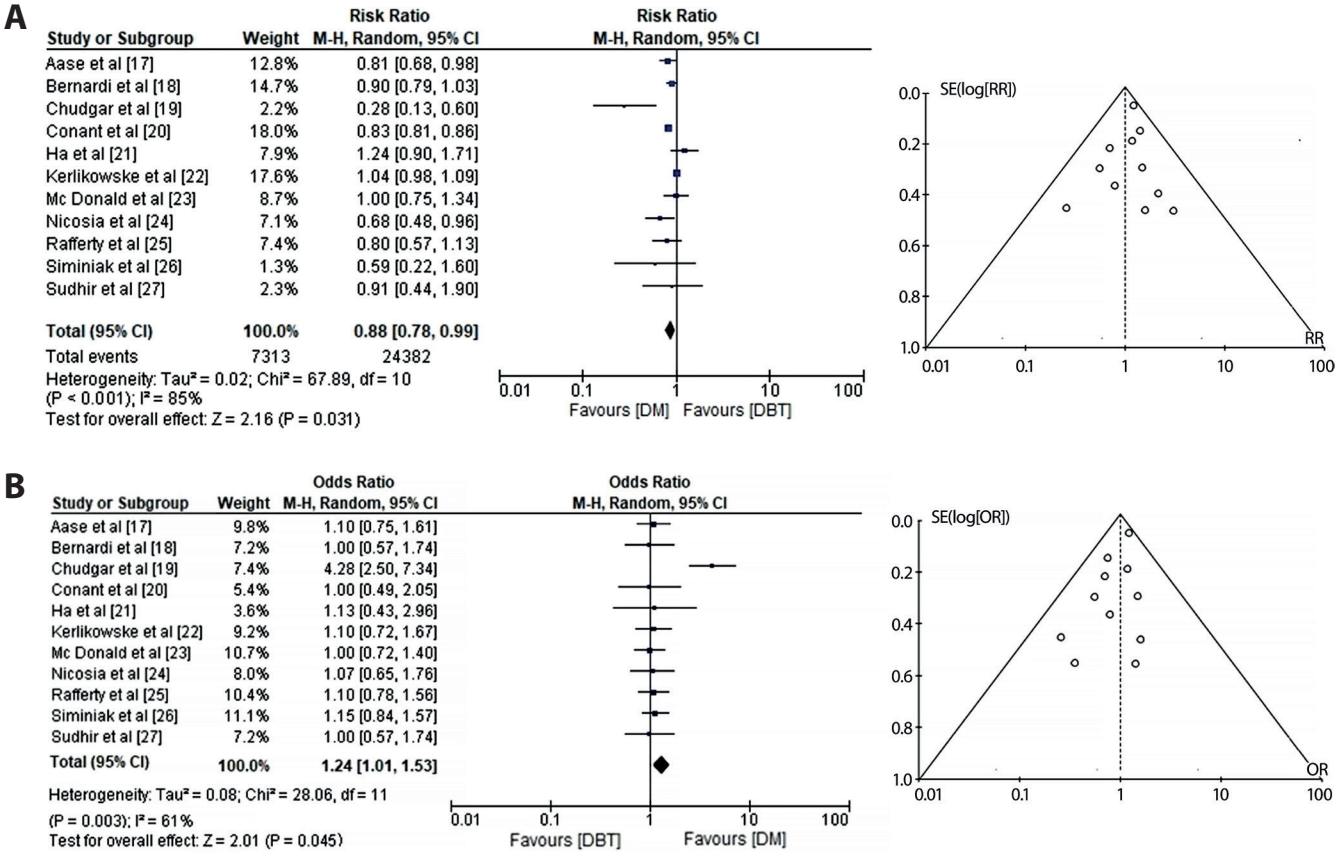

Fig. 6. Forest plot for primary outcomes and funnel plot for overall recall rate for digital breast tomosynthesis (DBT) and digital mammography (DM). A. Risk ratio (RR); B. Odds ratio (OR)

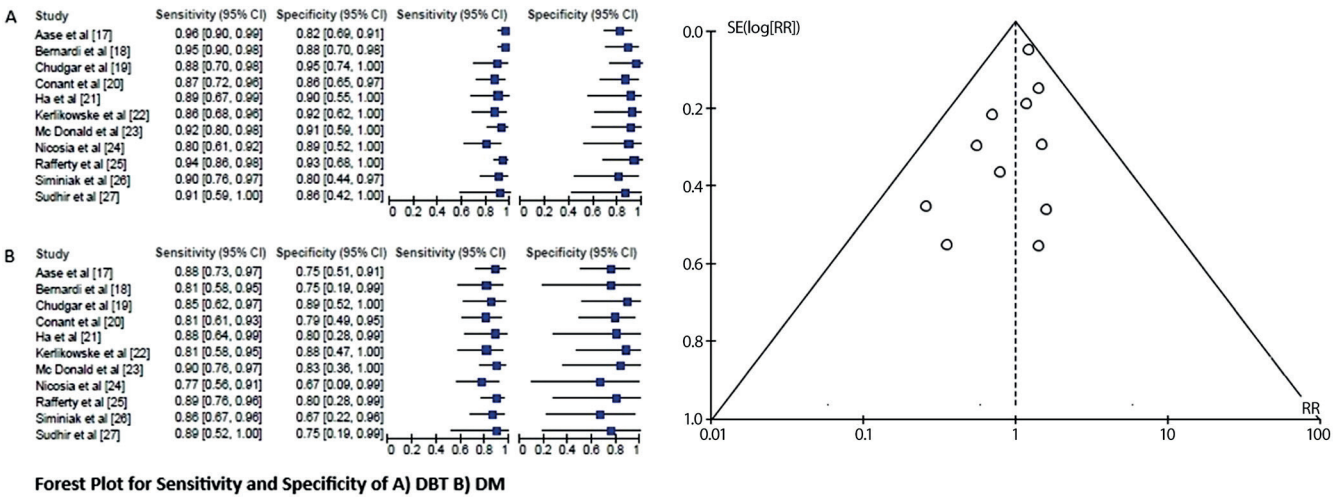

Fig. 7. Forest plot for primary outcomes and funnel plot for sensitivity and specificity of digital breast tomosynthesis (DBT) and digital mammography (DM). A. Risk ratio (RR); B. Odds ratio (OR)

indicate that DBT exhibited a pooled sensitivity of 0.91, with a 95% CI ranging from 0.59 to 0.99. Additionally, the pooled specificity for DBT was 0.90, with a 95% CI of 0.42 to 1.0. Conversely, Fig. 7B presents the findings for DM, revealing an overall sensitivity of 0.86, with a 95% CI ranging from 0.52 to 1.0. The pooled specificity for DM was 0.81, with a 95% CI of 0.12 to 1.0. We found that DBT exhibited greater sensitivity and specificity than DM in detecting BC.

Evaluation of DBT and DM screening results for accuracy and quality

To evaluate the diagnostic precision of the DBT and DM screening tools, an HSROC was generated for both using the sensitivity and specificity data derived from the 11 studies included in the analysis (Fig. 8). Figure 8A depicts the HSROC curve for DBT, whereas Fig. 8B illustrates the HSROC curve for DM. The circular symbols in the diagram represent individual studies, with the size of each circle corresponding to the number of patients included in that particular study. The height of the ovals represents the number of patients with BC, while the width represents the number of patients without BC. Additionally, the diagram includes a 95% prediction region. Analysis of the curves revealed that DBT exhibited higher accuracy, pooled sensitivity and specificity than DM, even when considering the presence of inter-study heterogeneity.

Variations in screening outcomes can occur during the implementation of DBT and DM due to the use of distinct devices, instruments and processes. Furthermore, the degree of control over factors that influence the magnitude of the results is constrained. Therefore, it is crucial to take into account the impact of these numerous stochastic, uncontrollable variables when interpreting and assessing the results. Hence, for the purpose of quality control and identification of measurement bias in the incorporated studies, the Youden plots, which are designed for interlaboratory comparisons, were also constructed. The Youden index (YI)[42] was computed using the sensitivity and specificity data obtained from the 11 studies incorporated in the analysis to evaluate the BC screening capability of the diagnostic tests. The findings indicated that DBT exhibited higher diagnostic accuracy than DM, as evidenced by DBT's YI of 81% and DM's YI of 67%, which are illustrated in Fig. 9, where Fig. 9A and Fig. 9B represent DBT and DM, respectively. A lack of bias in these diagrams is attributable to the closely matched datasets and ensures that the results are reliable and accurate.

Discussion

Mammography is an X-ray imaging technique used to assess the breast to identify cancer and other disorders early and for diagnostic and screening purposes. Digital mammography is a system in which the X-ray film utilized in SFM is substituted by solid-state detectors that convert X-rays into electrical impulses, similar to those used in digital cameras.[43] The European Society of Breast Imaging (EUSOBI) has issued its latest guidelines for the screening of women with highly dense breasts, as they are almost twice as likely to develop BC than a woman with normal breasts. Concurrently, the effectiveness of mammography is diminished due to the concealment of malignancies by the excessive projection of fibroglandular breast tissue. According to the EUSOBI guidelines set in 2022, it is strongly advised to do regular MRI screening exams every 2–3 years for individuals with breast composition type D, as defined by the American College of Radiology (ACR).[44] Also, DM is more expensive than traditional film technology and has lower spatial resolution. To address these limitations, DBT, a technology that captures numerous pictures of the breast rather than the customary single 2D image acquired with

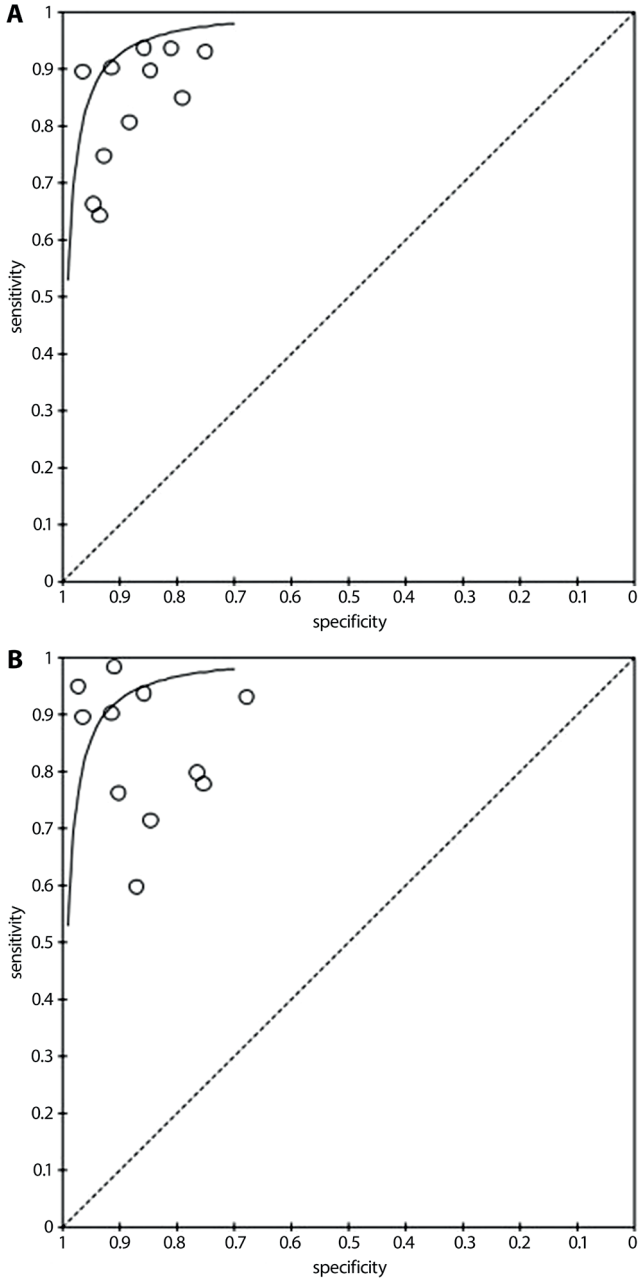

Fig. 8. Hierarchical summary receiver operating characteristic curve (HSROC) for digital breast tomosynthesis (DBT) and digital mammography (DM)

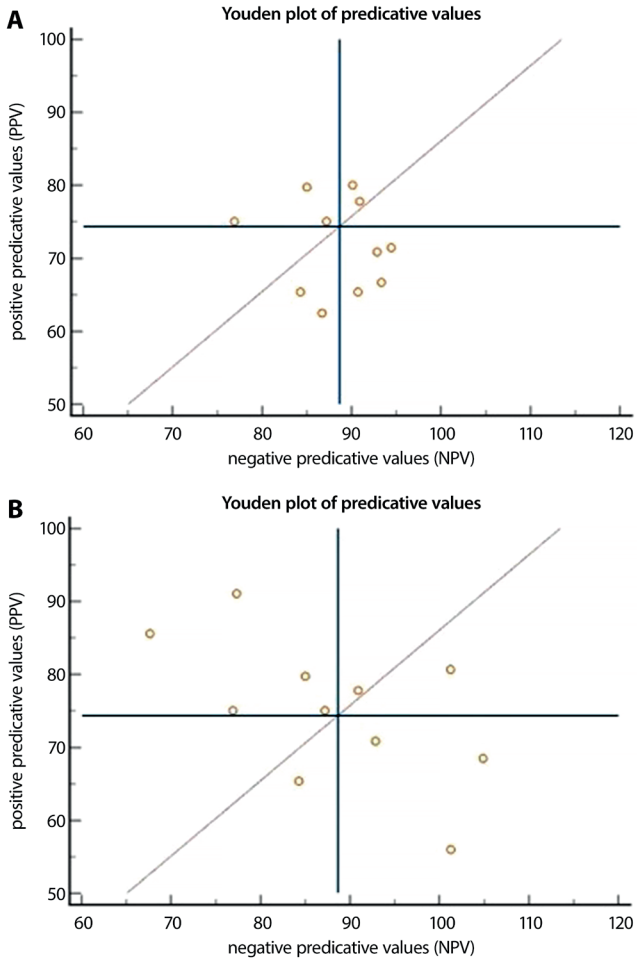

Fig. 9. Youden plot for digital breast tomosynthesis (DBT) and digital mammography (DM)

traditional mammography, is currently being used.[45] Digital breast tomosynthesis produces a more detailed picture and eliminates the problem of overlapping fibroglandular breast tissue that can disguise BC or imitate a pseudo-tumor, potentially enhancing the sensitivity for identifying breast malignancies and lowering the false positive rate.[46,47] Tomosynthesis, on the other hand, requires higher levels of radiation exposure and prolonged reading time.[48] The radiation doses employed for each test vary, though current technologies employ minimal radiation doses to obtain breast X-rays that exhibit superior image quality. The mean cumulative radiation dose for a standard mammography, which includes 2 views of each breast, is around 0.4 millisieverts (mSv). Digital breast tomosynthesis was linked to a radiation dosage that ranged from much lower to somewhat higher than DM. Specifically, the dose ratio ranges were 0.34–1.0 for 1-view DBT and 0.68–1.17 for 2-view DBT.[49]

The objective of this meta-analysis was to evaluate the diagnostic precision and dependability of DBT compared to DM for BC screening in women with either dense or non-dense breast tissue and included 11 trials encompassing 2,124,018 individuals. The study revealed that the DBT resulted in a higher CDR, as shown by an RR of 1.27 (95% CI: 1.14–1.41). Additionally, DBT demonstrated a lower recall rate, with an RR of 0.88 (95% CI: 0.78–0.99). The sensitivity and specificity of DBT were greater than those of DM. The pooled sensitivity for DBT was 0.91 (95% CI: 0.59–0.99) and the pooled specificity was 0.90 (95% CI: 0.42–1.0). In contrast, the pooled sensitivity for DM was 0.86 (95% CI: 0.52–1.0) and the pooled specificity was 0.81 (95% CI: 0.12–1.0). These differences in sensitivity and specificity between DBT and DM were statistically significant (Mantel–Haenszel method, $z = 2.53$; $p < 0.001$ for DBT and $z = 2.37$, $p < 0.001$ for DM).

The diagnostic accuracy of DBT was shown to be considerably superior to DM, as evidenced by the higher YI

values of 81% and 67% for DBT and DM, respectively. All of the obtained data exhibited reliability, lack of bias and statistical significance, indicated by a p-value of less than 0.05. The findings of our study are consistent with a previous systematic review and meta-analysis that examined the effectiveness of DBT and DM. In research conducted by Phi et al. in 2018,[50] it was shown that DBT had a high CDR (RR = 1.16, 95% CI: 1.02–1.31) and sensitivity (ranging from 84% to 90%) in women with mammographically dense breasts. Similarly, a study conducted by Li et al.[51] revealed that DBT exhibited varying levels of increased cancer detection (1/1,000 screens, 95% CI: 0.3–1.6, p = 0.003) and recall rates influenced by breast density (–0.9%, 95% CI: –1.4% to –0.4%, p < 0.001). In their systematic review and meta-analysis, Alabousi et al.[52] examined the performance of DBT, synthetic mammography (SM) and DM in the context of BC screening. They concluded that DBT alone or in conjunction with DM yielded optimal outcomes for BC screening.

The findings of this study demonstrate enhanced diagnostic outcomes when utilizing DBT in conjunction with Synthetic 2D (s2D) imaging compared to using DM alone. These results underscore the significance of incorporating DBT into BC screening practices. Nevertheless, it is essential to acknowledge that more research with longer observation periods and many screening iterations is necessary to develop definitive conclusions regarding the influence of enhanced detection of cancer on periodic rates of cancer and, perhaps, on BC mortality.

Limitations

This meta-analysis had several limitations. First, the inclusion of only 11 retrospective or prospective studies with moderate-to-high levels of heterogeneity limited the findings despite the study's strict adherence to the recommended methodological rigor. Second, the studies included in the analysis solely focused on the assessment of initial detection measures, neglecting to provide any insights into the potential long-term health consequences associated with DBT screening. Hence, the potential impact of DBT on reducing BC mortality through incremental screening remains unknown. Furthermore, a significant portion of the data presented pertains to the screening of prevalent cases of DBT at the first stage. It is probable that variations may arise in the screening outcomes acquired through using diverse devices, equipment and processes when employing DBT and DM for screening. As a result, it is plausible that the findings of our study may have limited generalizability. In addition, the fact that only English-language articles were included may have limited the scope of our meta-analysis. Lastly, it should be noted that the small number of studies and patient populations included in this analysis limits the generalizability of the findings to a larger population. Consequently, additional research is necessary to investigate this issue further.

Conclusions

The present meta-analysis offers an up-to-date comparison of the DBT and DM screening techniques, with the results suggesting that DBT exhibits superior performance compared to DM in terms of increased cancer detection, sensitivity and recall rate in screening and diagnostic scenarios. The potential improvement in CDR and reduction in missed diagnoses (recall rate) associated with DBT may indicate a more effective approach to screening or diagnostic assessment for women with dense and non-dense breast tissue. Hence, the findings presented in our study have the potential to contribute to screening policy development, research planning and individual screening recommendations. However, it is crucial to note that further studies with extended follow-up periods and multiple screening rounds are required to establish conclusive findings regarding the impact of improved cancer detection on interval cancer rates and, potentially, on BC mortality.

Supplementary data

The Supplementary materials are available at https://doi.org/10.5281/zenodo.10803079. The package includes the following files:

Supplementary Table 1: Standardized questionnaire for assessment of risk of bias of included studies.

ORCID iDs

Hao Lin https://orcid.org/ 0009-0002-5203-4520
Yimeng Zhang https://orcid.org/0009-0000-9637-5568
Lixia Wu https://orcid.org/0009-0000-1345-2434
Ceng Li https://orcid.org/ 0009-0000-8913-0028

References

1. Giaquinto AN, Sung H, Miller KD, et al. Breast cancer statistics, 2022. *CA Cancer J Clin*. 2022;72(6):524–541. doi:10.3322/caac.21754
2. Duffy SW, Tabár L, Yen AM, et al. Mammography screening reduces rates of advanced and fatal breast cancers: Results in 549,091 women. *Cancer*. 2020;126(13):2971–2979. doi:10.1002/cncr.32859
3. Elmore JG, Armstrong K, Lehman CD, Fletcher S. Screening for breast cancer. *JAMA*. 2005;293(10):1245. doi:10.1001/jama.293.10.1245
4. Nicholson BT, LoRusso AP, Smolkin M, Bovbjerg VE, Petroni GR, Harvey JA. Accuracy of assigned BI-RADS breast density category definitions. *Acad Radiol*. 2006;13(9):1143–1149. doi:10.1016/j.acra.2006.06.005
5. Tice JA, Gard CC, Miglioretti DL, et al. Comparing mammographic density assessed by digital breast tomosynthesis or digital mammography: The Breast Cancer Surveillance Consortium. *Radiology*. 2022;302(2):286–292. doi:10.1148/radiol.2021204579
6. Boyd NF, Guo H, Martin LJ, et al. Mammographic density and the risk and detection of breast cancer. *N Engl J Med*. 2007;356(3):227–236. doi:10.1056/NEJMoa062790
7. Mokhtary A, Karakatsanis A, Valachis A. Mammographic density changes over time and breast cancer risk: A systematic review and meta-analysis. *Cancers (Basel)*. 2021;13(19):4805. doi:10.3390/cancers13194805
8. Reynolds A. Breast density and digital breast tomosynthesis. *Radiol Technol*. 2013;85(1):63M–82M; quiz 83M–85M. PMID:24029897.
9. Destounis SV, Morgan R, Arieno A. Screening for dense breasts: Digital breast tomosynthesis. *Am J Roentgenol*. 2015;204(2):261–264. doi:10.2214/AJR.14.13554
10. Sprague BL, Coley RY, Lowry KP, et al. Digital breast tomosynthesis versus digital mammography screening performance on successive screening rounds from the breast cancer surveillance consortium. *Radiology*. 2023;307(5):e223142. doi:10.1148/radiol.223142

11. Gao Y, Moy L, Heller SL. Digital breast tomosynthesis: Update on technology, evidence, and clinical practice. *Radiographics*. 2021;41(2): 321–337. doi:10.1148/rg.2021200101
12. Lee JM, Ichikawa LE, Wernli KJ, et al. Digital mammography and breast tomosynthesis performance in women with a personal gistory of breast cancer, 2007–2016. *Radiology*. 2021;300(2):290–300. doi:10.1148/radiol.2021204581
13. Heywang-Köbrunner SH, Jänsch A, Hacker A, Weinand S, Vogelmann T. Digital breast tomosynthesis (DBT) plus synthesised two-dimensional mammography (s2D) in breast cancer screening is associated with higher cancer detection and lower recalls compared to digital mammography (DM) alone: Results of a systematic review and meta-analysis. *Eur Radiol*. 2022;32(4):2301–2312. doi:10.1007/s00330-021-08308-8
14. Bahl M, Mercaldo S, Dang PA, McCarthy AM, Lowry KP, Lehman CD. Breast cancer screening with digital breast tomosynthesis: Are initial benefits sustained? *Radiology*. 2020;295(3):529–539. doi:10.1148/radiol.2020191030
15. Paulis LE, Lobbes MBI, Lalji UC, et al. Radiation exposure of digital breast tomosynthesis using an antiscatter grid compared with full-field digital mammography. *Invest Radiol*. 2015;50(10):679–685. doi:10.1097/RLI.0000000000000168
16. Yang G, Qian X, Phan T, et al. Design and feasibility studies of a stationary digital breast tomosynthesis system. *Nucl Instrum Methods Phys Res A*. 2011;648(Suppl 1):S220–S223. doi:10.1016/j.nima.2010.11.147
17. Aase HS, Holen ÅS, Pedersen K, et al. A randomized controlled trial of digital breast tomosynthesis versus digital mammography in population-based screening in Bergen: Interim analysis of performance indicators from the To-Be trial. *Eur Radiol*. 2019;29(3):1175–1186. doi:10.1007/s00330-018-5690-x
18. Bernardi D, Belli P, Benelli E, et al. Digital breast tomosynthesis (DBT): Recommendations from the Italian College of Breast Radiologists (ICBR) by the Italian Society of Medical Radiology (SIRM) and the Italian Group for Mammography Screening (GISMa). *Radiol Med*. 2017; 122(10):723–730. doi:10.1007/s11547-017-0769-z
19. Chudgar AV, Conant EF, Weinstein SP, et al. Assessment of disease extent on contrast-enhanced MRI in breast cancer detected at digital breast tomosynthesis versus digital mammography alone. *Clin Radiol*. 2017;72(7):573–579. doi:10.1016/j.crad.2017.02.013
20. Conant EF, Beaber EF, Sprague BL, et al. Breast cancer screening using tomosynthesis in combination with digital mammography compared to digital mammography alone: A cohort study within the PROSPR consortium. *Breast Cancer Res Treat*. 2016;156(1):109–116. doi:10.1007/s10549-016-3695-1
21. Ha SM, Yi A, Yim D, et al. Digital breast tomosynthesis plus ultrasound versus digital mammography plus ultrasound for screening breast cancer in women with dense breasts. *Korean J Radiol*. 2023;24(4):274. doi:10.3348/kjr.2022.0649
22. Kerlikowske K, Su YR, Sprague BL, et al. Association of screening with digital breast tomosynthesis vs digital mammography with risk of interval invasive and advanced breast cancer. *JAMA*. 2022; 327(22):2220. doi:10.1001/jama.2022.7672
23. McDonald ES, Oustimov A, Weinstein SP, Synnestvedt MB, Schnall M, Conant EF. Effectiveness of digital breast tomosynthesis compared with digital mammography: Outcomes analysis from 3 years of breast cancer screening. *JAMA Oncol*. 2016;2(6):737. doi:10.1001/jamaoncol.2015.5536
24. Nicosia L, Bozzini AC, Pesapane F, et al. Breast digital tomosynthesis versus contrast-enhanced mammography: Comparison of diagnostic application and radiation dose in a screening setting. *Cancers (Basel)*. 2023;15(9):2413. doi:10.3390/cancers15092413
25. Rafferty EA, Durand MA, Conant EF, et al. Breast cancer screening using tomosynthesis and digital mammography in dense and non-dense breasts. *JAMA*. 2016;315(16):1784. doi:10.1001/jama.2016.1708
26. Siminiak N, Pasiuk-Czepczyńska A, Godlewska A, et al. Are contrast enhanced mammography and digital breast tomosynthesis equally effective in diagnosing patients recalled from breast cancer screening? *Front Oncol*. 2022;12:941312. doi:10.3389/fonc.2022.941312
27. Sudhir R, Sannapareddy K, Potlapalli A, Krishnamurthy PB, Buddha S, Koppula V. Diagnostic accuracy of contrast-enhanced digital mammography in breast cancer detection in comparison to tomosynthesis, synthetic 2D mammography and tomosynthesis combined with ultrasound in women with dense breast. *Br J Radiol*. 2021;94(1118): 20201046. doi:10.1259/bjr.20201046
28. Page MJ, McKenzie JE, Bossuyt PM, et al. The PRISMA 2020 statement: An updated guideline for reporting systematic reviews. *BMJ*. 2021;372:n71. doi:10.1136/bmj.n71
29. Huedo-Medina TB, Sánchez-Meca J, Marín-Martínez F, Botella J. Assessing heterogeneity in meta-analysis: Q statistic or I^2 index? *Psychol Methods*. 2006;11(2):193–206. doi:10.1037/1082-989X.11.2.193
30. Schmidt L, Shokraneh F, Steinhausen K, Adams CE. Introducing RAPTOR: RevMan Parsing Tool for Reviewers. *Syst Rev*. 2019;8(1):151. doi:10.1186/s13643-019-1070-0
31. McGuinness LA, Higgins JPT. Risk-of-bias VISualization (robvis): An R package and Shiny web app for visualizing risk-of-bias assessments. *Res Synth Methods*. 2021;12(1):55–61. doi:10.1002/jrsm.1411
32. George BJ, Aban IB. An application of meta-analysis based on DerSimonian and Laird method. *J Nucl Radiol*. 2016;23(4):690–692. doi:10.1007/s12350-015-0249-6
33. Begg CB, Mazumdar M. Operating characteristics of a rank correlation test for publication bias. *Biometrics*. 1994;50(4):1088–1101. PMID:7786990.
34. Van Enst WA, Ochodo E, Scholten RJ, Hooft L, Leeflang MM. Investigation of publication bias in meta-analyses of diagnostic test accuracy: A meta-epidemiological study. *BMC Med Res Methodol*. 2014;14(1):70. doi:10.1186/1471-2288-14-70
35. Sterne JAC, Egger M. Funnel plots for detecting bias in meta-analysis. *J Clin Epidemiol*. 2001;54(10):1046–1055. doi:10.1016/S0895-4356(01)00377-8
36. Elovic A, Pourmand A. MDCalc Medical Calculator App Review. *J Digit Imaging*. 2019;32(5):682–684. doi:10.1007/s10278-019-00218-y
37. Coucke W, Rida Soumali M, Badrick T. Improving Youden plots by including analytical performance specifications. *Clin Chim Acta*. 2022; 531:212–216. doi:10.1016/j.cca.2022.04.014
38. Takwoingi Y, Guo B, Riley RD, Deeks JJ. Performance of methods for meta-analysis of diagnostic test accuracy with few studies or sparse data. *Stat Methods Med Res*. 2017;26(4):1896–1911. doi:10.1177/0962280215592269
39. Godavitarne C, Robertson A, Ricketts DM, Rogers BA. Understanding and interpreting funnel plots for the clinician. *Br J Hosp Med*. 2018;79(10):578–583. doi:10.12968/hmed.2018.79.10.578
40. Lin L, Chu H. Quantifying publication bias in meta-analysis. *Biometrics*. 2018;74(3):785–794. doi:10.1111/biom.12817
41. Trevethan R. Sensitivity, specificity, and predictive values: Foundations, pliabilities, and pitfalls in research and practice. *Front Public Health*. 2017;5:307. doi:10.3389/fpubh.2017.00307
42. Fluss R, Faraggi D, Reiser B. Estimation of the Youden index and its associated cutoff point. *Biometrical J*. 2005;47(4):458–472. doi:10.1002/bimj.200410135
43. Lowry KP, Coley RY, Miglioretti DL, et al. Screening performance of digital breast tomosynthesis vs digital mammography in community practice by patient age, screening round, and breast density. *JAMA Netw Open*. 2020;3(7):e2011792. doi:10.1001/jamanetworkopen.2020.11792
44. Mann RM, Athanasiou A, Baltzer PAT, et al. Breast cancer screening in women with extremely dense breasts recommendations of the European Society of Breast Imaging (EUSOBI). *Eur Radiol*. 2022;32(6): 4036–4045. doi:10.1007/s00330-022-08617-6
45. Muttarak M. Digital mammography: Opportunities and limitations. *Singapore Med J*. 2007;48(9):795–796. PMID:17728956.
46. Fedon C, Caballo M, García E, et al. Fibroglandular tissue distribution in the breast during mammography and tomosynthesis based on breast CT data: A patient-based characterization of the breast parenchyma. *Med Phys*. 2021;48(3):1436–1447. doi:10.1002/mp.14716
47. Vedantham S, Shi L, Michaelsen KE, et al. Digital breast tomosynthesis guided near infrared spectroscopy: Volumetric estimates of fibroglandular fraction and breast density from tomosynthesis reconstructions. *Biomed Phys Eng Express*. 2015;1(4):045202. doi:10.1088/2057-1976/1/4/045202
48. Preibsch H, Siegmann-Luz KC. Digitale Tomosynthese der Mamma. *Radiologe*. 2015;55(1):59–70. doi:10.1007/s00117-014-2753-0
49. Svahn TM, Houssami N, Sechopoulos I, Mattsson S. Review of radiation dose estimates in digital breast tomosynthesis relative to those in two-view full-field digital mammography. *Breast*. 2015;24(2):93–99. doi:10.1016/j.breast.2014.12.002

50. Phi XA, Tagliafico A, Houssami N, Greuter MJW, De Bock GH. Digital breast tomosynthesis for breast cancer screening and diagnosis in women with dense breasts: A systematic review and meta-analysis. *BMC Cancer*. 2018;18(1):380. doi:10.1186/s12885-018-4263-3
51. Li T, Houssami N, Noguchi N, Zeng A, Marinovich ML. Differential detection by breast density for digital breast tomosynthesis versus digital mammography population screening: A systematic review and meta-analysis. *Br J Cancer*. 2022;127(1):116–125. doi:10.1038/s41416-022-01790-x
52. Alabousi M, Wadera A, Kashif Al-Ghita M, et al. Performance of digital breast tomosynthesis, synthetic mammography, and digital mammography in breast cancer screening: A systematic review and meta-analysis. *J Nat Cancer Inst*. 2021;113(6):680–690. doi:10.1093/jnci/djaa205

Forensic value of soft tissue detachments from the hyoid bone in death due to strangulation asphyxia

Giovanna Del Balzo[1,A,D], Guido Pelletti[2,C,E], Dario Raniero[1,B,C], Alessia Farinelli[1,B,D], Andrea Uberti[1,B,C], Elisa Vermiglio[1,C,D], Gabriele Molteni[3,4,E,F], Riccardo Nocini[5,C,E], Stefano Gobbo[6,C,F], Francesco Taus[1,C,E], Albino Eccher[7,C,F], Claudio Luchini[1,E,F], Matteo Brunelli[1,E,F]

[1] Department of Diagnostics and Public Health, University of Verona, Italy
[2] Department of Medical and Surgical Sciences, Unit of Legal Medicine, University of Bologna, Italy
[3] Department of Otorhinolaryngology Head and Neck Surgery, IRCCS Azienda Ospedaliero-Universitaria di Bologna, Policlinico Sant'Orsola-Malpighi, Italy
[4] Department of Medical and Surgical Sciences (DIMEC), Alma Mater Studiorum, University of Bologna, Italy
[5] Department of Surgery, Dentistry, Pediatrics and Gynecology, University of Verona, Italy
[6] Department of Translational Medicine, University of Ferrara, Italy
[7] Department of Medical and Surgical Sciences for Children and Adults, University Hospital of Modena, Italy

A – research concept and design; B – collection and/or assembly of data; C – data analysis and interpretation;
D – writing the article; E – critical revision of the article; F – final approval of the article

Advances in Clinical and Experimental Medicine, ISSN 1899–5276 (print), ISSN 2451–2680 (online) *Adv Clin Exp Med*. 2025;34(3):327–335

Address for correspondence
Guido Pelletti
E-mail: guidopelletti@gmail.com

Funding sources
None declared

Conflict of interest
None declared

Received on December 27, 2023
Reviewed on March 12, 2024
Accepted on March 27, 2024

Published online on April 29, 2024

Cite as
Del Balzo G, Pelletti G, Raniero D, et al. Forensic value of soft tissue detachments from the hyoid bone in death due to strangulation asphyxia. *Adv Clin Exp Med*. 2025;34(3):327–335. doi:10.17219/acem/186560

DOI
10.17219/acem/186560

Abstract

Background. There are no unequivocal histopathological findings for the diagnosis of fatal asphyxia due to neck compression. From the observation of a series of asphyxiation cases, we noted, during microscopic analysis, a high frequency of "detachment" of soft tissues from the hyoid bone. This specifically refers to the presence of an optical space between the surface of the hyoid bone and soft tissues.

Objectives. We aimed to evaluate the detachment of soft tissues from the hyoid bone as specific histological evidence of death due to strangulation asphyxia.

Materials and methods. Ten blocks were taken from deaths due to external mechanical compression of the neck (strangulation asphyxia, group A), 22 blocks were taken from deaths for other causes without trauma to the neck (group B), and 38 blocks were obtained from living subjects that have undergone laryngectomies (group C). The presence/absence of detachments were compared between the 3 groups (A, B and C) using Fisher's exact test.

Results. The detachment of soft tissues from the hyoid bone was observed in 5 cases (50%) in group A, 6 cases (27.2%) in group B, and 17 cases (44.3%) in group C. The sensitivity and specificity of the presence of the detachment in group A were 0.5 (95% confidence interval (95% CI): 0.38–0.62) and 0.57 (95% CI: 0.45–0.69), respectively. The comparison between the 3 groups and the presence/absence of soft tissue detachment showed no statistically significant differences between the groups ($p = 0.329$), clarifying that soft tissue detachment is a nonspecific variable for all 3 situations.

Conclusions. Detachment of soft tissues has poor value as a single element to favor the diagnosis of asphyxia due to violent compression of the neck and should be interpreted as an artifactual finding, unrelated to the neck injury or injury vitality.

Key words: histology, autopsy, strangulation, artifact, detachment of soft tissue from hyoid bone

Background

Asphyxia due to external compression of the neck (i.e., strangulation asphyxia) is a common issue in forensic pathology and can be seen in homicides, suicides, and, rarely, in accidental cases.[1] Compression can be caused by different mechanisms and can be classified as hanging, ligature strangulation and manual strangulation, depending on the means used to compress the neck (ligature vs hands) and the application of forces (assailant force vs gravity).[2] Ligature and manual strangulation are typically seen in homicides, whereas hanging is often encountered in suicide cases. Homicide by hanging and suicide by ligature strangulation is rare.[3,4]

Macroscopic and microscopic signs of strangulation have been broadly studied, and their specificity is well known for hanging[5,6] as well as manual and ligature strangulation.[7,8] Histological analysis of deaths due to strangulation is usually performed to identify signs of injuries of the skin and internal structures of the neck,[9–11] such as fractures with hemorrhages of the surrounding soft tissues. However, when there are no known hallmarks of asphyxia due to external forces, the cause of death determination can be challenging. In such cases, there are, as a rule, no (or only uncharacteristic) morphological macroscopic or microscopic findings, namely conjunctival petechiae and other findings during the histological examination of the lung, the so-called "hemorrhagic-dysphoric syndrome".[12] Nevertheless, none of the signs of asphyxia in internal organs is conclusive for asphyxia: the diagnosis of asphyxiation is typically made by collecting all relevant internal and external findings, expressing a different level of support for the hypothesis of asphyxia over other hypotheses, such as fatal drug intoxication or sudden death.

In recent years, the ultra-specialized research in legal medicine[13,14] on this topic has focused on studying signs of asphyxia and developing new techniques that can support the diagnosis.[15–17] A series of autopsy cases revealed a high frequency of soft tissue "detachment" from the hyoid bone during microscopic analysis.. This specifically refers to the presence of an optical space between the surface of the hyoid bone and soft tissues.

Objectives

Hypothesizing that the microscopic identification during light microscopy of soft tissue detachment from the hyoid bone could contribute to the challenging diagnosis of asphyxia resulting from neck compression, the objective of this study was to determine, through a retrospective case-control analysis, whether this finding is more frequent in cases of asphyxia or if it is an artifact resulting from sample processing. The findings in our casework will be compared to existing literature on mechanical asphyxia.

Materials and methods

We performed a retrospective study on whole neck blocks (including the tongue, hyoid bone, larynx, and the first tracheal ring) collected during forensic autopsies between 2019 and 2021 in the Section of Forensic Pathology of the University Hospital of Verona (Italy), which represents one of the main referral centers for forensic pathology in northeast Italy. Seventy whole neck blocks were available for the purposes of the study, including 10 blocks taken from deaths due to strangulation (group A), 22 blocks taken from deaths for other causes without inner cervical injuries (group B), and 38 blocks obtained from living subjects that had undergone laryngectomies for infiltrative squamous carcinoma (group C), as reported in Table 1 (groups A and B) and Table 2 (group C).

In group A, the cause and manner of death were determined after a comprehensive medico-legal evaluation, based on circumstantial data, external examination, autopsy, and, when needed, ancillary tests (i.e., histologic and toxicologic analyses). Group C specimens were selected after a review of the anatomy of the specimens following primary gross sampling for oncologic primary diagnosis and staging at the Pathology Department of the University Hospital of Verona. In group C, the invasion of the soft tissue directly surrounding the examined hyoid bone horn was an exclusion criterion. Tumors did invade the soft tissue and/or adjacent bones and were staged as pT3 in 13 cases and pT4 in 4 cases. All hyoid-larynx complexes included in the study were fixed in a 10% buffered formalin solution immediately after sampling/extraction. After formalin fixation, the histologic analysis was performed within 2 weeks for all cases.

Neck blocks from asphyxiation deaths were used as cases, while neck blocks from other deaths or laryngectomies in living patients were used as negative controls. The dissection techniques applied were identical, according to The National Association of Medical Examiners (NAME) recommendations.[18] Neck structures were dissected using a layer-by-layer technique following vascular decompression of the neck by removal of cephalic and thoracic organs to minimize the risk of misinterpretations. During neck dissection, each layer was contextually examined to search for any macroscopic lesions of the soft tissues. The hyoid-larynx complex collected during autopsies was obtained by incision of the oral floor and subsequent gentle dissection of the esophagus and anterior neck structures from the anterior aspect of the cervical spine. During the procedure, a layer of 0.5 cm of soft tissue adjacent to the hyoid bone (the greater hyoid bone horns) was preserved intact for histological analysis. The sampling for histological analysis was performed on surgical laryngectomies as samples according to the College of American Pathologists (CAP) protocol. All complexes were referred to the Section of Pathology of the University

Table 1. Detachment of soft tissue from hyoid bone in asphyxia deaths due to neck compression compared to other circumstances

ID	Sex	Age	Group	External injuries	Internal injuries	Cause of death	Manner of death	Presence of detachment/number of samples^	Maximum extent of the detachment	Near to hemorrhage	Near to fracture	PMI
1	M	58	A	petechial hemorrhages and skin sulcus	none	ligature strangulation	suicide	8/9 blocks	1250 µm	–	–	2
2	F	34	A	skin sulcus	fracture of the left greater cornu of hyoid bone, hemorrhages	hanging	suicide	4/4 blocks	1820 µm	no	no	2
3	F	68	A	skin discoloration	tongue hemorrhages	ligature strangulation*	homicide	4/4 blocks	230 µm	–	–	3
4	F	11	A	petechial hemorrhages and gum bruises	bilateral fracture of hyoid bone and hemorrhages	smothering and manual strangulation	homicide	4/4 blocks	510 µm	yes	no	3
5	F	43	A	skin sulcus	none	hanging	suicide	3/4 blocks	630 µm	–	–	4
6	M	64	A	brownish discoloration of the skin	brownish discoloration of soft tissues	ligature strangulation*	homicide	0/12 blocks	no	–	–	6
7	F	49	A	fingernail abrasions	hemorrhages	manual strangulation	homicide	0/8 blocks	no	no	–	4
8	M	37	A	irregular abrasions	hemorrhages in the left superior horn of thyroid cartilage	hanging	suicide	0/2 blocks	no	no	–	2
9	M	91	A	none	fracture of the superior horn of the thyroid cartilage, hemorrhages	smothering and manual strangulation	homicide	0/1 blocks	no	–	no	3
10	M	40	A	linear abrasion	none	hanging	suicide	0/2 blocks	no	–	–	2
11	M	89	B	none	none	sepsis*	natural death	1/4 blocks	480 µm	–	–	2
12	F	55	B	none	none	thoracic trauma	accident	0/3 blocks	no	–	–	2
13	M	69	B	none	none	drowning	suicide	0/2 blocks	no	–	–	3
14	M	34	B	none	none	gunshot	homicide	1/3 blocks	580 µm	–	–	4
15	M	62	B	none	none	cardiac death	natural death	0/1 blocks	no	–	–	3
16	F	26	B	none	none	drug overdose	accident	0/1 blocks	no	–	–	5
17	F	52	B	laceration	hemorrhages	choking	suicide	1/1 blocks	2110 µm	–	–	2
18	M	35	B	none	hemorrhages	polytrauma	accident	0/1 blocks	no	–	–	5
19	M	32	B	none	none	drug overdose	accident	0/1 blocks	no	–	–	2
20	F	77	B	none	none	cardiac death	natural death	1/3 blocks	1920 µm	–	–	3
21	M	58	B	none	none	head trauma	homicide	0/3 blocks	no	–	–	2

Table 1. Detachment of soft tissue from hyoid bone in asphyxia deaths due to neck compression vs other circumstances – cont.

ID	Sex	Age	Group	External injuries	Internal injuries	Cause of death	Manner of death	Presence of detachment/number of samples^	Maximum extent of the detachment	Near to hemorrhage	Near to fracture	PMI
22	F	49	B	none	none	polytrauma	suicide	0/2 blocks	no	–	–	3
23	M	29	B	none	none	CO poisoning	accident	0/3 blocks	no	–	–	4
24	M	38	B	none	none	cardiac death*	natural death	0/2 blocks	no	–	–	4
25	M	42	B	none	none	sepsis	natural death	0/4 blocks	no	–	–	3
26	M	79	B	none	none	polytrauma	accident	1/5 blocks	1110 µm	–	–	2
27	M	79	B	none	none	silicosis	natural death	0/3 blocks	no	–	–	2
28	M	66	B	none	none	gunshot	accident	0/4 blocks	no	–	–	3
29	F	51	B	abrasions, bruises	perihyoid tissue hemorrhages	polytrauma	homicide	0/3 blocks	no	–	–	4
30	F	27	B	petechial hemorrhages, mucosal contusion on the lips	none	smothering	homicide	0/2 blocks	no	–	–	3
31	F	52	B	none	none	pulmonary embolism	natural death	1/1 blocks	990 µm	–	–	2
32	F	3	B	petechial hemorrhages and abrasions	none	smothering	homicide	0/3 blocks	no	–	–	2

* advanced post-mortem decomposition stage; group A – deaths due to violent external compression of the neck; group B – deaths of other causes without trauma of the neck; Near to hemorrhage – the reported maximum extent of the detachment was reported on the slide where the horn fracture was present; Near to fracture – the reported maximum extent of the detachment was reported on the slide where the soft-tissue hemorrhage was present; PMI – post-mortem interval; M – male; F – female; CO – carbon monoxide.

Hospital of Verona and placed in a slow decalcifying solution. Serial withdrawals of the hyoid bone and adjacent soft tissue were obtained from each sample. A minimum of 3 and a maximum of 12 withdrawals for each autopsy were obtained and were dehydrated in an increasing ethanol ladder, diaphonized in xylene substitute, and embedded in a high fusion point paraffin (60°), resulting in a mean of 4.6 paraffin blocks per case. From each block, a single slice 3–5 µm-thick was cut using a microtome and stained with hematoxylin and eosin (H&E). Each slide was examined using a standard morphologic method, represented by vision with an Olympus BX microscope (Olympus Corp., Tokyo, Japan) performed by an expert pathologist, and a digital method by which the slides were scanned and digitalized using a Grundium Ocus scanner (Grundium/Nikon, Tampere, Finland). An expert pathologist analyzed the slides and digital images, focusing on the identification of detachment of the soft tissues from the hyoid bone (presence of an angular empty space in between soft tissue and bone on H&E staining), as well as any incidental microscopic findings, such as hemorrhages in cartilages, soft tissues and muscles, or microfractures of the hyoid bone and thyroid cartilage.

Statistical analyses

The following data were collected for each case: sex, presence of detachment, the number of blocks in which the detachment was observed, and the maximum extent of the detachment. Only for autopsy cases, external and internal injuries and the cause and the manner of death were included. Logistic regression is a statistical method allowing for the testing of models designed to predict binary outcomes, such as the presence or absence of detachment. In a single model, the independent predictor variable is categorical and pertains to 3 medico-legal/clinical settings, namely, groups A, B and C. To run a logistic regression, some assumptions regarding the sample size, multicollinearity and outliers were preliminarily checked. Since we only had 1 independent variable, we deemed the minimum sample size to be adequate (group A; n = 10). Additionally, we did not find any outliers. Statistical tests were performed using the IBM Statistical Package for the Social Sciences (SPSS) v. 29.0 (IBM Corp., Armonk, USA). Values were presented as absolute number of cases, frequency and, when appropriate, median and ranges. The presence/absence of detachment in cases

Table 2. Detachment of soft tissue from the hyoid bone in asphyxia deaths due to neck compression compared to other circumstances in group C – blocks obtained from living subjects that had undergone laryngectomies for infiltrative squamous carcinoma

ID	Sex	Age	Presence of detachment/ number of samples^	Maximum extent of the detachment
1	F	61	0/4 blocks	no
2	M	66	1/2 blocks	1210 µm
3	F	71	2/3 blocks	230 µm
4	F	77	0/1 blocks	no
5	M	67	0/4 blocks	no
6	F	75	0/1 blocks	no
7	F	67	1/3 blocks	1920 µm
8	F	66	0/4 blocks	no
9	M	66	0/4 blocks	no
10	M	78	0/4 blocks	no
11	F	87	0/4 blocks	no
12	F	78	1/3 blocks	230 µm
13	F	77	1/3 blocks	460 µm
14	F	75	0/2 blocks	no
15	F	66	1/3 blocks	1200 µm
16	F	64	0/4 blocks	no
17	F	59	1/3 blocks	580 µm
18	F	55	0/2 blocks	no
19	M	56	0/2 blocks	no
20	M	57	0/2 blocks	no
21	M	81	2/3 blocks	580 µm
22	M	67	1/2 blocks	613 µm
23	F	58	1/2 blocks	713 µm
24	M	60	1/2 blocks	619 µm
25	M	80	0/1 blocks	no
26	M	80	2/3 blocks	1920 µm
27	M	81	2/3 blocks	1821 µm
28	M	78	1/3 blocks	1218 µm
29	F	65	1/3 blocks	415 µm
30	F	78	1/3 blocks	1754 µm
31	F	67	0/1 blocks	no
32	M	56	0/1 blocks	no
33	M	65	0/4 blocks	no
34	F	67	0/1 blocks	no
35	F	56	0/1 blocks	no
36	M	69	2/3 blocks	2230 µm
37	M	80	0/4 blocks	no
38	F	81	0/4 blocks	no

*advanced post-mortem decomposition stage. External injuries not applicable in all cases; M – male; F – female

and controls was also compared within the 3 groups (A, B and C), using Fisher's exact test (level of significance < 0.05). The sensitivity and specificity of the tests were provided.

Results

In group A (asphyxia deaths due to the compression of the neck), the median age was 46 years (range: 11–91 years), and the male-to-female ratio was 1:1. In group B (deaths for other causes), the median age of the group was 51.5 years (range: 3–89 years), while the female-to-male ratio was 1.6:1. In group C (neck blocks from laryngectomies), the median age was 67 years (range: 61–87). The age of group C was significantly higher than the age of the other groups.

Table 1,2 report all the details of the study cohort. All hanging cases were suicidal "short-drop hangings" or "hangings without the drop", with the knot located behind the occiput, whereas manual strangulation cases were homicides. Internal injuries were totally absent in 2 hanging cases, while the other 2 cases presented hemorrhage alone and fracture of the left greater cornu of the hyoid bone with concomitant hemorrhage, respectively.

Detachments were identified in 6/22 (27.2%) autopsy specimens due to other causes than asphyxia and in 17/38 (44.7%) surgical laryngectomies. Representative images were captured in Fig. 1,2. Both hanging cases, which revealed the detachment of soft tissues from the hyoid bone, were associated with the skin sulcus to the neck, whereas only 1 of them was associated with injuries to the inner structures of the neck. Both ligature strangulation cases, in which the detachment of the soft tissues from the hyoid bone was found to be associated with internal injury, were homicides. This finding was associated with a fracture of the hyoid bone in a single case of manual strangulation with detachment of the soft tissues from the hyoid bone. A bar chart of the presence/absence of detachment is presented in Fig. 3.

Statistical analyses results

A direct logistic regression analysis was conducted to determine whether the likelihood of detecting a detachment of soft tissues from the hyoid bone was impacted by the medico-legal setting. The model featured a single independent variable, namely the medico-legal setting. However, the full model, which included the predictor, was statistically not significant (χ^2 (2, n = 70) = 2.319, p = 0.314). This indicates that the model was unable to differentiate between medico-legal settings that reported detecting a detachment of soft tissues from the hyoid bone and those that did not. As a result, there was no need for additional post hoc analyses with pairwise comparisons between groups, or for sensitivity and specificity analyses. A contingency table is provided in Table 3.

Finally, the comparison between the 3 groups and the presence/absence of soft tissue detachment showed no statistically significant differences between groups (p = 0.329), clarifying that soft tissue detachment is a non-specific variable for all 3 situations. In other words, it has no role in identifying any of these different situations.

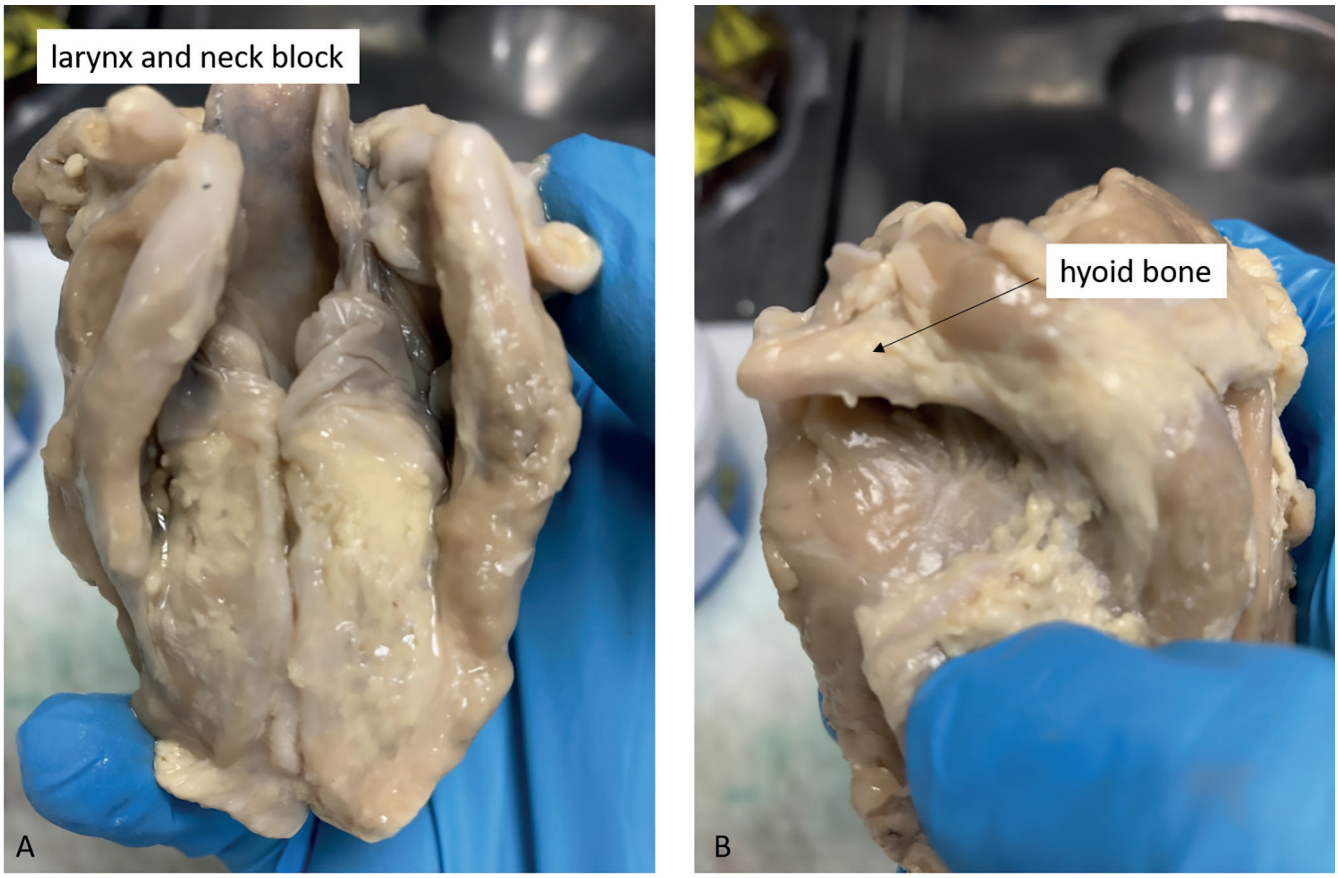

Fig.1. A. Hyoid-larynx complex, posterior view; B. Hyoid-larynx complex, lateral view with signature to the hyoid

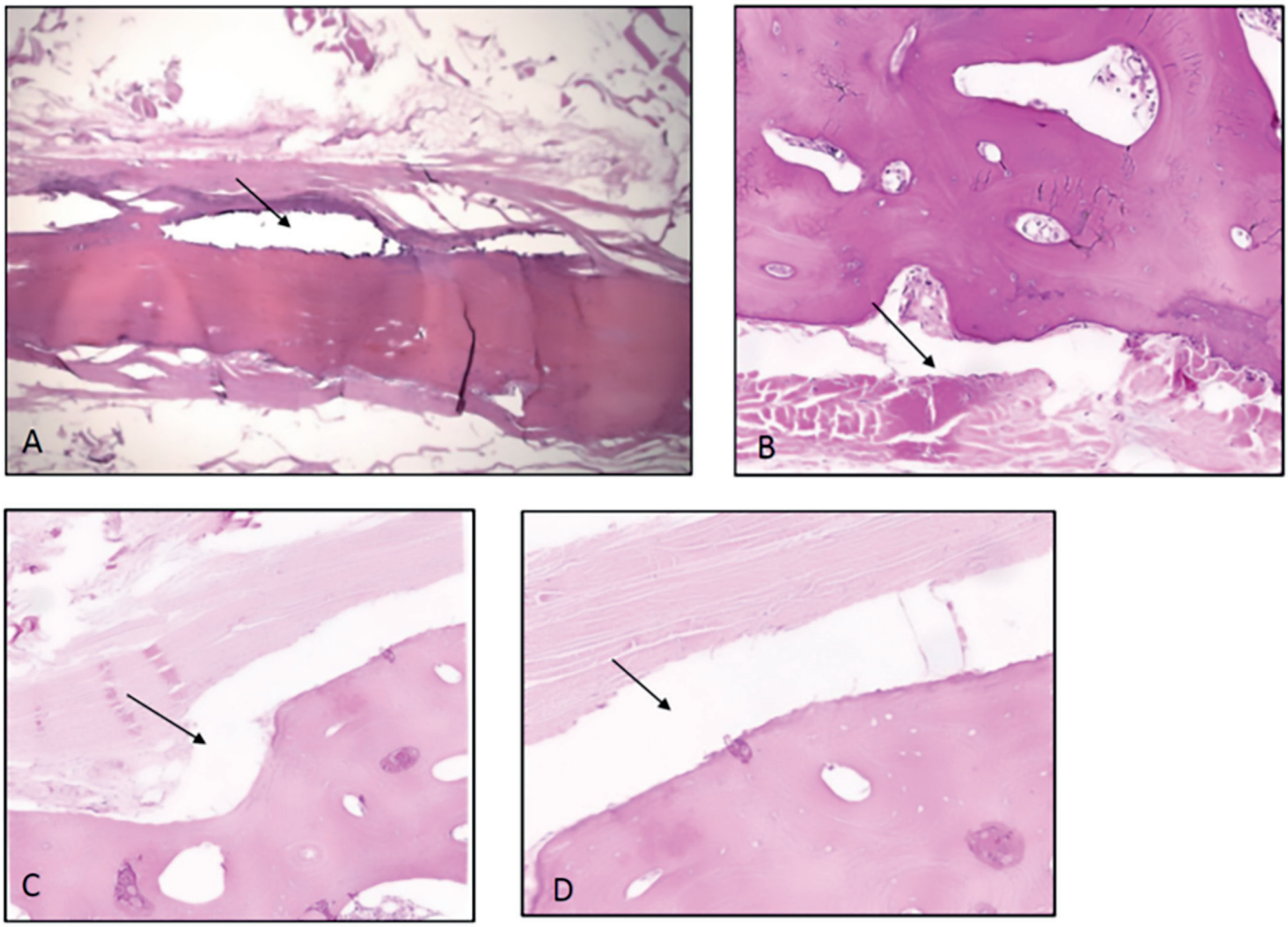

Fig. 2. Soft tissue detachment from the hyoid bone in a specimen obtained by: A. Legal autopsy case that occurred from a violent compression to the neck (study cohort); B. Surgical laryngectomy; C,D. Legal autopsy case in which no compression occurred to the neck (control cohort). Hematoxylin & eosin (H&E) staining (×10 magnification)

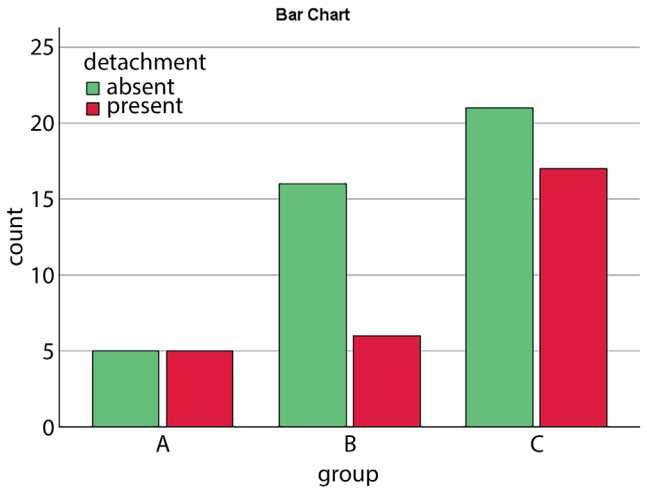

Fig. 3. Bar chart reporting the presence/absence of detachment in the 3 groups

Table 3. Contingency table

Group		Detachment		Total
		Absent	Present	
Group	A	5	5	10
	B	16	6	22
	C	21	17	38
Total		42	28	70

Group A – deaths due to violent external compression of the neck; group B – deaths for other causes without a trauma of the neck; group C – blocks obtained from living subjects that had undergone to laryngectomies for infiltrative squamous carcinoma.

Discussion

Histopathologic findings in relation to death due to strangulation asphyxia are poor, and literature mostly refers to the hemorrhagic infiltration of skin injuries produced by the mean used to cause asphyxia or other signs, such as a transverse laceration of the intimal layer of carotid arteries described in cases of hanging (Amussat's sign).[19,20] The NAME Forensic Autopsies Performance Standards released in 2006 (updated in 2020) detailed that muscles, soft tissues, airways, and vascular structures of the anterior neck must be examined to identify signs of disease and/or injury; thus, a layer-by-layer dissection is necessary for proper evaluation of trauma to the anterior neck. Removal and ex situ dissection of the upper airway, pharynx and upper esophagus is mandatory, and the dissection of the posterior neck is also necessary when an occult neck injury is suspected. The forensic pathologist shall examine in situ muscles and soft tissues of the anterior neck, ensure proper removal of neck organs and airways, examine neck organs and airways, dissect the posterior neck in cases of suspected occult neck injury, and perform anterior neck dissection in neck trauma cases.[18] All steps are usually performed during autopsies, and less frequently the anatomical whole neck regions are analyzed after the formalin-fixed process and after paraffin embedding. It is well known in any anatomic pathology and/or forensic laboratory that there is a chance to produce artifactual tissues when dealing with fixation and tissue sectioning. Therefore, when mechanical asphyxia is suspected as the cause of death, and forensics are requested to analyze the neck region after formalin-fixation, the artifacts must be known to avoid misinterpretation of final gross and histopathological morphological signs. Hemorrhages, soft tissue edematous congestion or bone fractures are the morphological details to search for. Some autopsy cases without pathognomonic external and internal macroscopic findings fail provide an effective element to allow expert anatomical or forensic pathologists to correctly diagnose the cause and manner of death with a high level of confidence.[21] This is due to the relatively low specificity of some of the common findings in asphyxia cases, which can be revealed in people who died due to causes other than strangulation asphyxia.[22,23]

Detachment of soft tissues from the hyoid bone can be easily examined by microscopy, and, to date, little was known about the value of this finding, which was observed with a high frequency in our casework. In fact, to our knowledge, no study on the diagnostic value of this finding has been published thus far. We observed a low sensitivity and specificity of the evidence of soft tissue detachments from the hyoid bone as a unique interpretation of the cause of death, particularly in the differentiation between mechanical strangulation asphyxia and death by other causes. The relatively high rate of soft tissue detachment from the hyoid bone in deaths due to other causes than asphyxia, as well as in group C, showed the non-specificity of the detachment, probably being an artifact occurring during the preparation of the sample. Again, this issue is supported by the relatively high rate of detachment found in the surgical laryngectomy group, where any sort of external compression to the neck was ruled out.

The detachment of soft tissues from the hyoid bone can be caused by several mechanisms. First, the dissection technique and an excessively rough extraction of the hyoid-larynx complex can lead to detachment of soft tissues, as well as other artificial findings such as fractures of the bone and cartilage.[24] Second, the complex processing of autopsy samples implies the use of aggressive chemicals, frequent manipulation and cutting forces with a scalpel, with the risk of artificially producing detachment of soft tissues from the hyoid bone.[25] The use of a slow decalcifying solution may help to reduce possible artifacts owing to its lower chemical aggressiveness compared to other strong decalcifying solutions. Moreover, the transition point from the dense structure of the hyoid bone to the lower density of the nearby soft tissues may represent a point of resistance that prevents easy running through the microtome blade. This resistance may artificially induce the detachment of soft tissues from the hyoid

bone.[26] As a consequence, the detachment of soft tissue from bones is not an uncommon finding during the technical histopathological processes after decalcification and tissue sectioning at the microtome. Bones are usually decalcified, and the process, although gently performed by using slow decalcifiers, usually shows detachments such as those observed in our study, even more in older patients. All technical processes are part of the pre-analytical standard operative procedures in an anatomic pathology and/or forensic laboratory.

With regard to the manner of death, our study is consistent with the results provided by other authors who found a clear prevalence of suicide in hanging cases and homicide in deaths due to strangulation.[9,27] Our single case of suicide by ligature strangulation showed no internal injuries, in contrast to other cases of ligature and manual strangulation, since internal injuries were found in all cases. This finding is consistent with Maxeiner et al.[28] and may be a consequence of the different forces involved in homicide and self-inflicted strangulation.

Taking into consideration the occurrence of fractures of the hyoid bone and thyroid cartilage, we found 2 fractures of the hyoid bone in a case of hanging and in a case of manual strangulation, whereas only 1 case of fracture of the thyroid cartilage occurred in a 91-year-old man who was a victim of manual strangulation. The occurrence of fractures of hyoid bones in asphyxia deaths is not uncommon. According to the literature, the prevalence of hyoid bone fractures in victims of hanging varies between 2% and 21%,[5,29] while the same injury can be found in approx. 35% of manual strangulation cases.[30] This difference is related to the major amount of energy applied by the hands of the assailant in contrast to the energy and the direction of the force provided by the ligature used in suicide by hanging.[30] The fracture of thyroid cartilage appears to be as frequent as that of the hyoid bone in hanging cases, ranging from 5% to 32%,[31,32] and it is more frequent in manual strangulation cases.[32] At the same time, it is well known that fractures of the thyroid cartilage are related to the age of the victim. The rate of fracture of the thyroid cartilage increases with age because of the ossification process of the cartilage as people age.[32,33] For this reason, the frequency and distribution of fractures of neck structures are commonly utilized to assist in interpreting the manner of death.[34,35]

In our study, we observed that the detachment of soft tissues has poor value as a single element to support the diagnosis of asphyxia due to violent compression of the neck. Moreover, the procedures regarding glass slide sectioning at a microtome and the decalcification process of the neck-hyoid blocks can justify the artifactual detachment of soft tissue from the hyoid bone. The design of this study seems appropriate for its purposes, having 2 independent control groups, 1 comprising deaths from other causes and the other consisting of samples taken from living individuals. The main limitation of the study is represented by the size and heterogeneity of group A compared to the other 2 groups. The exclusion criteria for group C, namely the absence of tumor invasion into the tissue near the hyoid bone, are also important to avoid sampling bias and improve the reproducibility of the study.

Limitations

The primary limitation of this study is the heterogeneity of mechanical asphyxia cases (group A), both in terms of the age of the subjects and the mode of death. It is possible that detachment may be more pronounced when greater force is applied to the neck. Additionally, the small number of cases in group A does not allow for quantitative considerations regarding a potential association between the extent of detachment and the cause of death.

Conclusions

Ongoing research for markers of strangulation asphyxia is necessary to achieve an adequate level of evidence in a judicial context. The exclusion of possible markers is also useful to avoid judicial errors. This observational retrospective study demonstrates that the detachment of soft tissues from the hyoid bone does not support the diagnosis of strangulation asphyxia in forensic autopsies and should be considered an artifact due to technical reasons. Therefore, in the absence of alterations to the structures of the neck, as is often the case in asphyxiation with soft means, the differential diagnosis must rely on the integrated assessment of all elements gathered during the forensic medical examination and autopsy. The forensic pathologist will then provide their evaluation, expressing support for the asphyxia cause, when requested. Further studies are required to draw more reliable conclusions on this forensic topic. Specifically, prospective studies, expanding the number of cases of asphyxia deaths, and improving the homogeneity of groups are needed to assess the nature and occurrence of the detachment of soft tissues from the hyoid bone.

ORCID iDs

Giovanna Del Balzo https://orcid.org/0000-0002-9147-9373
Guido Pelletti https://orcid.org/0000-0003-3263-1758
Dario Raniero https://orcid.org/0000-0002-0468-8602
Alessia Farinelli https://orcid.org/0000-0003-4279-5430
Andrea Uberti https://orcid.org/0000-0003-3609-0039
Gabriele Molteni https://orcid.org/0000-0001-7764-2122
Riccardo Nocini https://orcid.org/0000-0001-5086-4390
Stefano Gobbo https://orcid.org/0000-0001-5247-5233
Francesco Taus https://orcid.org/0000-0003-4728-6686
Albino Eccher https://orcid.org/0000-0002-9992-5550
Claudio Lucchini https://orcid.org/0000-0003-4901-4908
Matteo Brunelli https://orcid.org/0000-0002-3832-2676

References

1. Azmak D. Asphyxial deaths: A retrospective study and review of the literature. *Am J Forensic Med Pathol*. 2006;27(2):134–144. doi:10.1097/01.paf.0000221082.72186.2e
2. Sauvageau A, Boghossian E. Classification of asphyxia: The need for standardization. *J Forensic Sci*. 2010;55(5):1259–1267. doi:10.1111/j.1556-4029.2010.01459.x
3. Verma SK, Lal S. Strangulation deaths during 1993–2002 in East Delhi (India). *Leg Med (Tokyo)*. 2006;8(1):1–4. doi:10.1016/j.legalmed.2005.06.004
4. Jiwane AS, Zine KU, Bardale RV. Analysis of compression injuries over neck: One-year prospective study. *Indian J Forensic Commun Med*. 2021;7(4):203–209. doi:10.18231/j.ijfcm.2020.042
5. Sharma BR, Harish D, Sharma A, Sharma S, Singh H. Injuries to neck structures in deaths due to constriction of neck, with a special reference to hanging. *J Forensic Leg Med*. 2008;15(5):298–305. doi:10.1016/j.jflm.2007.12.002
6. Jayaprakash S, Sreekumari K. Pattern of injuries to neck structures in hanging: An autopsy study. *Am J Forensic Med Pathol*. 2012;33(4):395–399. doi:10.1097/PAF.0b013e3182662761
7. Demirci S, Dogan KH, Erkol Z, Gunaydin G. Ligature strangulation deaths in the province of Konya (Turkey). *J Forensic Leg Med*. 2009;16(5):248–252. doi:10.1016/j.jflm.2008.12.013
8. Pollanen MS, Chiasson DA. Fracture of the hyoid bone in strangulation: Comparison of fractured and unfractured hyoids from victims of strangulation. *J Forensic Sci*. 1996;41(1):110–113. PMID:8934706.
9. Sharma N, Shrivastava A, Vyas P. A study of morphology and histopathology of ligature marks in asphyxial deaths by compression of neck in Jodhpur region, Rajasthan. *J Med Sci Clin Res*. 2018;6(6):923–929. doi:10.18535/jmscr/v6i6.170
10. Jiwane AS, Zine KU, Bardale RV. Microscopic analysis of compression injury over neck: One-year prospective study. *Indian J Forensic Commun Med*. 2021;8(2):125–131. doi:10.18231/j.ijfcm.2021.025
11. Gentile G, Tambuzzi S, Andreola S, Zoja R. Histotopography of haemorrhagic infiltration in the hanging cutaneous furrow: Where to look for haemorrhagic infiltration in hanging. *Med Sci Law*. 2022;62(1):52–59. doi:10.1177/00258024211023246
12. Dettmeyer R, Verhoff MA, Schütz H. *Forensic Medicine: Fundamentals and Perspectives*. Berlin–Heidelberg, Germany: Springer; 2014. ISBN:978-3-642-38817-0.
13. Boscolo-Berto R, Viel G, Cecchi R, et al. Journals publishing biomedicolegal research in Europe. *Int J Legal Med*. 2012;126(1):129–137. doi:10.1007/s00414-011-0620-3
14. Viel G, Boscolo-Berto R, Cecchi R, Bajanowski T, Vieira ND, Ferrara SD. Bio-medicolegal scientific research in Europe. A country-based analysis. *Int J Legal Med*. 2011;125(5):717–725. doi:10.1007/s00414-011-0576-3
15. Scopetti M, Padovano M, Manetti F, et al. Molecular autopsy in asphyxia deaths: Diagnostic perspectives of miRNAs in the evaluation of hypoxia response. *Int J Med Sci*. 2023;20(6):749–753. doi:10.7150/ijms.79539
16. Shekhawat RS, Meshram VP, Rao M, et al. Further explorations into the role of mast cells in deaths associated with fatal asphyxia: An immunohistochemical study utilizing CD 117 marker. *Forensic Sci Int*. 2023;350:111689. doi:10.1016/j.forsciint.2023.111689
17. Barranco R, Tettamanti C, Bonsignore A, Ventura F. Otorrhagia in strangulations: An important but often underestimated finding in forensic pathology. *J Forensic Sci*. 2022;67(4):1739–1742. doi:10.1111/1556-4029.15030
18. Peterson GF, Clark SC. Forensic autopsy performance standards. *Am J Forensic Med Pathol*. 2006;27(3):200–225. doi:10.1097/01.paf.0000243580.43150.3c
19. Luigi Crudele GD, Galante N, Fociani P, et al. The forensic application of the Glycophorin A on the Amussat's sign with a brief review of the literature. *J Forensic Leg Med*. 2021;82:102228. doi:10.1016/j.jflm.2021.102228
20. Hejna P. Amussat's sign in hanging: A prospective autopsy study. *J Forensic Sci*. 2011;56(1):132–135. doi:10.1111/j.1556-4029.2010.01548.x
21. Rajs J, Thiblin I. Histologic appearance of fractured thyroid cartilage and surrounding tissues. *Forensic Sci Int*. 2000;114(3):155–166. doi:10.1016/S0379-0738(00)00299-1
22. Bux R, Padosch SA, Ramsthaler F, Schmidt PH. Laryngohyoid fractures after agonal falls: Not always a certain sign of strangulation. *Forensic Sci Int*. 2006;156(2-3):219–222. doi:10.1016/j.forsciint.2005.05.030
23. Advenier A, De La Grandmaison GL, Cavard S, Pyatigorskaya N, Malicier D, Charlier P. Laryngeal anomalies: Pitfalls in adult forensic autopsies. *Med Sci Law*. 2014;54(1):1–7. doi:10.1177/0025802413485731
24. Lockyer BE. Death by hanging: Examination of autopsy findings and best approach to the post-mortem examination. *Diagn Histopathol*. 2019;25(11):423–430. doi:10.1016/j.mpdhp.2019.07.006
25. Fieguth A, Albrecht UV, Bertolini J, Kleemann W. Intracartilaginous haemorrhagic lesions in strangulation? *Int J Legal Med*. 2003;117(1):10–13. doi:10.1007/s00414-002-0300-4
26. Sy J, Ang LC. Microtomy: Cutting formalin-fixed, paraffin-embedded sections. *Methods Mol Biol*. 2019;1897:269–278. doi:10.1007/978-1-4939-8935-5_23
27. Godin A, Kremer C, Sauvageau A. Fracture of the cricoid as a potential pointer to homicide: A 6-year retrospective study of neck structures fractures in hanging victims. *Am J Forensic Med Pathol*. 2012;33(1):4–7. doi:10.1097/PAF.0b013e3181d3dc24
28. Maxeiner H, Bockholdt B. Homicidal and suicidal ligature strangulation: A comparison of the post-mortem findings. *Forensic Sci Int*. 2003;137(1):60–66. doi:10.1016/s0379-0738(03)00279-2
29. Green MA. Morbid anatomical findings in strangulation. *Forensic Sci*. 1973;2(3):317–323. doi:10.1016/0300-9432(73)90046-0
30. Lebreton-Chakour C, Godio-Raboutet Y, Torrents R, et al. Manual strangulation: Experimental approach to the genesis of hyoid bone fractures. *Forensic Sci Int*. 2013;228(1-3):47–51. doi:10.1016/j.forsciint.2013.02.014
31. Tse R, Langlois N, Winskog C, Byard RW. An assessment of the usefulness of routine histological examination in hanging deaths. *J Forensic Sci*. 2012;57(4):976–978. doi:10.1111/j.1556-4029.2012.02104.x
32. Giovannini E, Franchetti G, Ridolfi M, et al. An unusual case of corpse concealment driven by emotional distress. *Legal Medicine*. 2024;67:102379. doi:10.1016/j.legalmed.2023.102379
33. Di Nunno N, Lombardo S, Costantinides F, Di Nunno C. Anomalies and alterations of the hyoid-larynx complex in forensic radiographic studies. *Am J Forensic Med Pathol*. 2004;25(1):14–19. doi:10.1097/01.paf.0000113931.49721.e4
34. Wilson R, McFadden C, Rowbotham S. A meta-analytic review of the frequency and patterning of laryngohyoid and cervical fractures in cases of suicide by hanging. *J Forensic Sci*. 2023;68(3):731–742. doi:10.1111/1556-4029.15234
35. Zátopková L, Janík M, Urbanová P, Mottlová J, Hejna P. Laryngohyoid fractures in suicidal hanging: A prospective autopsy study with an updated review and critical appraisal. *Forensic Sci Int*. 2018;290:70–84. doi:10.1016/j.forsciint.2018.05.043

Comparison of the efficacy of two preoxygenation techniques using oxygen reserve index

Yesim Cokay Abut[A,C–F], Ece Kisa[B–D]

Department of Anesthesiology and Reanimation, Istanbul Education and Training Hospital (SUAM), University of Health Sciences, Turkey

A – research concept and design; B – collection and/or assembly of data; C – data analysis and interpretation;
D – writing the article; E – critical revision of the article; F – final approval of the article

Advances in Clinical and Experimental Medicine, ISSN 1899–5276 (print), ISSN 2451–2680 (online) *Adv Clin Exp Med*. 2025;34(3):337–342

Address for correspondence
Yesim Cokay Abut
E-mail: yesimabut2000@yahoo.com

Funding sources
None declared

Conflict of interest
None declared

Acknowledgements
We would like to express our gratitude to Prof. Dr. Feyza Karagoz Guzey for her invaluable contributions to the application of statistical methods in our study.

Received on July 30, 2023
Reviewed on January 23, 2024
Accepted on May 3, 2024

Published online on September 9, 2024

Cite as
Abut YC, Kisa E. Comparison of the efficacy of two preoxygenation techniques using oxygen reserve index. *Adv Clin Exp Med*. 2025;34(3):337–342. doi:10.17219/acem/188259

DOI
10.17219/acem/188259

Abstract

Background. Preoxygenation is very important to protect the patient from hypoxia before intubation. However, pulse oximetry has some limitations in detecting hypoxia.

Objectives. We aimed to compare the effectiveness of 2 preoxygenation techniques based on oxygen reserve index (ORI) levels.

Materials and methods. Twenty healthy male volunteers were included in the study. They inhaled 100% FiO_2 oxygen administered at 5 L/min as the 1st technique (M1) with a ventilation mask as much as their tidal volumes for 3 min. The 2nd technique (M2) applied 100% FiO_2 oxygen at 10 L/min flow using the same mask and 8 deep inspiratory volumes, which was aimed to be completed within 1 min. Maximum ORI levels, duration to reach that level, and time needed to reach the target ORI level (0.35) and return back to the "0" were measured.

Results. In the M1 group, ORI levels were significantly higher during and after 60 s, according to post hoc tests. In the M2 groups, ORI levels were significantly higher during and after the 4th inspiration, according to post hoc tests. Oxygen reserve index values at the 60th 2nd (M1) and 8th inspiration (M2) were compared as the 8th inspiration corresponded to the 60th second. The maximum ORI values were significantly lower in the M1 group compared to the M2 group ($p < 0.001$ and $p = 0.006$, respectively). Seven volunteers (36.8%) in the M1 group and 2 volunteers (10.5%) in the M2 group could not reach the target ORI (McNemar's test, test statistic 3.2, degrees of freedom (df) = 1, $p = 0.063$). The time to reach the target ORI value and to reach maximum ORI values was significantly longer in the M1 group than in the M2 group ($p = 0.008$ and $p < 0.001$, respectively).

Conclusions. We observed that the 8-deep breath technique is more effective in preoxygenation compared to the 3-min tidal volume technique.

Key words: preoxygenation, oxygen reserve index (ORI), hypoxia prevention, 8-deep breath technique, 3-min tidal volume technique

Background

Administration of 100% oxygen before a "rapid-sequence" induction of anesthesia is recommended to prevent hypoxia during induction.[1]

Historically, many preoxygenation techniques have been described.[2,3] Currently, there are 4 methods of preoxygenation used in routine anesthetic practice: (1) the deep breathing technique; (2) the rapid breathing using a fraction of inspired oxygen (FiO_2) of 1 (100%) for 2 to 5 min; (3) the 4 or 8-vital capacity methods; and (4) the Transnasal Humidified Rapid Insufflation Ventilator Exchange (THRIVE) technique.[4]

The use of intraoperative pulse oximetry (SpO_2) enhances the prevention of hypoxic events and is mandatory in anesthesia and critical care practices.[5,6]

However, because the relationship between the arterial partial pressure of oxygen (PaO_2) and arterial oxygen saturation (SaO_2) is not linear but rather sigmoid, SpO_2 may not provide an additional warning below the levels of 98% until PaO_2 decreases below 70 mm Hg.[7–9]

On the other hand, increasing the PaO_2 above 90–100 mm Hg or more will no longer affect the SpO_2. As a consequence, when SpO_2 is ≥97%, the PaO_2 levels could be anywhere between 90 and 600 mm Hg.[10–12]

These major limitations in clinical practice have forced researchers to develop new methods to measure tissue oxygenation levels. The oxygen reserve index (ORI™; Masimo Corp., Irvine, USA) is a new variable that represents oxygenation status, with a scale between 0.00 and 1.00, and enables noninvasive and continuous measurement of PaO_2 ranging from 100 to 200 mm Hg. Oxygen reserve index has significant potential for predicting both hypoxemia and hyperoxia.[13,14]

Objectives

Considering that SpO_2 monitoring is not sufficient to show hypoxic or hyperoxic events, we aimed to compare the effectiveness of 2 preoxygenation techniques using ORI measurements.

Materials and methods

Following the approval of the Institutional Ethics Committee of the University of Health Sciences Istanbul SUAM (dated 12/22/23, No. 398, and UMIN: 000051009/08/05/23) and the provision of informed consent by each participant, 20 healthy male volunteers with an American Society of Anesthesiology (ASA) of 1 status, ranging in age from 18 to 32 years, were recruited to the study. The study size was assessed using biostatistical methods based on relevant previous studies. All study participants were nonsmokers with no evidence of cardiovascular, respiratory or other systemic diseases. Additional exclusion criteria included hemodynamic disturbances in the operating room and pre-procedural anxiety. Patients with nonivasive blood pressure (NIBP) over 140/90 mm Hg and a preprocedural State Trait Anxiety Inventory (STAI) test level over 41 were also excluded. Each study participant was monitored continuously using electrocardiography (ECG), NIBP sensors and the Masimo Root Radical-7 (Masimo Corp., Irvine, USA) incorporating both ORI-PVI and SpO_2 sensors, which were the disposable adhesive type and were placed on the 4th finger of the contralateral side of the NIBP monitoring and protected under a light-shielding cover. The ORI was based on Masimo Rainbow SET (Masimo Inc, Irvine, USA) technology, in which the pulsatile signals were extracted from 8 wavelengths ranging between 500 and 1,400 nm, enabling the detection of changes in PaO_2 after SaO_2 was maximally saturated according to changes in the peripheral venous oxygen saturation. Oxygen reserve index is a novel, multiwavelength pulse oximeter-based, non-dimensional index that ranges from 0 to 1 as PaO_2 increases from about 80 to 200 mm Hg.

As a result of the reliable measurement of peripheral perfusion, the participants' skin temperature was monitored using a thermocouple and maintained at 36.5°C throughout the experiment. During the experiment, oxygen gas flow was tightly controlled using a semi-open anesthesiology circuit and a proper face mask. The SpO_2 and ORI values were displayed and stored using Root with a Radical-7 device (Masimo Corp., Irvine, USA). A universal serial bus (USB) data output port on the Root monitor was connected to a computer (Ideapad 5 14ITL05; Lenovo, Beijing, China) running proprietary Pulse Oximetry Automatic Data Collection software (Masimo Instrument Configuration Tool (MICT) v. V1.2.4.5; Masimo Corp.) to create and store data files that were subsequently analyzed offline.

Each study participant underwent 2 different techniques of preoxygenation. Oxygen was administered by the following 2 methods using the following preoxygenation techniques in each study participant. The 1st method (M1) oxygenated volunteers with 100% FiO_2 at a 5 L/min flow for 3 min while they were breathing normally, which means the inspired volume was as much as their usual tidal volumes (without any leakage, which was ensured by proper mask usage). In the meantime, we recorded SpO_2, ORI, total hemoglobin (SpHb), and Pleth variability index (PVI) values every 30 s and noted their maximum quantities. At the end of the 3 min, we took the masks off the volunteers and waited for ORI values to reach "0" again and noted its duration. Approximately 1 h after the administration of M1, the 2nd method (M2) was employed to oxygenate the volunteers. This involved the administration of 100% FiO_2 and a 10 L/min flow, with the volunteers instructed to take 8 breaths in 1 min, with maximal effort, to reach their maximum forced inspired volumes. In the meantime, we recorded SpO_2, ORI, SpHb, and PVI values after each deep inspiration, and we also noted their maximum quantities, just like in the M1 group.

An ORI of 0.35 was used as the target to be reached, and the duration to achieve this level was recorded in each technique. In addition, after the oxygenation period, maximum ORI levels, time to reach maximum ORI levels, and time for the return of the ORI to its baseline value in room air after cessation of oxygen supplementation (3 min for the M1 technique; 1 min for the M2 technique) were recorded and compared. There was no potential source of bias.

Statistical analyses

Statistical evaluations were performed using the PICOS program on the E-PICOS website, and post hoc analyses using a Friedman's test were performed with the R software (R Foundation for Statistical Computing, Vienna, Austria). Categorical values were given as percentages. Numerical values were given as median and min/max levels because of the small volunteer size of the group (n < 25). Categorical values, such as the ability to reach target ORI levels, were compared between the 2 methods using the McNemar's test. A Wilcoxon signed-rank test was employed to assess the statistical significance of numerical variables between the 2 methods, given the limited number of study participants. Oxygen reserve index changes over time in the M1 and M2 groups were separately evaluated using the Friedman's test, and post hoc analyses were made using the Nemenyi test. P-values <0.05 were accepted as statistically significant.

Results

Twenty volunteers aged 18–32 years with an ASA 1 status were recruited for the study. One volunteer was excluded because of high blood pressure levels altering high STAI 1 test results. Demographic data of the volunteers are provided in Table 1.

Oxygen reserve index changes over time in the M1 group and during inspirations 1–8 in the M2 group are shown in Table 2 and as boxplot graphics in Fig. 1,2. The values of 6 measurements in the M1 group were compared using Friedman's test (n = 19, degrees of freedom (df) = 5, test statistic = 42.322, p < 0.01). Oxygen reserve index levels were significantly higher during and after 60 s, according to post hoc tests (Table 3). In addition, values of 8 measurements in the M2 group were also compared with the Friedman's test (n = 19, df = 7, test statistic = 104.759, p < 0.01). Oxygen reserve index levels were significantly higher during and after the 4th inspiration, according to post hoc tests (Table 4).

Oxygen reserve index values in the 60th second (values of M1ORI60 for the M1 and M2ORI 8th for the M2 groups were compared because the 8th inspiration corresponded to the 60th second in M1 technique and maximum ORI values were significantly lower in the M1 than in the M2

Table 1. Descriptive data of the study group (n = 19)

Patient data	Q1	Median	Q3
Age	23	27	29
BMI	22.53	24.91	26.57
Temperature	36.4	36.5	36.5
STAI	23	31	34
SBP	122	126	131
DBP	72	75	79
ISPO2	98	98	99
IHB	13.1	13.9	14.5

BMI – body mass index; STAI – State Trait Anxiety Inventory; SBP – systolic blood pressure; DBP – diastolic blood pressure; ISPO2 – saturation of oxygen; IHB – blood hemoglobin; Q1 – 1st quartile; Q3 – 3rd quartile.

Table 2. The changes of ORI during time in method 1 and during inspirations in method 2 (n = 19)

Parameters	Min	Max	25th percentile	50th percentile	75th percentile
M1ORI 30	0.00	0.31	0.0000	0.0000	0.0400
M1 ORI 60	0.00	1.00	0.1500	0.3200	0.3700
M1 ORI 90	0.03	1.00	0.2000	0.3700	0.4500
M1 ORI 120	0.15	0.91	0.3000	0.3600	0.5100
M1 ORI 150	0.15	0.96	0.3000	0.3400	0.4900
M1 ORI 180	0.14	0.85	0.2800	0.3400	0.4900
M2 ORI 1st	0.00	0.07	0.0000	0.0000	0.0000
M2 ORI 2nd	0.00	0.41	0.0000	0.0000	0.0000
M2 ORI 3rd	0.00	0.45	0.0000	0.0000	0.0000
M2 ORI 4th	0.00	0.63	0.0000	0.0100	0.0700
M2 ORI 5th	0.00	0.95	0.0100	0.1700	0.4100
M2 ORI 6th	0.00	1.00	0.1600	0.3600	0.4900
M2 ORI 7th	0.00	1.00	0.2600	0.4300	0.5600
M2 ORI 8th	0.00	1.00	0.3300	0.4400	0.5600

M1 – method 1; M2 – method 2.

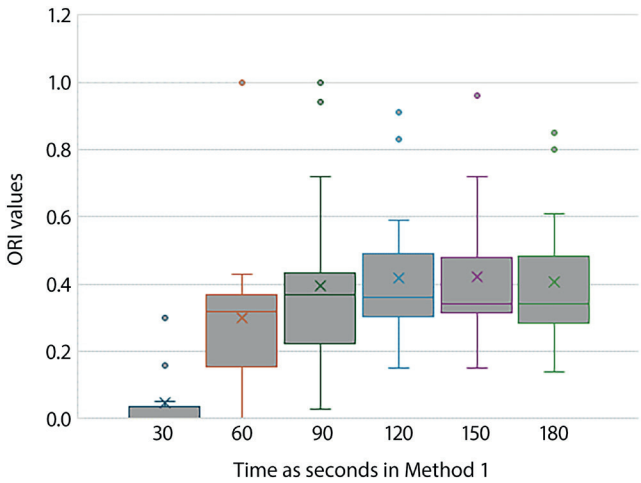

Fig. 1. Boxplot representing changes of oxygen reserve index (ORI) in time in method 1. M1ORI30, 60, 90… etc. showed ORI values measured at 30th, 60th, 90th… etc. seconds

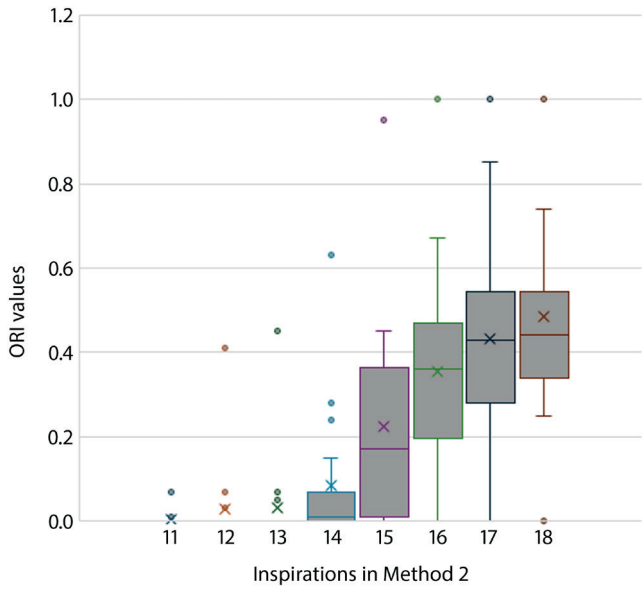

Fig. 2. Boxplot representing changes of oxygen reserve index (ORI) during inspirations from the 1st to the 8th in method 2. M2I1, 2, 3, …, etc. showed ORI values measured during the 1st, 2nd, 3rd, …, etc. inspirations

group ($p < 0.001$ and $p = 0.006$, respectively, Table 5). Seven volunteers (36.8%) in the M1 group and 2 volunteers (10.5%) in the M2 group could not reach the target ORI (McNemar's, test statistic 3.2, df = 1, $p = 0.063$). Times to reach the target values of ORI and to reach maximum ORI values were significantly longer in the M1 than in the M2 group ($p = 0.008$ and $p < 0.001$, respectively). Time to return to baseline ORI values were not significantly different between the 2 groups ($p = 0.071$, Table 5).

Discussion

Preoxygenation is a mandatory technique that extends the safe apnea time for endotracheal intubation, particularly in a "cannot intubate/cannot oxygenate" (CICO) scenario.[15] The procedure is carried out by supplying 100%

Table 3. Comparisons of oxygen reserve index (ORI) values according to time using Friedman test and post hoc Nemenyi test in method 1

Time [s]	Test statistics/p-values&				
	60	90	120	150	180
30	**34.5/<0.001**	**61/<0.001**	**57.5/<0.001**	**59.5/<0.001**	**45.5/<0.001**
60	–	**26.5/0.008**	25/0.033	**23/<0.022**	11/0.56
90	–	–	3.5/0.844	1.5/0.778	15.5/0.776
120	–	–	–	2/0.812	12/0.394
150	–	–	–	–	14/0.144
p-value*	**42.322/<0.001**				

*Friedman test; & – post hoc Nemenyi test; significant p-values are in bold.

Table 4. Comparisons of oxygen reserve index (ORI) values during inspirations using Friedman test and post hoc Nemenyi test in method 2

Ins.	Test statistics/p-values&						
	2	3	4	5	6	7	8
1	2/0.180	1.5/0.285	22/0.006	47/0.001	**66/<0.001**	**81/<0.001**	**92.5/<0.001**
2	–	1.6/0.276	20.5/0.006	45/0.001	**64/<0.001**	**79/<0.001**	**90.5/<0.001**
3	–	–	20/0.005	45.5/0.001	**84.5/<0.001**	**79.5/<0.001**	**91/<0.001**
4	–	–	–	25/0.002	44/0.001	**59/<0.001**	**70.5/<0.001**
5	–	–	–	–	19/0.003	34/0.001	**45.5/<0.001**
6	–	–	–	–	–	15/0.005	26.5/0.002
7	–	–	–	–	–	–	11.5/0.024
p-value*	**104.759/<0.001**						

Ins. – inspirations; * – Friedman test; & – post hoc Nemenyi test; significant p-values are in bold.

Table 5. Comparisons of various oxygen reserve index (ORI) parameters between methods 1 and 2

Parameters	M1 (median)	M2 (median)	Test statistic	p-value*
ORI in the 60th s&	0.32	0.44	3.517	**<0.001**
Maximum ORI	0.46	0.51	2.769	**0.006**
ORI target time	57.5	48	–2.672	**0.008**
ORI max time	110	59	–3.542	**<0.001**
ORI zeroing time	78	114	1.808	0.071

M1– method 1; M2 – method 2; *Wilcoxon paired signed rank test; significant p-values are in bold. & – comparison was made between M1ORI 60 for method 1 and M2 ORI 8th for method 2.

oxygen (FiO_2 of 1.0) before the induction of general anesthesia, and several methods of preoxygenation have been described in the literature. Two of the commonly known standardized approaches are 8 deep breaths in 1 min and tidal volume breathing for 3–5 min, both using 100% inspired oxygen, but there are studies questioning whether the techniques are effective or not.[16–20]

Today, we know a lot about the oxygen cascade. The definition of hypoxia is typically based on SpO_2 measurements. However, it is recognized that SpO_2 does not provide sufficient information about hypoxia at the tissue and cellular levels. However, while we try to protect the patient from hypoxia, we have concerns about the hyperoxia and its side effects at the same time.[21–28] Because some studies have shown that SpO_2 and the partial oxygen pressure changes in arterial blood gas analysis do not match exactly, a new and more sensitive pulse oximeter-based indexing system (ORI) obtained with pulsatile multiple wavelength analysis was defined. Researchers have discussed that ORI may be more sensitive in the measurement of hypoxia, hyperoxia or both. For this purpose, we tried to evaluate 2 major preoxygenation techniques and their benefits on the ORI.

This study is distinct from previous investigations that have established safe apnea times and preoxygenation techniques based on SpO_2 levels. In our study, we observed the effects of different preoxygenation techniques on tissue oxygenation reserve according to the ORI. Furthermore, the M2 group exhibited a more pronounced increase in ORI values and a longer duration of elevated values than the M1 group, which can be a time-saving method in emergency intubations, rapid sequential induction, and in the case of a cesarean section, morbid obesity, etc.[29–32]

We found that the maximum ORI levels varied between volunteers, which shows that oxygen reserve capacity may be different individually, but whatever this level is, it can be reached more quickly with the M2 technique.

According to the literature, Applegate et al. found that an ORI > 0.24 can be considered a $PaO_2 \geq 100$ mm Hg when SpO_2 levels are over 98%.[33] In a study by Szmuk et al.[14] conducted with Masimo, an ORI value of 0.3 provided 85% sensitivity and 80% specificity for a $PaO_2 < 150$ mm Hg.[14] However, an ORI > 0.55 appears to correlate with a $PaO_2 \geq 150$ mm Hg level in light of this data. Our target ORI value was 0.35 because our aim was to put into practice the results of this study in difficult intubation situations.

The time to reach the target ORI was also shorter in the M2 group. Moreover, while 7 study participants in the M1 group could not reach their personal maximum ORI levels, there were only 2 cases that failed in the M2 group. We observed that the study participants adapted better to the M2 technique.

Although the presence of a safe apnea time has been shown to be important in procedures such as bronchoscopy, which is reported in case reports, especially in which apneic oxygenation is used, there are not enough data from clinical studies.[34,35] Instead of safe apnea time, we used reset duration of ORI. We saw that the ORI reset time was longer in the M2 technique.

In addition, while doing this study as we saw in Fig. 2, the 3–4 deep breath technique which was defined in previous years failed, because the ORI values start to increase from the 4th breath. Therefore, study participants need more time to raise their oxygen reserves to the target and max levels.

During preoxygenation, the saturation levels of the study participants were 100%; therefore, we reached the end of that monitoring parameter, indicating it was not a clinically effective tool in comparing the 2 preoxygenation techniques. This finding was similar to the results obtained by Koishi et al., which reported that SpO_2 began to decrease 72 s (mean) after ORI reached 0.00 and the SpO_2 was 99 (98–99%).[36]

Limitations

The study group consisted of healthy volunteers. Therefore, it was not possible to examine the results of patients with different comorbidities. It would have been possible to perform simultaneous matching of the ORI measurements with PaO_2 levels in arterial blood gas analysis. Consequently, it would have been possible to directly measure the oxygen status of the study participants.

Conclusions

We compared 2 preoxygenation techniques using ORI in healthy volunteers. We observed that the M2 technique is more effective in preoxygenation compared to the 3-min tidal volume technique. The M2 technique is preferable, particularly in emergency or difficult intubation situations.

Data availability

The datasets generated and/or analyzed during the current study are available from the corresponding author on reasonable request.

Consent for publication

Not applicable.

ORCID IDs

Yesim Cokay Abut https://orcid.org/0000-0001-8763-605X
Ece Kisa https://orcid.org/0009-0009-4493-3690

References

1. American Society of Anesthesiologists Task Force on Management of the Difficult Airway. Practice Guidelines for Management of the Difficult Airway. *Anesthesiology*. 2003;98(5):1269–1277. doi:10.1097/00000542-200305000-00032
2. Hamilton WK, Eastwood DW. A study of denitrogenation with some inhalahon anesthetic systems. *Anesthesiology*. 1955;16(6):861–867. doi:10.1097/00000542-195511000-00004
3. Gold MI, Duarte I, Muravchick S. Arterial oxygenation in conscious patients after 5 minutes and after 30 seconds of oxygen breathing. *Anesth Analg*. 1981;60(5):313–315. PMID:7194597.
4. Nimmagadda U, Salem MR, Crystal GJ. Preoxygenation: Physiologic basis, benefits, and potential risks. *Anesth Analg*. 2017;124(2):507–517. doi:10.1213/ANE.0000000000001589
5. Checketts MR, Alladi R, Ferguson K, et al. Recommendations for standards of monitoring during anaesthesia and recovery 2015: Association of Anaesthetists of Great Britain and Ireland. *Anaesthesia*. 2016;71(1):85–93. doi:10.1111/anae.13316
6. American Society of Anesthesiologists (ASA). Standards for Basic Anesthetic Monitoring. American Society of Anesthesiologists Committee of Origin: Standards and Practice Parameters. Approved by the ASA House of Delegates on October 21, 1986, and last amended on October 20,2010, with an effective date of July,1,2011. Schamburg, USA: American Society of Anesthesiologists (ASA); 2010. https://www.asahq.org/standards-and-practice-parameters/standards-for-basic-anesthetic-monitoring. Accessed July 25, 2023.
7. Hsia CCW. Respiratory function of hemoglobin. *N Engl J Med*. 1998; 338(4):239–248. doi:10.1056/NEJM199801223380407
8. Biebuyck JF, Severinghaus JW, Kelleher JF. Recent developments in pulse oximetry. *Anesthesiology*. 1992;76(6):1018–1038. doi:10.1097/00000542-199206000-00024
9. Beasley R, McNaughton A, Robinson G. New look at the oxyhaemoglobin dissociation curve. *Lancet*. 2006;367(9517):1124–1126. doi:10.1016/S0140-6736(06)68488-2
10. Pedersen T, Nicholson A, Hovhannisyan K, Møller AM, Smith AF, Lewis SR. Pulse oximetry for perioperative monitoring. *Cochrane Database Syst Rev*. 2014;2014(3):CD002013. doi:10.1002/14651858.CD002013.pub3
11. Lee LA, Domino KB. The Closed Claims Project: Has it influenced anesthetic practice and outcome? *Anesthesiol Clin North Am*. 2002; 20(3):485–501. doi:10.1016/S0889-8537(02)00006-8
12. Lee LA, Caplan RA, Stephens LS, et al. Postoperative opioid-induced respiratory depression: A closed claims analysis. *Anesthesiology*. 2015; 122(3):659–665. doi:10.1097/ALN.0000000000000564
13. Simpao AF, Gálvez JA. When seconds count, buy more time: The oxygen reserve index and its promising role in patient monitoring and safety. *Anesthesiology*. 2016;124(4):750–751. doi:10.1097/ALN.0000000000001036
14. Szmuk P, Steiner JW, Olomu PN, Ploski RP, Sessler DI, Ezri T. Oxygen reserve index: A novel noninvasive measure of oxygen reserve. A pilot study anesthesiology. *Anesthesiology*. 2016;124(4):779–784. doi:10.1097/ALN.0000000000001009
15. Frerk C, Mitchell VS, McNarry AF, et al. Difficult Airway Society 2015 guidelines for management of unanticipated difficult intubation in adults. *Br J Anaesth*. 2015;115(6):827–848. doi:10.1093/bja/aev371
16. Baillard C, Depret F, Levy V, Boubaya M, Beloucif S. Incidence and prediction of inadequate preoxygenation before induction of anaesthesia. *Ann Fr Anesth Reanim*. 2014;33(4):e55–e58. doi:10.1016/j.annfar.2013.12.018
17. Battaglini D, Robba C, Rocco PRM, De Abreu MG, Pelosi P, Ball L. Perioperative anaesthetic management of patients with or at risk of acute distress respiratory syndrome undergoing emergency surgery. *BMC Anesthesiol*. 2019;19(1):153. doi:10.1186/s12871-019-0804-9
18. Benumof JL. Preoxygenation: Best method for both efficacy and efficiency? *Anesthesiology*. 1999;91(3):603–603. doi:10.1097/00000542-199909000-00006
19. Mccrory JW, Matthews JNS. Comparison of four methods of preoxygenation. *Br J Anaesth*. 1990;64(5):571–576. doi:10.1093/bja/64.5.571
20. Chiron B, Laffon M, Ferrandiere M, Pittet JF, Marret H, Mercier C. Standard preoxygenation technique versus two rapid techniques in pregnant patients. *Int J Obstet Anesth*. 2004;13(1):11–14. doi:10.1016/S0959-289X(03)00095-5
21. Baquero H, Alviz R, Castillo A, Neira F, Sola A. Avoiding hyperoxemia during neonatal resuscitation: Time to response of different SpO_2 monitors. *Acta Paediatr*. 2011;100(4):515–518. doi:10.1111/j.1651-2227.2010.02097.x
22. Hedenstierna G, Edmark L. Mechanisms of atelectasis in the perioperative period. *Best Pract Res Clin Anaesthesiol*. 2010;24(2):157–169. doi:10.1016/j.bpa.2009.12.002
23. Edmark L, Kostova-Aherdan K, Enlund M, Hedenstierna G. Optimal oxygen concentration during induction of general anesthesia. *Anesthesiology*. 2003;98(1):28–33. doi:10.1097/00000542-200301000-00008
24. Jamieson D, Chance B, Cadenas E, Boveris A. The relation of free radical production to hyperoxia. *Annu Rev Physiol*. 1986;48(1):703–719. doi:10.1146/annurev.ph.48.030186.003415
25. Turrens JF, Freeman BA, Levitt JG, Crapo JD. The effect of hyperoxia on superoxide production by lung submitochondrial particles. *Arch Biochem Biophys*. 1982;217(2):401–410. doi:10.1016/0003-9861(82)90518-5
26. Lumb AB, Walton LJ. Perioperative oxygen toxicity. *Anesthesiol Clin*. 2012;30(4):591–605. doi:10.1016/j.anclin.2012.07.009
27. Farquhar H, Weatherall M, Wijesinghe M, et al. Systematic review of studies of the effect of hyperoxia on coronary blood flow. *Am Heart J*. 2009;158(3):371–377. doi:10.1016/j.ahj.2009.05.037
28. Yilmaz Ak H, Özşahin Y, Yeşiltaş MA, Sandal B, Salihoglu Z, Erkalp K. Early outcomes of a high PaO_2/FiO_2 ratio during cardiopulmonary bypass. *J Tehran Heart Cent*. 2022;17(2):41–47. doi:10.18502/jthc.v17i2.9834
29. Yoshida K, Isosu T, Noji Y, et al. Usefulness of oxygen reserve index (ORi™), a new parameter of oxygenation reserve potential, for rapid sequence induction of general anesthesia. *J Clin Monit Comput*. 2018; 32(4):687–691. doi:10.1007/s10877-017-0068-1
30. Russell EC, Wrench I, Feast M, Mohammed F. Pre-oxygenation in pregnancy: The effect of fresh gas flow rates within a circle breathing system. *Anaesthesia*. 2008;63(8):833–836. doi:10.1111/j.1365-2044.2008.05502.x
31. Berthoud MC, Peacock JE, Reilly CS. Effectiveness of preoxygenation in morbidly obese patients. *Br J Anaesth*. 1991;67(4):464–466. doi:10.1093/bja/67.4.464
32. Dixon BJ, Dixon JB, Carden JR, et al. Preoxygenation is more effective in the 25° head-up position than in the supine position in severely obese patients. *Anesthesiology*. 2005;102(6):1110–1115. doi:10.1097/00000542-200506000-00009
33. Applegate RL, Dorotta IL, Wells B, Juma D, Applegate PM. The relationship between oxygen reserve index and arterial partial pressure of oxygen during surgery. *Anesth Analg*. 2016;123(3):626–633. doi:10.1213/ANE.0000000000001262
34. Niwa Y, Shiba J, Fujita H, Oka R, Takeuchi M. Oxygen reserve index (ORi™) contributes to prediction of hypoxemia and patient safety during tracheal stent insertion using rigid bronchoscopy: A case report. *J Clin Monit Comput*. 2019;33(6):1011–1014. doi:10.1007/s10877-018-0232-2
35. Ray S, Kulkarni K, Dave N, Chincholi I. The utility of the oxygen reserve index™ in a neonate undergoing re-exploration of a tracheoesophageal fistula. *Indian J Anaesth*. 2018;62(3):233. doi:10.4103/ija.IJA_778_17
36. Koishi W, Kumagai M, Ogawa S, Hongo S, Suzuki K. Monitoring the oxygen reserve index can contribute to the early detection of deterioration in blood oxygenation during one-lung ventilation. *Minerva Anestesiol*. 2018;84(9):1063–1069. doi:10.23736/S0375-9393.18.12622-8

Efficacy of topical local anesthetic, topical cooling spray, and audiovisual distraction on relief of needle-related pain during blood collection: A randomized controlled trial

Siwatus Puangrab[1,A–D,F], Weeratian Tawanwongsri[2,3,A,D–F], Auemphon Mordmuang[4,A,E,F], Wiphada Khocharoen[5,C], Pimchanok Krainukun[5,C]

[1] Department of Anesthesiology, School of Medicine, Walailak University, Nakhon Si Thammarat, Thailand
[2] Division of Dermatology, Department of Internal Medicine, School of Medicine, Walailak University, Nakhon Si Thammarat, Thailand
[3] Center of Excellence in Data Science and Health Study, Walailak University, Nakhon Si Thammarat, Thailand
[4] Department of Medical Sciences, School of Medicine, Walailak University, Nakhon Si Thammarat, Thailand
[5] Walailak University Hospital, Nakhon Si Thammarat, Thailand

A – research concept and design; B – collection and/or assembly of data; C – data analysis and interpretation; D – writing the article; E – critical revision of the article; F – final approval of the article

Advances in Clinical and Experimental Medicine, ISSN 1899–5276 (print), ISSN 2451–2680 (online) *Adv Clin Exp Med*. 2025;34(3):343–350

Address for correspondence
Weeratian Tawanwongsri
E-mail: weeratian.ta@gmail.com

Funding sources
This study was funded by Walailak University (WU65256).

Conflict of interest
None declared

Acknowledgements
We extend our heartfelt gratitude to Asst. Prof. Dr. Wanida Limmun for her invaluable statistical expertise and meticulous review of our manuscript. Her insights and suggestions were crucial in enhancing the rigor and clarity of our analysis. We deeply appreciate her dedication and assistance throughout this project.

Received on November 7, 2023
Reviewed on February 6, 2024
Accepted on April 29, 2024

Published online on August 29, 2024

Cite as
Puangrab S, Tawanwongsri W, Mordmuang A, Khocharoen W, Krainukun P. Efficacy of topical local anesthetic, topical cooling spray, and audiovisual distraction on relief of needle-related pain during blood collection: A randomized controlled trial. *Adv Clin Exp Med*. 2025;34(3):343–350. doi:10.17219/acem/188106

DOI
10.17219/acem/188106

Abstract

Background. Venipuncture is one of the most common invasive procedures in healthcare, often resulting in the experience of pain. While audiovisual distraction, topical anesthesia and cold spray application have been reported as methods to reduce pain, there is a lack of studies that focus on comparing their efficacy and safety.

Objectives. We aimed to compare the efficacy and safety of pain reduction during venipuncture using audiovisual distraction, topical anesthesia and cold spray application.

Materials and methods. A randomized controlled study was conducted at Walailak University (Nakhon Si Thammarat, Thailand) from April 2023 to July 2023. Eligible adult participants voluntarily enrolled in the study and were randomly assigned to 1 of 4 groups: group 1 (control), group 2 (topical anesthetic), group 3 (cooling spray), and group 4 (audiovisual distraction). Pain scores and satisfaction levels were assessed following the venipuncture procedure on the upper extremities.

Results. Forty-seven participants were included in the final analysis. The participants had a mean age of 42.3 years (standard deviation (±SD): 13.1), with the majority being female (66.0%). The participants in the intervention groups reported lower pain scores than those in group 1. The mean differences were 2.67 points in group 2 (95% confidence interval (95% CI): 1.49–3.84; $p < 0.001$), 1.56 points in group 3 (95% CI: 0.15–2.98; $p = 0.077$), and 1.67 points in group 4 (95% CI: 0.37–2.96; $p = 0.042$). However, the pain reduction did not reach statistical significance when comparing these 3 interventions. All groups reported a median satisfaction level of 3, with no significant difference among them ($H(3) = 6.050$, $p = 0.109$).

Conclusions. Pain reduction interventions, including topical anesthetic, cooling spray and audiovisual distraction, are effective methods for alleviating pain during venipuncture. Participants who received a topical anesthetic reported the lowest pain scores and highest levels of satisfaction.

Key words: pain, venipuncture, topical anesthetic, cooling spray, audiovisual distraction

Background

Pain is defined as an unpleasant sensory and emotional experience associated with, or similar to, actual or potential tissue damage.[1] The perceived intensity varies depending on biological, psychological and social factors. The nociceptive signal emanating from an injury undergoes modulation through endogenous mechanisms that can amplify or diminish both the signal and the perceived pain.[2] Failing to alleviate acute pain can lead to physiological and psychological effects. These effects include stress and inflammation, as well as a range of impacts on the cardiovascular, gastrointestinal and respiratory systems.[3] Also, this can result in increased anxiety, sleep disturbances, and a diminished quality of life across biological, psychological and social aspects of health.[4]

Venipuncture involves the process of drawing blood and remains one of the most prevalent invasive procedures in healthcare, often leading to the experience of pain.[5] The pain score varies across studies, ranging approx. from 3 to 7 out of 10.[6–9] Although our comprehension of the intricacies surrounding pain remains partial,[2] the existing theories serve as guiding principles for interventions aimed at pain reduction. At present, methods for pain reduction encompass both pharmacological and non-pharmacological interventions. Common interventions include audiovisual distraction, topical anesthesia and the use of cold spray.[10–14] The reduction of perceived pain through audiovisual distraction occurs due to the inherent limitations of human attention capacity. When a person's attention is diverted from the stimulus, the perception of pain diminishes.[15,16] Topical anesthetics reversibly block nerve conduction by targeting free nerve endings and competing with calcium-binding sites that control sodium permeability. This results in decreased permeability, depolarization and an increased excitability threshold.[17,18] The utilization of cold spray for pain reduction was elucidated by its ability to induce vasoconstriction and alter nerve conduction patterns.[19] Based on the gate control theory, the perception of cool sensations is primarily detected by A-delta fibers, which in turn exert inhibitory effects on the active C fibers.[20] Additionally, pain signal transmission is decelerated at lower tissue temperatures.[14,21]

However, there is still a lack of randomized controlled trials that compare the efficacy and safety of these interventions. This study was conducted to determine the extent of pain alleviation through the use of common methods during venipuncture. The findings can provide valuable insights to establish optimal clinical practices in the context of venipuncture procedures.

Objectives

We aimed to compare the efficacy of pain reduction during venipuncture using audiovisual distraction, topical anesthesia and cold spray application.

Methods

Participants

This randomized controlled study was conducted from April 2023 to July 2023 at the Walailak University (Nakhon Si Thammarat, Thailand). We posted online announcements about this study and asked for volunteers on our academic websites. To minimize undue influence, we had our co-investigators organize the registration and withdrawal processes. The inclusion criteria included: (1) being 18–40 years old; (2) willing to participate in the study; and (3) being able to read, write and understand Thai and English as well as the capacity to provide informed consent. The exclusion criteria included: (1) mental restriction or being unable to rate pain scores; (2) needle insertion with more than 2 attempts; (3) body mass index (BMI) >30 kg/m^2; (4) being unable to collect blood from the antecubital area; (5) history of allergy to topical anesthesia; (6) audiovisual impairment with a decreased quality of life; (7) psychiatric disorders; (8) peripheral neuropathy; (9) cold intolerance; (10) peripheral arterial disease affecting the antecubital areas; and (11) history of taking non-steroidal anti-inflammatory drugs within 1 week of the intervention.

This prospective study was approved by the Walailak Ethics Committee (No. WUEC-23-070-01). Written informed consent was obtained from all participants after a full explanation of the study. This study complied with the principles of the Declaration of Helsinki and the International Conference on Harmonization of Good Clinical Practice. Participants were permitted to withdraw from the study at any time for any reason without consequence.

This clinical trial was registered in the Thai Clinical Trials Registry (No. TCTR20230324007). The ethics committee took into account and complied with the laws of Thailand, including the Personal Data Protection Act. All data files and sensitive personal information were encrypted, password-protected, and saved to a secure computer that was only accessible to the study coordinators to ensure confidentiality. Participants could access their own data by directly contacting study coordinators. No information that could link an individual to the data was revealed. Twelve months after completion of the study, all data were deleted.

Intervention and study design

After eligible participants were voluntarily recruited, they were randomly assigned to 1 of 4 groups using Excel 2019 (Microsoft Corp., Armonk, USA) with allocation concealment using sealed envelopes: group 1 (control), group 2 (topical anesthetic), group 3 (cooling spray), and group 4 (audiovisual distraction). To anesthetize the skin at the needle insertion area of 10 cm^2, 1 g of EMLA cream (5% emulsion containing 2.5% each of lidocaine and prilocaine; Recipharm Karlskoga AB, Karlskoga, Sweden)

was applied in the topical anesthetic group for 1 h before venipuncture. In the cooling spray group, the needle insertion site was sprayed with Perskindol cool spray (0.5% Menthol; IGS Aerosols GmbH, Wehr, Germany). The spray was administered for 5 s at a distance of 15 cm and a 90° angle from the skin. After allowing the spray to evaporate from the skin for 10 s, vascular access was performed after skin disinfection. In the audiovisual distraction group, participants were instructed to watch a 1.22-min video clip (https://youtu.be/vJG698U2Mvo) while doing venipuncture. This intervention, the selective attention test, consisted of 6 players playing with 2 basketballs. Participants were asked to count and answer how many times the players wearing white passed the basketball. In the control group, participants underwent venipuncture after skin disinfection without additional intervention.

A blood pressure cuff was placed 5 cm proximal to the antecubital fossa and was then inflated to 40–60 mm Hg. The needle insertion sites were sterilized with 70% alcohol patches and allowed to dry. The venipuncture was performed using a 21-gauge needle by 1 medical staff member. The total blood volume collected was 5–15 mL, with the specific vein selected depending on the number of laboratory tests requested by the attending physicians. Baseline characteristics were collected through structured questionnaires and medical records, including age, gender, height, weight, and vital signs. Pain scores, satisfaction levels and adverse events resulting from the intervention were accessed and recorded by a blinded investigator. Pain scores ranged from 0 (indicating no pain) to 10 (indicating extreme pain), while satisfaction levels ranged from 0 (representing extreme dissatisfaction) to 3 (representing extreme satisfaction).

Sample size and power

To estimate sample size, the effect sizes were based on outcomes from a previous study.[22] A sample size of 9 in each group was initially planned, which had a 90% power to detect an effect size of 2.1, comparing each intervention arm and the control arm using a 2-sample t-test. All t-tests were 2-sided with a 0.01 significance level. Assuming an approx. 25% loss to follow-up, we proposed to recruit and randomize 12 participants per intervention group to give a total sample size of 48 participants.

Statistical analyses

For descriptive statistics, means and standard deviations (SDs) were used to describe normally distributed continuous data, while medians and interquartile ranges (IQRs) were applied for continuous data that were not normally distributed. Additionally, 95% confidence intervals (95% CIs) were calculated to estimate the precision of the mean values. Frequency and percentages were utilized for analyzing categorical data. For inferential statistics, the study incorporated a variety of tests. Normally distributed variables were evaluated, as shown in Supplementary Table 1. We verified the equality of variances across the groups prior to conducting the statistical tests to assess differences in pain scores among the groups. The results of this analysis are provided in Supplementary Table 3. Following this verification, a one-way analysis of variance (ANOVA) was conducted to assess the significance of differences in age and BMI among the different groups. Due to the limited sample size, a Fisher's exact test was utilized to assess proportion comparisons among independent groups. According to pain scores and satisfaction levels, as non-parametric data, differences among the 4 groups were tested using the Kruskal–Wallis test, and Dunn's test was used for the post hoc analysis for pairwise comparisons. A multiple comparisons correction was performed to adjust the significance level (α) for comparing pain scores between the groups. To address the issue of the family-wise error rate, the Bonferroni correction method was applied. This approach involves dividing α by the number of comparisons to control the family-wise error rate, with α specifically divided by 6 for our 6 pairwise comparisons. For comparisons of pain across different factors between the 2 groups, the Mann–Whitney U test or independent t-test was selected depending on the normality of the data. Additionally, Spearman's rho was utilized to measure the strength and direction of association between 2 ranked variables in the context of non-normal data. To investigate the link between BMI and pain, we created scatter plots with locally estimated scatterplot smoothing (LOESS) curves for an initial visual analysis. We then applied a range of regression models (Linear, Logarithmic, Inverse, Quadratic, and Cubic) to precisely examine this relationship, aiming to capture the complex dynamics between BMI and pain experiences. In this study, all the statistical tests, including the Fisher's exact test, one-way ANOVA, Mann–Whitney U test, independent t-test, and Kruskal–Wallis test, were conducted as two-tailed tests. For each of these two-tailed tests, a p-value of < 0.05 was required to indicate statistical significance. All statistical analyses were conducted using SPSS software v. 15 (SPSS Inc., Chicago, USA) and the R programming environment (R Foundation for Statistical Computing, Vienna, Austria). This comprehensive analysis included a range of model fittings (Linear, Logarithmic, Inverse, Quadratic, Cubic, and LOESS) to assess the association between BMI and pain. The utilization of both SPSS and R enabled a thorough investigation of the data through various statistical lenses, ensuring a robust examination of the underlying relationships.

Results

Forty-eight eligible volunteers were recruited for the study; however, 1 participant had to be excluded due to extreme, intolerable pain. As a result, 47 participants

Table 1. Baseline characteristics (n = 47)

Characteristics		Group 1 (n = 12)	Group 2 (n = 12)	Group 3 (n = 11)	Group 4 (n = 12)	Test name and p-value
Sex, n (%)	male	4 (33.3)	1 (8.3)	4 (36.4)	7 (58.3)	p = 0.080[a]
	female	8 (66.7)	11 (91.7)	7 (63.6)	5 (41.7)	
Age [years] ±SD		43.5 (±13.0)	36.8 (±13.9)	45.3 (±14.0)	43.8 (±11.5)	F(3) = 0.993, p = 0.405[b]
BMI [kg/m^2] ±SD		23.0 (±2.2)	22.5 (±3.3)	24.9 (±4.5)	21.6 (±2.6)	F(3) = 2.165, p = 0.106[b]
Education, n (%)	secondary education	3 (25.0)	1 (8.3)	5 (45.5)	2 (16.7)	p = 0.209[a]
	higher education	9 (75.0)	11 (91.7)	6 (54.5)	10 (83.3)	
Dominant hand, n (%)	right	7 (58.3)	11 (91.7)	11 (100.0)	12 (100.0)	p = 0.010[a]
	left	5 (41.7)	1 (8.3)	0 (0.0)	0 (0.0)	
Correlation between punctured site and dominant hand, n (%)	same side	7 (58.3)	3 (25.0)	4 (36.4)	4 (33.3)	p = 0.429[a]
	different side	5 (41.7)	9 (75.0)	7 (63.6)	8 (66.7)	
Punctured vessel, n (%)	median vein	11 (91.7)	9 (75.0)	11 (100.0)	8 (66.7)	p = 0.038[a]
	cephalic vein	1 (8.3)	2 (16.7)	0 (0.0)	0 (0.0)	
	basilic vein	0 (0.0)	1 (8.3)	0 (0.0)	4 (33.3)	
History of blood sampling, number of times (%)	0	1 (8.3)	5 (41.7)	2 (18.2)	2 (16.7)	p = 0.756[a]
	1–3	2 (16.7)	2 (16.7)	3 (27.3)	2 (16.7)	
	4–6	2 (16.7)	1 (8.3)	1 (9.1)	1 (8.3)	
	7–10	0 (0.0)	1 (8.3)	0 (0.0)	0 (0.0)	
	>10	7 (58.3)	3 (25.0)	5 (45.5)	7 (58.3)	

BMI – body mass index; SD – standard deviation. Group 1 – control group; group 2 – topical anesthetic group; group 3 – cooling spray group; group 4 – audiovisual distraction group. Statistical test notations: [a] Fisher's exact test; [b] one-way analysis of variance (ANOVA).

Table 2. Comparison of pain scores and satisfaction levels across the 4 participant groups (n = 47)

Group	n	Pain score		Satisfaction level	
		median	IQR	median	IQR
Group 1	12	4.00	2.00	3.00	1.00
Group 2	12	1.00	2.00	3.00	0.00
Group 3	11	2.00	3.00	3.00	1.00
Group 4	12	2.00	2.00	3.00	0.00
All	47	2.00	3.00	3.00	0.00

Group 1 – control; group 2 – topical anesthetic; group 3 – cooling spray; group 4 – audiovisual distraction; IQR – interquartile range. Pain scores were measured on a scale from 0 to 10, with 0 indicating no pain and 10 indicating extreme pain. Satisfaction levels were gauged on a scale from 0 to 3, where 0 represented extreme dissatisfaction and 3 represented extreme satisfaction.

remained for the final analysis. The mean age of the participants was 42.3 years (SD ±13.1). The majority of participants were female (66.0%), held higher education qualifications (76.6%) and exhibited right-hand dominance (87.2%). Common comorbidities included essential hypertension (33.0%), hypothyroidism (27.0%), dyslipidemia (20.0%), type 2 diabetes mellitus (13.0%), and others (33.0%), such as coronary artery disease, allergic rhinitis, and hepatitis B infections. Table 1 displays the baseline characteristics of the participants in each group.

Comparison of pain scores and satisfaction levels across the four intervention groups are demonstrated in Table 2 and Fig. 1,2. The participants in the intervention groups reported lower pain scores than those in group 1. The mean differences were 2.67 points in group 2 (95% CI: 1.49–3.84; $p < 0.001$), 1.56 points in group 3 (95% CI: 0.15–2.98; $p = 0.077$), and 1.67 points in group 4 (95% CI: 0.37–2.96; $p = 0.042$), as shown in Table 3. Multiple t-tests using Dunn's test with Bonferroni correction revealed a statistically significant difference in pain between group 1 and group 2 (test statistic = 3.716, $p < 0.001$). The median satisfaction level in all groups was 3.00 (interquartile range (IQR) 0.00), and the Kruskal–Wallis test indicated no significant difference in satisfaction levels across all groups ($H(3) = 6.050$, $p = 0.109$). The study revealed no statistically significant differences in pain scores based on sex, educational level, hand dominance, puncture side, type of vessel, or history of blood sampling, as shown in Supplementary

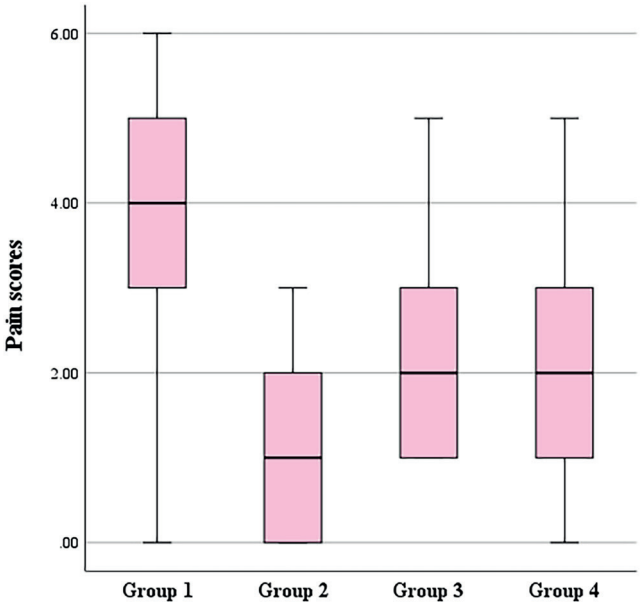

Fig. 1. Pain scores across the 4 participant groups (n = 47)

The midline of the box represents the median of the data. The bottom and top of the box depict the 25th and 75th percentiles, respectively. The whiskers extend to show the range of the data, from the minimum to the maximum values.

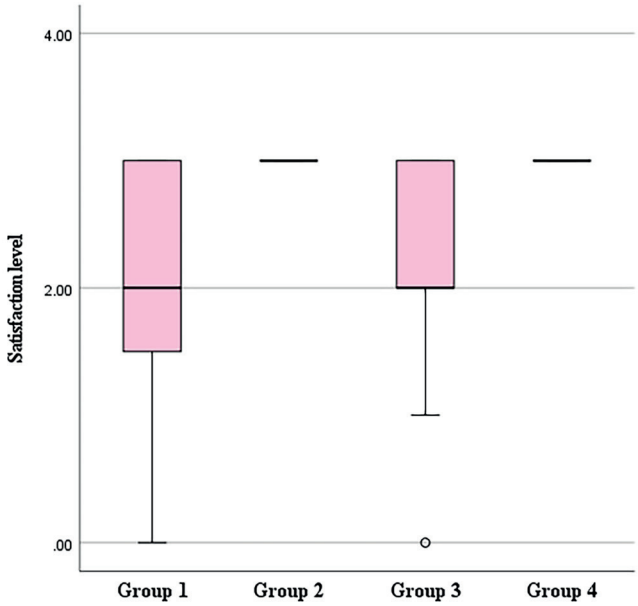

Fig. 2. Satisfaction levels across the 4 participant groups (n = 47)

The midline of the box represents the median of the data. The bottom and top of the box depict the 25th and 75th percentiles, respectively. The whiskers extend to show the range of the data, from the minimum to the maximum values.

Table 3. Comparison of pain scores and satisfaction levels across different groups (n = 47)

Comparisons	Mean differences (95% CI)	Test value and p-value*
Pain scores		
Among 4 groups	N/A	H(3) = 14.020, p = 0.003[a]
Group 1 and 2	2.67 (1.49, 3.84)	test statistic = 3.716, p < 0.001[b]*
Group 1 and 3	1.56, (0.15, 2.98)	test statistic = 2.143, p = 0.096[b]*
Group 1 and 4	1.67 (0.37, 2.96)	test statistic = 2.177, p = 0.089[b]*
Group 2 and 3	−1.11 (−2.31, 0.10)	test statistic = −1.492, p = 0.407[b]*
Group 2 and 4	−1.00 (−2.05, 0.05)	test statistic = −1.540, p = 0.371[b]*
Group 3 and 4	0.11 (−1.22, 1.43)	test statistic = −0.014, p = 1.000[b]*
Satisfaction levels		
Among 4 groups	N/A	H(3) = 6.050, p = 0.109[a]

95% CI – 95% confidence interval; N/A – not applicable. Statistical test notations: [a] Kruskal–Wallis test; [b] Dunn's test. * To adjust the significance level (α) for multiple comparisons of pain scores among groups, multiple Dunn's tests were used. The family-wise error rate was controlled by applying the Bonferroni correction, which involved dividing α by the number of comparisons (e.g., α/6 for 6 comparisons).

Table 4. Correlation between each factor and pain

Variables	Correlation coefficient and p-value
Age	r = 0.243, p = 0.100
Weight	r = −0.197, p = 0.184
Height	r = −0.083, p = 0.578
BMI	r = −0.200, p = 0.178

BMI – body mass index. Spearman's rho was employed as the statistical method for analyzing the correlations presented in the data set.

Table 2. However, the Kruskal–Wallis test indicated significant differences among weight categories (H(3) = 8.368, p = 0.039). Compared with participants having a BMI over 27.5 kg/m², those with a BMI of 18.5–22.9 kg/m² and those with a BMI of 23.0–27.5 kg/m² reported significantly higher pain scores, with test statistics of 2.593 (p = 0.029) and 2.490 (p = 0.038), respectively. The Spearman's rho correlation analysis was conducted due to the non-normal distribution of the data, aiming to identify any monotonic component in the association between pain and other factors, including age (r = 0.243, p = 0.100), weight (r = −0.197, p = 0.184), height (r = −0.083, p = 0.578), and BMI (r = −0.200, p = 0.178). The results, detailed in Table 4, indicate the absence of a significant monotonic component in these associations. However, this does not preclude the existence of non-monotonic components between these variables.

No immediate serious adverse reactions were noted across all groups. In group 3, a notable observation involved 3 participants (27.3%) reporting minor side effects associated with the use of vapocoolant sprays, which manifested as transient erythema at the application site. This erythema typically resolved spontaneously within 5–10 min.

Discussion

Pain is a common adverse effect of the venipuncture procedure. While most people experience mild pain, failing to alleviate acute pain can lead to both physiological and psychological effects.[3] To date, several methods have been proposed to alleviate pain during the procedure. However, there is still a lack of randomized controlled trials that compare the efficacy and safety of these interventions. To the best of our knowledge, our study was the first to compare the efficacy of pain reduction during venipuncture using audiovisual distraction, topical anesthesia and cold spray application. Our findings revealed that participants in each intervention group reported lower pain scores compared to those in the control group. Participants who received the topical anesthetic reported the lowest pain scores, and this difference was statistically significant. Additionally, they expressed high levels of satisfaction.

Consistent with our findings, previous research has demonstrated a significant reduction in pain scores with 3 specific interventions. First, local anesthetics have shown a substantial and statistically significant effect in reducing pain during venipuncture procedures (mean = 1.04, 95% CI: 0.92–1.34) and intravenous insertions (mean = 1.05, 95% CI: 0.84–1.46).[10] Second, the application of vapocoolants has been associated with a significant decrease in pain scores (median = 1, range: 0–3) compared to a control group (median = 3, range: 1.2–5) during venipuncture ($p = 0.001$).[9] Third, audiovisual distraction techniques have been effective in significantly reducing needle-related pain. Gandhar et al. found that the mean pain score for a group watching cartoons during venipuncture was significantly lower (mean 4.6, SD ±1.5) than that of the control group (mean 7.7, SD ±0.8, $p < 0.001$).[8] Similarly, Orhan and Gozen demonstrated that the post-venipuncture pain score for a group engaged in virtual reality was significantly lower (mean 1.46, SD ±1.49) than that of a control group (mean 4.44, SD ±2.26, $p = 0.001$).[11]

Our findings emphasize that all 3 interventions (topical anesthetic application, cooling spray and audiovisual distraction techniques) successfully lowered pain scores associated with venipuncture procedures. However, the pain reduction did not reach statistical significance when comparing these 3 interventions. The ideal anesthetic intervention should be effective, quick, painless, inexpensive, and side-effect-free. The audiovisual distraction, therefore, appears to be a practical choice in real-world applications in the venipuncture procedure due to its advantages, including time efficiency, non-invasiveness and the absence of disposable materials. Prior to venipuncture, the patients need to wait for the topical anesthetic to reach its peak effects. The cream needs time to be absorbed and the pain to be relieved. The average insertion depths with acceptable pain following 60 min and 120 min of lidocaine and prilocaine local anesthetic application were 2.9 mm and 4.5 mm, respectively.[23] The average depths of the basilic, median cubital, and cephalic veins after applying a tourniquet are 2.9 mm (SD ±1.7), 1.7 mm (SD ±0.8) and 1.7 mm (SD ±0.6), respectively.[24] Therefore, if blood needs to be collected from the deeper parts of these veins, it may take longer than 1 h to achieve the desired effect.

Adverse effects related to EMLA cream are exceedingly rare and mostly limited to localized, temporary reactions, such as blanching, redness, altered temperature sensation, edema, pruritus, burning, purpura, and contact hypersensitivity.[25] The major concern for systemic toxicity is the development of methemoglobinemia. Thus, caution is advised when administering EMLA cream to patients with glucose-6-phosphate deficiency, those concurrently using methemoglobin-inducing medications, and infants below 3 months of age.[26] Correspondingly, no local or systemic side effects were observed in our findings. Previous studies reported a total of 8 adverse events out of 279 participants (2.9%). All of the reactions were minor, including cold sensations, 3 temporary instances of erythema at the spray site and 1 case of a burning sensation.[27] We also observed that 3 participants developed temporary erythema, with no further consequences or concerns.

Individuals show substantial differences in their perception of pain. Distinctive individual variations result from biological, psychological and social factors. Nevertheless, these factors do not directly influence pain themselves; instead, they signify the various processes that modify pain.[28] Kivrak et al.[29] revealed that anxiety may predict pain, but other factors like sex, depression, somatosensory amplification, age, and weight do not seem to influence the perception of pain during the venipuncture procedure. Pain tolerance thresholds in the upper extremity veins can vary. Yoshida et al.[30] found that the superficial dorsal vein had a significantly higher pain tolerance threshold at 250 Hz in response to pinprick sensations compared to the median cubital, basilic and cephalic veins at the wrist. There was no significant difference between the pain tolerance thresholds of the cephalic vein at the cubitus and the superficial dorsal vein. Previous studies have provided support for the impact of hand laterality on pain perception, revealing that the non-dominant hand tends to be more sensitive to pain than the dominant hand.[31,32] Our findings, in relation to pain and obesity, align with those of Emerson et al.,[33] who suggested that obesity had a limited effect on pain sensitivity. This indicates that obesity alone may not significantly increase the risk of developing chronic pain by intensifying nociceptive mechanisms. In contrast, Mendonça et al.[34] reported significant prevalences of musculoskeletal and severe pain among severely obese individuals. They identified the factors contributing to pain in adults with severe obesity, including clinical conditions, a sedentary lifestyle, the extent of obesity, and overall body fat. Additionally, Majchrzak et al.[35] found that obese lung cancer patients undergoing thoracic surgery experienced more intense and longer-lasting pain than their non-obese counterparts. The reasons behind the varying pain thresholds observed between obese and non-obese patients remain unclear.

Possible explanations for this phenomenon could include chronic inflammation associated with obesity, the release of inflammatory mediators by macrophages, genetic variations, and nocturnal hypoxemia.[36–39] Our study found a non-significant trend suggesting an inverse relationship between obesity and pain sensitivity. This observation might be explained by various factors, including differences in participant characteristics, psychological influences, biological mechanisms, and the limitations of a small sample size.[1] Future research, potentially involving larger sample sizes or incorporating a broader range of variables, including comprehensive biological, psychological and social factors, might, therefore, provide clearer insights into the nuanced relationship between BMI and the experience of pain.

Limitations

We acknowledge several limitations of this study. First, our study is limited to a single center, which may restrict its applicability to a broader population. To enhance the external validity of our findings, it is essential to conduct multicenter randomized controlled trials involving larger and more diverse populations and settings. Second, psychological factors such as anxiety and depression, as well as social factors, were not comprehensively assessed. These factors can influence the perceived intensity of pain. Nevertheless, we screened for them through history-taking and physical examinations and excluded individuals with psychiatric disorders. Third, certain baseline characteristics across the 4 groups, including the participant's dominant hand and the correlation between the punctured site and punctured vessels, differed significantly. Further studies are needed to control for these differences to confirm the pain reduction findings across interventions. Lastly, the combined interventions were not evaluated or compared with single interventions. Further studies should be conducted to assess the additional effects of combining interventions.

Conclusions

The intervention for pain reduction, which includes topical anesthetic, cooling spray and audiovisual distraction, is an effective method for alleviating pain during venipuncture. Participants who received a topical anesthetic reported the lowest pain scores and high levels of satisfaction. When selecting the intervention, consideration should be given to the availability of resources, patient preferences and time constraints.

Supplementary data

The Supplementary materials are available at https://doi.org/10.5281/zenodo.11079400. The package includes the following files:

Supplementary Table 1. Evaluating normal distribution in each variable group.

Supplementary Table 2. Comparison of pain across different factors.

Supplementary Table 3. The assessment of equal variances.

Supplementary Table 4. The numbers of expected observations.

Supplementary Fig. 1. Correlation between age and pain scores (n = 47).

Supplementary Fig. 2. Correlation between weight and pain scores (n = 47).

Supplementary Fig. 3. Correlation between height and pain scores (n = 47).

Supplementary Fig. 4. Correlation between body mass index (BMI) and pain scores (n = 47).

Supplementary Fig. 5. Correlation between body mass index (BMI) and pain scores (n = 47) using Locally Weighted Scatterplot Smoothing (LOESS) curves.

Data availability

The datasets generated and/or analyzed during the current study are available from the corresponding author on reasonable request.

Consent for publication

Not applicable.

ORCID IDs

Siwatus Puangrab https://orcid.org/0000-0003-2784-6500
Weeratian Tawanwongsri https://orcid.org/0000-0002-1949-7323
Auemphon Mordmuang https://orcid.org/0000-0002-3979-9599
Wiphada Khocharoen https://orcid.org/0009-0003-7849-4055
Pimchanok Krainukun https://orcid.org/0009-0001-3460-4182

References

1. Raja SN, Carr DB, Cohen M, et al. The revised International Association for the Study of Pain definition of pain: Concepts, challenges, and compromises. *Pain*. 2020;161(9):1976–1982. doi:10.1097/j.pain.0000000000001939
2. Marchand S. Mechanisms challenges of the pain phenomenon. *Front Pain Res*. 2021;1:574370. doi:10.3389/fpain.2020.574370
3. Macintyre PE, Shug S, Scott D, Visser EJ, Walker SM, eds. *Acute Pain Management: Scientific Evidence*. 4th ed. Melbourne, Australia: Australian and New Zealand College of Anaesthetists and Faculty of Pain Medicine; 2015. https://www.anzca.edu.au/getattachment/4c3b03b7-52bf-4c10-9115-83d827c0fc38/Acute-Pain-Management-Scientific-Evidence. Accessed April 29, 2024.
4. Duenas M, Ojeda B, Salazar A, Mico JA, Failde I. A review of chronic pain impact on patients, their social environment and the health care system. *J Pain Res*. 2016;9:457–467. doi:10.2147/JPR.S105892
5. World Health Organization. *WHO Guidelines on Drawing Blood: Best Practices in Phlebotomy*. Geneva, Switzerland: World Health Organization (WHO); 2010. https://iris.who.int/bitstream/handle/10665/44294/9789241599221_eng.pdf?sequence=1. Accessed April 29, 2024.
6. Ballesteros-Peña S, Vallejo-De La Hoz G, Fernández-Aedo I. Pain scores for venipuncture among ED patients. *Am J Emerg Med*. 2017;35(4):653–654. doi:10.1016/j.ajem.2017.01.034

7. Basak T, Aciksoz S, Savasci U, Yilmaz S. Effectiveness of vapocoolant spray on venipuncture pain in young male donors: A randomized controlled trial. *J Infus Nurs*. 2021;44(6):339–345. doi:10.1097/NAN.0000000000000443
8. Gandhar SS, Deshpande J, Borude S. Effectiveness of cartoon movies as distractor on pain among children undergoing venipuncture. *Int J Sci Res*. 2016;5(6):2241–2242. https://www.ijsr.net/archive/v5i6/NOV164843.pdf. Accessed January 3, 2024.
9. Mace SE. Prospective, randomized, double-blind controlled trial comparing vapocoolant spray vs placebo spray in adults undergoing venipuncture. *Am J Emerg Med*. 2016;34(5):798–804. doi:10.1016/j.ajem.2016.01.002
10. Fetzer SJ. Reducing venipuncture and intravenous insertion pain with eutectic mixture of local anesthetic: A meta-analysis. *Nurs Res*. 2002;51(2):119–124. doi:10.1097/00006199-200203000-00008
11. Orhan E, Gozen D. The effect of virtual reality on pain experienced by school-age children during venipuncture: A randomized controlled study. *Games Health J*. 2023;12(4):330–339. doi:10.1089/g4h.2022.0232
12. Rezai MS, Goudarzian AH, Jafari-Koulaee A, Bagheri-Nesami M. The effect of distraction techniques on the pain of venipuncture in children: A systematic review. *J Pediatr Rev*. 2017;5(1):26–37. doi:10.17795/jpr-9459
13. Semerci R, Akarsu Ö, Kılıç D. The effect of buzzy and cold spray on pain, anxiety, and fear of children during venipuncture in pediatric emergency department in Turkey; A randomized controlled study. *J Pediatr Nurs*. 2023;68:e1–e7. doi:10.1016/j.pedn.2022.08.019
14. Wang L, Fang L, Zhou Y, Fang X, Liu J, Qu G. Efficacy and safety of vapocoolant spray for vascular puncture in children and adults: A systematic review and meta-analysis. *PLoS One*. 2023;18(2):e0279463. doi:10.1371/journal.pone.0279463
15. Gurav KM, Kulkarni N, Shetty V, et al. Effectiveness of audio and audio-visual distraction aids for management of pain and anxiety in children and adults undergoing dental treatment: A systematic review and meta-analysis. *J Clin Pediatr Dent*. 2022;46(2):86–106. doi:10.17796/1053-4625-46.2.2
16. McCaul KD, Malott JM. Distraction and coping with pain. *Psychol Bull*. 1984;95(3):516–533. PMID:6399756.
17. Kumar M, Chawla R, Goyal M. Topical anesthesia. *J Anaesthesiol Clin Pharmacol*. 2015;31(4):450. doi:10.4103/0970-9185.169049
18. Navarro-Rodriguez JM, Suarez-Serrano C, Martin-Valero R, Marcen-Roman Y, de-la-Casa-Almeida M. Effectiveness of topical anesthetics in pain management for dermal injuries: A systematic review. *J Clin Med*. 2021;10(11):2522. doi:10.3390/jcm10112522
19. Majidinejad S, Heidari F, Famil Chitgarian A. Skin cooling to reduce the pain associated with local anesthetic injection: A randomized controlled trial. *Arch Acad Emerg Med*. 2022;10(1):e20. PMID:35573720, PMCID:PMC9078070.
20. Campbell TS, Johnson JA, Zernicke KA. Gate control theory of pain. In: Gellman MD, ed. *Encyclopedia of Behavioral Medicine*. Cham, Switzerland: Springer International Publishing; 2020:914–916. doi:10.1007/978-3-030-39903-0_1134
21. Baxter AL, Cohen LL, McElvery HL, Lawson ML, Von Baeyer CL. An integration of vibration and cold relieves venipuncture pain in a pediatric emergency department. *Pediatr Emerg Care*. 2011;27(12):1151–1156. doi:10.1097/PEC.0b013e318237ace4
22. İnal S, Kelleci M. Relief of pain during blood specimen collection in pediatric patients. *MCN Am J Matern Child Nurs*. 2012;37(5):339–345. doi:10.1097/NMC.0b013e31825a8aa5
23. Wahlgren CF, Quiding H. Depth of cutaneous analgesia after application of a eutectic mixture of the local anesthetics lidocaine and prilocaine (EMLA cream). *J Am Acad Dermatol*. 2000;42(4):584–588. PMID:10727302.
24. Mukai K, Nakajima Y, Nakano T, et al. Safety of venipuncture sites at the cubital fossa as assessed by ultrasonography. *J Patient Saf*. 2020;16(1):98–105. doi:10.1097/PTS.0000000000000441
25. Friedman PM, Mafong EA, Friedman ES, Geronemus RG. Topical anesthetics update: EMLA and beyond. *Dermatol Surg*. 2001;27(12):1019–1026. doi:10.1046/j.1524-4725.2001.01855.x
26. Huang W, Vidimos A. Topical anesthetics in dermatology. *J Am Acad Dermatol*. 2000;43(2):286–298. doi:10.1067/mjd.2000.106506
27. Griffith RJ, Jordan V, Herd D, Reed PW, Dalziel SR. Vapocoolants (cold spray) for pain treatment during intravenous cannulation. *Cochrane Database Syst Rev*. 2016;2016(4):CD009484. doi:10.1002/14651858.CD009484.pub2
28. Fillingim RB. Individual differences in pain: Understanding the mosaic that makes pain personal. *Pain*. 2017;158(Suppl 1):S11–S18. doi:10.1097/j.pain.0000000000000775
29. Kose Ozlece H, Kivrak Y, Ustündag MF, Asoglu M. Pain perception: Predictive value of sex, depression, anxiety, somatosensory amplification, obesity, and age. *Neuropsychiatr Dis Treat*. 2016;12:1913–1918. doi:10.2147/NDT.S106974
30. Yoshida M, Shiiba S, Sago T, Nunomaki M, Harano N, Watanabe S. Comparison of pain tolerance thresholds of upper limb to identify the most appropriate venipuncture site. *J Oral Maxillofac Surg*. 2015;73(5):850.e1–850.e5. doi:10.1016/j.joms.2015.01.027
31. Ozawa M, Kanda K, Hirata M, Kusakawa I, Suzuki C. Effect of gender and hand laterality on pain processing in human neonates. *Early Hum Dev*. 2011;87(1):45–48. doi:10.1016/j.earlhumdev.2010.09.371
32. Pud D, Golan Y, Pesta R. Hand dominancy: A feature affecting sensitivity to pain. *Neurosci Lett*. 2009;467(3):237–240. doi:10.1016/j.neulet.2009.10.048
33. Emerson NM, Nahman-Averbuch H, Peugh JL, Coghill RC. Pain sensitivity does not differ between obese and healthy weight individuals. *Pain Rep*. 2021;6(3):e942. doi:10.1097/PR9.0000000000000942
34. Mendonça CR, Noll M, De Carvalho Santos ASEA, Rodrigues APDS, Silveira EA. High prevalence of musculoskeletal pain in individuals with severe obesity: Sites, intensity, and associated factors. *Korean J Pain*. 2020;33(3):245–257. doi:10.3344/kjp.2020.33.3.245
35. Majchrzak M, Brzecka A, Daroszewski C, et al. Increased pain sensitivity in obese patients after lung cancer surgery. *Front Pharmacol*. 2019;10:626. doi:10.3389/fphar.2019.00626
36. Divella R, De Luca R, Abbate I, Naglieri E, Daniele A. Obesity and cancer: The role of adipose tissue and adipo-cytokines-induced chronic inflammation. *J Cancer*. 2016;7(15):2346–2359. doi:10.7150/jca.16884
37. Elmallah RK, Ramkumar PN, Khlopas A, et al. Postoperative pain and analgesia: Is there a genetic basis to the opioid crisis? *Surg Technol Int*. 2018;32:306–314. PMID:29791710.
38. Doufas AG, Tian L, Davies MF, Warby SC. Nocturnal intermittent hypoxia is independently associated with pain in subjects suffering from sleep-disordered breathing. *Anesthesiology*. 2013;119(5):1149–1162. doi:10.1097/ALN.0b013e3182a951fc
39. Chin SH, Huang WL, Akter S, Binks M. Obesity and pain: A systematic review. *Int J Obes*. 2020;44(5):969–979. doi:10.1038/s41366-019-0505-y

Association of anion gap and albumin corrected anion gap with acute kidney injury in patients with acute ischemic stroke

*Haiqian Yao[1,A,D–F], *Jianan Tian[1,B,C,F], Shi Cheng[2,A,E,F]

[1] Department of Neurology, The Second Affiliated Hospital of Harbin Medical University, China
[2] Department of Orthopedic Surgery, The Second Affiliated Hospital of Harbin Medical University, China

A – research concept and design; B – collection and/or assembly of data; C – data analysis and interpretation;
D – writing the article; E – critical revision of the article; F – final approval of the article

Advances in Clinical and Experimental Medicine, ISSN 1899–5276 (print), ISSN 2451–2680 (online) *Adv Clin Exp Med*. 2025;34(3):351–359

Address for correspondence
Shi Cheng
E-mail: schengdoc_Ort@outlook.com

Funding sources
None declared

Conflict of interest
None declared

* Haiqian Yao and Jianan Tian contributed equally to this work.

Received on November 10, 2023
Reviewed on March 6, 2024
Accepted on April 4, 2024

Published online on June 11, 2024

Abstract

Background. Acute kidney injury (AKI) has become a common complication of acute ischemic stroke (AIS) and may have a significant impact on clinical outcomes. Anion gap (AG)/albumin corrected anion gap (ACAG) are used to assess acid-base balance status and help identify the severity of metabolic acidosis.

Objectives. To explore the association of AG and ACAG with the risk of AKI in AIS patients admitted to the intensive care unit (ICU).

Materials and methods. Data of AIS patients in this retrospective cohort study were extracted from the electronic ICU (eICU) databases (2014–2015). The outcome was the occurrence of AKI after ICU admission. The covariates included demographic data, vital signs, comorbidities, laboratory parameters, and medication use. The association of AG and ACAG levels with AKI risk in AIS patients was evaluated using univariate and multivariate logistic regression models with odds ratios (ORs) and 95% confidence intervals (95% CIs). The predictive performance of AG and ACAG for the risk of AKI in AIS patients was assessed with the area under the curve (AUC). To further explore the association of AG and ACAG levels with AKI risk, subgroup analyses were performed according to comorbidities.

Results. Of the 1,260 AIS patients, 546 (43%) developed AKI. Elevated AG (OR = 1.73, 95% CI: 1.32–2.29) and ACAG (OR = 1.57, 95% CI: 1.21–2.04) were associated with the risk of AKI in AIS patients. The AUC of ACAG was superior to AG for predicting the risk of AKI (0.581 vs 0.558; p = 0.024). Elevated ACAG levels were associated with the risk of AKI in AIS patients without ischemic heart disease (OR = 1.60, 95% CI: 1.19–2.15), diabetes (OR = 1.58, 95% CI: 1.19–2.10) and hypertension (OR = 1.69, 95% CI: 1.24–2.30).

Conclusions. Albumin corrected anion gap was a better predictor than AG for AKI risk in AIS patients, which may help clinicians identify high-risk patients for AKI.

Key words: acute kidney injury, acute ischemic stroke, anion gap, albumin corrected anion gap

Cite as
Yao H, Tian J, Cheng S. Association of anion gap and albumin corrected anion gap with acute kidney injury in patients with acute ischemic stroke. *Adv Clin Exp Med*. 2025;34(3):351–359. doi:10.17219/acem/186814

DOI
10.17219/acem/186814

Background

Acute ischemic stroke (AIS) is a cerebral infarction caused by cerebral vascular occlusion or hemorrhage and is a common vascular event of the central nervous system.[1] Acute ischemic stroke affects approx. 95 individuals per 100,000 population worldwide every year and is a significant cause of disability and death.[2] Evidence showed that a common complication in patients with AIS is acute kidney injury (AKI), which occurs in about 19% of patients with AIS.[3,4] Acute kidney injury can deteriorate the medical status of patients with AIS and predict a worse clinical prognosis, including longer hospital stay and higher mortality.[5,6] Identification of high-risk patients who may develop AKI is essential for the management and improvement of outcomes in patients with AIS.

Acid-base disorders (particularly metabolic acidosis) are common problems in critically ill patients and are closely related to patient morbidity and mortality.[7] Evidence shows that acid-base disorders and altered electrolyte concentrations are early biochemical responses in AIS, leading to continuous tissue oxidative damage and increased inflammation.[8] The serum anion gap (AG) is an index reflecting the concentration of unmeasured anions, which is used to assess acid-base balance status.[9] However, due to albumin molecules carrying a charge, the results will appear falsely negative, leading to misjudgment of the AG level, a situation that often occurs in critically ill patients with hypoalbuminemia.[10] To avoid the fluctuation of the AG with differing albumin concentrations, the albumin-corrected anion gap (ACAG) was proposed.[11] The AG level is a significant predictor of in-hospital mortality in patients with AIS, and high AG levels are linked to high mortality in AIS patients.[12] However, the relationship between ACAG levels and the prognosis of AIS patients is unclear. Moreover, AG and ACAG levels have been reported to be linked to a higher incidence of and mortality in AKI.[13,14] The link between AG and ACAG levels and the risk of AKI in AIS patients deserves to be explored.

Objectives

This study aimed to evaluate the associations of AG and ACAG levels with AKI risk in patients with AIS who were admitted to the intensive care unit (ICU) and assessed the predictive effect of AG and ACAG for AKI risk.

Materials and methods

Study population

This retrospective cohort study extracted AIS patient data from the electronic ICU (eICU) database (https://eicu-crd.mit.edu/gettingstarted/overview/). The eICU database is a publicly available multicenter database that covers highly granular data on more than 200,000 patients admitted to ICUs across the continental USA from 2014 to 2015.[15] The overall information includes vital sign measurements, severity of illness measures, care plan documentation, treatment information, and diagnosis information. The participant's informed consent was waived because the data were anonymized.

The inclusion criteria included: 1) participants ≥18 years of age and 2) participants diagnosed with AIS at ICU admission.[16] The exclusion criteria were: 1) ICU stay shorter than 24 h; 2) patients with missing data about survival; 3) patients with missing data of sodium, potassium, chloride, bicarbonate, albumin, and AKI grade; 4) patients diagnosed with end-stage renal disease (ESRD)[17,18]; and 5) patients with a history of kidney transplantation.

Definition of AG and ACAG

Anion gap and ACAG were calculated based on the following equation[19]: AG (mmol/L) = (sodium + potassium) – (chloride + bicarbonate) and ACAG (mmol/L) = [4.4 – {albumin(g/dL)}] * 2.5 + AG. The measurements of sodium, potassium, chloride, bicarbonate, and albumin were based on the patient's records at the time of initial admission to the ICU. The AG and ACAG levels were categorized into high- and low-level groups based on the value corresponding to the maximum of Youden's J statistic as the cutoff value (Supplementary Fig. 1). The AG and ACAG levels were categorized as AG levels (low-level (<12.15 mmol/L) and high-level (≥12.15 mmol/L)) and ACAG levels (low-level (<15.075 mmol/L) and high-level (≥15.075 mmol/L)).

Potential covariates

Potential covariates were age, gender, race, height, weight, ICU type, body mass index (BMI), cardiogenic shock, ischemic heart disease, diabetes, hypertension, vasopressor therapy, thrombolysis, thrombectomy, antiplatelet, anticoagulation, antihypertension, ventilation, diastolic blood pressure (DBP), respiratory rate, heart rate, alanine aminotransferase (ALT), systolic blood pressure (SBP), aspartate aminotransferase (AST), serum creatinine (SCR), blood urea nitrogen (BUN), mean arterial pressure (MAP), platelets, white blood cell count (WBC), red blood cell distribution width (RDW), hemoglobin, bilirubin, glucose, international normalized ratio (INR), and estimated glomerular filtration rate (eGFR).

Outcome and follow-up

The AKI was defined by the Kidney Disease Improving Global Outcomes (KDIGO)[20] as follows: an increase in SCR level ≥0.3 mg/dL within 48 h, an increase in SCR levels to ≥1.5 times than the level at ICU admission within 7 days, or urine volume <0.5 mL/kg/h for 6 h. The outcome in this

cohort was the occurrence of AKI after ICU admission. Follow-up began on ICU admission and was terminated when the patient was discharged from the ICU or AKI developed.

Statistical analyses

Normally distributed continuous data were reported as the mean ± standard deviation (mean (±SD)) and tested using t-tests. Non-normally continuous data were presented as medians and quartiles (Me (Q1, Q3)) and tested using a Mann–Whitney U test. Categorical data were presented as the number and percentage (n (%)) and tested using a χ^2 test or Fisher's exact test.

The outcome and exposure variables were not missing, covariates with greater than 20% missing were deleted, and covariates with less than 20% missing were interpolated using multiple interpolations (Supplementary Table 1). Missing data were interpolated 5 times using multiple interpolations through the R package "mice" (v. 3.15.0),[21] with the means of the 5 interpolations taken for continuous variables and the mode of the 5 interpolations taken for categorical variables. Sensitivity analyses were performed on the data before and after interpolation (Supplementary Table 2). Covariates were screened using the adaptive best–subset selection (ABESS) method.[22] All variables except exposure and composite index calculation variables (e.g., height, weight, SBP, DBP, SCR, sodium, potassium, chloride, bicarbonate, and albumin) were selected using the "abbess" R package (v. 0.4.8) based on the generalized information criterion (GIC) (Supplementary Table 3).[22] A variance inflation factor (VIF) was used to assess the linearity between variables, and a VIF ≥ 5 was considered multicollinearity (Supplementary Table 4). The Box–Tidwell test was applied to evaluate the linearity of numerical variables using Logit(P), and a p-value >0.05 satisfied the linear requirement (Supplementary Table 5). The best subsets of covariates after screening were BMI, ischemic heart disease, ventilation, WBC, and platelets. The logistic regression models were used for analyzing the association between AG and ACAG levels and AKI risk in AIS patients, and the results were presented as odds ratios (ORs) with 95% confidence intervals (95% CIs). Model 1 was adjusted for all covariates, including BMI, ischemic heart disease, ventilation, WBC, and platelets. Model 2 was adjusted for albumin based on Model 1. The area under the curve (AUC) was applied to evaluate the predictive effect of AG and ACAG on the AKI risk of AIS patients. The Hosmer–Lemeshow test was utilized to assess the model's goodness-of-fit (Supplementary Table 6). The associations were performed in different subgroups of ischemic heart disease (yes or no), diabetes (yes or no) and hypertension (yes or no).

Data cleaning, missing value imputation, covariate screening, data modeling, prediction performance evaluation, and subgroup analysis were performed using R software v. 4.2.2 (R Foundation for Statistical Computing, Vienna, Austria). SAS 9.4 software (SAS Institute Inc., Cary, USA) was used for descriptive statistical analysis and sensitivity analysis. A p-value <0.05 was considered statistically significant for all analyses.

Results

Patients' characteristics

A flowchart of AIS patients is presented in Fig. 1. A total of 3,005 patients with AIS admitted to ICU were screened. Among them, 1,745 patients were excluded from the study, including 97 patients aged <18 years, 280 patients with an ICU stay of less than 24 h, 1,331 patients with missing sodium, potassium, chloride, bicarbonate, albumin, and AKI grade data, and 37 patients with a diagnosis of ESRD. The mean age of all patients was 67.70 ±13.38 years, with a median follow-up time of 2 (1, 4) days. Table 1 displays AIS patient characteristics with and without AKI. There were significant differences in age, weight, BMI, ICU type, cardiogenic shock, ischemic heart disease, diabetes, hypertension, vasopressor, ventilation, thrombolysis, antiplatelet therapy, heart rate, respiratory rate, WBC, hemoglobin, RDW, bilirubin, SCR, INR, albumin, BUN, glucose, AST, bicarbonate, and eGFR.

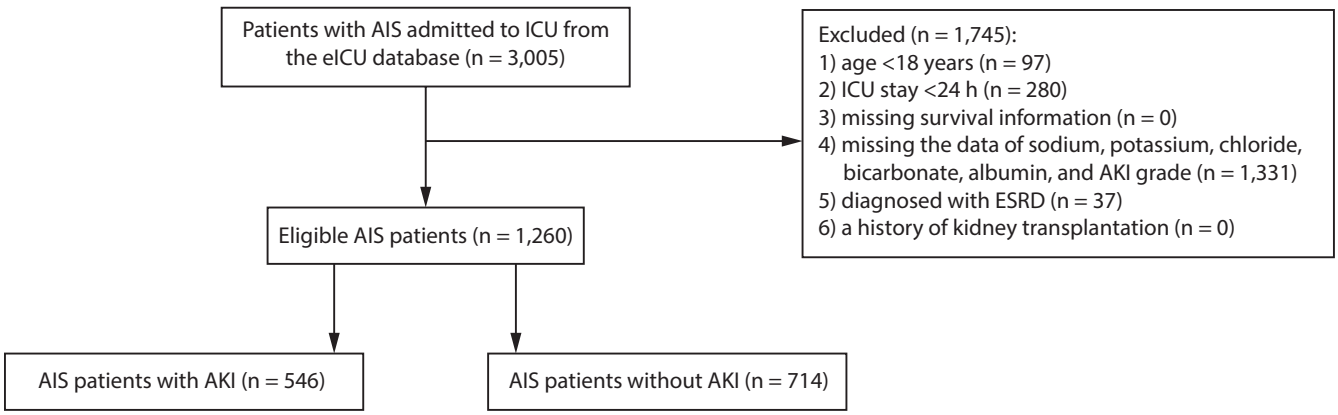

Fig. 1. The screening flowchart of acute ischemic stroke (AIS) patients

ICU – intensive care unit; AKI – acute kidney injury; ESRD – end-stage renal disease.

Table 1. Characteristics of patients with acute ischemic stroke (AIS)

Variables		Total (n = 1,260)	Non-AKI (n = 714)	AKI (n = 546)	Statistics	p-value
AG [mmol/L] mean ±SD		14.52 ±4.32	14.12 ±4.20	15.03 ±4.42	t = –3.73	<0.001
AG, n (%)	high-level (≥12.15 mmol/L)	880 (69.84)	463 (64.85)	417 (76.37)	χ^2 = 19.520	<0.001
	low-level (<12.15 mmol/L)	380 (30.16)	251 (35.15)	129 (23.63)		
ACAG [mmol/L], mean ±SD		16.84 ±4.32	16.23 ±4.14	17.65 ±4.41	t = –5.87	<0.001
ACAG, n (%)	high-level (≥15.075 mmol/L)	823 (65.32)	416 (58.26)	407 (74.54)	χ^2 = 36.193	<0.001
	low-level (<15.075 mmol/L)	437 (34.68)	298 (41.74)	139 (25.46)		
Age [years] mean ±SD		67.70 ±13.38	67.04 ±14.00	68.56 ±12.47	t = –2.03	0.043
Age, years, n (%)	<65	477 (37.86)	285 (39.92)	192 (35.16)	χ^2 = 2.969	0.085
	≥65	783 (62.14)	429 (60.08)	354 (64.84)		
Gender, n (%)	female	609 (48.33)	346 (48.46)	263 (48.17)	χ^2 = 0.010	0.918
	male	651 (51.67)	368 (51.54)	283 (51.83)		
Race, n (%)	African-American	124 (9.84)	72 (10.08)	52 (9.52)	χ^2 = 0.236	0.889
	Caucasian	982 (77.94)	557 (78.01)	425 (77.84)		
	other	154 (12.22)	85 (11.90)	69 (12.64)		
Height [cm], mean ±SD		168.99 ±11.57	169.46 ±10.67	168.37 ±12.63	t = 1.63	0.103
Weight [kg], mean ±SD		82.54 ±22.44	81.28 ±21.47	84.18 ±23.56	t = –2.25	0.025
BMI [kg/m^2], Me (Q1, Q3)		27.58 (24.08, 32.02)	27.31 (23.84, 31.09)	28.02 (24.52, 33.43)	Z = 2.815	0.005
BMI [kg/m^2], n (%)	<25	391 (31.03)	237 (33.19)	154 (28.21)	χ^2 = 8.652	0.013
	25–30	431 (34.21)	253 (35.43)	178 (32.60)		
	≥30	438 (34.76)	224 (31.37)	214 (39.19)		
ICU type, n (%)	CICU	114 (9.05)	50 (7.00)	64 (11.72)	χ^2 = 10.336	0.016
	NICU	440 (34.92)	266 (37.25)	174 (31.87)		
	SICU	72 (5.71)	42 (5.88)	30 (5.49)		
	other	634 (50.32)	356 (49.86)	278 (50.92)		
Cardiogenic shock, n (%)	no	1,250 (99.21)	712 (99.72)	538 (98.53)	–	0.024
	yes	10 (0.79)	2 (0.28)	8 (1.47)		
Ischemic heart disease, n (%)	no	964 (76.51)	593 (83.05)	371 (67.95)	χ^2 = 39.274	<0.001
	yes	296 (23.49)	121 (16.95)	175 (32.05)		
Diabetes, n (%)	no	1074 (85.24)	632 (88.52)	442 (80.95)	χ^2 = 14.065	<0.001
	yes	186 (14.76)	82 (11.48)	104 (19.05)		
Hypertension, n (%)	no	905 (71.83)	532 (74.51)	373 (68.32)	χ^2 = 5.867	0.015
	yes	355 (28.17)	182 (25.49)	173 (31.68)		
Vasopressor, n (%)	no	1137 (90.24)	675 (94.54)	462 (84.62)	χ^2 = 34.581	<0.001
	yes	123 (9.76)	39 (5.46)	84 (15.38)		
Ventilation, n (%)	no	959 (76.11)	619 (86.69)	340 (62.27)	χ^2 = 101.507	<0.001
	yes	301 (23.89)	95 (13.31)	206 (37.73)		
Thrombolysis, n (%)	no	874 (69.37)	467 (65.41)	407 (74.54)	χ^2 = 12.153	<0.001
	yes	386 (30.63)	247 (34.59)	139 (25.46)		
Thrombectomy, n (%)	no	1243 (98.65)	706 (98.88)	537 (98.35)	χ^2 = 0.648	0.421
	yes	17 (1.35)	8 (1.12)	9 (1.65)		
Antiplatelet, n (%)	no	1122 (89.05)	647 (90.62)	475 (87.00)	χ^2 = 4.157	0.041
	yes	138 (10.95)	67 (9.38)	71 (13.00)		
Anticoagulation, n (%)	no	1197 (95.00)	681 (95.38)	516 (94.51)	χ^2 = 0.496	0.481
	yes	63 (5.00)	33 (4.62)	30 (5.49)		
Antihypertension, n (%)	no	1056 (83.81)	604 (84.59)	452 (82.78)	χ^2 = 0.747	0.387
	yes	204 (16.19)	110 (15.41)	94 (17.22)		
Heart rate [bpm], mean ±SD		84.37 ±19.84	82.66 ±18.72	86.62 ±21.04	t = –3.48	<0.001
Respiratory rate [times/min], mean ±SD		19.07 ±4.99	18.72 ±4.54	19.54 ±5.50	t = –2.82	0.005

Table 1. Characteristics of patients with acute ischemic stroke (AIS) – cont.

Variables		Total (n = 1,260)	Non-AKI (n = 714)	AKI (n = 546)	Statistics	p-value
SBP [mm Hg], mean ±SD		146.38 ±28.94	147.32 ±27.46	145.14 ±30.74	t = 1.31	0.191
DBP [mm Hg], mean ±SD		80.47 ±19.45	81.10 ±18.36	79.64 ±20.78	t = 1.30	0.193
MAP [mm Hg], mean ±SD		102.44 ±20.03	103.18 ±18.91	101.47 ±21.40	t = 1.47	0.141
WBC [k/mcL], Me (Q_1, Q_3)		9.40 (7.30, 12.60)	8.82 (7.20, 11.20)	10.51 (7.60, 14.30)	Z = 6.075	<0.001
Platelets [K/mcL], Me (Q_1, Q_3)		218.50 (176.00, 267.50)	222.00 (180.00, 267.00)	215.00 (169.00, 269.00)	Z = –1.814	0.070
Hemoglobin [g/dL], mean ±SD		13.05 ±2.32	13.19 ±2.23	12.86 ±2.41	t = 2.44	0.015
RDW [%], mean ±SD		14.38 ±1.87	14.23 ±1.73	14.58 ±2.02	t = –3.22	0.001
Billirubin [mg/dL], Me (Q_1, Q_3)		0.60 (0.40, 0.80)	0.50 (0.40, 0.70)	0.60 (0.40, 0.90)	Z = 5.461	<0.001
SCR [mg/dL], Me (Q_1, Q_3)		0.97 (0.78, 1.27)	0.94 (0.76, 1.20)	1.00 (0.80, 1.40)	Z = 3.655	<0.001
INR, Me (Q_1, Q_3)		1.06 (1.00, 1.20)	1.00 (1.00, 1.10)	1.10 (1.00, 1.24)	Z = 7.382	<0.001
Albumin [g/dL], mean ±SD		3.47 ±0.61	3.56 ±0.58	3.35 ±0.63	t = 5.88	<0.001
BUN [mg/dL], Me (Q_1, Q_3)		18.00 (13.00, 25.00)	17.00 (13.00, 23.00)	19.00 (14.00, 28.00)	Z = 3.859	<0.001
Glucose [mg/dL], Me (Q_1, Q_3)		128.00 (105.00, 161.00)	121.00 (102.00, 148.00)	138.00 (110.00, 178.00)	Z = 6.165	<0.001
ALT [U/L], Me (Q_1, Q_3)		23.90 (17.00, 35.00)	24.00 (17.00, 34.00)	23.00 (17.00, 36.00)	Z = 0.016	0.987
AST [U/L], Me (Q_1, Q_3)		24.00 (18.00, 34.00)	23.00 (18.00, 31.00)	25.00 (19.00, 41.00)	Z = 5.088	<0.001
Sodium [mmol/L], mean ±SD		138.73 ±4.42	138.62 ±4.11	138.88 ±4.79	t = –1.01	0.313
Potassium [mmol/L], mean ±SD		4.03 ±0.57	4.00 ±0.51	4.06 ±0.64	t = –1.85	0.065
Chloride [mmol/L], mean ±SD		103.71 ±5.41	103.70 ±5.04	103.73 ±5.86	t = –0.11	0.916
Bicarbonate [mmol/L], mean ±SD		24.53 ±3.92	24.80 ±3.64	24.18 ±4.23	t = 2.75	0.006
eGFR [mL/min/1.7 3m^2], Me (Q_1, Q_3)		77.28 (56.89, 93.57)	80.58 (61.31, 95.81)	71.75 (52.34, 91.22)	Z = –4.525	<0.001
Status, n (%)	survival	1169 (92.78)	696 (97.48)	473 (86.63)	χ^2 = 54.348	<0.001
	dead	91 (7.22)	18 (2.52)	73 (13.37)		

t – statistics for t-test; Z – statistics of Wilcoxon–Mann–Whitney test; χ^2 – statistics for χ^2 test. These tests were used to compare the differences in characteristics between patients with acute kidney injury (AKI) and those without AKI. SD – standard deviation; Me – median; Q1 – 1st quartile; Q3– 3rd quartile; AG – anion gap; ACAG – albumin corrected anion gap; BMI – body mass index; CICU – cardiac intensive care unit; NICU – neuro intensive care unit; SICU – surgical intensive care unit; SBP – systolic blood pressure; DBP – diastolic blood pressure; MAP – mean arterial pressure; WBC – white blood cell count; RDW – red cell volume distribution width; SCR – serum creatinine; INR – international normalized ratio; BUN – blood urea nitrogen; ALT – alanine aminotransferase; AST – aspartate aminotransferase; eGFR – estimated glomerular filtration rate.

Association between AG and ACAG levels and the AKI risk in patients with AIS

The relationship between AG and ACAG levels and the risk of AKI in AIS patients is presented in Table 2. An elevated AG was associated with the AKI risk in patients with AIS (OR = 1.73, 95% CI: 1.32–2.29; p < 0.001), after adjustments for BMI, ischemic heart disease, ventilation, WBC, platelets, and albumin. A high level of ACAG was associated with the AKI risk in AIS patients (OR = 1.57, 95% CI: 1.21–2.04; p = 0.001), after adjustments for BMI, ischemic heart disease, ventilation, WBC, and platelets.

The predictive performance of AG and ACAG for the risk of AKI in AIS patients

Figure 2 shows the predictive performance of AG and ACAG concerning AKI risk in patients with AISs. The AUC for predicting the AKI risk was 0.558 (95% CI: 0.533–0.583) and 0.581 (95% CI: 0.556–0.607) for AG and ACAG, respectively (Table 3). Moreover, the predictive performance of ACAG was superior to that of AG (p = 0.024).

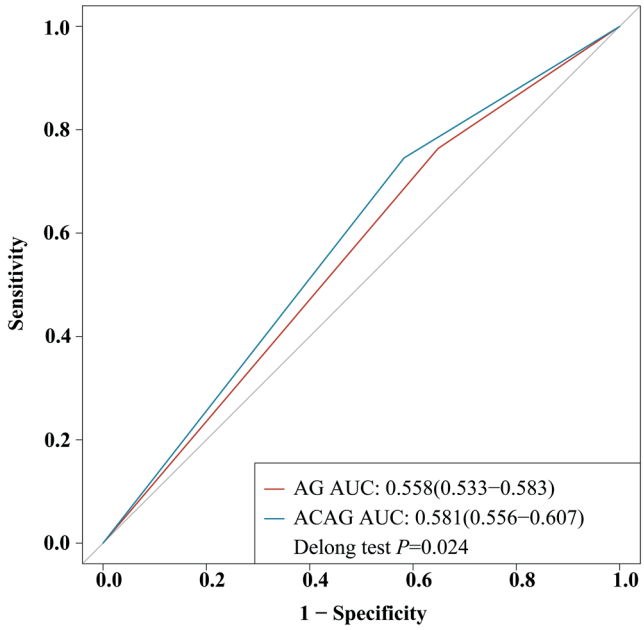

Fig. 2. The receiver operating characteristic (ROC) curves of AG and ACAG for predicting the risk of AKI in AIS patients

AG – anion gap; ACAG – albumin corrected anion gap; AKI – acute kidney injury; AIS – acute ischemic stroke; AUC – area under the curve

Table 2. Associations of AG and ACAG with the risk of AKI in AIS patients

Variables		Crude model		Model 1		Model 2	
		OR (95% CI)	p-value	OR (95% CI)	p-value	OR (95% CI)	p-value
AG	low-level	Ref.	–	Ref.	–	Ref.	–
	high-level	1.75 (1.37–2.25)	<0.001	1.57 (1.20–2.05)	0.001	1.73 (1.32–2.29)	<0.001
ACAG	low-level	Ref.	–	Ref.	–	–	–
	high-level	2.10 (1.65–2.68)	<0.001	1.57 (1.21–2.04)	0.001	–	–

OR – odd ratio; 95% CI – 95% confidence interval; AG – anion gap; ACAG – albumin corrected anion gap; AKI – acute kidney injury; AIS – acute ischemic stroke; AG levels (low-level (<12.15 mmol/L) and high-level (≥12.15 mmol/L)); ACAG levels (low-level (<15.075 mmol/L) and high-level (≥15.075 mmol/L)). Crude model – univariate model; Model 1 – adjusted for body mass index (BMI), ischemic heart disease, ventilation, white blood cells count (WBC), and platelets; Model 2 – adjusted for BMI, ischemic heart disease, ventilation, WBC, platelets, and albumin.

Table 3. The predictive performance of AG and ACAG for the AKI risk in patients with AIS

Variables	AG	ACAG
AUC (95% CI)	0.558 (0.533–0.583)	0.581 (0.556–0.607)
Accuracy (95% CI)	0.530 (0.502–0.558)	0.560 (0.532–0.587)
Specificity (95% CI)	0.352 (0.317–0.387)	0.417 (0.381–0.454)
Sensitivity (95% CI)	0.764 (0.728–0.799)	0.745 (0.709–0782)
PPV (95% CI)	0.474 (0.441–0.507)	0.495 (0.460–0.529)
NPV (95% CI)	0.661 (0.613–0.708)	0.682 (0.638–0726)

AG – anion gap; ACAG – albumin corrected anion gap; AKI – acute kidney injury; AIS – acute ischemic stroke; AUC – area under the curve; 95% CI – 95% confidence interval; PPV – positive predictive value; NPV – negative predictive value.

Association of ACAG with AKI in AIS patients based on ischemic heart disease, diabetes and hypertension

Further analyses were conducted to explore this association in AIS patients with regard to different subgroups of ischemic heart disease, diabetes and hypertension patients (Fig. 3). The results showed that the high ACAG levels were associated with the AKI risk in AIS patients without ischemic heart disease (OR = 1.60, 95% CI: 1.19–2.15), diabetes (OR = 1.58, 95% CI: 1.19–2.10) and hypertension (OR = 1.69, 95% CI: 1.24–2.30).

Discussion

We investigated the effects of AG and ACAG levels on AKI risk in AIS patients. Our findings showed that high AG and ACAG levels were associated with AKI risk in AIS patients. The performance of ACAG was superior to AG for predicting the risk of AKI. We also found that high levels of ACAG were associated with the AKI risk in AIS patients without ischemic heart disease, diabetes and hypertension.

The AG and ACAG are clinical indicators to evaluate acid-base imbalances, and high AG and ACAG levels indicate the occurrence of metabolic acidosis.[23,24] Previous studies have found that high levels of AG and ACAG were positively associated with poor outcomes in a variety of diseases, including AKI and AIS.[12,25–28] Jhou et al.[12] reported that an elevated AG was associated with poor outcomes and a higher in-hospital mortality risk in patients with AIS. Cheng et al.[25] found that an elevated AG was associated with increased short-term and long-term all-cause mortality in AKI patients. Zhao et al.[28] reported that a high level of ACAG was associated with the AKI risk in patients who were admitted to the ICU. However, the association of AG and ACAG levels with AKI risk in AIS patients remains unclear. In our study, we found that an elevated AG and ACAG were associated with AKI risk in patients with AIS. Our findings regarding the relationship between AG and ACAG and the risk of AKI in AIS patients are consistent with previous studies on AKI risk. The receiver operating characteristic (ROC) curve showed that both AG and ACAG could predict the AKI risk in AIS patients, and the predictive performance of ACAG was superior to AG. As mentioned earlier, ACAG is a more accurate predictor of metabolic acidosis in critically ill patients with hypoalbuminemia. Hu et al.[24] reported the association of high ACAG levels with the risk of 1-year mortality in critically ill patients with sepsis, and the predictive performance of ACAG was superior to AG.

We further evaluated the relationship between ACAG levels and AKI risk in different populations. Our study indicated that a high level of ACAG was associated with AKI risks in AIS patients without ischemic heart disease, diabetes and hypertension. The high ACAG levels were not associated with an increased AKI risk in AIS patients with ischemic heart disease, diabetes and hypertension. This reason may be that the values of acid-base imbalance markers change with the progression of the disease. Evidence suggests that ischemic heart disease, diabetes and hypertension can cause low serum albumin levels, hyperlactatemia and electrolyte disturbances, which may affect ACAG levels.[29–33] Dinh et al.[34] conducted a retrospective study that found ACAG to perform poorly in the diagnosis of hyperlactatemia.

The mechanism by which a high level of ACAG was associated with higher odds of AKI in patients with AIS may involve acid-base disorders. The kidneys are an important organ system for regulating acid-base balance, which mainly

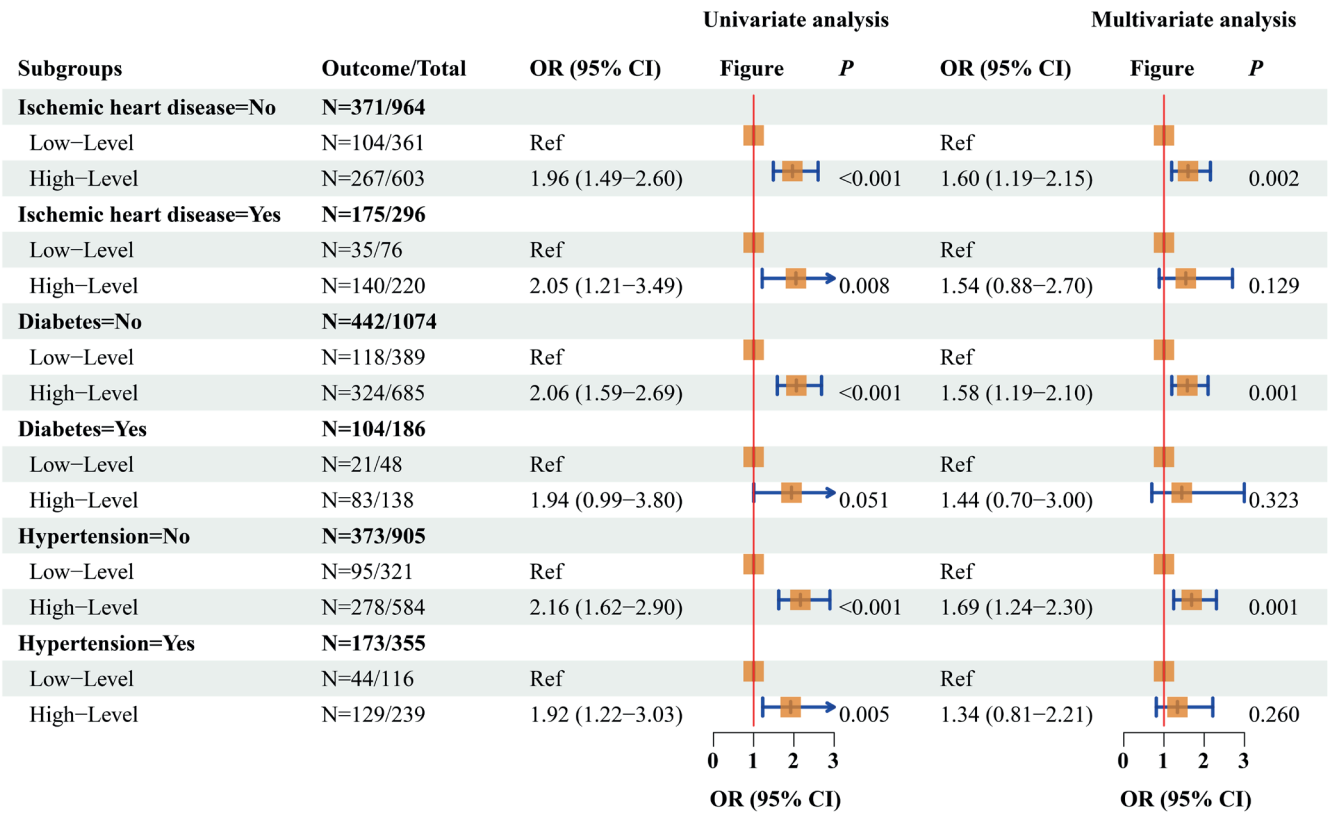

Fig. 3. Association between ACAG and AKI in AIS patients based on ischemic heart disease, diabetes and hypertension. Multivariate analysis adjusted for body mass index (BMI), ischemic heart disease (unadjusted for analysis of ischemic heart disease), ventilation, white blood cells count (WBC), and platelets

ACAG – albumin corrected anion gap; AKI – acute kidney injury; AIS – acute ischemic stroke. OR – odds ratio; 95% CI – 95% confidence interval.

promotes acid-base balance by maintaining bicarbonate homeostasis and acid excretion.[35] Acute kidney injury occurs in 9.62% of patients with ischemic stroke[4,36]; such patients are characterized by high SCR levels and kidney function impairments such as acid-base balance, electrolytes and fluids, and is associated with high mortality.[37,38] In addition, acid-base disorders and altered electrolyte concentrations are early biochemical responses in AIS, leading to continuous tissue oxidative damage and increased inflammation, further aggravating kidney injury and metabolic acidosis.[8]

Clinically, the ACAG level may be used as a potential prognostic indicator for the pre-bed management of AIS patients, which can help clinicians in the early identification of AIS patients with a high risk for AKI. This may provide certain references for risk stratification management and early intervention treatment of AIS patients.

Limitations

When interpreting our findings, it is important to consider the limitations of this retrospective cohort study. The database did not record AIS infarct size. This study highlights the relationship between AG and ACAG at ICU admission and AKI risk in AIS patients. However, the AG and ACAG at different time points were not explored due to the lack of data. Moreover, the association between dynamic changes in AG and ACAG levels during ICU admission and the risk of AKI is still not clear. Future well-designed prospective studies should be conducted to confirm our findings.

Conclusions

Our results demonstrated that high levels of AG and ACAG were linked to higher odds of AKI in AIS patients. In AIS patients, ACAG levels are a better predictor of AKI risk than AG. Monitoring ACAG levels before bed can help clinicians identify individuals at risk for AKI and intervene with treatment early.

Supplementary data

The Supplementary materials are available at https://doi.org/10.5281/zenodo.10851301. The package includes the following files:

Supplementary Table 1. Proportion of missing values for variables.

Supplementary Table 2. Comparison for the missing data before and after data interpolation.

Supplementary Table 3. The optimum subset of covariates and their coefficients screened using the ABESS method.

Supplementary Table 4. Multicollinearity test between variables using VIF.

Supplementary Table 5. The Box–Tidwell test for subsets of optimal covariates.

Supplementary Table 6. The Hosmer–Lemeshow test for the model goodness-of-fit.

Supplementary Fig. 1. Youden's J statistic for categorizing AG and ACAG levels.

Data availability

The datasets generated and/or analyzed during the current study are available from the corresponding author on reasonable request.

Consent for publication

Not applicable.

ORCID iDs

Haiqian Yao https://orcid.org/0000-0001-6028-1383
Jianan Tian https://orcid.org/0000-0002-8956-3031
Shi Cheng https://orcid.org/0000-0002-6215-7842

References

1. Phipps MS, Cronin CA. Management of acute ischemic stroke. *BMJ*. 2020;368:l6983. doi:10.1136/bmj.l6983
2. Feigin VL, Stark BA, Johnson CO, et al. Global, regional, and national burden of stroke and its risk factors, 1990–2019: A systematic analysis for the Global Burden of Disease Study 2019. *Lancet Neurol*. 2021; 20(10):795–820. doi:10.1016/S1474-4422(21)00252-0
3. Lewington AJP, Cerdá J, Mehta RL. Raising awareness of acute kidney injury: A global perspective of a silent killer. *Kidney Int*. 2013;84(3): 457–467. doi:10.1038/ki.2013.153
4. Zorrilla-Vaca A, Ziai W, Connolly Jr ES, Geocadin R, Thompson R, Rivera-Lara L. Acute kidney injury following acute ischemic stroke and intracerebral hemorrhage: A meta-analysis of prevalence rate and mortality risk. *Cerebrovasc Dis*. 2018;45(1–2):1–9. doi:10.1159/000479338
5. Yoo J, Hong JH, Lee SJ, et al. Acute kidney injury after endovascular treatment in patients with acute ischemic stroke. *J Clin Med*. 2020; 9(5):1471. doi:10.3390/jcm9051471
6. Qureshi AI, Aslam H, Zafar W, et al. Acute kidney injury in acute ischemic stroke patients in clinical trials. *Crit Care Med*. 2020;48(9):1334–1339. doi:10.1097/CCM.0000000000004464
7. Schricker S, Schanz M, Alscher MD, Kimmel M. Metabolic acidosis: Diagnosis and treatment [in German]. *Med Klin Intensivmed Notfmed*. 2020;115(4):275–280. doi:10.1007/s00063-019-0538-y
8. Martha SR, Fraser JF, Pennypacker KR. Acid–base and electrolyte changes drive early pathology in ischemic stroke. *Neuromol Med*. 2019;21(4):540–545. doi:10.1007/s12017-019-08555-5
9. Kraut JA, Madias NE. Serum anion gap: Its uses and limitations in clinical medicine. *Clin J Am Soc Nephrol*. 2007;2(1):162–174. doi:10.2215/CJN.03020906
10. Pratumvinit B, Lam L, Kongruttanachok N, et al. Anion gap reference intervals show instrument dependence and weak correlation with albumin levels. *Clin Chim Acta*. 2020;500:172–179. doi:10.1016/j.cca.2019.10.012
11. Figge J, Bellomo R, Egi M. Quantitative relationships among plasma lactate, inorganic phosphorus, albumin, unmeasured anions and the anion gap in lactic acidosis. *J Crit Care*. 2018;44:101–110. doi:10.1016/j.jcrc.2017.10.007
12. Jhou HJ, Chen PH, Yang LY, Chang SH, Lee CH. Plasma anion gap and risk of in-hospital mortality in patients with acute ischemic stroke: Analysis from the MIMIC-IV database. *J Pers Med*. 2021;11(10):1004. doi:10.3390/jpm11101004
13. Fu S, Wang Q, Chen W, Liu H, Li H. Development and external validation of a nomogram for predicting acute kidney injury in cardiogenic shock patients in intensive care unit. *Int J Gen Med*. 2022;15: 3965–3975. doi:10.2147/IJGM.S353697
14. Zhong L, Xie B, Ji XW, Yang XH. The association between albumin corrected anion gap and ICU mortality in acute kidney injury patients requiring continuous renal replacement therapy. *Intern Emerg Med*. 2022;17(8):2315–2322. doi:10.1007/s11739-022-03093-8
15. Pollard TJ, Johnson AEW, Raffa JD, Celi LA, Mark RG, Badawi O. The eICU Collaborative Research Database, a freely available multicenter database for critical care research. *Sci Data*. 2018;5(1):180178. doi:10.1038/sdata.2018.178
16. Huang X, Zhang Y. Relationship between serum bicarbonate levels and the risk of death within 30 days in ICU patients with acute ischemic stroke. *Front Neurol*. 2023;14:1125359. doi:10.3389/fneur.2023.1125359
17. Ge H, Liang Y, Fang Y, et al. Predictors of acute kidney injury in patients with acute decompensated heart failure in emergency departments in China. *J Int Med Res*. 2021;49(9):030006052110162. doi:10.1177/03000605211016208
18. He T, Li G, Xu S, Guo L, Tang B. Blood urea nitrogen to serum albumin ratio in the prediction of acute kidney injury of patients with rib fracture in intensive care unit. *Int J Gen Med*. 2022;15:965–974. doi:10.2147/IJGM.S348383
19. Li P, Shi L, Yan X, et al. Albumin corrected anion gap and the risk of in-hospital mortality in patients with acute pancreatitis: A retrospective cohort study. *J Inflamm Res*. 2023;16:2415–2422. doi:10.2147/JIR.S412860
20. Kellum JA, Lameire N; for the KDIGO AKI Guideline Work Group. Diagnosis, evaluation, and management of acute kidney injury: A KDIGO summary (Part 1). *Crit Care*. 2013;17(1):204. doi:10.1186/cc11454
21. Buuren SV, Groothuis-Oudshoorn K. MICE: Multivariate imputation by chained equations in R. *J Stat Soft*. 2011;45(3):1–67. doi:10.18637/jss.v045.i03
22. Zhu J, Wen C, Zhu J, Zhang H, Wang X. A polynomial algorithm for best-subset selection problem. *Proc Natl Acad Sci U S A*. 2020;117(52): 33117–33123. doi:10.1073/pnas.2014241117
23. Chen J, Dai C, Yang Y, et al. The association between anion gap and in-hospital mortality of post-cardiac arrest patients: A retrospective study. *Sci Rep*. 2022;12(1):7405. doi:10.1038/s41598-022-11081-3
24. Hu T, Zhang Z, Jiang Y. Albumin corrected anion gap for predicting in-hospital mortality among intensive care patients with sepsis: A retrospective propensity score matching analysis. *Clin Chim Acta*. 2021;521:272–277. doi:10.1016/j.cca.2021.07.021
25. Cheng B, Li D, Gong Y, Ying B, Wang B. Serum anion gap predicts all-cause mortality in critically Ill patients with acute kidney injury: Analysis of the MIMIC-III database. *Dis Markers*. 2020;2020:6501272. doi:10.1155/2020/6501272
26. Aydın SŞ, Aksakal E. Relationship between albumin-corrected anion gap and mortality in hospitalized heart failure patients. *Cureus*. 2023; 15(9):e45967. doi:10.7759/cureus.45967
27. Xu H, Xia J, Wang A, Zong L, An X, Sun X. Serum anion gap is associated with mortality in intensive care unit patients with diastolic heart failure. *Sci Rep*. 2023;13(1):16670. doi:10.1038/s41598-023-43928-8
28. Zhao X, Han J, Hu J, et al. Association between albumin-corrected anion gap level and the risk of acute kidney injury in intensive care unit. *Int Urol Nephrol*. 2023;56(3):1117–1127. doi:10.1007/s11255-023-03755-2
29. Arques S. Human serum albumin in cardiovascular diseases. *Eur J Intern Med*. 2018;52:8–12. doi:10.1016/j.ejim.2018.04.014
30. Oda E. Decreased serum albumin predicts hypertension in a Japanese health screening population. *Intern Med*. 2014;53(7):655–660. doi:10.2169/internalmedicine.53.1894
31. Ghionzoli N, Sciaccaluga C, Mandoli G, et al. Cardiogenic shock and acute kidney injury: The rule rather than the exception. *Heart Fail Rev*. 2021;26(3):487–496. doi:10.1007/s10741-020-10034-0
32. Gonçalves SEAB, Gonçalves TJM, Guarnieri A, Risegato RC, Guimarães MP, De Freitas DC. Association between thiamine deficiency and hyperlactatemia among critically ill patients with diabetes infected by SARS-CoV-2. *J Diabetes*. 2021;13(5):413–419. doi:10.1111/1753-0407.13156
33. Masharani U, Strycker LA, Lazar AA, Wu K, Brooks GA. Hyperlactatemia in diabetic ketoacidosis. *Diabet Med*. 2022;39(4):e14723. doi:10.1111/dme.14723

34. Dinh CH, Ng R, Grandinetti A, Joffe A, Chow DC. Correcting the anion gap for hypoalbuminaemia does not improve detection of hyperlactataemia. *Emerg Med J*. 2006;23(8):627–629. doi:10.1136/emj.2005.031898
35. Wagner CA, Imenez Silva PH, Bourgeois S. Molecular pathophysiology of acid-base disorders. *Semin Nephrol*. 2019;39(4):340–352. doi:10.1016/j.semnephrol.2019.04.004
36. Arnold J, Ng KP, Sims D, Gill P, Cockwell P, Ferro C. Incidence and impact on outcomes of acute kidney injury after a stroke: A systematic review and meta-analysis. *BMC Nephrol*. 2018;19(1):283. doi:10.1186/s12882-018-1085-0
37. Orieux A, Boyer A, Dewitte A, Combe C, Rubin S. Acute kidney injury in intensive care unit: A review [in French]. *Nephrol Ther*. 2022;18(1):7–20. doi:10.1016/j.nephro.2021.07.324
38. Albeladi F. Essence core: Fluid management in acute kidney injury. *Saudi J Kidney Dis Transpl*. 2021;32(1):9. doi:10.4103/1319-2442.318552

Serum HMGB1 as a predictor for postoperative delirium in elderly patients undergoing total hip arthroplasty surgery

Yan Zou[1,A,D–E], Yuan Wu[2,B,C], An Wei[3,B,C], Hao Nie[1,B,D], Shan Hui[1,C], Cuizhong Liu[2,C], Tingzhi Deng[1,A,E,F]

[1] Department of Geriatrics, Hunan Provincial People's Hospital (The First Affiliated Hospital of Hunan Normal University), Changsha, China
[2] Department of General Medicine, Hunan Provincial People's Hospital (The First Affiliated Hospital of Hunan Normal University), Changsha, China
[3] Department of Ultrasound, Hunan Provincial People's Hospital (The First Affiliated Hospital of Hunan Normal University), Changsha, China

A – research concept and design; B – collection and/or assembly of data; C – data analysis and interpretation;
D – writing the article; E – critical revision of the article; F – final approval of the article

Advances in Clinical and Experimental Medicine, ISSN 1899–5276 (print), ISSN 2451–2680 (online) *Adv Clin Exp Med*. 2025;34(3):361–368

Address for correspondence
Tingzhi Deng
E-mail: TingzhiDeng@163.com

Funding sources
None declared

Conflict of interest
None declared

Received on July 17, 2023
Reviewed on March 23, 2024
Accepted on May 23, 2024

Published online on August 29, 2024

Abstract

Background. Postoperative delirium (POD) is an acute mental disorder that occurs after surgery requiring general anesthesia. In animal studies, high-mobility group box 1 (HMGB1) plays a key role in mediating postoperative neuroinflammation and may have a direct impact on POD.

Objectives. The objective of this prospective observational study was to investigate the serum levels of HMGB1 in elderly POD patients undergoing total hip arthroplasty.

Materials and methods. This prospective observational study included 287 elderly patients who underwent total hip arthroplasty in our hospital from October 2019 to September 2022. Patients were assessed for the presence of POD using the Confusion Assessment Method (CAM) within 72 h of surgery. Serum HMGB1, interleukin (IL)-6, IL-1β, tumor necrosis factor alpha (TNF-α), and C-reactive protein (CRP) levels were measured using enzyme-linked immunosorbent assay (ELISA) before surgery, as well as at 24 h, 48 h and 72 h after surgery. Demographic and clinical data of all elderly patients were collected.

Results. The anesthesia time and surgical time in the POD group were significantly higher than those in the non-POD group. The serum levels of HMGB1, IL-6 and IL-1β in the POD group were significantly elevated compared to those in the non-POD group at all time points after surgery ($p < 0.05$). In addition, the serum levels of HMGB1 were positively correlated with TNF-α, IL-6 and IL-1β levels. HMGB1, IL-6 and IL-1β could be potential predictive biomarkers for the occurrence of POD in elderly patients undergoing total hip arthroplasty. Finally, we found that anesthesia time, surgical time, HMGB1, TNF-α, IL-6, and IL-1β were risk factors for POD in elderly patients undergoing total hip arthroplasty.

Conclusions. Serum HMGB1 levels were markedly elevated in elderly POD patients undergoing total hip arthroplasty. In addition, HMGB1 could serve as a potential predictive biomarker for POD in elderly patients undergoing total hip arthroplasty.

Key words: cytokines, prognosis, HMGB1, total hip arthroplasty, postoperative delirium

Cite as
Yan Zou Y, Wu Y, Wei A, et al. Serum HMGB1 as a predictor for postoperative delirium in elderly patients undergoing total hip arthroplasty surgery. *Adv Clin Exp Med*. 2025;34(3):361–368. doi:10.17219/acem/189227

DOI
10.17219/acem/189227

Background

Postoperative delirium (POD) is an acute mental disorder that manifests as confusion, cognitive dysfunction and reduced attention following general anesthesia surgery. It typically occurs within 24 to 72 h after surgery.[1,2] Elderly individuals, aged 65 years or older, are particularly susceptible to developing POD, with the risk increasing by 1.15 times for each additional year of age.[3] Postoperative delirium is considered the most common surgical complication in elderly hip fracture patients, which significantly affects the postoperative recovery of patients and increases hospitalization time and costs.[4,5] Therefore, there is a pressing need for early preventive strategies and comprehensive care for elderly patients at risk of developing POD.

Postoperative delirium is associated with metabolic disorders, oxidative stress and inflammatory responses within the nervous system.[6–8] High-mobility group box 1 (HMGB1) is a DNA-binding protein that is highly abundant within the nuclei of eukaryotic cells and is involved in a variety of physiopathological responses, including inflammation and oxidative stress.[9,10] The activation of immune cells and subsequent inflammatory responses can be induced by HMGB1.[11] Moreover, elevated levels of HMGB1 have been linked to poor prognoses in various inflammatory diseases and cancers.[12,13] In addition, in animal studies, HMGB1 plays a key role in mediating postoperative neuroinflammation and may have a direct impact on POD.[14] However, there is a dearth of clinical research exploring the specific involvement of HMGB1 in the development of POD in elderly patients undergoing total hip arthroplasty.

Objectives

The objective of this prospective observational research was to investigate the serum levels of HMGB1 in elderly POD patients undergoing total hip arthroplasty. Our study aims to shed light on the clinical significance of HMGB1 in elderly POD patients.

Methods

Patients

This prospective observational study included 287 elderly patients who underwent total hip arthroplasty in Hunan Provincial People's Hospital (The First Affiliated Hospital of Hunan Normal University; Changsha, China) from October 2019 to September 2022. The inclusion criteria for the patients were: 1) age over 65; 2) American Society of Anesthesiologists (ASA) grade I–III) planned unilateral total hip arthroplasty under spinal anesthesia. The exclusion criteria were: 1) patients with a Mini-Mental State Examination (MMSE) score ≤23 before surgery; 2) patients with a history of severe mental or neurological illness; 3) patients with severe infection, cardiac, hepatic, renal insufficiency, or malignancy; 4) patients with severe complications during or after surgery; and 5) patients treated with anti-inflammatory or immunosuppressive drugs before surgery. All patients received anesthesia, total hip arthroplasty and postoperative care from the same team in our hospital. Patients were assessed for the presence of POD using the Confusion Assessment Method (CAM)[15] within 72 h of surgery. The CAM includes 4 aspects: 1) acute onset of cognitive changes, 2) inattention, 3) disorganized thinking, and 4) altered level of consciousness. If the patient demonstrates a positive reaction to 1, 2 and either 3 or 4 during the assessment, they are considered to have delirium at that particular time point. For the POD diagnosis, the same anesthesiologist evaluated the participant twice daily on postoperative days 1–3. This study received ethical approval from the ethics committee of Hunan Provincial People's Hospital (The First Affiliated Hospital of Hunan Normal University; approval No. Scientific Research 2023-29). Written informed consent was obtained from all participants.

Blood sampling measurement

Serum levels of HMGB1, interleukin (IL)-6, IL-1β, tumor necrosis factor alpha (TNF-α), and C-reactive protein (CRP) were assessed using the enzyme-linked immunosorbent assay (ELISA) method. Within 24 h of admission, fasting vena cava blood samples (5 mL) were collected from the patients for analysis and centrifuged at 2000 g for 15 min and tested according to a commercially available kit (HMGB1 MBS3803280, IL-6 MBS175877, IL-1β MBS3803011, TNF-α MBS824943, and CRP MBS8123937; MyBioSource, San Diego, USA). The serum biomarker levels were measured in all patients before surgery, as well as at 24 h, 48 h and 72 h after surgery.

Data collection and scale scoring

Before the operation, the clinical and demographic data of all elderly patients were collected, including age, gender, body mass index (BMI), comorbidities (hypertension, diabetes, coronary heart disease), diastolic blood pressure (DBP), systolic blood pressure (SBP), and ASA classification. In addition, we also recorded the surgical time, anesthesia time and intraoperative blood loss of all patients.

Statistical analyses

All statistical analyses were conducted using IBM SPSS v. 26.0 (IBM Corp., Armonk, USA). Normally distributed data were presented as means ± standard deviations (±SD), while non-normally distributed data were presented as medians (interquartile ranges (IQR)). To compare differences between the 2 study groups, the Mann–Whitney test, Student's t-test or χ^2 test was utilized. The probability of a type 1 error was

not controlled, and inferences about statistical significance may be unreliable. Pearson's correlation analysis was employed to assess the relationship between serum biomarkers. Linear discriminant analysis (LDA) was used to classify whether elderly patients undergoing total hip arthroplasty would develop POD. Receiver operating characteristic (ROC) curve analysis was performed to evaluate the predictive value of HMGB1 in POD. Additionally, we established binary logistic regression models to identify risk factors for POD. We conducted Box–Tidwell tests to assess the linear relationship between the predictor variables and the logit of the response variables. Furthermore, variance inflation factor (VIF) tests were performed to examine the presence of multicollinearity among variables. Additionally, Cook's distance test has been utilized to identify any extreme outliers. A p-value <0.05 was regarded as a significant difference.

Results

The clinical profiles of all enrolled individuals

Our prospective observational study included 287 elderly patients who underwent total hip arthroplasty surgery, and all patients were classified into a POD group (n = 83) or a non-POD group (n = 204) according to the CAM scale performed 72 h postoperatively. Compared to the non-POD group, the anesthesia time and surgical time in the POD group were remarkably increased (Table 1, $p < 0.05$). No significant differences were found between the 2 groups in terms of age, gender, BMI, SBP, DBP, comorbidities, ASA classification, and intraoperative blood loss.

Dynamic changes of HMGB1 and cytokines in the postoperative

Subsequently, we examined the serum HMGB1, IL-6, IL-1β, CRP, and TNF-α levels of all study participants before surgery, as well as at 24, 48 and 72 h after surgery. According to Fig. 1, the serum HMGB1, IL-6, IL-1β, CRP, and TNF-α levels in elderly patients undergoing total hip arthroplasty were significantly elevated in the first 24 h after surgery, followed by a gradual decline. The serum levels of HMGB1 and IL-1β in the POD group were markedly elevated compared to those in the non-POD group at all time points after surgery ($p < 0.05$), although there were no significant differences in the serum levels of these biomarkers before surgery. Furthermore, we conducted Pearson's correlation analysis on the serum levels of HMGB1 and inflammatory factors 24 h after surgery and found that the serum HMGB1 levels were positively correlated with IL-1β and IL-6 levels (Table 2, $p < 0.05$). This suggested an association between the patient's serum IL-1β, IL-6 and HMGB1 levels at 24 h postoperatively.

Predictive value of HMGB1 for POD in elderly patients undergoing total hip arthroplasty

We performed LDA to classify whether elderly patients undergoing total hip arthroplasty would develop POD using significantly different serum cytokines (HMGB1, IL-6, IL-1β, and TNF-α) as independent variables. The results, as shown in Table 3, demonstrated that the LDA achieved a sensitivity of 75.9%, specificity of 79.9% and

Table 1. Demographic and clinical data of all study participants

Variable	POD group (n = 83)	non-POD group (n = 204)	p-value
Age [years]	76 (12)	77 (12)	0.275
Sex, female (%)	45 (54.22)	117 (57.35)	0.679
BMI [kg/m^2]	25.35 ±2.18	25.34 ±2.31	0.996
SBP [mm Hg]	123.03 ±13.60	120.68 ±14.41	0.204
DBP [mm Hg]	76.63 ±8.23	77.31 ±8.51	0.536
History of disease			
Hypertension, n (%)	38 (45.78)	89 (43.63)	0.760
Diabetes, n (%)	15 (18.07)	31 (15.20)	0.586
Coronary heart disease, n (%)	19 (22.89)	33 (16.18)	0.231
ASA classification	2 (2)	2 (2)	0.991
Surgical time [min]	152.49 ±17.47	135.65 ±15.88	<0.001
Anesthesia time [min]	176.60 ±21.63	155.32 ±18.22	<0.001
Intraoperative blood loss [mL]	31.23 ±6.50	31.38 ±6.25	0.851

POD – postoperative delirium; BMI – body mass index; SBP – systolic blood pressure; DBP – diastolic blood pressure; ASA – American Society of Anesthesiologists. Continuous data presented non-normal distribution (age and ASA classification) were expressed as median (interquartile range (IQR)) and analyzed with Mann–Whitney U test. Continuous data presented normal distribution (BMI, SBP, DBP, surgical time, anesthesia time, and intraoperative blood loss) were expressed by mean ±standard deviation (±SD) and analyzed using Student's t-test, while χ^2 test was used for comparing rates (sex and history of disease).

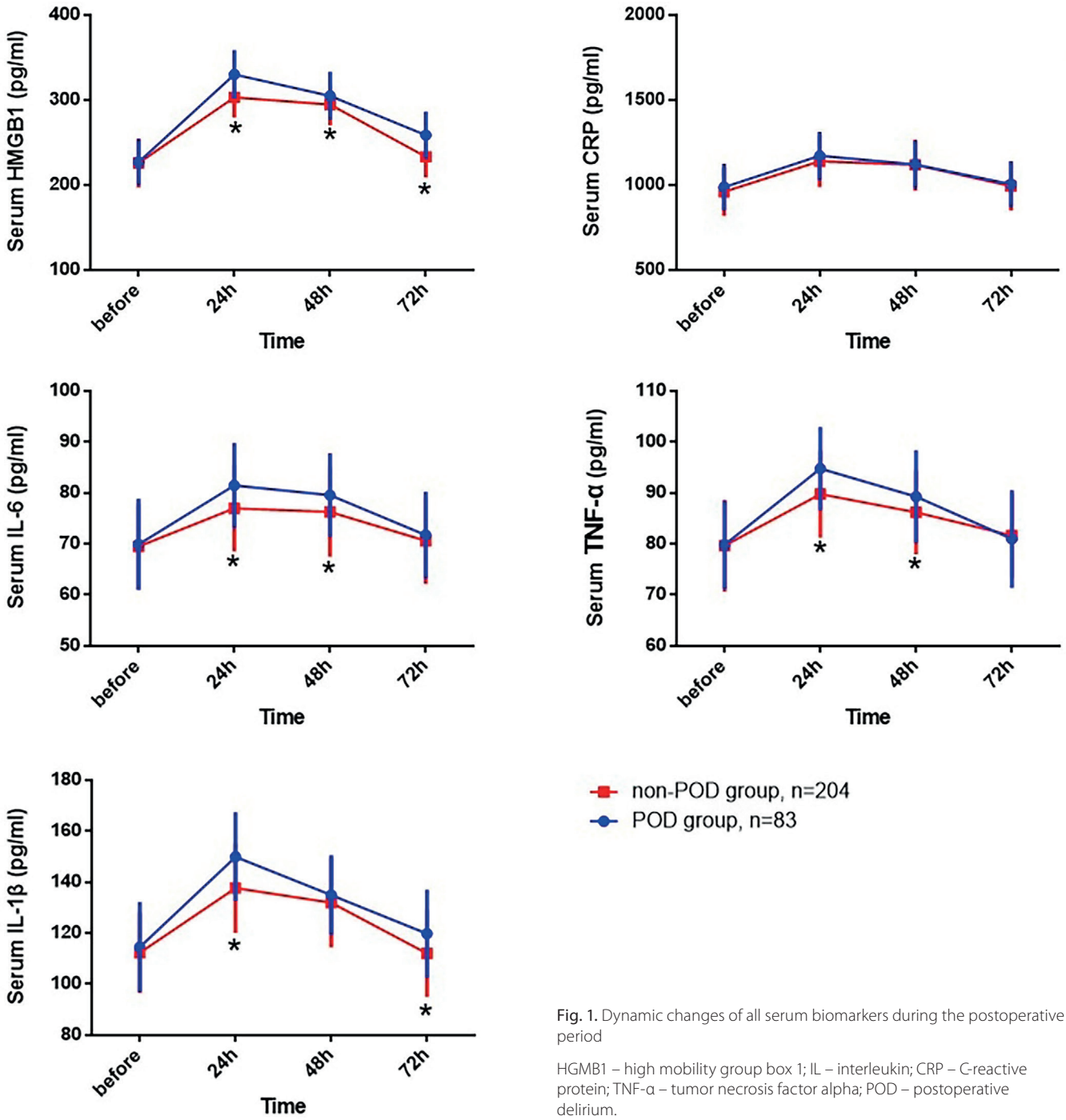

Fig. 1. Dynamic changes of all serum biomarkers during the postoperative period

HGMB1 – high mobility group box 1; IL – interleukin; CRP – C-reactive protein; TNF-α – tumor necrosis factor alpha; POD – postoperative delirium.

accuracy of 78.7% in the classification. To further evaluate the classification performance of LDA for POD in elderly patients undergoing total hip arthroplasty and assess the predictive value of HMGB1 and inflammatory factors for POD, we conducted a ROC curve analysis. The results showed that HMGB1, IL-6 and IL-1β could be potential predictive biomarkers for the occurrence of POD in elderly patients undergoing total hip arthroplasty, with HMGB1 showing a better diagnostic value (Fig. 2). The AUC of HMGB1 was 0.789, the cutoff value was 319.2 pg/mL, the sensitivity was 75.90%, and the specificity was 67.16%. This suggested that based on these cytokine levels, it might be possible to predict the occurrence of POD in elderly patients undergoing total hip arthroplasty.

Risk factors of POD in elderly patients undergoing total hip arthroplasty

We conducted a logistic regression analysis using the enter method to identify risk factors for POD in elderly patients undergoing total hip arthroplasty. We used 2 models: Model 1 including demographic and clinical data (age, sex, BMI, SBP, DBP, ASA classification, surgery

Table 2. Correlation analysis among HMGB1, TNF-α, IL-6, IL-1β, and CRP

Variables		HMGB1	CRP	IL-6	IL-1β	TNF-α
HMGB1	Pearson's correlation	1	–0.001	0.136	0.221	0.089
	p-value	–	0.988	0.021	<0.001	0.132
CRP	Pearson's correlation	–0.001	1	0.066	0.060	0.090
	p-value	0.988	–	0.267	0.315	0.129
IL-6	Pearson's correlation	0.136	0.066	1	–0.003	0.026
	p-value	0.021	0.267	–	0.956	0.656
IL-1β	Pearson's correlation	0.221	0.060	–0.003	1	0.123
	p-value	<0.001	0.315	0.956	–	0.038
TNF-α	Pearson's correlation	0.089	0.090	0.026	0.123	1
	p-value	0.132	0.129	0.656	0.038	–

HMGB1 – high-mobility group box 1; IL – interleukin; TNF-α – tumor necrosis factor alpha; CRP-C –reactive protein. Pearson's correlation analysis was employed to assess the relationship between serum biomarkers.

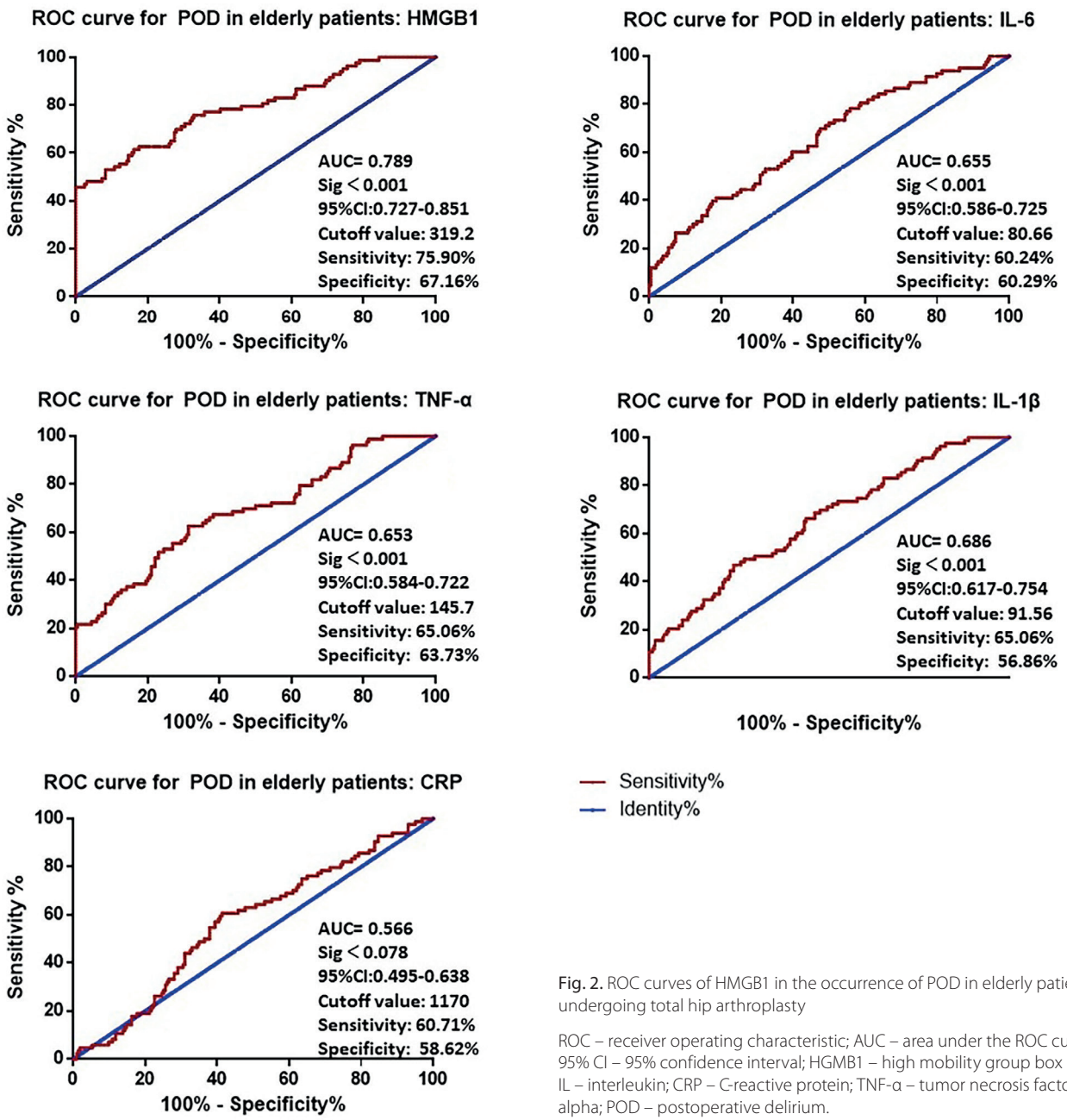

Fig. 2. ROC curves of HMGB1 in the occurrence of POD in elderly patients undergoing total hip arthroplasty

ROC – receiver operating characteristic; AUC – area under the ROC curve; 95% CI – 95% confidence interval; HGMB1 – high mobility group box 1; IL – interleukin; CRP – C-reactive protein; TNF-α – tumor necrosis factor alpha; POD – postoperative delirium.

Table 3. Linear discriminant analysis for classify patients with postoperative delirium (POD)

Statistical method	Accuracy (%)	Error (%)	Sensitivity (%)	Specificity (%)
LDA	78.7	21.3	75.9	79.9

LDA – linear discriminant analysis.

Table 4. Logistic regression for POD in elderly patients undergoing total hip arthroplasty

Variables	Wald	OR	95% CI	p-value
Age	0.957	1.023	0.977–1.071	0.328
Sex	0.386	1.230	0.640–2.361	0.535
BMI	0.174	1.031	0.893–1.190	0.677
SBP	1.286	0.987	0.964–1.010	0.257
DBP	0.244	1.009	0.972–1.048	0.621
ASA classification	0.119	1.073	0.718–1.605	0.731
Intraoperative blood loss	0.008	0.998	0.947–1.051	0.927
Anesthesia time	32.653	0.950	0.934–0.967	<0.001
Surgical time	30.787	0.942	0.922–0.962	<0.001
HMGB1	40.774	0.954	0.940–0.968	<0.001
CRP	1.467	0.999	0.996–1.001	0.266
IL-6	12.601	0.923	0.883–0.965	<0.001
IL-1β	12.130	0.964	0.944–0.984	<0.001
TNF-α	15.898	0.914	0.874–0.955	<0.001

POD – postoperative delirium; OR – odds ratio; 95% CI – 95% confidence interval; BMI – body mass index; SBP – systolic blood pressure; DBP – diastolic blood pressure; ASA – American Society of Anesthesiologists; HMGB1 – high-mobility group box 1; IL – interleukin; TNF-α – tumor necrosis factor alpha; CRP-C – reactive protein.

time, anesthesia time, and intraoperative blood loss), with the results of the Hosmer–Lemeshow test (p = 0.100) and Nagelkerke R^2 (0.435) showing a well goodness of fit. Model 2 including cytokines (HMGB1, TNF-α, CRP, IL-6, and IL-1β), with the results of the Hosmer–Lemeshow test (p = 0.261), and Nagelkerke R^2 (0.510) and showed a well goodness of fit. Both models satisfied the assumptions of logistic regression, including the presence of a linear relationship between the predictor variables and the logarithm of the response variables, the absence of multicollinearity among variables and the absence of extreme outliers. The results showed that anesthesia time, surgical time, HMGB1, IL-1β, IL-6, and TNF-α were risk factors for POD in elderly patients undergoing total hip arthroplasty (Table 4).

Discussion

The occurrence of POD has significant implications for patient outcomes and prognosis. In severe cases, it can even pose a life-threatening risk. As a result, experts increasingly recommend the implementation of systematic interventions through various approaches to reduce the incidence and duration of delirium. Therefore, predicting elderly patients who are at risk of developing POD in advance and intervening is of great significance.[16,17] In this research, we investigated serum biomarkers for predicting POD and found that the serum level of HMGB1 24 h after surgery can be used to predict the occurrence of POD in elderly patients undergoing total hip arthroplasty.

Postoperative patients often experience a massive release of inflammatory mediators in the body, such as cytokines, inflammatory cells and immune cells, all of which can pass through the blood-brain barrier to trigger an inflammatory response that causes toxic effects on neurons, resulting in the occurrence of POD.[18,19] A growing body of research has demonstrated a strong association between the inflammatory state of patients after surgery and the development of POD. Zhang et al. showed that serum levels of IL-6, CRP and TNF-α in POD patients increased significantly early after surgery, and gradually decreased on the 3rd day after surgery, which is consistent with our research results.[20] Other evidence also suggested that high preoperative plasma IL-6 levels were significantly correlated with the onset of POD.[21] In addition, a meta-analysis indicated that IL-6 appears to be a consistent predictor of delirium in surgical samples, while CRP cannot predict the occurrence of delirium in patients after surgery.[22] Interestingly, another meta-analysis confirmed that early postoperative CRP levels in POD patients were substantially increased compared to non-POD patients and could predict the onset of POD. The results in Fig. 1 showed that postoperative serum IL-1β and IL-6 levels in POD patients were significantly elevated compared to non-POD patients, with no

significant difference in CRP levels. The different results of these studies may be related to the age of the study participants, sample size and the time of serum collection.

High-mobility group box 1 can activate inflammatory cells and promote the release of inflammatory mediators such as IL-6 and IL-1β by binding to Toll-like receptors (TLR) 2, 4 and 9.[23] Additionally, HMGB1 can also activate the NF-κB signaling pathway, further promoting the occurrence and progression of inflammation.[24] Therefore, we analyzed the correlation between serum HMGB1 and inflammatory factor levels in elderly patients undergoing total hip arthroplasty. The results in Table 2 showed that serum HMGB1 levels were positively correlated with IL-6 and IL-1β, which is consistent with the results of Kim et al.,[25] Kamiya et al.[26] and Huo et al.[27] We further analyzed the difference in serum HMGB1 levels between POD patients and non-POD patients and found that serum HMGB1 levels were significantly elevated in POD patients (Fig. 1). This may be related to the upregulation of HMGB1, which can promote neuroinflammation and enhance cognitive impairment in related brain diseases.[28] In addition, as shown in Fig. 2, our study also revealed that HMGB1 can serve as a potential predictive biomarker for POD in elderly patients undergoing total hip arthroplasty, suggesting a potential underlying association between HMGB1 and the occurrence of POD. It has been reported that HMGB1 disrupts the blood–brain barrier and releases pro-inflammatory cytokines, which in turn impairs synaptic plasticity and disrupts memory formation and maintenance, leading to postoperative cognitive dysfunction.[29] Furthermore, evidence suggests that the inhibition of HMGB1-related signaling pathways can mediate hippocampal neuroinflammation and regulate M1/M2 polarization, thereby providing neuroprotective effects.[30] These studies elucidate the specific mechanisms underlying the association between HMGB1 and POD. Additionally, in Table 4, logistic regression analysis demonstrated that increased postoperative serum HMGB1 levels are a risk factor for POD, implying that HMGB1 may serve as a novel therapeutic target for POD. This possibility has already been explored in animal studies, such as by Li et al., who showed that the downregulation of HMGB1 may activate new protective measures, preventing delayed neurocognitive recovery after challenges such as anesthesia and surgery.28 Other evidence indicates that HMGB1 mediates postoperative neuroinflammation and may have a direct impact on POD and cognitive dysfunction[14] while inhibiting the HMGB1/RAGE/TLR4 signaling pathway could emerge as a potential novel therapeutic approach for mitigating HMGB1-induced neuroinflammation, seizures and cognitive impairment.[31]

Limitations

This study has some limitations. First, the sample size was relatively small. Second, our analysis assessed only a small number of inflammatory factors, which may have excluded other potentially relevant variables. Third, the probability of type 1 errors was not controlled, and inferences about statistical significance may be unreliable. Lastly, the molecular mechanisms underlying the involvement of HMGB1 in POD development remain unclear and warrant further investigation.

Conclusions

Our results suggested that the serum HMGB1 levels were markedly enhanced in elderly POD patients undergoing total hip arthroplasty. In addition, HMGB1 could serve as a potential predictive biomarker for POD in elderly patients undergoing total hip arthroplasty. This study may provide new targets and a comprehensive approach for treating elderly patients with POD.

Supplementary data

The Supplementary materials are available at https://doi.org/10.5281/zenodo.11093429. The package includes the following files:

Supplementary Table 1. Data distribution.

Supplementary Table 2. SPSS output for homogeneity of variance teste and Student t-test.

Supplementary Table 3. SPSS output for paired sample t-test.

Supplementary Table 4. SPSS output for Student t-test bootstrap.

Supplementary Table 5. The assumptions of the LDA.

Supplementary Table 6. The assumptions of logistic regression.

Supplementary Table 7. SPSS output for logistic regression analysis.

Supplementary Fig. 1. Scatter plots of Pearson correlation.

Data availability

The datasets generated and/or analyzed during the current study are available from the corresponding author on reasonable request.

Consent for publication

Not applicable.

ORCID iDs

Yan Zou https://orcid.org/0009-0006-0176-1292
Yuan Wu https://orcid.org/0009-0006-1403-2304
An Wei https://orcid.org/0009-0001-3109-4316
Hao Nie https://orcid.org/0009-0005-8983-526X
Shan Hui https://orcid.org/0009-0004-8302-504X
Cuizhong Liu https://orcid.org/0009-0001-0633-3282
Tingzhi Deng https://orcid.org/0009-0007-2887-7647

References

1. Deiner S, Silverstein JH. Postoperative delirium and cognitive dysfunction. *Br J Anaesth*. 2009;103:i41–i46. doi:10.1093/bja/aep291
2. Duning T, Ilting-Reuke K, Beckhuis M, Oswald D. Postoperative delirium: Treatment and prevention. *Curr Opin Anaesth*. 2021;34(1):27–32. doi:10.1097/ACO.0000000000000939
3. Wang Y, Shen X. Postoperative delirium in the elderly: The potential neuropathogenesis. *Aging Clin Exp Res*. 2018;30(11):1287–1295. doi:10.1007/s40520-018-1008-8
4. Ho M, Nealon J, Igwe E, et al. Postoperative delirium in older patients: A systematic review of assessment and incidence of postoperative delirium. *Worldviews Evid Based Nurs*. 2021;18(5):290–301. doi:10.1111/wvn.12536
5. O'Regan NA, Law TW, Dunne D, et al. Delirium in older postoperative hip fracture patients. *Hip Int*. 2013;23(4):424–425. doi:10.5301/hipint.5000067
6. Zhang J, Gao J, Guo G, et al. Anesthesia and surgery induce delirium-like behavior in susceptible mice: The role of oxidative stress. *Am J Transl Res*. 2018;10(8):2435–2444. PMID:30210682. PMCID: PMC6129548.
7. Guo Y, Li Y, Zhang Y, et al. Post-operative delirium associated with metabolic alterations following hemi-arthroplasty in older patients. *Age Ageing*. 2020;49(1):88–95. doi:10.1093/ageing/afz132
8. Noah AM, Almghairbi D, Evley R, Moppett IK. Preoperative inflammatory mediators and postoperative delirium: Systematic review and meta-analysis. *Br J Anaesth*. 2021;127(3):424–434. doi:10.1016/j.bja.2021.04.033
9. Zhang H, Ding L, Shen T, Peng D. HMGB1 involved in stress-induced depression and its neuroinflammatory priming role: A systematic review. *Gen Psych*. 2019;32(4):e100084. doi:10.1136/gpsych-2019-100084
10. Yu Y, Tang D, Kang R. Oxidative stress-mediated HMGB1 biology. *Front Physiol*. 2015;6:93. doi:10.3389/fphys.2015.00093
11. Lee W, Ku S, Yoo H, Song K, Bae J. Andrographolide inhibits HMGB 1-induced inflammatory responses in human umbilical vein endothelial cells and in murine polymicrobial sepsis. *Acta Physiol*. 2014;211(1):176–187. doi:10.1111/apha.12264
12. Cámara-Quílez M, Barreiro-Alonso A, Rodríguez-Bemonte E, Quindós-Varela M, Cerdán ME, Lamas-Maceiras M. Differential characteristics of HMGB2 versus HMGB1 and their perspectives in ovary and prostate cancer. *Curr Med Chem*. 2020;27(20):3271–3289. doi:10.2174/0929867326666190123120338
13. Fang J, Ge X, Xu W, et al. Bioinformatics analysis of the prognosis and biological significance of HMGB1, HMGB2, and HMGB3 in gastric cancer. *J Cell Physiol*. 2020;235(4):3438–3446. doi:10.1002/jcp.29233
14. Terrando N, Yang T, Wang X, et al. Systemic HMGB1 neutralization prevents postoperative neurocognitive dysfunction in aged rats. *Front Immunol*. 2016;7:441. doi:10.3389/fimmu.2016.00441
15. Wei LA, Fearing MA, Sternberg EJ, Inouye SK. The confusion assessment method: A systematic review of current usage. *J Am Geriatr Soc*. 2008;56(5):823–830. doi:10.1111/j.1532-5415.2008.01674.x
16. Collinsworth AW, Priest EL, Campbell CR, Vasilevskis EE, Masica AL. A review of multifaceted care approaches for the prevention and mitigation of delirium in intensive care units. *J Intensive Care Med*. 2016;31(2):127–141. doi:10.1177/0885066614553925
17. Aldecoa C, Bettelli G, Bilotta F, et al. European Society of Anaesthesiology evidence-based and consensus-based guideline on postoperative delirium. *Eur J Anaesthesiol*. 2017;34(4):192–214. doi:10.1097/EJA.0000000000000594
18. Kotfis K, Ślozowska J, Safranow K, Szylińska A, Listewnik M. The practical use of white cell inflammatory biomarkers in prediction of postoperative delirium after cardiac surgery. *Brain Sci*. 2019;9(11):308. doi:10.3390/brainsci9110308
19. Liu X, Yu Y, Zhu S. Inflammatory markers in postoperative delirium (POD) and cognitive dysfunction (POCD): A meta-analysis of observational studies. *PLoS One*. 2018;13(4):e0195659. doi:10.1371/journal.pone.0195659
20. Zhang W, Wang T, Wang G, Yang M, Zhou Y, Yuan Y. Effects of dexmedetomidine on postoperative delirium and expression of IL-1β, IL-6, and TNF-α in elderly patients after hip fracture operation. *Front Pharmacol*. 2020;11:678. doi:10.3389/fphar.2020.00678
21. Capri M, Yani SL, Chattat R, et al. Pre-operative, high-IL-6 blood level is a risk factor of post-operative delirium onset in old patients. *Front Endocrinol (Lausanne)*. 2014;5:173. doi:10.3389/fendo.2014.00173
22. Adamis D, Van Gool WA, Eikelenboom P. Consistent patterns in the inconsistent associations of Insulin-like growth factor 1 (IGF-1), C-reactive protein (C-RP) and interleukin 6 (IL-6) levels with delirium in surgical populations: A systematic review and meta-analysis. *Arch Gerontol Geriatr*. 2021;97:104518. doi:10.1016/j.archger.2021.104518
23. Heim KR, Mulla MJ, Potter JA, Han CS, Guller S, Abrahams VM. Excess glucose induce trophoblast inflammation and limit cell migration through HMGB 1 activation of Toll-Like receptor 4. *Am J Reprod Immunol*. 2018;80(5):e13044. doi:10.1111/aji.13044
24. Meng L, Li L, Lu S, et al. The protective effect of dexmedetomidine on LPS-induced acute lung injury through the HMGB1-mediated TLR4/NF-κB and PI3K/Akt/mTOR pathways. *Mol Immunol*. 2018;94:7–17. doi:10.1016/j.molimm.2017.12.008
25. Kim EJ, Park SY, Baek SE, et al. HMGB1 increases IL-1β production in vascular smooth muscle cells via NLRP3 inflammasome. *Front Physiol*. 2018;9:313. doi:10.3389/fphys.2018.00313
26. Kamiya N, Kim HK. Elevation of proinflammatory cytokine HMGB1 in the synovial fluid of patients with Legg–Calvé–Perthes disease and correlation with IL-6. *JBMR Plus*. 2021;5(2):e10429. doi:10.1002/jbm4.10429
27. Huo R, Liu H, Chen J, Sheng H, Miao L. Serum HMGB1 level is correlated with serum I-FABP level in neonatal patients with necrotizing enterocolitis. *BMC Pediatr*. 2021;21(1):355. doi:10.1186/s12887-021-02818-6
28. Xiong Y, Yang J, Tong H, Zhu C, Pang Y. HMGB1 augments cognitive impairment in sepsis-associated encephalopathy by binding to MD -2 and promoting NLRP3 -induced neuroinflammation. *Psychogeriatrics*. 2022;22(2):167–179. doi:10.1111/psyg.12794
29. Saxena S, Kruys V, De Jongh R, Vamecq J, Maze M. High-mobility group Box-1 and its potential role in perioperative neurocognitive disorders. *Cells*. 2021;10(10):2582. doi:10.3390/cells10102582
30. Wang J, Xin Y, Chu T, Liu C, Xu A. Dexmedetomidine attenuates perioperative neurocognitive disorders by suppressing hippocampal neuroinflammation and HMGB1/RAGE/NF-κB signaling pathway. *Biomed Pharmacother*. 2022;150:113006. doi:10.1016/j.biopha.2022.113006
31. Paudel YN, Shaikh MF, Chakraborti A, et al. HMGB1: A common biomarker and potential target for TBI, neuroinflammation, epilepsy, and cognitive dysfunction. *Front Neurosci*. 2018;12:628. doi:10.3389/fnins.2018.00628

Prognostic factors and clinical characteristics of patients with newly diagnosed non-secretory multiple myeloma in the era of new drugs in "real-world" study: Experiences of the Polish Myeloma Group

Grzegorz Charliński[1,2,A–F], Aneta Szudy-Szczyrek[3,B], Martyna Podgajna[3,B], Michał Mielnik[3,B], Anna Kopińska[4,B], Agata Tyczyńska[5,B], Lidia Usnarska-Zubkiewicz[6,B], Łukasz Bołkun[7,B], Elżbieta Wiater[2,B], Mateusz Krzystański[8,C], David H. Vesole[9,10,E,F], Artur Jurczyszyn[11,E,F]

[1] Department of Nephrology, Hypertension and Internal Medicine, Faculty of Medicine, University of Warmia and Mazury, Olsztyn, Poland
[2] Department of Hematology and Bone Marrow Transplantation, Nicolaus Copernicus Hospital, Toruń, Poland
[3] Chair and Department of Hematooncology and Bone Marrow Transplantation, Medical University of Lublin, Poland
[4] Department of Hematology and Bone Marrow Transplantation, Medical University of Silesia, School of Medicine in Katowice, Poland
[5] Department of Hematology and Transplantology, Medical University of Gdańsk, Poland
[6] Department of Hematology, Blood Neoplasms and Bone Marrow Transplantation, Wroclaw Medical University, Poland
[7] Department of Hematology, Medical University of Bialystok, Poland
[8] Independent IT Specialist, Cracow, Poland
[9] Department of Hematology/Oncology, Medstar Georgetown University Hospital, Washington, D.C., USA
[10] John Theurer Cancer Center at Hackensack Meridian School of Medicine, USA
[11] Plasma Cell Dyscrasias Center, Department of Hematology, Faculty of Medicine, Jagiellonian University Medical College, Cracow, Poland

A – research concept and design; B – collection and/or assembly of data; C – data analysis and interpretation;
D – writing the article; E – critical revision of the article; F – final approval of the article

Advances in Clinical and Experimental Medicine, ISSN 1899–5276 (print), ISSN 2451–2680 (online) *Adv Clin Exp Med*. 2025;34(3):369–378

Address for correspondence
Grzegorz Charliński
E-mail: grzegorzcharlinski0508@gmail.com

Funding sources
None declared

Conflict of interest
None declared

Received on August 27, 2023
Reviewed on December 25, 2023
Accepted on May 27, 2024

Published online on August 29, 2024

Cite as
Charliński G, Szudy-Szczyrek A, Podgajna M, et al. Prognostic factors and clinical characteristics of patients with newly diagnosed non-secretory multiple myeloma in the era of new drugs in "real-world" study: Experiences of the Polish Myeloma Group. *Adv Clin Exp Med*. 2025;34(3):369–378. doi:10.17219/acem/189390

DOI
10.17219/acem/189390

Abstract

Background. Non-secretory multiple myeloma (NSMM) accounts for approx. 2–3% of multiple myeloma (MM) cases. Due to the rare occurrence and ineligibility of patients with NSMM to participate in clinical trials, we have limited data on treatment efficacy and the clinical course in these patients. Most of the literature consists of case reports and small retrospective studies.

Objectives. The study aimed to analyze patient characteristics, prognostic factors and treatment outcomes in newly diagnosed (ND) NSMM.

Materials and methods. This is a multicenter, retrospective analysis of 43 patients with NSMM diagnosed between June 2010 and September 2021, conducted in 8 Polish hematology centers.

Results. The median overall survival (OS) was 103 months (95% confidence interval (95% CI): 20–72). The most common cause of death was MM disease progression. The overall response rate (ORR) was 84.6%; complete response (CR), very good partial response (VGPR), partial response (PR), and no response (NR) rates were 20.5%, 46.2%, 17.9%, and 15.4%, respectively. In multivariable analysis, factors contributing to worse OS included International Staging System stage 3 (ISS-3) ($p = 0.0277$), anemia (Hb <10 g/dL or >2 below upper limit of normal value (ULN), $p = 0.0270$), renal insufficiency (RI, serum creatinine >2 mg/dL, $p = 0.0476$), and serum albumin <5.5 mg/L (0.0408).

Conclusions. Non-secretory multiple myeloma is a rare subtype of MM. This small study demonstrates that outcomes are comparable to secretory MM. However, the inclusion of this subset of patients in clinical trials is essential to assess prognosis, treatment efficacy and clinical outcomes.

Key words: clinical characteristics, non-secretory multiple myeloma, prognostic factors

Background

Multiple myeloma (MM) is a bone marrow (BM) cancer characterized by uncontrolled proliferation of clonal plasmocytes (CP) in the BM, which, in most cases, produces a monoclonal (M) protein found in the serum and/or urine.[1] Approximately 2,600 new MM cases are diagnosed annually in Poland.[2] The criteria for the diagnosis of MM include the presence of CP producing an M-protein and the presence of at least 1 indicator of organ damage defined by the acronym SLiM-CRAB (≥60% CPBM, serum free light chain (sFLC) ratio ≥100 or <0.01, presence of 1 or more bone lesions on magnetic resonance imaging (MRI), hypercalcemia, renal insufficiency (RI), anemia, and bone lesions).[3] In approx. 97–98% of patients with MM, an M-protein can be detected in the serum and urine using electrophoresis and immunofixation.[3]

On the other hand, in free light chain (FLC) MM, CP produce an M-protein consisting solely of the light chains of immunoglobulins.[4] In the remaining 2–3% of MM, there is no detectable M-protein in the serum and/or Bence–Jones proteins in the urine using electrophoresis or immunofixation assays.[5,6] This type of MM is generally defined as non-secretory (NS) MM.[7,8]

The introduction of nephelometric testing to detect and measure sFLC concentrations in clinical practice has changed the definition. About 3/4 of MMs identified as NSMM have elevated clonal FLC levels and an abnormal FLC ratio; these cases are called oligosecretory MM (M-protein <10 g/L, Bence–Jones protein <200 mg/24 h and sFLC <100 mg/L).[9] True NSMM, i.e., lack of M-protein synthesis, is found in approx. 2% of MM patients.[10] The pathophysiology of NSMM includes reduced M-protein synthesis, impaired secretion and rapid degradation of the M-protein intra- or extracellularly.[7]

Virtually all clinical trials exclude patients with NSMM from participation since the trials require measurable parameters to determine therapy efficacy. Thus, we have limited data on the treatment efficacy and clinical course of NSMM.[11–13] Most of the literature consists of case reports and small retrospective studies.[14–25]

Objectives

Our study aimed to analyze patient characteristics, prognostic factors and treatment of newly diagnosed (ND) NSMM.

Materials and methods

A multicenter retrospective study was conducted in 8 Polish hematology centers. Patients were identified through database searches at each study center. Each center's institutional review board approved the study following the ethical guidelines of the Declaration of Helsinki. Patients with ND NSMM between June 2010 and September 2021 were included in the analysis. Non-secretory multiple myeloma was defined by the International Myeloma Working Group (IMWG) as the absence of M-protein in serum and urine using immunofixation testing. According to the updated IMWG criteria for MM, a sFLC <100 mg/L with an abnormal sFLC ratio was defined as "oligosecretory," and "non-producing" was defined by a sFLC <100 mg/L with a normal sFLC ratio.[26,27] Patients diagnosed with monoclonal gammopathy of undetermined significance (MGUS), asymptomatic MM and organ involvement with light-chain amyloidosis (AL) were excluded from our analysis. Staging and response criteria utilized the IMWG definitions.[4,28–30]

Progression-free survival (PFS) was expressed in months and was defined as the time from diagnosis to disease progression, change of treatment or death. Overall survival (OS) was described in months as the time from diagnosis until death or last follow-up.

Statistical analyses

Continuous and categorical variables are presented using descriptive statistics. The Kaplan–Meier (K–M) method was used for survival analysis, and survival curves were generated.

The log-rank test was used to compare the differences between groups. The Cox proportional hazards regression method was applied for fitting univariable survival models, expressed as hazard ratios (HR) with 95% confidence intervals (95% CI). The Cox regression model was used to examine potential prognostic factors for ND NSMM. The univariable Cox regression and group comparisons using the log-rank test were conducted as separate analyses and do not constitute a family of hypotheses. Tests based on the Schoenfeld residuals were used to test the proportional hazards assumptions in Cox regression assumptions (cox.zph function in survival package). The Cox regression assumptions were also verified by confirming the absence of correlation between predictors based on a correlation matrix. To assess the quality of the obtained regression models, parameters such as p-value and Nagelkerke R^2 were used. All reported p-values were 2-sided and considered significant if they were less than 0.05. Variable selection for the multivariable Cox proportional hazards regression model was based on Akaike's information criterion (AIC).

The following steps were applied to construct the multiple Cox regression model using AIC criteria:

- a model that includes all considerable variables was created;
- the dredge function in the MuMIn package was used to conduct a comprehensive analysis, considering all possible combinations of variables;
- for each combination, the AIC criterion was calculated; and
- the variables from models that achieved the lowest AIC values were selected for the multivariable model.

Finally, a multivariable Cox regression model was built, and the results were interpreted, focusing on the statistical significance of independent variables, interpretability of parameters, and the sensibility of predictions in the context of the research problem and practical application of the model. The sFLC ratio variable was excluded from the analysis because the survival curves (normal compared to abnormal sFLC ratio) crossed. Such a case suggests complexity in interpreting the impact of that variable, and excluding it reduces the complexity of the required statistical analysis. The data used in the statistical analysis were complete, and there were no missing data in the dataset, except for cytogenetic studies performed in only 56% of patients. This variable was not included in the selection variable procedures.

Statistical analysis and graphics were obtained using the software PQStat v. 1.8.4.140 (PQStat Software, Poznań, Poland) and a package dedicated to survival analysis. The software R-studio v. 1.3.959 (http://www.R-exams.org) with dedicated packages was used for variable selection for the multivariable analysis.

Results

Patient characteristics

Forty-three patients with an established diagnosis of ND NSMM were included in the analysis. The median follow-up was 24 months (range: 1–137). The median age at NSMM diagnosis was 62 years (range: 41–80). Sixteen patients (37.2%) were ≥65 years old and 4 patients (9.3%) were older than 75 years. The study included 25 men (58.1%). At diagnosis, the sFLC in 25 patients (58.1%) had a ratio <0.25 or >1.65, but all patients had an absolute sFLC <100 mg/L.

All patients were monitored using laboratory tests, sFLC assays, BM aspiration, and imaging.

Laboratory tests and sFLC determinations were performed before the start of each chemotherapy cycle and every 2 months (median; range: 1–3) after the end of treatment. Depending on the hematological center, BM aspiration in the assessment of CP (multiparameter flow cytometry – MPF) was repeated every 3–6 months during and every 6 months after treatment. At the initial diagnosis, positron emission tomography/computed tomography (PET/CT) imaging was performed in 28 patients (65.1%), MRI in 6 patients (13.9%), whole-body low-dose computed tomography (WBLD-CT) in 5 patients (11.6%), and radiological imaging of the skeletal system in 4 patients (9.4%). After treatment ended, imaging studies were repeated every 6 months (median).

Using the International Staging System (ISS), 11 patients (25.6%), 10 patients (23.2%) and 22 patients (51.2%) were diagnosed with stages ISS-1, ISS-2 and ISS-3 MM, respectively. Baseline cytogenetics by fluorescent in situ hybridization (FISH) was available in 24 patients (55.8%) with NSMM. High-risk cytogenetic abnormalities were found in 11 patients (45.8%) and the t(11;14) in 2 (8.3%) of the tested patients. Patient characteristics and clinical features are listed in Table 1.

Table 1. Baseline clinical characteristics of the patients with non-secretory multiple myeloma

Variable	Value (n = 43)
Median age (min, max) [Q1, Q3]	62 (41, 80) [54.5, 66]
Age ≥65 years, n (%)	16 (37.2)
Male sex, n (%)	25 (58.1)
ISS stage, n (%)	
ISS-1	11 (25.6)
ISS-2	10 (23.2)
ISS-3	22 (51.2)
Cytogenetics	24 (55.8)
High-risk cytogenetics[a], n (%)	11 (45.8)
t(11;14), n (%)	2 (8.3)
First-line chemotherapy, n (%)	
Bort + IMiD-based	23 (53.5)
Bort-based	11 (25.6)
Thal-based	9 (20.9)
Autologous stem cell transplantation, n (%)	16 (37.2)
Dialysis, n (%)	4 (9.3)
Response after 1st-line therapy[b], n (%)	
ORR (≥PR)	33 (84.6)
≥VGPR	26 (66.7)
CR	8 (20.5)
VGPR	18 (46.2)
PR	7 (17.9)
SD	2 (5.1)
PD	4 (10.3)
Laboratory tests	
CPBM ≥ 60%, n (%)	11 (25.6)
Abnormal sFLC ratio, n (%)	25 (58.1)
Serum Hb <10 g/dL or >2 below ULN, n (%)	21 (48.8)
Serum albumin <3.5 g/dL, n (%)	11 (25.6)
Serum creatinine >2.0 mg/dL, n (%)	9 (20.9)
Serum β2-microglobulin ≥5.5 mg/L, n (%)	18 (41.9)
Serum calcium >2.75 mmol/L, n (%)	10 (23.2)
Serum LDH >ULN, n (%)	32 (74.4)
Bone lesions presence, n (%)	39 (90.7)

Q1, Q3 – 1st and 3rd quartile; max – maximum; min – minimum; ASCT – autologous stem cell transplantation; Bort – bortezomib; CPBM – clonal plasmocytes infiltration in the bone marrow; IMiD – immunomodulatory drug; Hb – hemoglobin concentration; IMiD – immunomodulatory drug; ISS – International Staging System; LDH – lactate dehydrogenase; sFLC – serum free light chain; Thal – thalidomide; ULN – upper limit of normal value; VGPR – very good partial response; [a] defined as presence of t(4;14), t(14;16), t(14;20) or del17p in the absence of any trisomy; [b] response: ORR – overall response rate; CR – complete response; PR – partial response; VGPR – very good partial response; SD – stabile disease; PD – progression disease.

NSMM treatment

Thirty-four patients (79.1%) received bortezomib (Bort)-based therapy. Twenty-three (53.5%) patients received Bort in combination with an immunomodulatory drug (IMiD, thalidomide (Thal) – 21 patients, lenalidomide – 2 patients), and 11 patients (25.6%) were treated with Bort in combination with other drugs. Nine patients (20.9%) received Thal-based treatment. After induction therapy, 16 (37.2%) patients received high-dose chemotherapy followed by an autologous stem cell transplantation (ASCT). Maintenance therapy was not used after ASCT.

After 1st-line treatment, the ORR (≥PR) was 84.6%, while CR, VGPR, PR, and NR ratios were 20.5%, 46.2%, 17.9%, and 15.4%, respectively (Table 1). Complete response was achieved in 31.2% of patients treated with chemotherapy, followed by ASCT and in 11.1% of patients treated with chemotherapy only.

The median PFS was 16 months (95% CI: 9–34, Fig. 1A). Comparing patients treated with ASCT following induction therapy with patients not treated with ASCT, the median PFS was 34 months compared to 9 months, respectively (log-rank HR: 0.288, 95% CI: 0.137–0.606; p = 0.0034). Additionally, we found a trend towards longer PFS in patients who achieved a greater PR after 1st-line treatment compared to patients who did not; median PFS was 26 months compared to 4 months, respectively (log-rank HR: 0.263, 95% CI: 0.074–0.928; p = 0.0004).

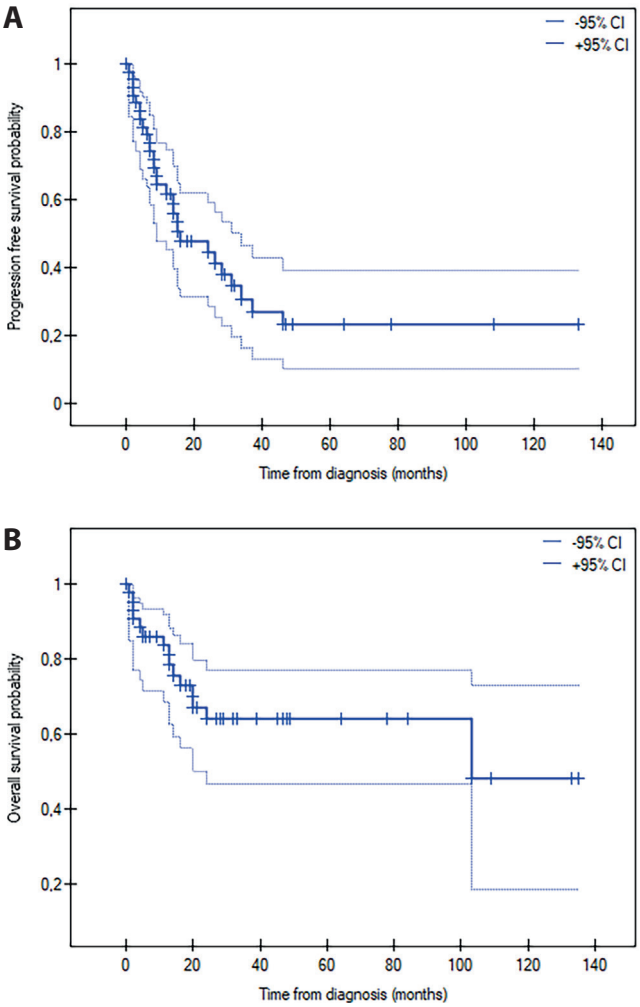

Fig. 1. The Kaplan–Meier curve for progression-free survival (A) and overall survival (B) in 43 patients with non-secretory multiple myeloma

Twenty-two patients (51.2%) received 2nd-line therapy. Ten patients received Vd-based therapy, including 3 patients with Vd in combination with daratumumab (Dara-Vd), 3 patients with doxorubicin (PAD) and 3 patients with Thal (VTd). Nine patients received Rd-based treatment, including 1 patient receiving Rd in combination with carfilzomib (KRd) and 1 patient in combination with ixazomib (Ixa-Rd). One patient was treated with Thal in combination with dex (Td), 1 patient with belantamab mafodotin and 1 patient with melflufen + dex. Six patients additionally received an ASCT. The effectiveness of treatment was assessed in 18 patients. The ORR was 77.8%, while CR, VGPR, PR, and NR rates were 22.2%, 16.7%, 38.9%, and 22.2%, respectively. The median PFS (PFS2) was 12 months (95% CI: 2–57).

Eight patients (18.6%) received 3rd-line therapy. Four patients received Vd-based therapy, including 3 who received Vd in combination with daratumumab (Dara-Vd), and 4 patients received Rd-based therapy, including 1 who received Rd in combination with carfilzomib (KRd). Due to the limited number of patients, the assessment of the effectiveness of 3rd-line treatment was not statistically analyzed.

Survival analyses and prognostic factors

The median OS for the entire group was 103 months (95% CI: 20–72, Fig. 1B). During the follow-up, 15 patients (34.9%) died. The most common cause of death was NSMM progression in 10 patients (66.7%), infection in 4 patients (26.6%), including COVID-19 disease in 1 patient, and a 2nd primary malignancy in 1 patient (6.7%).

Analyzing the effect of age on OS, a significant prolongation of OS was found in patients aged <65 years compared to ≥65 years; median OS, not achieved (NA) compared to 16 months, respectively (log-rank HR: 3.230; 95% CI: 1.089–9.583; p = 0.0171).

A significant prolongation of OS was observed in patients with stages ISS-1 and ISS-2 compared to ISS-3, and the median was NA compared to 24 months (log-rank HR: 4.394; 95% CI: 1.595–12.105; p = 0.0111). Patients with a CP infiltration of the BM (CPBM) <60% had a longer OS than patients with a CPBM ≥60%; the median OS was NA compared to 20 months (log-rank HR: 3.079; 95% CI: 0.910–10.422; p = 0.0198). Other factors identified as having a significant impact on OS were anemia (Hb <10 g/dL or >2 below the ULN, log-rank HR: 9.397; 95% CI: 3.357–26.305; p = 0.0002) and RI (serum creatinine >2 mg/dL, log-rank HR: 3.202; 95% CI: 0.838–12.230; p = 0.0180). There was a trend towards prolonged OS in patients with normal serum calcium (sCa) levels compared to hypercalcemia

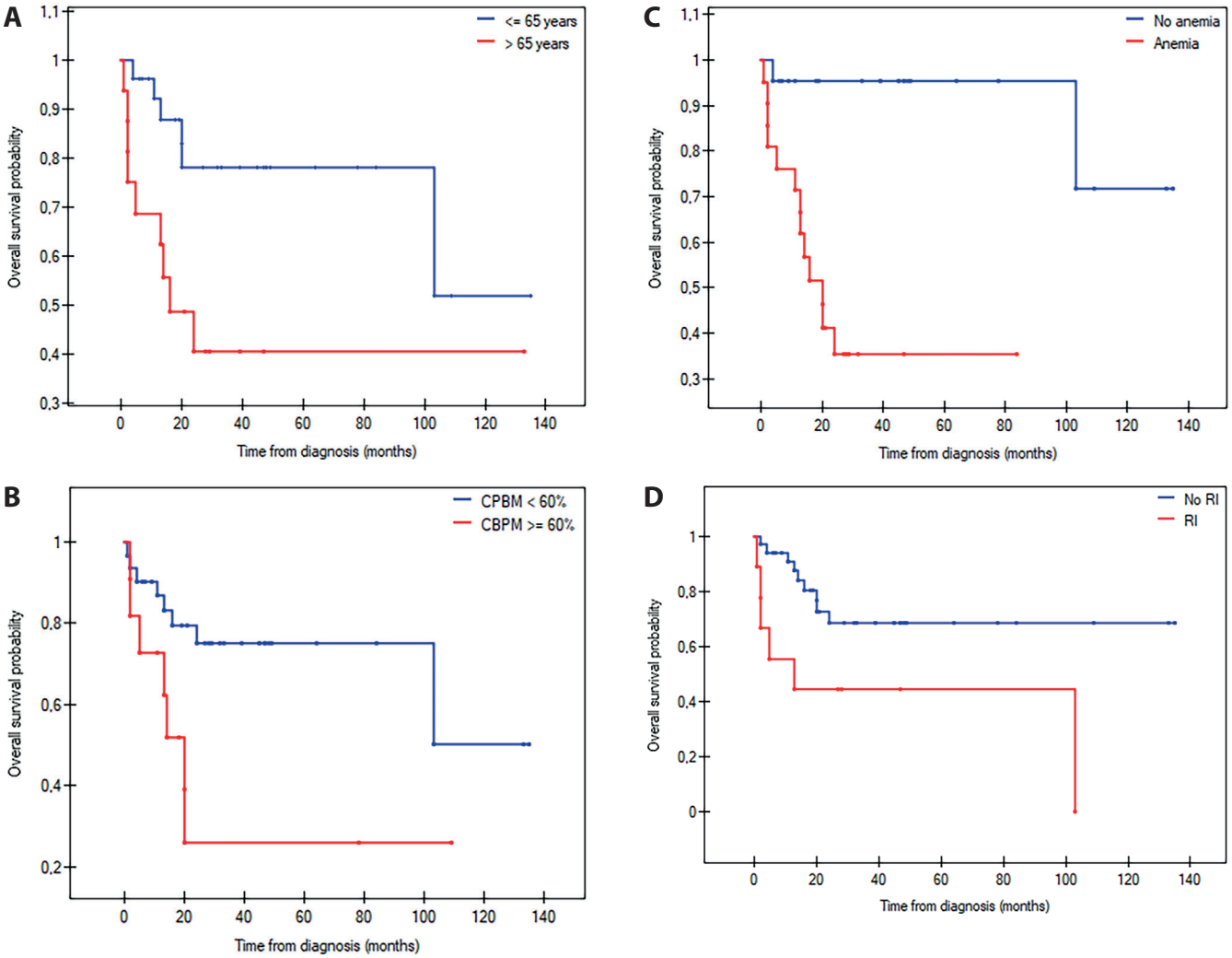

Fig. 2. The Kaplan–Meier overall survival curves in 43 patients with non-secretory multiple myeloma by age (A), clonal plasmocytes infiltration in the bone marrow (B), anemia (C), andrenal insufficieny (D)

(log-rank HR: 2.575; 95% CI: 0.653–10.145; p = 0.0647). The K–M curves of selected baseline factors related to OS (age, ISS system, CPBM, anemia, and RI) are shown in Fig. 2.

In a univariable analysis of OS, age ≥65 years, CPBM ≥60%, anemia, RI, serum albumin <3.5 g/dL, serum β2-microglobulin ≥5.5 mg/L, and bone lytic lesions contributed to a worse OS (Table 2). In a multivariable analysis, ISS-3, anemia, RI, a serum albumin <3.5 g/dL, and a serum β2-microglobulin ≥5.5 mg/L contributed to a worse OS (Table 3).

Considering 1st-line chemotherapy, we found a trend for prolonged OS in patients treated with Bort + IMiD-based compared to Bort-based and Thal-based therapy; median OS was NA compared to 24 months, respectively (log-rank HR: 2.751; 95% CI: 1.004–7.576; p = 0.0578). Furthermore, we found a significantly longer OS in patients who received ASCT after induction treatment. The median OS in the patients treated compared to untreated with ASCT groups was NA compared to 104 months (log-rank HR: 0.225; 95% CI: 0.080–0.629; p = 0.0289). We found a significantly longer OS in patients who achieved a greater PR compared to a lesser PR after 1st-line treatment with a median OS of NA compared to 4 months, respectively (log-rank HR: 0.184; 95% CI: 0.043–0.796; p = 0.0002). The K–M curves of selected factors related to 1st-line treatment (type of 1st-line treatment, ASCT, the response after 1st-line treatment) are presented in Fig. 3.

Discussion

Non-secretory multiple myeloma is a rare subtype of MM. Due to patients' low incidence and ineligibility for clinical trials, this type of MM is not fully understood. The lack of measurable M-protein probably delays the diagnosis of NSMM and makes it difficult to assess the effectiveness of treatment and disease recurrence.[22] Disease assessment requires either BM analysis and/or radiographic imaging. Our multicenter retrospective study evaluated the clinical characteristics, prognostic factors, clinical outcomes, and OS in patients with NSMM. Due to the inability to compare our results with the results

Table 2. Univariable analyses for overall survival in patients with non-secretory multiple myeloma

Variable		Univariable analysis							
		variable β	lower 95% CI	upper 95% CI	HR	lower 95% CI	upper 95% CI	Nagelkerke R^2	p-value
Age [years]	≥65	1.181	0.144	2.217	3.265	1.155	9.181	0.2883	0.0256
	<65								
Gender	male	0.059	–0.976	1.094	1.061	0.376	2.987	0.0008	0.9112
	female								
Cytogenetic risk	high-risk	0.646	–0.855	2.146	1.907	0.425	8.551	0.0982	0.3989
	standard-risk								
CPBM [%]	≥60	1.146	0.119	2.172	3.144	1.126	8.776	0.2578	0.0287
	<60								
Hb [g/dL]	<10 or >2 below ULN	2.833	0.796	4.870	17.005	2.218	130.388	0.6458	0.0064
	>10 or <2 below ULN								
Serum albumin [g/dL]	<3.5	1.539	0.501	2.577	4.660	1.650	13.158	0.4133	0.0037
	≥3.5								
Serum creatinine [mg/dL]	>2.0	1.173	0.135	2.210	3.231	1.145	9.121	0.2519	0.0267
	≤2.0								
Serum β2-microglobulin [mg/L]	≥5.5	1.144	0.065	2.224	3.141	1.067	9.248	0.2670	0.0378
	<5.5								
Serum calcium [mmol/L]	>2.75	1.003	–0.116	2.121	2.726	0.891	8.341	0.1681	0.0789
	≤2.75								
LDH	>ULN	1.049	–0.519	2.618	2.856	0.595	13.712	0.1415	0.1897
	≤ULN								
Bone lytic lesions	yes	–1.590	–2.882	–0.298	0.204	0.056	0.742	0.2471	0.0158
	no								

95% CI – 95% confidence interval; CPBM – clonal plasmocytes infiltration in the bone marrow; Hb – hemoglobin concentration; HR – hazard ratio; LDH – lactate dehydrogenase; ULN – upper limit of normal value.

Table 3. Multivariable analyses for overall survival in patients with non-secretory multiple myeloma

Variable	Multivariable analysis						
	variable β	lower 95% CI	upper 95% CI	HR	lower 95% CI	upper 95% CI	p-value
ISS-3	0.830	0.091	1.569	2.293	1.095	4.801	0.0277
CPBM ≥60%	1.246	–0.401	2.893	3.476	0.669	18.050	0.1382
Hb <10 g/dL or >2 below ULN	2.395	0.272	4.518	10.965	1.312	91.635	0.0270
Serum albumin <3.5 g/dL	1.560	0.192	2.928	4.758	1.211	18.691	0.0254
Serum creatinine >2.0 mg/dL	1.516	0.016	3.016	0.048	1.016	20.417	0.0476
Serum β2-microglobulin ≥5.5 mg/L	–2.152	–4.215	–0.090	0.116	0.015	0.914	0.0408
Serum calcium >2.75 mmol/L	–0.388	–2.006	1.230	0.678	0.134	3.423	0.6384

Nagelkerke R^2 = 0.244; p = 0.0003; 95% CI – 95% confidence interval; CPBM – clonal plasmocytes infiltration in the bone marrow; Hb – hemoglobin concentration; HR – hazard ratio; ISS – International Staging System; ULN – upper limit of normal value.

of clinical trials, we compared our results to available observational studies.

The median age at diagnosis in the general population of MM patients is 69 years.[31] In comparison, the median age of Polish patients with NSMM was 62 years and was comparable to the results of other observational studies of patients with NSMM and with the results of an observational study of patients with MM from Central Europe, where the median age was 64 years old.[8,20,32] At the time of MM diagnosis, 2/5 of patients were >65 years and 1/10 were over 75 years old. Although an age >65 affected OS in the univariable analysis, we did not find such a relationship in the multivariable analysis.

New drugs (Thal, lenalidomide and Bort) were used as 1st-line therapy in all Polish patients. However, in studies by Chawla et al.,[8] Sun et al.[20] and Wålinder et al.,[21]

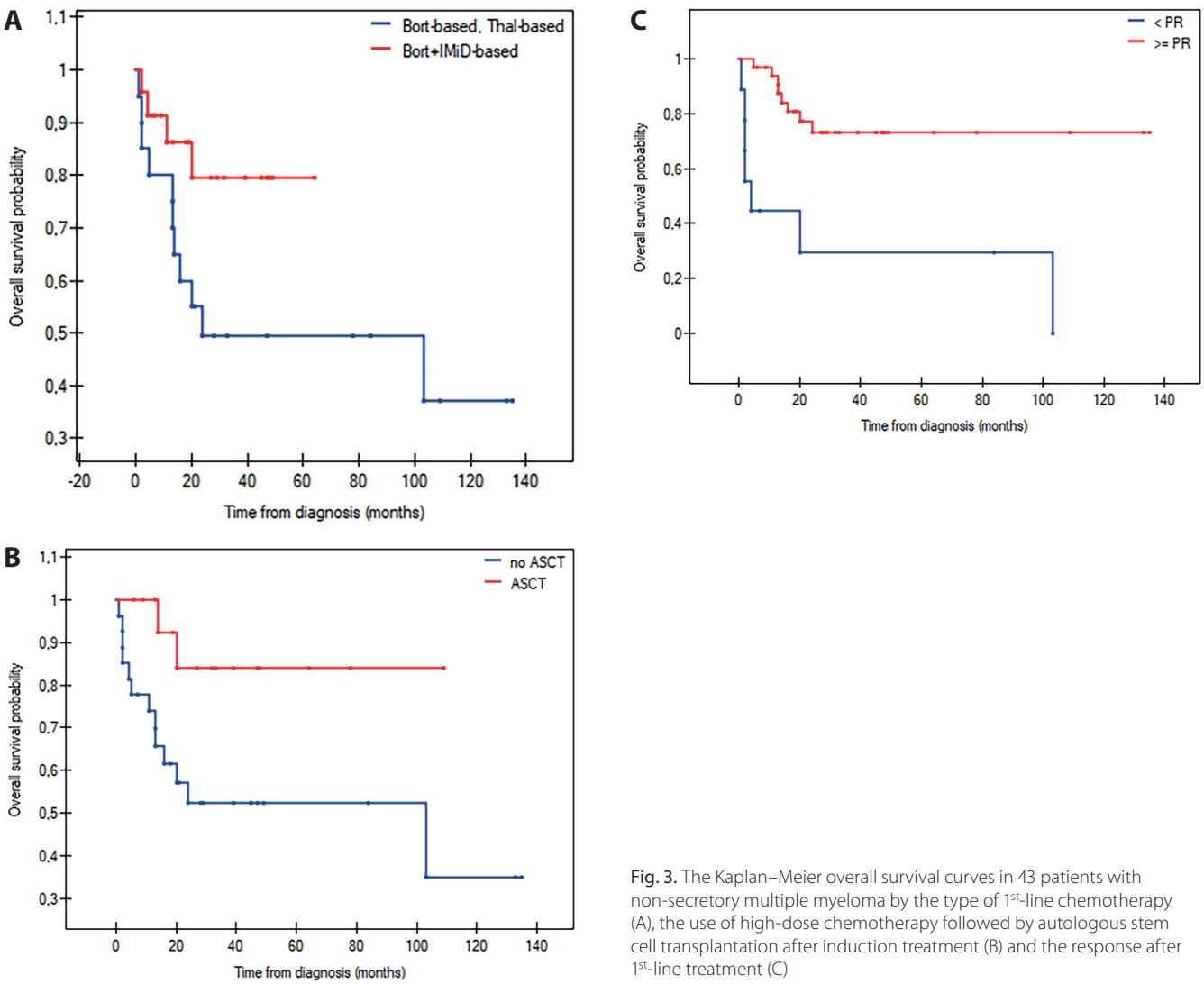

Fig. 3. The Kaplan–Meier overall survival curves in 43 patients with non-secretory multiple myeloma by the type of 1st-line chemotherapy (A), the use of high-dose chemotherapy followed by autologous stem cell transplantation after induction treatment (B) and the response after 1st-line treatment (C)

treatment based on new drugs (Thal, lenalidomide and Bort) was used in 22%, 54% and 94% of patients, respectively. In our population, 20.5% of patients achieved CR after 1st-line treatment, which is comparable to the report by Wålinder et al.[21] (26% of patients achieved CR) and lower than in the study by Chawla et al.[8] and Sun et al.,[20] where CR was achieved in 44% (patients treated with new drugs) and 65.8% of patients, respectively. In a Chinese study,[20] a higher CR rate did not improve survival, unlike the American[8] and Swedish[21] studies, which showed a trend toward better survival in patients who achieved CR.

The use of new drugs as 1st-line therapy, followed by ASCT, and the achievement of CR significantly prolonged the OS of patients with NSMM, similar to the trend observed in the general population of MM patients.[24] We found a significant difference in OS in the group of patients who received ASCT compared to those who did not receive ASCT as 1st-line therapy. This result may be because all patients in the induction treatment were treated with new drugs. However, this requires further research.

In our group, the percentage of patients with ASCT after induction treatment was 37%, comparable to the Swedish study[21] and higher than in American[8] and Chinese studies,[20] where ASCT was used in 18% and 27% of patients, respectively. In our study group, CR was achieved in 31.2% of patients with NSMM treated with ASCT. The Center for International Blood and Marrow Transplant Research showed that ASCT results are comparable in patients with NSMM and secretory MM.[14] Comparing the effectiveness of ASCT treatment in patients with NSMM and secretory MM, Kumar et al. found similar 3-year OS and PFS rates of 66% compared to 61% ($p = 0.26$) and 40% compared to 33% ($p = 0.05$), respectively.[14] Beneficial effects of ASCT in NSMM were also reported by Terpos et al.[24] Therefore, it seems that patients with NSMM should receive an ASCT as the standard of care.

We found that 41.9% of patients had an average baseline sFLC ratio, and the median OS in this subgroup of patients was comparable to that of patients with an abnormal sFLC ratio. Our results are similar to those obtained by Sun et al.[20] and Wålinder et al.,[21] and opposite to those obtained

by Chawla et al.[8] In addition, we found that an abnormal baseline sFLC ratio was not an adverse prognostic factor and median OS was comparable in both subgroups.

At the time of diagnosis, we found anemia in 49% of patients, which is comparable to the results obtained by Sun et al.[20] but higher than those reported by Wålinder et al.[21] and Migkou et al.,[22] which were 35%, 21%, and 15% respectively. We found that anemia at diagnosis is one of the essential laboratory predictors of OS in both univariable and multivariable analyses. Anemia at diagnosis is one of the most important prognostic factors affecting OS in the univariable and multivariable analyses. This may be explained by the finding that we found CPBM > 60% in a quarter of patients, indicative of a higher disease burden.

Since sFLC levels were low in our study group by definition, RI (sCr >2 mg/dL) was found in only 21% of patients and probably was not associated with FLC-associated renal pathology. Wålinder et al.[21] found RI in the unmeasurable, oligosecretory and NSMM groups to be 11%, 13% and 6% of patients, respectively. A similar incidence of RI (eGFR <30 mL/min) was found in the study by Migkou et al., 11% and 7%, respectively, in patients with oligosecretory and SMM.[22] The incidence of RI in the cited studies may be due to the definition of RI adopted in these studies and the coexistence of hypercalcemia.

Bone changes and hypercalcemia were found in 91% and 23% of Polish patients with NSMM, respectively. Wålinder et al. found bone lesions in 90% of patients, while hypercalcemia was found in only 10–12%.[21] A similar incidence of bone lesions was observed in a study by Migkou et al., where bone lesions were found in 85% of patients with NSMM and 81% of patients with oligosecretory MM, and their incidence was comparable to that of SMM (75%).[22] The same study found hypercalcemia in 5% of patients with oligosecretory MM, 16% with NSMM and 17% with SMM.[14] The slightly higher incidence of bone lesions and hypercalcemia in our study may be due to the severity of NSMM (51% of patients were diagnosed with NSMM at a clinical stage of ISS-3), more extensive infiltration of CPBM and perhaps a difference in NSMM biology.

Monitoring the effectiveness of NSMM treatment remains a challenge for hematologists. Serial histopathological examinations combined with imaging are currently considered the "gold standard" for monitoring patients with NSMM.[25] Bone marrow biopsies increase costs and patient discomfort. It should be remembered that cytological and histopathological examination of the BM reveals heterogeneous involvement of CPBM. For this reason, it is recommended that MPF be performed to assess CPBM. This study is justified because minimal residual disease (MRD) is now recognized as an important prognostic factor influencing the OS of MM patients. Further development of MPF techniques assessing circulating CP in the peripheral blood may contribute to further progress in the monitoring of NSMM. Mass spectrometry (MS) is another method that can be used to assess the effectiveness of treatment in patients with NSMM. Detection of M-proteins using matrix-assisted laser desorption/ionization-time-of-light (MALDI-TOF) MS may be an alternative to conventional immunofixation, especially in patients with NSMM. Further clinical studies using this method are undoubtedly needed.[33]

Due to the limited use of serum protein electrophoresis (SPEP), urine protein electrophoresis (UPEP) and FLC assays in patients with NSMM, it has a minimal application; for this reason, the use of MPF together with MRI and/or PET/CT is currently the optimal way to assess the response to treatment in patients with NSMM.[34,35] Although MRI is a susceptible method for detecting bone changes at the time of diagnosis of NSMM, due to the static image of bone changes in patients who have achieved MM remission, it is an insufficient method for detecting pathological changes.[36,37] However, patients with NSMM whose lesions were detected on PET/CT at diagnosis should have the examination repeated at intervals depending on the duration of treatment cycles and clinical conditions. In aggressive forms of NSMM or lack of clinical indicators indicating response to treatment, more frequent PET/CT follow-up examinations are recommended. However, the slow course of NSMM and the reduction/resolution of clinical symptoms allow for fewer routine check-ups. In patients achieving long-term remission, the frequency of PET/CT depends on the depth of response obtained and the characteristics of the patients before treatment. In patients in whom PET/CT cannot be performed, disease monitoring is based on serial BM aspirations and biopsies of extramedullary lesions.

Due to the lack of guidelines for monitoring patients with NSMM, which may cause a delay in the diagnosis of disease relapse/progression, we propose introducing guidelines as part of the recommendations of the Polish Myeloma Group. Analyzing the results obtained during NSMM treatment, we suggest performing laboratory tests assessing organ performance, known as CRAB, before each cycle of chemotherapy and BM biopsy with MPF evaluation every 3–6 months. We recommend repeating a WBLD-CT, MRI or PET/CT (depending on the test performed at the time of diagnosis) of the entire body every 3–6 months or more often, depending on the clinical situation. In patients who have achieved remission after treatment or are undergoing maintenance treatment, we suggest repeating laboratory tests assessing organ function (CRAB) every 2 months and BM biopsy with cytometric assessment and a WBLD-CT every 3–6 months or more often, depending on the clinical situation.[38] In patients with oligosecretory MM, we suggest performing the sFLC assay repeatedly during treatment every 2 months or more often, depending on the clinical situation.

Limitations

Certain limitations of our study should be considered. First, it is a retrospective study with a small number of patients analyzed. Second, the chemotherapy protocols used for 1st-line therapy were heterogeneous. In addition, cytogenetic studies were available on only a few patients. For this reason, we could not draw firm conclusions regarding the cytogenetic profile of NSMM. Another weakness of our study is selection bias, which we minimized by enrolling consecutive patients at each participating center. The relatively long median OS in our population is probably due to the long follow-up period of the analyzed patients, the relatively young age (median 62 years) of the patients, the high percentage of ASCT recipients (37%), and biological factors, such as a lower risk of renal complications. Moreover, all patients, both in the 1st and subsequent lines of treatment, were treated with chemotherapy protocols based on new drugs (Bort, Thal and lenalidomide). Additionally, in the treatment of relapsed/refractory NSMM, 45.5% of patients received chemotherapy based on daratumumab (27.3% of patients) and 2nd-generation proteasome inhibitors (carfilzomib and ixazomib – 9.1% of patients), as well as with belantamab mafodotin and melphalan flufenamide (9.1% of patients).

Conclusions

Our study showed that the most important prognostic factors with the most significant impact on OS in patients with NSMM, identified using multivariate Cox analysis, are ISS clinical stage, anemia and RI.

Non-secretory multiple myeloma makes up a small subset of MM patients. Extrapolating the statistical data to the number of reported cases of MM in Poland, approx. 50 new cases of NSMM should be expected annually. Undoubtedly, further research is needed to understand the disease's biology better and qualify patients with NSMM for randomized clinical trials to assess the effectiveness of treatment using modern diagnostic methods (MS, MPF of CPBM, and CP circulating in the peripheral blood) and to determine prognostic factors affecting OS.

Data availability

The datasets generated and/or analyzed during the current study are available from the corresponding author on reasonable request.

Consent for publication

Not applicable.

ORCID iDs

Grzegorz Charliński https://orcid.org/0000-0002-0595-5864
Aneta Szudy-Szczyrek https://orcid.org/0000-0003-2352-394X
Martyna Podgajna https://orcid.org/0000-0002-2863-5142
Michał Mielnik https://orcid.org/0000-0003-4473-5319
Anna Kopińska https://orcid.org/0000-0002-6821-7033
Agata Tyczyńska https://orcid.org/0000-0002-2067-2715
Lidia Usnarska-Zubkiewicz https://orcid.org/0000-0002-5893-1989
Łukasz Bołkun https://orcid.org/0000-0002-6629-8626
Elżbieta Wiater https://orcid.org/0009-0002-0319-7534
David H. Vesole https://orcid.org/0000-0001-7721-3870
Artur Jurczyszyn https://orcid.org/0000-0001-9796-8365

References

1. Bladé J, Samson D, Reece D, et al. Criteria for evaluating disease response and progression in patients with multiple myeloma treated by high-dose therapy and haemopoietic stem cell transplantation. Myeloma Subcommittee of the EBMT. European Group for Blood and Marrow Transplant. *Br J Haematol*. 1998;102(5):1115–1123. doi:10.1046/j.1365-2141.1998.00930.x
2. Kruszewska M, Łańda K. Leczenie szpiczaka plazmocytowego (mnogiego) w Polsce – choroba, pacjent, system. Warsaw,Poland: Fundacja Watch Health Care; 2022. https://pthit.pl/wp-content/uploads/2023/01/Raport-WHC-Szpiczak-Choroba-Pacjent-System.pdf.
3. Bourantas K. Nonsecretory multiple myeloma. *Eur J Haematol*. 1996; 56(1–2):109–111. doi:10.1111/j.1600-0609.1996.tb00312.x
4. Rajkumar SV, Dimopoulos MA, Palumbo A, et al. International Myeloma Working Group updated criteria for the diagnosis of multiple myeloma. *Lancet Oncol*. 2014;15(12):e538–e548. doi:10.1016/S1470-2045(14)70442-5
5. Cavo M, Galieni P, Gobbi M, et al. Nonsecretory multiple myeloma. *Acta Haematol*. 1985;74(1):27–30. doi:10.1159/000206159
6. Charliński G, Jurczyszyn A. Non-secretory multiple myeloma: Diagnosis and management. *Adv Clin Exp Med*. 2021;31(1):95–100. doi:10.17219/acem/141455
7. Coriu D, Weaver K, Schell M, et al. A molecular basis for nonsecretory myeloma. *Blood*. 2004;104(3):829–831. doi:10.1182/blood-2004-02-0477
8. Chawla SS, Kumar SK, Dispenzieri A, et al. Clinical course and prognosis of non-secretory multiple myeloma. *Eur J Haematol*. 2015;95(1):57–64. doi:10.1111/ejh.12478
9. Shaw GR. Nonsecretory plasma cell myeloma: Becoming even more rare with serum free light-chain assay. A brief review. *Arch Pathol Lab Med*. 2006;130(8):1212–1215. doi:10.5858/2006-130-1212-NPCMEM
10. Dispenzieri A, Kyle R, Merlini G, et al. International Myeloma Working Group guidelines for serum-free light chain analysis in multiple myeloma and related disorders. *Leukemia*. 2009;23(2):215–224. doi:10.1038/leu.2008.307
11. Drayson M, Tang LX, Drew R, Mead GP, Carr-Smith H, Bradwell AR. Serum free light-chain measurements for identifying and monitoring patients with nonsecretory multiple myeloma. *Blood*. 2001;97(9): 2900–2902. doi:10.1182/blood.V97.9.2900
12. Dreicer R, Alexanian R. Nonsecretory multiple myeloma. *Am J Hematol*. 1982;13(4):313–318. doi:10.1002/ajh.2830130406
13. Durie BGM, Harousseau JL, Miguel JS, et al. International uniform response criteria for multiple myeloma. *Leukemia*. 2006;20(9): 1467–1473. doi:10.1038/sj.leu.2404284
14. Kumar S, Pérez WS, Zhang MJ, et al. Comparable outcomes in onsecretory and secretory multiple myeloma after autologous stem cell transplantation. *Biol Blood Marrow Transplant*. 2008;14(10):1134–1140. doi:10.1016/j.bbmt.2008.07.011
15. Kumar SK, Dispenzieri A, Lacy MQ, et al. Continued improvement in survival in multiple myeloma: Changes in early mortality and outcomes in older patients. *Leukemia*. 2014;28(5):1122–1128. doi:10.1038/leu.2013.313
16. Kumar SK, Rajkumar V, Kyle RA, et al. Multiple myeloma. *Nat Rev Dis Primers*. 2017;3(1):17046. doi:10.1038/nrdp.2017.46
17. Kyle RA, Gertz MA, Witzig TE, et al. Review of 1027 patients with newly diagnosed multiple myeloma. *Mayo Clin Proc*. 2003;78(1):21–33. doi:10.4065/78.1.21

18. Larson D, Kyle RA, Rajkumar SV. Prevalence and monitoring of oligosecretory myeloma. *N Engl J Med*. 2012;367(6):580–581. doi:10.1056/NEJMc1206740
19. Lu J, Lu J, Chen W, et al. Clinical features and treatment outcome in newly diagnosed Chinese patients with multiple myeloma: Results of a multicenter analysis. *Blood Cancer J*. 2014;4(8):e239–e239. doi:10.1038/bcj.2014.55
20. Sun H, Liu A, Liu L, et al. Outcome and characteristics of nonsecretory multiple myeloma compared with secretory multiple myeloma: A retrospective multicenter study from China. *BMC Cancer*. 2023;23(1):930. doi:10.1186/s12885-023-11223-4
21. Wålinder G, Samuelsson J, Näsman P, et al. Outcome and characteristics of non-measurable myeloma: A cohort study with population-based data from the Swedish Myeloma Registry. *Eur J Haematol*. 2020;104(5):376–382. doi:10.1111/ejh.13351
22. Migkou M, Avivi I, Gavriatopoulou M, et al. Clinical characteristics and outcomes of oligosecretory and non-secretory multiple myeloma. *Ann Hematol*. 2020;99(6):1251–1255. doi:10.1007/s00277-020-03984-w
23. Smith DB, Harris M, Gowland E, Chang J, Scarffe JH. Non-secretory multiple myeloma: A report of 13 cases with a review of the literature. *Hematol Oncol*. 1986;4(4):307–313. doi:10.1002/hon.2900040407
24. Terpos E, Apperley JF, Samson D, et al. Autologous stem cell transplantation in multiple myeloma: Improved survival in nonsecretory multiple myeloma but lack of influence of age, status at transplant, previous treatment and conditioning regimen. A single-centre experience in 127 patients. *Bone Marrow Transplant*. 2003;31(3):163–170. doi:10.1038/sj.bmt.1703818
25. Nandakumar B, Kumar SK, Dispenzieri A, et al. Cytogenetic features and clinical outcomes of patients with non-secretory multiple myeloma in the era of novel agent induction therapy. *Clin Lymphoma Myeloma Leuk*. 2020;20(1):53–56. doi:10.1016/j.clml.2019.09.624
26. Fonseca R. Non-secretory myeloma: clinical and biologic implications. *Oncology (Williston Park)*. 2013;27(9):932–933. PMID:24282995.
27. Kumar S, Paiva B, Anderson KC, et al. International Myeloma Working Group consensus criteria for response and minimal residual disease assessment in multiple myeloma. *Lancet Oncol*. 2016;17(8):e328–e346. doi:10.1016/S1470-2045(16)30206-6
28. Greipp PR, Miguel JS, Durie BGM, et al. International staging system for multiple myeloma. *J Clin Oncol*. 2005;23(15):3412–3420. doi:10.1200/JCO.2005.04.242
29. Palumbo A, Avet-Loiseau H, Oliva S, et al. Revised international staging system for multiple myeloma: A report from International Myeloma Working Group. *J Clin Oncol*. 2015;33(26):2863–2869. doi:10.1200/JCO.2015.61.2267
30. Kaplan EL, Meier P. Nonparametric estimation from incomplete observations. *J Am Stat Assoc*. 1958;53(282):457–481. doi:10.1080/01621459.1958.10501452
31. National Cancer Institute. Cancer stat facts: Myeloma. Bethesda, USA: National Cancer Institute; 2022. https://seer.cancer.gov/statfacts/html/mulmy.html. Accessed March 28, 2023.
32. Coriu D, Dytfeld D, Niepel D, et al. Real-world multiple myeloma management practice patterns and outcomes in six Central and Eastern European countries. *Pol Arch Intern Med*. 2018;128(9):500–511. doi:10.20452/pamw.4305
33. Murray DL, Puig N, Kristinsson S, et al. Mass spectrometry for the evaluation of monoclonal proteins in multiple myeloma and related disorders: An International Myeloma Working Group Mass Spectrometry Committee Report. *Blood Cancer J*. 2021;11(2):24. doi:10.1038/s41408-021-00408-4
34. Paiva B, Martinez-Lopez J, Vidriales MB, et al. Comparison of immunofixation, serum free light chain, and immunophenotyping for response evaluation and prognostication in multiple myeloma. *J Clin Oncol*. 2011;29(12):1627–1633. doi:10.1200/JCO.2010.33.1967
35. Corso A, Mangiacavalli S. Non-secretory myeloma: Ready for a new definition? *Mediterr J Hematol Infect Dis*. 2017;9(1):e2017053. doi:10.4084/mjhid.2017.053
36. Lin C, Luciani A, Belhadj K, et al. Multiple myeloma treatment response assessment with whole-body dynamic contrast-enhanced MR imaging. *Radiology*. 2010;254(2):521–531. doi:10.1148/radiol.09090629
37. Bannas P, Hentschel HB, Bley TA, et al. Diagnostic performance of whole-body MRI for the detection of persistent or relapsing disease in multiple myeloma after stem cell transplantation. *Eur Radiol*. 2012;22(9):2007–2012. doi:10.1007/s00330-012-2445-y
38. Regelink JC, Minnema MC, Terpos E, et al. Comparison of modern and conventional imaging techniques in establishing multiple myeloma-related bone disease: A systematic review. *Br J Haematol*. 2013;162(1):50–61. doi:10.1111/bjh.12346

Validation of the Polish version of the Hand Function Scoring system

Maciej Belka[1,A–F], Mateusz Koziej[2,A–F], Jan Banach[3,A–F], Marta Dagmara Banach[4,A–F], Marek Trybus[5,A–F]

[1] University Hospital in Cracow, Poland
[2] Department of Anatomy, Jagiellonian University Medical College, Cracow, Poland
[3] Faculty of Health Sciences, Jagiellonian University Medical College, Cracow, Poland
[4] Department of Neurology, Jagiellonian University Medical College, Cracow, Poland
[5] 2nd Department of General Surgery, Jagiellonian University Medical College, Cracow, Poland

A – research concept and design; B – collection and/or assembly of data; C – data analysis and interpretation;
D – writing the article; E – critical revision of the article; F – final approval of the article

Advances in Clinical and Experimental Medicine, ISSN 1899–5276 (print), ISSN 2451–2680 (online) *Adv Clin Exp Med*. 2025;34(3):379–384

Address for correspondence
Marta Dagmara Banach
E-mail: martabanach@yahoo.com

Funding sources
None declared

Conflict of interest
None declared

Received on November 2, 2023
Reviewed on January 4, 2024
Accepted on March 12, 2024

Published online on April 17, 2024

Abstract

Background. The Hand Function Scoring (HFS) system was created to assess the results of rehabilitation treatment after hand injuries. A perceived hand function improvement in patients who underwent carpal tunnel syndrome surgery prompted us to use the Watts HFS questionnaire in our study.

Objectives. The study aimed to: 1) translate and validate the new questionnaire into Polish; 2) analyze the usefulness of the scale in the pre- and post-operative assessment of patients with carpal tunnel syndrome; and 3) compare the results with other questionnaires recognized as the gold standard in carpal tunnel treatment evaluation.

Materials and methods. Patients with electromyographically confirmed carpal tunnel syndrome (n = 317) were enrolled in the study. Participants completed the HFS, Boston Carpal Tunnel Questionnaire (BCTQ), Michigan Hand Outcomes Questionnaire (MHQ), and the Quality-of-Life Scale (QoLS) on their first visit to our clinic. Two weeks later, 84 patients completed the same questionnaires again, and 6–12 months after the operation, we received 90 additional responses.

Results. The analysis showed that the HFS questionnaire met the validation criteria and had a strong correlation with the BCTQ questionnaire for the Symptoms Severity Scale (SSS) (Rho = 0.70, $p < 0.001$) and the Functional Status Scale (FSS) (Rho = 0.89, $p < 0.001$).

Conclusions. The HFS questionnaire was successfully employed in the subjective assessment of carpal tunnel symptom syndrome severity and the analysis of treatment results, and would complement the clinical assessment of patients during treatment. The questionnaire could also be used in future scientific research.

Key words: quality of life, carpal tunnel syndrome, Hand Function Scoring (HFS) system, Boston Carpal Tunnel Questionnaire (BCTQ), Michigan Hand Outcomes Questionnaire (MHQ)

Cite as
Belka M, Koziej M, Banach J, Banach MD, Trybus M. Validation of the Polish version of the Hand Function Scoring system. *Adv Clin Exp Med*. 2025;34(3):379–384. doi:10.17219/acem/185977

DOI
10.17219/acem/185977

Background

Carpal tunnel syndrome is a disease that significantly reduces the quality of life (QoL),[1,2] mostly due to pain, numbness and muscle weakness that consequently lead to difficulties with everyday activities.[1]

One of the critical elements of diagnostics is a thorough pre-operative assessment of the patient.[2] The literature often confirms that, apart from the objective results of tests such as electromyography or ultrasound, understanding patient's subjective opinions on their health is equally important.[3,4] These opinions might be influenced by many factors that cannot be easily measured and quantified, such as current mental state, motivation and involvement in the treatment process, or socio-economic status.[3,5] Questionnaires, especially those tailored or adapted to a single disease, are the most useful methods of assessing the disease severity subjectively experienced by patients and allow for the assessment of treatment progress via different methods.

The HFS questionnaire created by Watts et al. to assess the results of rehabilitation after hand injury consists of 25 questions rated on a scale of 1 to 4 points. The result of the questionnaire is the sum of all points obtained, with 100 points signifying the worst possible impairment of hand function.[4] The questionnaire was used to assess hand function after fractures of the distal end of the radius[6] and showed a positive correlation with injury severity and the time needed to return to work.[4,6,7] Another study found that it correlated with the Disabilities of the Arm, Shoulder and Hand (DASH) questionnaire ($R = 0.903$, $p < 0.05$),[6] which has been consistently used to assess carpal tunnel syndrome.[8,9] However, HFS alone has never been used to evaluate such patients. To this end, we aimed to simultaneously assess patients using the Michigan Hand Outcomes Questionnaire (MHQ), previously used in upper limb diseases, and the Boston Carpal Tunnel Questionnaire (BCTQ), adapted to assess carpal tunnel syndrome symptoms. In our opinion, introducing a new questionnaire for more extensively evaluating the ability to cope with everyday activities would complement the clinical evaluation of patients and help understand patient-perceived disease severity.

Objectives

The study aimed to: 1) translate into Polish and validate the HFS questionnaire; 2) assess its usefulness in the evaluation of surgical treatment progress in patients suffering from carpal tunnel syndrome; and 3) compare and analyze the obtained results with other questionnaires recognized as the gold standard in this disease.

Materials and methods

Study design, setting and eligibility criteria

The questionnaire was initially translated into Polish according to the scheme proposed by Beaton et al.,[10] with 340 patients treated in the Trauma and Orthopaedics Clinical Department of the University Hospital in Cracow (Poland) between April 2019 and May 2021 qualified for the study. During the first visit to the clinic, patients were informed in detail about the study plan, completed a short personal questionnaire about gender, age, weight, height, and place of residence, and provided signed informed consent to participate. When patients reported bilateral symptoms of carpal tunnel syndrome, the more affected limb was examined, and when the symptoms were similarly severe, the dominant limb was examined. Afterward, patients completed the HFS, BCTQ, MHQ, and Quality-of-Life Scale (QoLS) questionnaires. Two weeks later, patients completed the HFS questionnaire again before the surgery, with the next check-up taking place 6–12 months later. The median differences between measurements, along with their quartiles and minimum and maximum range, are presented in Fig. 1.

Study inclusion criteria were: 1) age between 18 and 75 years; 2) a diagnosis of carpal tunnel syndrome confirmed with electrophysiological examination; 3) fluent Polish language; 4) a recommendation for carpal tunnel syndrome surgical treatment; 5) no other pre-existing neurological, psychiatric or musculoskeletal disorders affecting the upper limbs; and 6) no expected changes in carpal tunnel syndrome severity within 2 weeks. Exclusion criteria included: 1) ongoing rehabilitation and 2) recent wrist injury. Based on this criteria, 23 patients were excluded from the study, with 317 taking part. Implementing such inclusion and exclusion criteria facilitated the selection of a more homogenous patient cohort, with this approach aiming to enhance the internal validity of the study by ensuring a more uniform and representative group of individuals with the specified condition.

The Bioethics Comittee of the Jagiellonian University approved the study (approval No. 1072.6120.32.2018), which was conducted in line with the 1964 Helsinki Declaration and its subsequent amendments.[11]

Hand Function Scoring system

The HFS questionnaire contains 25 questions about difficulties in performing daily activities, some of which coincide with those included in the BCTQ questionnaire. The results ranged from 25 to 100 points, with higher scores indicating worse hand function.[4]

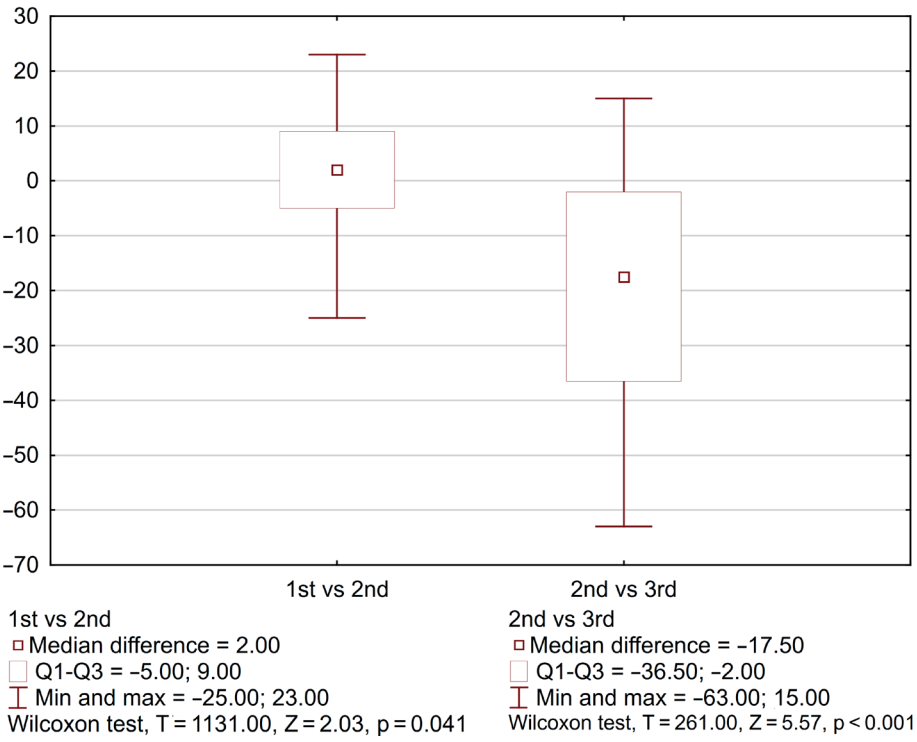

Fig. 1. Median differences in the Hand Function Scoring (HFS) system results between the 1st and 2nd measurements and the 2nd and 3rd measurements

Boston Carpal Tunnel Questionnaire

The BCTQ consists of several questions divided into 2 parts, one assessing carpal tunnel syndrome symptom severity and the other evaluating its impact on daily functioning. The final result is the mean score obtained from individual questions, with a lower score indicating a better subjective assessment of limb functioning.[12] The study used the Polish version of the questionnaire.[2]

Michigan Hand Outcomes Questionnaire

The MHQ is the only one that allows for simultaneous assessment of both upper limbs in terms of general functioning, problems with performing daily activities, pain intensity, and a subjective assessment of the aesthetics and general satisfaction with hand functioning. The questionnaire was designed to assess many upper limb diseases,[13] with its usefulness in evaluating patients with carpal tunnel syndrome confirmed in multiple studies.[14–16] The higher the final score, the better the limb function, except for pain assessment, where a lower score indicates less pain. The Polish version of the questionnaire was used in this study.[15]

Quality of Life Scale

The questionnaire proposed by Spitzer et al. in 1986 assessed QoL. The tool is a simple questionnaire consisting of 5 questions assessing the level of activity, daily life, health, support, and appearance.[15,17] The Polish version of the questionnaire was used in this study.[18]

Statistical analyses

All calculations employed Statistica v. 13.3 software (StatSoft Inc., Tulsa, USA), with data analyzed for normal distribution and presented using the mean and standard deviation (±SD) if normally distributed and quartiles (Q1–Q3) if the data failed the normality test. For correlations between variables, Pearson's correlation was used when both quantitative variables were normally distributed, with Spearman's rank order correlation used when this condition was not met. Correlations between pre- and post-surgery results were evaluated.

Analysis of differences between men and women was undertaken to assess if the results revealed factors that might influence the study outcomes. Student's t-test for independent variables was employed if quantitative variables were normally distributed and there was homogeneity of variance (evaluated using the t-test for variance), while the Mann–Whitney U test was applied when a normal distribution was not met. Differences between pre- and post-operative results were also analyzed using the Student's t-test for normally distributed dependent variables and the Wilcoxon test for non-normal data. A p-value below 0.05 was considered statistically significant.

Tests evaluating repeatability of measurements, internal consistency and analysis of measurement errors were used for reliability analysis. The repeatability of the measurements was assessed using the interclass correlation coefficient (ICC), a model of absolute agreement of two-way mixed effects. The value of this coefficient varies between 0 and 1, with the expected value for this type of work being

above 0.7. The 2nd method for assessing repeatability was Bland–Altman plots, in which the vertical axis shows the difference between the two HFS results and the horizontal axis the average value of the 2 pre-operative measurements, with a 2-week break in between. The graph shows the 95% confidence interval (95% CI) for mean measurements defined as ±1.96 × SD.[19]

The analysis of internal consistency employed Cronbach's alpha parameters to evaluate whether individual questions correlated with each other. To assess measurement errors, the standard error of measurement (SEM) coefficient was calculated according to the formula SEM = SD × √(1 – ICC), which indicates perfect questionnaire reliability when equal to 0. In addition, the minimum detectable change with a 95% CI was calculated according to the formula MDC95 = 1.96 × SEM × √2, which tells us what the minimum change in the questionnaire answers is to be considered correct and exclude measurement error.

Determining the validation criterion involved investigating correlations between the HFS questionnaire and the current gold standard for carpal tunnel syndrome patient assessment (the BCTQ questionnaire)[12] to calculate the correlation coefficient.[10] In addition, the analysis of marginal effects used the 15% criterion, meaning that the proportion of patients who achieved the maximum and minimum number of possible points should not exceed 15% of the study group.[20]

Cohen's standard mean response factor

$$SRM = (Me_{preoperative} - Me_{postoperative})/SD_{\text{of the mean difference}}$$

was used to analyze responsiveness to produce values above 0.8 (large), 0.5 (medium) and 0.3 (small).[21]

Study size

The sample size of 50 participants was determined with the intention of adequately powering the study to detect significant HFS changes, the primary outcome measure of interest. The sample size was calculated based on an Cronbach's alpha level of 0.05, an absolute error rate of 5% and a presumed SD of 20 for the HFS scores. These parameters were chosen to ensure that the study would have sufficient statistical power to detect meaningful differences or correlations in HFS scores before and after the intervention, allowing for robust and reliable conclusions.

Results

No significant differences were found between the original and translated copies in the translation process. In the initial questionnaire comprehension analysis conducted on 10 patients, no problems with understanding questions were reported. The final Polish version of the questionnaire was created (Supplementary Material 1). Ultimately, 317 patients were enrolled in the study, with 84 answering the questionnaire again before surgical treatment and 90 responding 6–12 months after. All individuals who responded to the 2nd pre-operative questionnaire also provided responses post-operatively. However, due to missing data and an inability to calculate the questionnaire outcome, several individuals were excluded from the analysis of the 2nd pre-operative response.

Most patients were women (73.19%), the mean duration of symptoms was 22.77 ±25.31 months, and carpal tunnel syndrome was more common on the right side (53.00%). The mean age was 59.05 years (SD = ±14.24) for both men and women, while men were heavier (90.0 kg (Q1–Q3 = 80.0–98.0) compared to 70.0 kg (Q1–Q3 = 62.0–80.0 kg)) and taller (175.0 cm (Q1–Q3 = 170.0–179.0) compared to 163.0 cm (Q1–Q3 = 158.0–168.0 cm)) than women. The overall body mass index (BMI) was 27.69 kg/m^2, with men having a higher median BMI (29.01 kg/m^2, Q1–Q3 = 27.74–32.65 kg/m^2) than women (26.36 kg/m^2, Q1–Q3 = 23.23–29.64 kg/m^2).

The mean pre-operative HFS value was 44.0 (Q1–Q3 = 25.0–59.0), the 2nd was 49.0 (Q1–Q3 = 35.0–61.0) and the 3rd was 25.0 (Q1–Q3 = 25.0–26.0), while ICC = 0.909, Cronbach's alpha = 0.95, SEM = 5.54, and MDC95 = 15.31. The difference between pre- and post-operative measurements for paired samples was statistically significant (p = 0.001). The median with quartiles of the BCTQ, MHQ and QoLS questionnaires are presented in Table 1. We did not observe ceiling or floor effects in our study.

The Bland–Altman analysis indicated that the agreement limit for HFS was between –20.81 (95% CI = –24.41––17.22) and 16.69 (95% CI = 13.10–20.29). The results of this analysis showed that there was high agreement between 2 measurements in a short interval, confirming good repeatability of the results.

The Polish version of the HSF correlated strongly with the symptom severity section of the BCTQ (Rho = 0.70,

Table 1. Median scores with 1st quartile (Q1)–3rd quartile (Q3) for the 1st measurement in each questionnaire

Questionnaire	Median	Q1–Q3
MHQ OHF	50.00	25.00–75.00
MHQ ADL	68.21	30.71–100.00
MHQ Work	75.00	25.00–100.00
MHQ Pain	70.00	70.00–80.00
MHQ Aesthetic	100.00	81.25–100.00
MHQ Satisfaction	41.67	25.00–75.00
MHQ total	63.38	46.49–79.23
BCTQ SSS	3.00	2.09–4.00
BCTQ FSS	2.38	1.00–3.38
QoLS1	10.00	8.00–10.00

HFS – Hand Function Score; MHQ – Michigan Hand Outcome Questionnaire; OHF – Overall Hand Function; ADL – Activities of Daily Living; BCTQ – Boston Carpal Tunnel Questionnaire; SSS – Symptoms Severity Scale; FSS – Functional Severity Scale; QoLS – Quality of Life Scale.

Table 2. Spearman's correlations between the Hand Function Scoring (HFS) system questionnaire results and those used for comparison in the study

Questionnaires	HFS correlation	
	Rho	p-value
MHQ OHF	−0.77	<0.001
MHQ ADL	−0.92	<0.001
MHQ Work	−0.76	<0.001
MHQ Pain	0.53	<0.001
MHQ Aesthetic	−0.38	0.001
MHQ Satisfaction	−0.77	<0.001
MHQ total	−0.85	<0.001
QoLS	−0.50	<0.001
BCTQ SSS	0.70	<0.001
BCTQ FSS	0.89	<0.001

MHQ – Michigan Hand Outcome Questionnaire; OHF – Overall Hand Function; ADL – Activities of Daily Living; BCTQ – Boston Carpal Tunnel Questionnaire; SSS – Symptoms Severity Scale; FSS – Functional Severity Scale; QoLS – Quality of Life Scale.

$p < 0.001$) and the BCTQ section evaluating upper limb function (Rho = 0.89, $p < 0.001$), meeting the validation condition. Moreover, the HSF questionnaire correlated strongly with the MHQ results (Rho= −0.85, $p < 0.001$), with the result being negative due to the inverse calculation used. As expected, HFS correlated the most with the part evaluating hand function in everyday activities (Rho = −0.92, $p < 0.001$). In addition, the HFS score moderately correlated with the QoL (Rho = −0.50, $p < 0.001$). Table 2 presents all HFS questionnaire correlation results.

The standard Cohen's d value for HFS was 0.69. Figure 1 shows the median differences between the 1st and 2nd preoperative measurements and those recorded post-operatively, both of which were statistically significant (pre-surgery (T = 1131.00, Z = 2.03, p = 0.041) and post-surgery (T = 261.00, Z = 5.57, $p < 0.001$)).

Discussion

In this study, we translated the HFS questionnaire into Polish and validated it using a group of carpal tunnel syndrome patients. The questionnaire's high correlation with the BCTQ symptom severity scale (SSS) (Rho = 0.89) suggests it can be effectively used for the clinical assessment of treatment results in such patients. Furthermore, Cronbach's alpha coefficient of 0.95, a measure of the compliance of answers given by patients to individual questions, demonstrates the high quality of the tool. Analysis of the original work by Watts et al. revealed the HFS to be of higher quality,[4] though Cronbach's alpha coefficient for the Polish version of the BCTQ and MHQ were at a similar level, with 0.906 for the BCTQ SSS, 0.924 for the BCTQ FSS,[2] and individual MHQ subscales ranging from 0.79 to 0.96.[15] Therefore, the HFS questionnaire can be used to assess carpal tunnel syndrome patients.

Our institution mainly uses the BCTQ to assess patients with carpal tunnel syndrome. However, in our opinion, introducing a new questionnaire to more extensively assess coping with everyday activities would support the clinical evaluation of treatment effects. In addition, HFS allows for a more comprehensive comparison of treatment results between different research centers. As such, HFS could be employed in further scientific works.

The available evidence demonstrates that the HFS can assess patients with wrist fractures, and the results correlated with the time off work, with worse hand function causing more time off.[5,6] The HFS authors then used the results to assess post-injury hand function improvement after rehabilitation.[4] These findings indicate that the HFS would be a useful tool for assessing carpal tunnel syndrome treatment effectiveness.

Our analysis showed that the HFS questionnaire correlated with the QoLS (Rho = −0.50, $p < 0.001$). There are only a few studies reporting the impact of carpal tunnel syndrome on QoL using questionnaires evaluated in the current study, with 1 such study showing a correlation between the BCTQ and the QoLS ($r = 0.50$, $p < 0.05$). This finding is similar to ours, though the correlation with the 36-item short-form survey (SF-36) was as high as 0.70.[8] In turn, the MHQ correlation with SF-36 was much lower, and in individual subscales of the SF-36, it ranged between $r = 0.254$ and $r = 0.520$.[15]

The strength of the current study lies within its prospective nature and the simultaneous analysis of comparisons between questionnaires used. In addition, the usefulness of the newly validated questionnaire in the assessment of patients with carpal tunnel syndrome was demonstrated.

Study limitations

Study limitations include its single-center nature, the inability to eliminate patient selection bias, and the fact that participating patients did not fully or completely reflect the entire population of those suffering from carpal tunnel syndrome. Further research with more participants is needed to obtain a broader scope for using the questionnaires in patients with carpal tunnel syndrome.

Conclusions

The current work translated the HFS questionnaire into Polish and validated it. The results strongly correlate with the BCTQ questionnaire, meaning it can be used to assess patients with carpal tunnel syndrome throughout the treatment process, allowing for a more extensive and subjective assessment of hand functioning during everyday activities. Furthermore, the HFS can compare therapy results between treatment centers and in future scientific research.

Supplementary data

The Supplementary materials are available at https://doi.org/10.5281/zenodo.10723897. The package includes the following files:

Supplementary Material 1. Polish version of the validated HFS system.

Supplementary Material 2. Results of the Shapiro–Wilk tests for the variables used in the research.

Data availability

The datasets generated and/or analyzed during the current study are available from the corresponding author on reasonable request.

Consent for publication

Not applicable.

ORCID iDs

Maciej Belka https://orcid.org/0000-0001-5058-5914
Mateusz Koziej https://orcid.org/0000-0002-2635-0776
Marta Dagmara Banach https://orcid.org/0000-0002-4656-3656
Marek Trybus https://orcid.org/0000-0003-2750-8608

References

1. Malakootian M, Soveizi M, Gholipour A, Oveisee M. Pathophysiology, diagnosis, treatment, and genetics of carpal tunnel syndrome: A review. *Cell Mol Neurobiol*. 2023;43(5):1817–1831. doi:10.1007/s10571-022-01297-2
2. Trybus M, Koziej M, Belka M, Bednarek M, Banach M. The Polish version of the Boston Carpal Tunnel Questionnaire: Associations between patient-rated outcome measures and nerve conduction studies. *J Plast Reconstr Aesthet Surg*. 2019;72(6):924–932. doi:10.1016/j.bjps.2018.12.032
3. Belka M, Koziej M, Trybus M, Fijałkowska M, Banach M. The adaptation of Polish version of Six-Item Carpal Tunnel Syndrome Symptoms Scale. *J Orthop Sci*. 2022;27(5):1039–1043. doi:10.1016/j.jos.2021.06.008
4. Watts AMI, Greenstock M, Cole RP. Outcome following the rehabilitation of hand trauma patients: The importance of a subjective functional assessment. *J Hand Surg*. 1998;23(4):485–489. doi:10.1016/S0266-7681(98)80128-9
5. Roesler ML, Glendon AI, O'Callaghan FV. Recovering from traumatic occupational hand injury following surgery: A biopsychosocial perspective. *J Occup Rehabil*. 2013;23(4):536–546. doi:10.1007/s10926-013-9422-4
6. Buchanan D, Prothero D, Field J. Which are the most relevant questions in the assessment of outcome after distal radial fractures? *Adv Orthop*. 2015;2015:460589. doi:10.1155/2015/460589
7. Opsteegh L, Reinders-Messelink HA, Schollier D, et al. Determinants of return to work in patients with hand disorders and hand injuries. *J Occup Rehabil*. 2009;19(3):245–255. doi:10.1007/s10926-009-9181-4
8. Boyd KU, Gan BS, Ross DC, Richards RS, Roth JH, MacDermid JC. Outcomes in carpal tunnel syndrome: Symptom severity, conservative management and progression to surgery. *Clin Invest Med*. 2005;28(5):254–260. PMID:16265997.
9. Greenslade JR, Mehta RL, Belward P, Warwick DJ. Dash and Boston Questionnaire assessment of carpal tunnel syndrome outcome: What is the responsiveness of an outcome questionnaire? *J Hand Surg*. 2004;29(2):159–164. doi:10.1016/j.jhsb.2003.10.010
10. Beaton DE, Bombardier C, Guillemin F, Ferraz MB. Guidelines for the process of cross-cultural adaptation of self-report measures. *Spine (Phila Pa 1976)*. 2000;25(24):3186–3191. doi:10.1097/00007632-200012150-00014
11. Cochran WG. *Sampling Techniques*. 3rd ed. New York, USA: Wiley & Sons; 1977. ISBN: 978-0-471-16240-7, 978-0-471-02939-7.
12. Leite JCDC, Jerosch-Herold C, Song F. A systematic review of the psychometric properties of the Boston Carpal Tunnel Questionnaire. *BMC Musculoskelet Disord*. 2006;7(1):78. doi:10.1186/1471-2474-7-78
13. Chung KC, Pillsbury MS, Walters MR, Hayward RA. Reliability and validity testing of the Michigan Hand Outcomes Questionnaire. *J Hand Surg*. 1998;23(4):575–587. doi:10.1016/S0363-5023(98)80042-7
14. Koziej M, Trybus M, Banach M, et al. Comparison of patient-reported outcome measurements and objective measurements after cubital tunnel decompression. *Plast Reconstr Surg*. 2018;141(5):1171–1181. doi:10.1097/PRS.0000000000004291
15. Koziej M, Trybus M, Mydłowska A, et al. The Polish version of the Michigan Hand Outcomes Questionnaire: Cross-cultural adaptation, reliability, construct validity, and measurement error. *J Hand Surg Eur Vol*. 2018;43(2):199–208. doi:10.1177/1753193417729579
16. Zyluk A, Piotuch B. Use of questionnaires in outcome measurement in hand surgery [in Polish]. *Chir Narzadow Ruchu Ortop Pol*. 2009;74(4):193–201. PMID:19999612.
17. Spitzer WO, Dobson AJ, Hall J, et al. Measuring the quality of life of cancer patients. *J Chronic Dis*. 1981;34(12):585–597. doi:10.1016/0021-9681(81)90058-8
18. Leppert W, Forycka M, de Walden-Gałuszko K, Majkowicz M, Buss T. Ocena jakości życia u chorych na nowotwory – zalecenia dla personelu oddziałów onkologicznych i medycyny paliatywnej. *Psychoonkologia*. 2014;1:17–29. https://www.termedia.pl/Ocena-jakosci-zycia-u-chorych-na-nowotwory-zalecenia-dla-personelu-oddzialow-onkologicznych-i-medycyny-paliatywnej,63,22979,1,0.html. Accessed November 1, 2023.
19. Bland JM, Altman DG. Measuring agreement in method comparison studies. *Stat Methods Med Res*. 1999;8(2):135–160. doi:10.1177/096228029900800204
20. Terwee CB, Bot SDM, De Boer MR, et al. Quality criteria were proposed for measurement properties of health status questionnaires. *J Clin Epidemiol*. 2007;60(1):34–42. doi:10.1016/j.jclinepi.2006.03.012
21. Cohen J. *Statistical Power Analysis for the Behavioral Sciences*. New York, USA: Routledge; 2013. doi:10.4324/9780203771587

Stabilization of the hypoplastic thumb type Blauth IIIB using a non-vascularized proximal interphalangeal joint from the toe as an alternative reconstruction when pollicization is not accepted: Description of the surgical technique

Michał Górecki[A–E], Piotr Czarnecki[A,D–F], Leszek Romanowski[A,E,F]

Department of Traumatology, Orthopedics and Hand Surgery, Poznan University of Medical Sciences, Poland

A – research concept and design; B – collection and/or assembly of data; C – data analysis and interpretation;
D – writing the article; E – critical revision of the article; F – final approval of the article

Advances in Clinical and Experimental Medicine, ISSN 1899–5276 (print), ISSN 2451–2680 (online) *Adv Clin Exp Med*. 2025;34(3):385–392

Address for correspondence
Michał Górecki
E-mail: michalmgorecki@gmail.com

Funding sources
The research was financed by a Big Research Grant (No. 5330) from statutory funding for young researchers – doctoral students for 2022 from Poznan University of Medical Sciences.

Conflict of interest
None declared

Received on December 23, 2023
Reviewed on March 1, 2024
Accepted on March 25, 2024

Published online on April 17, 2024

Cite as
Górecki M, Czarnecki P, Romanowski L. Stabilization of the hypoplastic thumb type Blauth IIIB using a non-vascularized proximal interphalangeal joint from the toe as an alternative reconstruction when pollicization is not accepted: Description of the surgical technique. *Adv Clin Exp Med*. 2025;34(3):385–392. doi:10.17219/acem/186477

DOI
10.17219/acem/186477

Abstract

Background. A Blauth IIIB hypoplastic thumb is a significant functional and cosmetic problem for the developing hand in children. The gold standard in treatment is amputation and index pollicization. Despite the good functional results, some parents do not consent to the operation, mainly for cosmetic reasons.

Objectives. The aim is to present a detailed description and features of the technique used in our department for stabilization of a hypoplastic thumb type Blauth IIIB with a non-vascularized proximal interphalangeal joint from the toe. This is the first description of this surgery for this kind of congenital defect, together with the largest group of patients analyzed compared to alternative techniques described in the literature.

Materials and methods. Sixteen patients were included in the analysis. The mean age was 3 years (standard deviation (SD) ±2). In most cases, it was a unilateral and isolated defect. We described the surgical technique and postoperative management in detail and assessed intraoperative factors such as donor selection, operative time, technical problems, stabilization time, complication rate, and reoperations. Appropriate statistics were performed.

Results. Most often, the graft was taken from the 3rd toe. The average operation time was 59 ±17.5 min. No technical problems were found during the surgery. The Kirschner wire was removed after an average of 6.5 weeks. The complication rate was 25%, which included the destabilization of Kirschner wires or graft non-union, but it decreased to 6% after reoperation. Five patients underwent tendon transfers.

Conclusions. The presented technique is based on principles such as vascularized metatarsophalangeal joint transplants. It may be an option for stabilizing a hypoplastic thumb if parents do not consent to pollicization. Having microsurgical skills is unnecessary. The operation and anesthesia times are significantly shorter, resulting in less burden on the child's body. The study will continue assessing long-term postoperative functions and the comparison to pollicization.

Key words: proximal interphalangeal joint, thumb hypoplasia, Blauth IIIB, PIP joint transfer, thumb stabilization

Background

Congenital disabilities occur in approx. 1% of newborns, and 10% are associated with upper limb anomalies. Of all hand defects, only 11% relate to thumb hypoplasia or aplasia, which is part of radial longitudinal hand deficiency. It can occur as an isolated defect or be associated with such syndromes as Apert syndrome, Rubinstein syndrome, Holt–Oram syndrome, Fanconi anemia, VACTERL association, and congenital radial deficiency.[1–3] The modified Blauth classification, based on the clinical picture and X-ray images, describes the degree of thumb hypoplasia and helps to select an appropriate surgical treatment.[4,5]

Thumb aplasia or hypoplasia significantly impairs the hand grip function and the proper physical and mental development of the child.[6] Surgical treatment can help to reduce the degree of disability, improve the child's development and reduce restrictions in everyday life. It is essential to implement appropriate treatment early to prevent the formation of inappropriate grip patterns, which – when preserved in the cerebral cortex – can significantly hinder rehabilitation and subsequent grip development.[6–8] The choice of a surgical method depends on the degree of thumb hypoplasia and on cosmetic and ethical aspects, which increasingly influence the parents' decisions.[5,9–11]

Grade IIIB thumb hypoplasia, according to the modified Blauth classification, is characterized by shortening and narrowing, flattening of the thumb's commissure, underdevelopment of the thenar muscles, tendons of the flexor pollicis longus (FPL), extensor pollicis longus (EPL), extensor pollicis brevis (EPB), and abductor pollicis longus (APL), as well as proximal 2/3 of the first metacarpal and instability of the metacarpophalangeal and carpometacarpal joints. The gold standard of treatment is the amputation of the thumb and index finger pollicization. This operation is associated with good functional effects. The range of motion of the transferred finger is equivalent to 50% of an average thumb movement, while the force of the global and 2-point grip is equivalent to 63–67% and 55–60% of a healthy hand force, respectively. Over 70% of patients are satisfied with the surgery results.[2,12–15]

Despite the treatment's outcomes, some parents do not accept the amputation since it forms a 4-fingered hand. In the literature, few reconstructive surgeries are presented that are aimed at increasing the stability of the hypoplastic thumb, where hypermobility and instability are the leading causes of dysfunction. [9–11,16–23]

Objectives

We want to present an alternative technique used for over 20 years in the authors' workplace, partly based on principles described in the literature. It consists of stabilizing the hypoplastic thumb with a non-vascularized proximal interphalangeal joint (PIP) graft from the toe to reconstruct the first carpometacarpal joint (CMC) and stabilize the thumb (Fig. 1). This technique can be supplemented with tendon or muscle transfers to improve active movements of the thumb and add more stability, e.g., transfer of the superficial flexor tendon of the ring finger or a Huber transfer for thumb opponensplasty and an extensor indicis proprius tendon transfer for extension and radial abduction of the thumb.[18,20]

The article aims to present a detailed description of the technique and evaluates the technical aspects of the surgery. This is the first description of this surgery for this kind of congenital disability, together with the largest group of patients analyzed compared to alternative techniques.

Materials and methods

Study design

This is a retrospective study, assessing clinical data included in the medical records from the hospital and outpatient treatments, preseting also a detailed description of the surgical technique. The data were summarized, and basic statistical operations were performed.

Participants

With this technique, 16 patients were operated on (9 men and 7 women) in the years 2005–2022. The mean age at the operation was 3 years. All patients underwent reconstructive

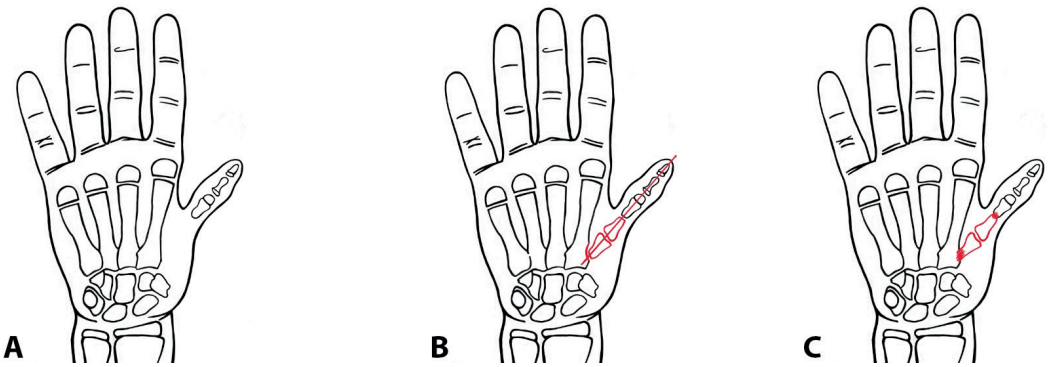

Fig. 1. Schematic drawing showing stabilization of the hypoplastic thumb type Blauth IIIB using a non-vascularized proximal interphalangeal joint from the toe. A. Hypoplastic thumb type Blauth IIIB before the operation; B. Thumb after the procedure; transferred joint and K-wire are marked in red; C. Thumb after obtaining bone union of the graft

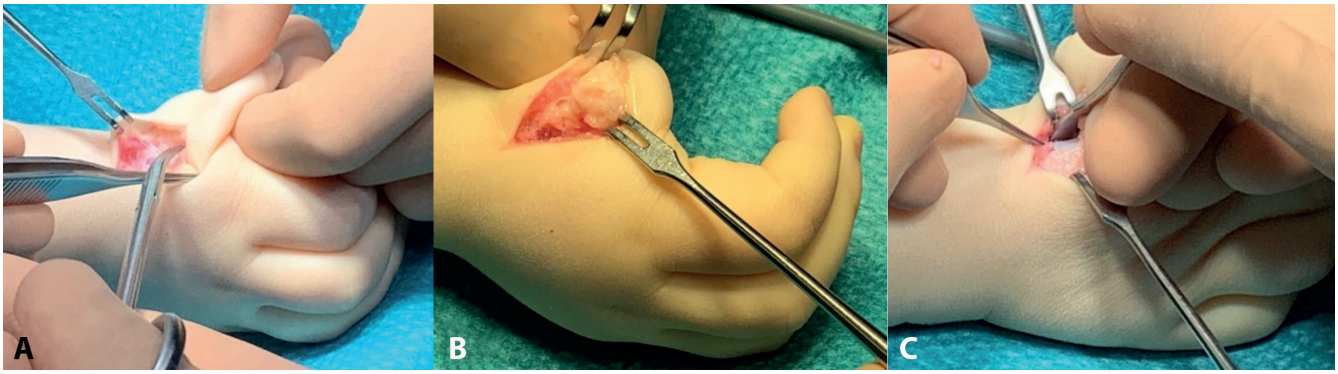

Fig. 2. A. An incision on the dorsal-radial side of the base of the thumb; B. Exposure and release of the proximal part of the first metacarpal bone; C. Preparing a space for a proximal interphalangeal joint (PIP) joint graft

Table 1. Details of the patients

Number of patients	Gender	Mean age at the operation [years]	Blauth classification	Unilateral defect	Complex defect
16	male – 9 female – 7	3 (SD ±2)	III B – 16	yes – 13 no – 3	yes – 3 no – 10

SD – standard deviation.

surgery of a type IIIB hypoplastic thumb, consisting of its stabilization using a non-vascularized PIP joint graft from the foot. In 13 cases, it was unilateral, and in 10 cases, it was an isolated defect of the thumb; in 3 cases, it was a complex upper extremity defect like congenital radial deficiency, and in 4 patients, an additional diagnosis of Poland's syndrome, congenital hearing loss, hydrocephalus, and an extra thumb or thumb aplasia in the contralateral hand was present.

Before the operation, parents were presented with the possibility of performing index finger pollicization, which they disagreed with because of the adverse cosmetic effect of a 4-fingered hand (Table 1).

Nine right hands and 7 left hands were operated on. The donor of the PIP joint was harvested from the right foot 11 times and the left foot 5 times, of which 63% (10/16) of grafts were taken from the same side as the operated hand. Most often, the graft was taken from the 3rd toe in 50% of cases, while in the remaining cases, the 4th and 2nd toes were used as the donor, 5 (31%) and 3 (19%) times, respectively.

Description of the operating technique

Four orthopedists performed all surgeries under the same operating room conditions. The surgery was performed in a bloodless field with a tourniquet through a longitudinal dorsal radial incision at the base of the thumb. Visualization of the first metacarpal bone was achieved. Exposure and release of its proximal part and preparation of the proximal stump to cancellous bone were performed to increase the chance of osseointegration with the graft. A space was prepared for the graft from the base of the first metacarpal bone to the proximal shaft of the second metacarpal bone (Fig. 2).

Our preferred joint donor from the foot is the 3rd or 4th toe because their size resembles the CMC I joint. In our experience, its absence did not cause significant dysfunctions of the foot, which does not prevent possible microsurgical transfers from the 2nd toe (Fig. 3).

A longitudinal dorsal incision of the toe is made above the PIP joint, next to the extensor tendon with its protection. Using a bone cutter, an osteotomy of the proximal and medial phalanges is performed to collect the joint graft with capsule and collateral ligaments. We harvest a graft length to fill the distance between the second metacarpal proximal metaphysis and the hypoplastic first metacarpal stump after maximum traction of the thumb, so that after the graft is introduced, there is compression between the bones, which increases the chance of osseointegration. We close the space with stitches. The toe is stabilized with a centrally inserted 1.0 or 0.8 mm Kirschner wire (Fig. 4).

Through the PIP joint graft, one 1.0 mm Kirschner wire is inserted longitudinally (Fig. 5). We prepare a bed for the graft from the radial proximal 1/3 side of the second metacarpal bone shaft. The harvested joint is stabilized on the first metacarpal stump by inserting the Kirschner wire antegrade. Then, it is stabilized to the previously prepared bed on the second metacarpal bone retrograde using the same axial wire to set the thumb at about 30° radial and palmar abduction (Fig. 6).

Additionally, 5 patients underwent tendon transfers to improve the active movement of the thumb, like flexor digitorum superficialis tendon 3rd or 4th finger to flexor pollicis longus tendon, abductor digiti minimi tendon or flexor digitorum superficialis tendon 4th finger to thumb opposition, extensor carpi radialis longus and flexor digitorum superficialis tendon 3rd finger on thumb's proximal phalanx for metararpophalangeal joint extensor and flexon, and extensor indicis proprius tendon to extensor pollicis longus. To close the skin wound, an absorbable suture of 4-0 or 5-0 is used,

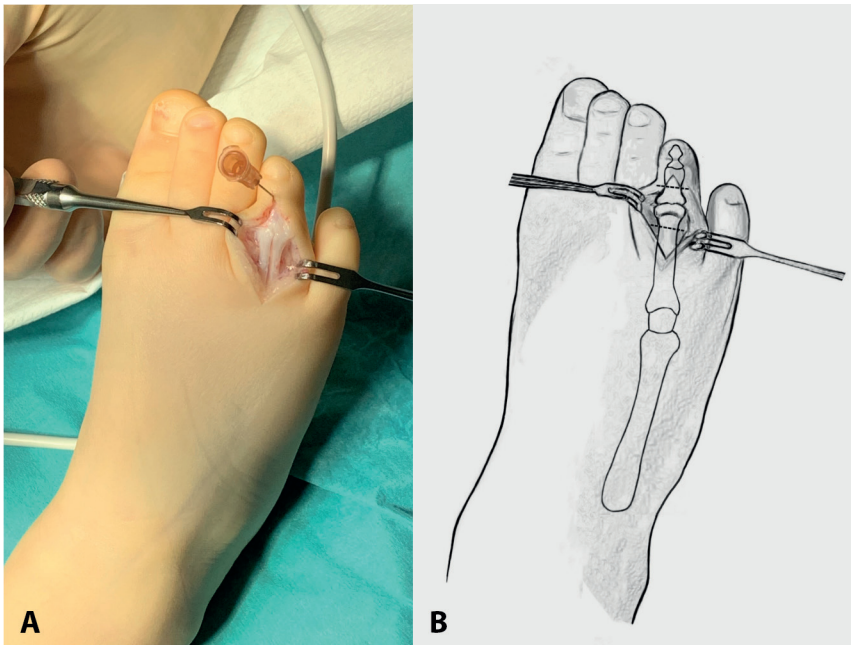

Fig. 3. A. Dorsal skin incision and exposure of the proximal interphalangeal joint (PIP) joint; B. Schematic drawing showing the harvesting of the PIP joint from the foot (osteotomy marked with a dashed line)

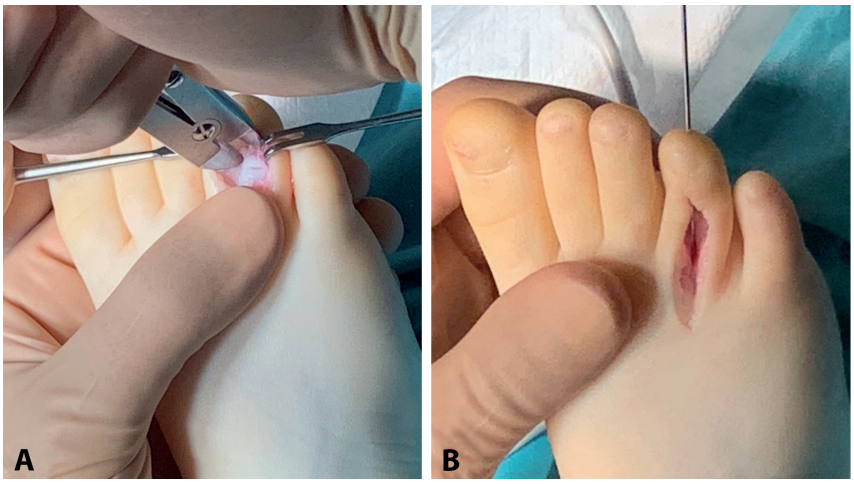

Fig. 4. A. Harvesting of the proximal interphalangeal joint (PIP) joint from the foot using a bone cutter; B. The toe is stabilized with Kirschner wire 1.0 or 0.8 mm inserted longitudinally

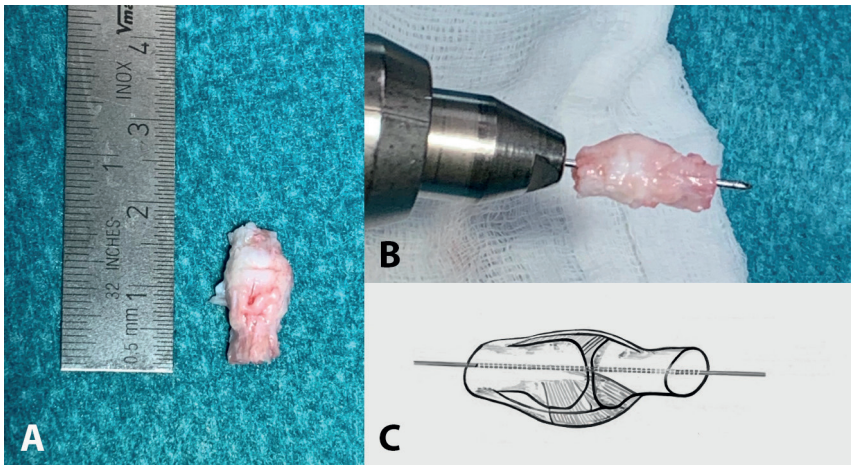

Fig. 5. A. The harvested proximal interphalangeal joint (PIP) joint graft with capsule and collateral ligaments is measured; B. One Kirschner wire (1.0 mm) is inserted centrally; C. Schematic drawing

depending on the size of the thumb. We secure the operated area with a large amount of cotton wool dressing, which protects and keeps the thumb in a fixed position. Additionally, the operated thumb is secured with an above-elbow cast.

The first change of dressing is performed 2 weeks after the surgery. The wire is removed at 6–8 weeks after the evaluation of bone fusion using an X-ray.

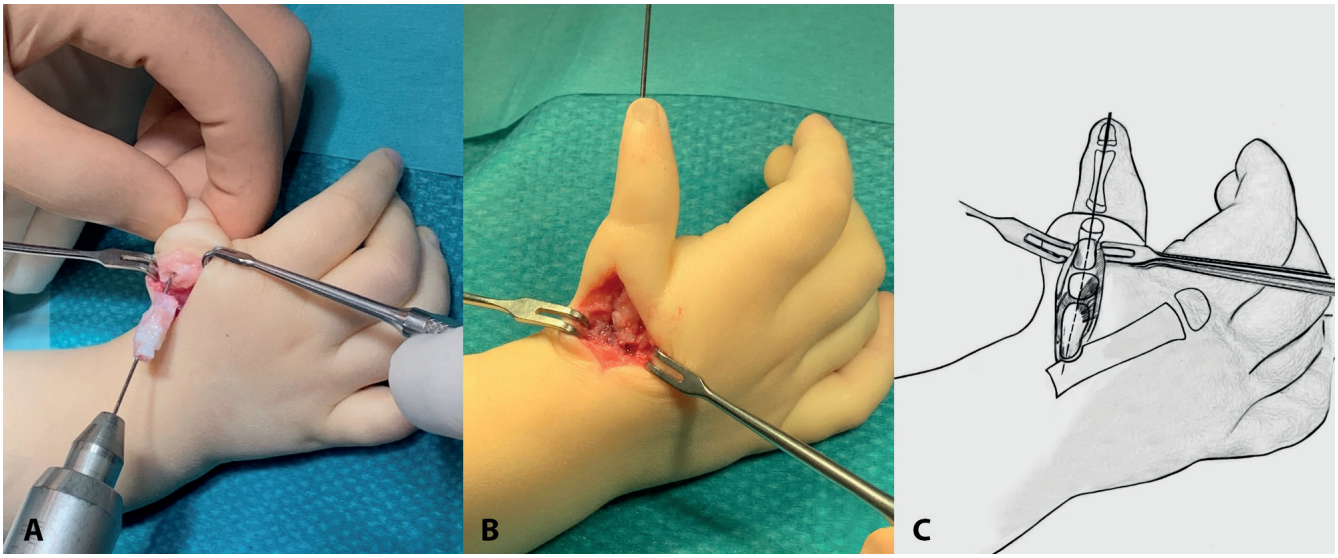

Fig. 6. A harvested joint graft is stabilized on the first metacarpal bone stump by inserting the Kirschner wire (A) and then into the previously prepared bed on the second metacarpal bone using the same axial K-wire (B); C. Schematic drawing

Table 2. Summary of data regarding surgical technique

Number of patients	Hand operated	Foot donor	PIP joint donor – toe	Average time of surgery	Technical problems during operation	Average time of Kirschner wire stabilization	Complication	Reoperations	Tendon transfer
16	right – 9 left – 7	right – 11 left – 5	2nd – 3 3rd – 8 4th – 5	59 min (SD ±17.5)	none	6.5 weeks (SD ±2.5)	4 cases*	3 cases*	5 cases*

* Details included in the text. SD – standard deviation; PIP – proximal interphalangeal joint.

Results

No significant technical problems were found during surgery in any patient. After surgery, the Kirschner wire was removed after an average of 6.5 weeks (Fig. 7,8). The average operation time was almost 1 h. The complication rate was 25% (4 patients), and there were 2 cases of destabilization and earlier removal of Kirschner wires where, in 1 case, graft union was not achieved, and there were 2 cases of non-union of the graft to the 1st or 2nd metacarpal bones. For this reason, reoperation was performed in 3 cases, consisting of only graft restabilization in 1 case, and in 2 cases, resection of the pseudoarthrosis, filling the defect with a bone graft and restabilization was required. After surgery in these 3 patients, union was achieved in 2, while pseudoarthrosis persisted in 1 (Table 2).

Discussion

The generally accepted gold standard of treatment in type IIIB thumb hypoplasia, according to the modified Blauth classification, is amputation of the thumb and index finger pollicization.[2]

Some parents do not accept this treatment method, as it results in an unfavorable cosmetic appearance in the form of a 4-fingered hand. Therefore, surgical techniques that preserve a hypoplastic thumb and improve thumb stability and function are being developed.

The main goal of reconstructive techniques described in the literature is to increase the stability of the hypermobile thumb, i.e., vascularized/non-vascularized metatarsophalangeal joint (MTP) transplant, free toe phalanx transplant, transfer of half the width or the entire metatarsal bone, vascularized metatarsal bone transplant with a full-thickness skin graft, and a non-vascularized structural transplant from the iliac crest.[9–11,14,17–19,23–28]

Allogenic (vascularized/non-vascularized) transfer of all or part of the PIP joint from the foot is widely described in the literature, both in adults and children, as an alternative to arthrodesis or endoprosthesis of the joint. The main indication is a congenital/post-traumatic/post-infectious deformation of the PIP joint.[29–31]

Kuzu et al.[30] presented the results of 7 adult patients after a transfer of a vascularized PIP II joint from the foot to improve the range of motion of the PIP joint of the finger. At 1-year follow-up, there was an increase in the amplitude of passive movement from 5° to 53° and active movement from 2° to 43°.

Dautel[29] presented the results after reconstructing 43 PIP joints in children and adults, with a 5-year follow-up. The average amplitude of active movement was

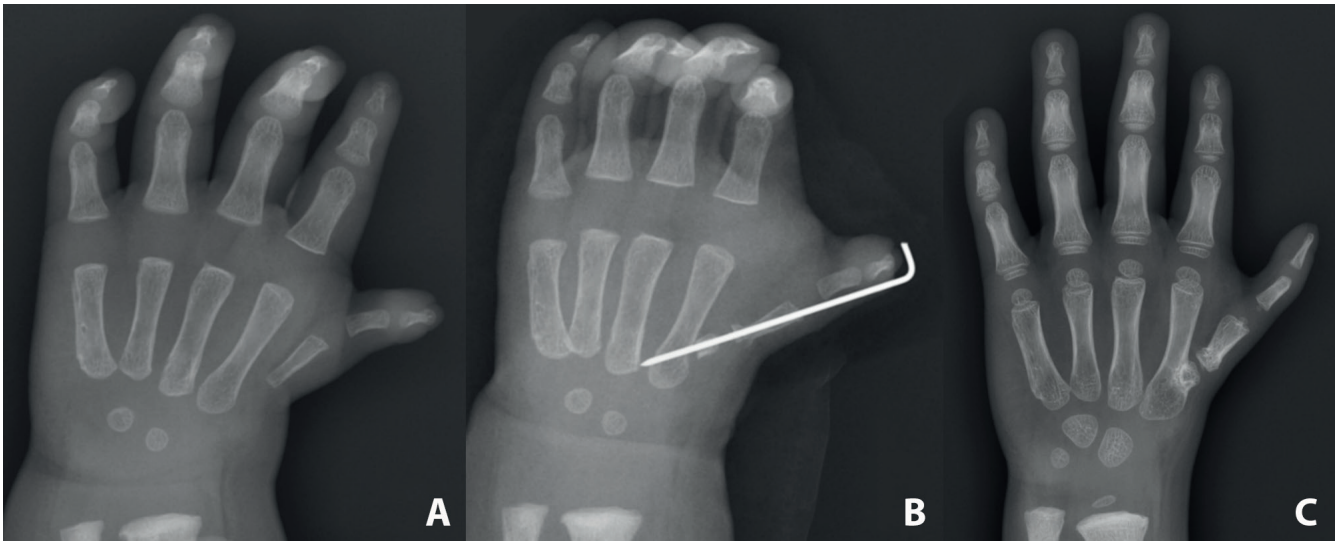

Fig. 7. X-ray of one of the operated patients: hand in anterior-posterior (AP) position before (A), after the operation (B) and after 3 years (C)

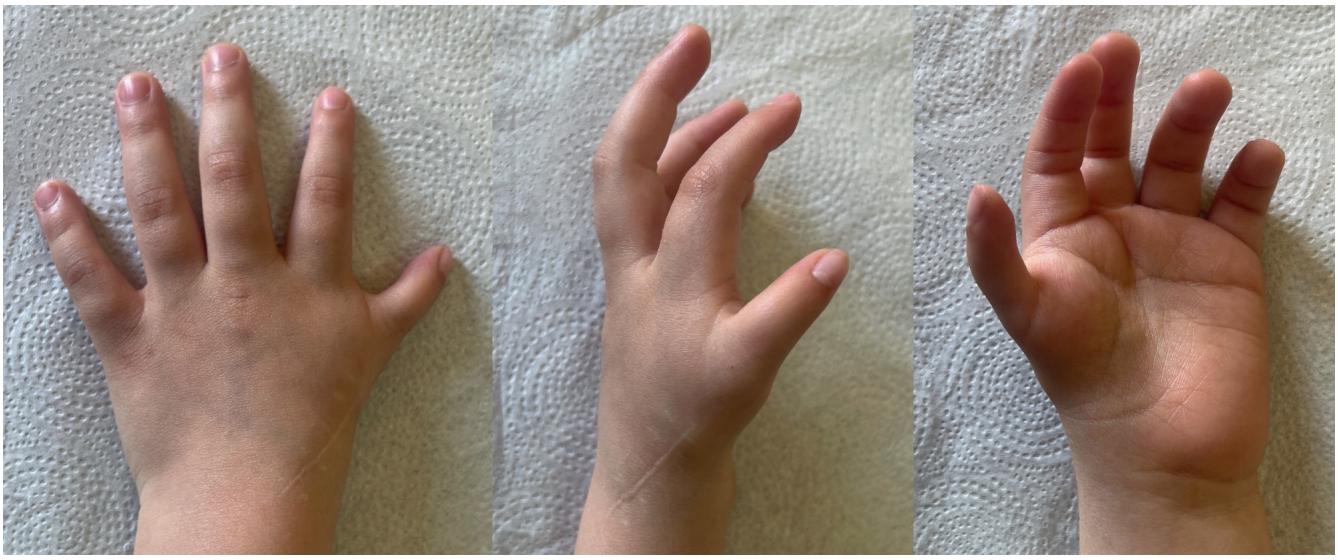

Fig. 8. A 4-year-old boy with a type IIIB hypoplastic thumb, 3 years after proximal interphalangeal joint (PIP) joint transfer. There is a visible shortening of the thumb, with atrophy of the thenar muscles, which is in an intermediate position

45°, with an average range of motion (ROM) of 34–79°. In 2 cases, the author observed total ankylosis of the transplanted joint.

Finding papers describing the use of the PIP joint to reconstruct a type IIIB hypoplastic thumb is difficult. Several authors described using a vascularized MTP graft for reconstruction as an alternative to pollicization.[14,18,25] We used a non-vascularized PIP joint graft, most often from the 3rd toe, where, in our opinion, this joint has adequate size to reconstruct the CMC I joint.

In cited works, the operation was performed on 9 patients with an average age of 9, whereas in our group of 16 patients, the average age was approx. 3 years. The parents did not accept pollicization in younger patients like many of our older patient cases. In older patients,[14] the surgery was performed to improve the stability of the thumb without a prior proposal of pollicization. In all cited cases, appropriate tendon transfers were performed to recreate the active movements of the thumb during the same operation[25] or in the next stage.[14,18] In this group of patients, just over 30% of cases had tendon transfers performed in the next stage of treatment. The parents of the remaining patients were not willing to undergo further operations, or the patient did not seek further treatment.

All authors achieved better thumb stability after surgery; however, only 1 article[18] described the ROM of the transplanted joint – 45° of radial and 75° of palmar adduction. In some patients, the force of the global grip was 3 times higher, and the key grip was 1.5 times lower compared to the patients after the pollicization.[25] Another article described it as 40% of the global grip strength and 14% of the 2-point grip strength compared to the opposite, healthy hand.[14] In 2 studies,[18,25] all patients could grasp small and large objects using the operated thumb. Foucher

et al.[14] stated that more than half of the patients could grasp small things using the thumb. However, in their daily activities, they used it only occasionally. Most of the patients were able to hold larger objects.

Unfortunately, the description of the technique and postoperative procedures in the cited works is not detailed enough to allow them to be appropriately compared. Additionally, those papers are based on a few clinical cases.

All cited works[14,18,20,24,25] are based on a vascularized joint transplant compared to our technique, where we use a non-vascularized graft. This means that it is not necessary to have highly specialized microsurgical skills. The risk of blood circulation disorders in the operated finger is significantly reduced, and the operating time is shortened from 6 h[24] to less than 1 h on average. As a result, the child's anesthesia time is also significantly shorter. The surgical approach of all authors, both on the foot (dorsal) and on the hand (dorsal-radial), was similar to our technique. We inserted the graft between the first and second metacarpal bone, as Foucher et al.[14] or Nishijima et al.[20] described. At the same time, Matsuzaki et al.[18] and Shibata et al.[25] placed the graft between the first metacarpal bone and the wrist bones. All authors used Kirschner wires to stabilize the graft as we do, but differently. Three papers[18,20,25] described 2 crossed wires, and 1 paper[14] an axial wire that only stabilizes the graft. However, our technique involves an axial wire inserted from the distal phalanx to the second metacarpal bone. In our group, the Kirschner wire was removed after an average of 6.5 weeks, similar to the paper by Foucher at al.,[14] which kept the wire in place for 5 weeks.

No complications were presented in any of the cited studies; only Foucher et al.[14] stated that all patients had graft ingrowth. In our work, 3 cases (19% of cases) were a non-union of the graft, and 1 case has been linked to wire destabilization. After reoperation in these 3 patients, union was achieved in 2, while pseudoarthrosis persisted in 1.

Long-term follow-up and evaluation of the donor site in the foot should be considered because as Garagnani et al. described in their work, the harvest of bone from the toes causes consequences that can only be identified after long-term follow-up. This is very important because if a deformity can be identified, the patients and their families should be informed about it before the operation.[32]

Limitations

The article presents a detailed description of the technique and an assessment of the technical aspects of the procedure. Despite the small group of patients who underwent surgery, this is the largest group analyzed compared to alternative techniques described in the literature. Slight differences in technique may be present due to the fact that more than 1 orthopedist performed all the surgeries. However, they took place in the same operating room conditions. It is necessary to continue research with long-term follow-up and functional assessment studies (both short-term and long-term).

Conclusions

The presented technique of reconstruction of the IIIB hypoplastic thumb with a non-vascularized PIP joint from the foot is based on principles like those reported in the literature on vascularized MTP transplants. It may be considered as one of the options for stabilizing a hypoplastic thumb in patients whose parents do not consent to pollicization. The main difference in the technique is that having highly specialized microsurgical skills is unnecessary. Also, the operation time and, consequently, the anesthesia time is significantly shorter, resulting in less burden on the child's body.

In the following research stage, it is necessary to examine the function of the hand after the operation described above. It will be valuable to compare the obtained results with patients after index pollicization as the gold standard for treating grade IIIB thumb hypoplasia.

ORCID iDs

Michał Górecki https://orcid.org/0000-0001-9902-0770
Piotr Czarnecki https://orcid.org/0000-0002-2890-8139

References

1. Sayadi L, Chopan M, Laub D. Thumb hypoplasia. *Eplasty*. 2015;15:ic62. PMID:26759691. PMCID:PMC4693184.
2. Tay SC, Moran SL, Shin AY, Cooney WP. The hypoplastic thumb. *J Am Acad Orthop Surg*. 2006;14(6):354–366. doi:10.5435/00124635-200606000-00005
3. Górecki M, Redman M, Romanowski L, Czarnecki P. Evaluation of the ulna lengthening by distraction osteogenesis in congenital radial deficiency. *Eur J Orthop Surg Traumatol*. 2022;33(5):1981–1987. doi:10.1007/s00590-022-03381-1
4. Tonkin MA. On the classification of congenital thumb hypoplasia. *J Hand Surg Eur Vol*. 2014;39(9):948–955. doi:10.1177/1753193413516246
5. Soldado F, Zlotolow DA, Kozin SH. Thumb hypoplasia. *J Hand Surg*. 2013;38(7):1435–1444. doi:10.1016/j.jhsa.2013.03.021
6. Tonkin MA. Assessment of surgery for the underdeveloped thumb. *J Hand Surg Eur Vol*. 2016;41(3):251–252. doi:10.1177/1753193415625146
7. Flatt AE. Our thumbs. *Proc (Bayl Univ Med Cent)*. 2002;15(4):380–387. doi:10.1080/08998280.2002.11927870
8. Buck-Gramcko D. Congenital malformations of the hand and forearm. *Chir Main*. 2002;21(2):70–101. doi:10.1016/S1297-3203(02)00103-8
9. Balakrishnan G, Vijayaragavan S, Somesh B. Restoration of five digit hand in type III B & C thumb hypoplasia: A game changer in surgical management. *Indian J Plast Surg*. 2020;53(3):349–356. doi:10.1055/s-0040-1718858
10. Chow CS, Ho PC, Tse WL, Hung LK. Reconstruction of hypoplastic thumb using hemi-longitudinal metatarsal transfer. *J Hand Surg Eur Vol*. 2012;37(8):738–744. doi:10.1177/1753193411432677
11. Liu B, Chen S, Chow ECS, Li P, Liu K, Yang C. Type IIIB and IV hypoplastic thumb reconstruction with non-vascularized fourth metatarsal. *J Hand Surg Eur Vol*. 2020;45(7):722–728. doi:10.1177/1753193420937547
12. Roper BA, Turnbull TJ. Functional assessment after pollicisation. *J Hand Surg*. 1986;11(3):399–403. doi:10.1016/0266-7681_86_90166-X
13. Kozin SH, Weiss AA, Webber JB, Betz RR, Clancy M, Steel HH. Index finger pollicization for congenital aplasia or hypoplasia of the thumb. *J Hand Surg*. 1992;17(5):880–884. doi:10.1016/0363-5023(92)90460-7

14. Foucher G, Medina J, Navarro R. Microsurgical reconstruction of the hypoplastic thumb, type IIIB. *J Reconstr Microsurg*. 2001;17(01): 009–016. doi:10.1055/s-2001-12683
15. Sykes PJ, Chandraprakasam T, Percival NJ. Pollicisation of the index finger in congenital anomalies: A retrospective analysis. *J Hand Surg*. 1991;16(2):144–147. doi:10.1016/0266-7681(91)90164-J
16. Hu W, Gasnier P, Le Nen D, Kerfant N, Boloorchi A. Description of an original conservative method for the surgical management of the Blauth IIIb thumb hypoplasia: "Relative lengthening – thumb stabilization" [in French]. *Ann Chir Plast Esthet*. 2012;57(4):342–349. doi:10.1016/j.anplas.2010.09.014
17. Kawabata H, Tamura D, Goldfarb CA. Treatment of Blauth type IIIB thumb hypoplasia using a nonvascularized toe phalanx. *J Hand Surg*. 2021;46(1):68.e1–68.e7. doi:10.1016/j.jhsa.2020.07.007
18. Matsuzaki H, Toishi S, Yoshizu T. A Blauth IIIB hypoplastic thumb reconstructed with a vascularised metatarso-phalangeal joint transfer: A case report with 28 years of follow up. *Hand Surg*. 2009;14(1):63–68. doi:10.1142/S0218810409004244
19. Nakada M, Tada K, Nakajima T, Matsuta M, Tsuchiya H. A case of a 5-year-old boy with a Blauth type IIIB hypoplastic thumb reconstructed with a nonvascularized, hemilongitudinal metatarsal transfer. *Case Rep Orthop*. 2018;2018:8205285. doi:10.1155/2018/8205285
20. Nishijima N, Matsumoto T, Yamamuro T. Two-stage reconstruction for the hypoplastic thumb. *J Hand Surg*. 1995;20(3):415–419. doi:10.1016/S0363-5023(05)80098-X
21. Tan J, Tu YK. Comparative study of outcomes between pollicization and microsurgical second toe-metatarsal bone transfer for congenital radial deficiency with hypoplastic thumb. *J Reconstr Microsurg*. 2013; 29(9):587–592. doi:10.1055/s-0033-1348063
22. Tu Y, Yeh W, Sananpanich K, et al. Microsurgical second toe-metatarsal bone transfer for reconstructing congenital radial deficiency with hypoplastic thumb. *J Reconstr Microsurg*. 2004;20(3):215–225. doi:10.1055/s-2004-823109
23. Zhong W, Tian W, Zhao J, et al. Nonvascularized iliac crest bone graft for reconstruction of the first metacarpal in type IIIB thumb hypoplasia: A radiographic follow-up study. *J Hand Surg*. 2023;48(2):196.e1–196.e8. doi:10.1016/j.jhsa.2021.09.032
24. Luangjarmekorn P, Pongernnak N, Kitidumrongsook P. Vascularized toe joint transfer for hypoplastic thumb type IV. *Tech Hand Up Extrem Surg*. 2021;25(4):226–234. doi:10.1097/BTH.0000000000000339
25. Shibata M, Yoshizu T, Seki T, Goto M, Saito H, Tajima T. Reconstruction of a congenital hypoplastic thumb with use of a free vascularized metatarsophalangeal joint. *J Bone Joint Surg*. 1998;80(10):1469–1476. doi:10.2106/00004623-199810000-00008
26. Tong DD, Wu LH, Li PC, et al. Reversed vascularized second metatarsal flap for reconstruction of Manske type IIIB and IV thumb hypoplasia with reduced donor site morbidity. *Chin Med J (Engl)*. 2019; 132(21):2565–2571. doi:10.1097/CM9.0000000000000477
27. Liu B, Bai F, Chen S. Revisiting the management of Manske Type 3B and 4 thumb hypoplasia. *J Hand Surg Eur Vol*. 2021;46(1):21–29. doi:10.1177/1753193420967240
28. Tonkin M. Surgical reconstruction of congenital thumb hypoplasia. *Indian J Plast Surg*. 2011;44(2):253. doi:10.4103/0970-0358.85347
29. Dautel G. Vascularized toe joint transfers to the hand for PIP or MCP reconstruction. *Hand Surg Rehabil*. 2018;37(6):329–336. doi:10.1016/j.hansur.2018.03.008
30. Kuzu İM, Kayan RB, Öztürk K, Güneren E. Functional improvement with free vascularized toe-to-hand proximal interphalangeal (PIP) joint transfer. *Plast Reconstr Surg Glob Open*. 2018;6(7):e1775. doi:10.1097/GOX.0000000000001775
31. Leclère FM, Haug L, Meier R, Surke C, Unglaub F, Vögelin E. Non-vascularized partial joint transfer for finger proximal interphalangeal joint reconstruction: A series of 9 patients. *Arch Orthop Trauma Surg*. 2020;140(1):139–144. doi:10.1007/s00402-019-03301-9
32. Garagnani L, Gibson M, Smith PJ, Smith GD. Long-term donor site morbidity after free nonvascularized toe phalangeal transfer. *J Hand Surg*. 2012;37(4):764–774. doi:10.1016/j.jhsa.2011.12.010

Comparison of T cell maturation profiles in the 1st and 5th wave of COVID-19 in the Polish population

Elżbieta Rutkowska[1,A–E], Iwona Kwiecień[1,A–D], Agata Raniszewska[1,B,C], Krzysztof Kłos[3,B], Iwona Melnicka[2,B], Piotr Rzepecki[3,E,F], Andrzej Chciałowski[2,A,E,F]

[1] Department of Internal Medicine and Hematology, Military Institute of Medicine–National Research Institute, Laboratory of Hematology and Flow Cytometry, Warsaw, Poland
[2] Department of Infectious Diseases and Allergology, Military Institute of Medicine–National Research Institute, Warsaw, Poland
[3] Department of Internal Medicine and Hematology, Military Institute of Medicine–National Research Institute, Warsaw, Poland

A – research concept and design; B – collection and/or assembly of data; C – data analysis and interpretation;
D – writing the article; E – critical revision of the article; F – final approval of the article

Advances in Clinical and Experimental Medicine, ISSN 1899–5276 (print), ISSN 2451–2680 (online) *Adv Clin Exp Med*. 2025;34(3):393–405

Address for correspondence
Elżbieta Rutkowska
E-mail: erutkowska@wim.mil.pl

Funding sources
This research was funded by Military Institute of Medicine, Warsaw, Poland (grant No. 585).

Conflict of interest
None declared

Received on November 2, 2023
Reviewed on February 16, 2024
Accepted on April 4, 2024

Published online on May 31, 2024

Cite as
Rutkowska E, Kwiecień I, Raniszewska A. Comparison of T cell maturation profiles in the 1st and 5th wave of COVID-19 in the Polish population. *Adv Clin Exp Med*. 2025;34(3):393–405. doi:10.17219/acem/186813

DOI
10.17219/acem/186813

Abstract

Background. The coronavirus pandemic has become the most critical global health threat of this century and the greatest challenge to the human population. The search for simple and quick diagnostic methods enabling the identification of patients infected with the SARS-CoV-2 virus may be a valuable method to track infection.

Objectives. The aim of the study was the clinical and immunological characterization of patients by assessing the degrees of maturity of T lymphocytes from the 1st and 5th waves of coronavirus disease 2019 (COVID-19) in comparison to a healthy control group (HC).

Materials and methods. We determined leukocyte and T lymphocyte subpopulations (recent thymic emigrant (RTE), naïve, effector, central memory and effector memory) in patients from the 1st COVID-19 wave ($n = 23$), the 5th COVID-19 wave ($n = 38$) and HC ($n=20$) using a panel of monoclonal antibodies using multiparameter flow cytometry.

Results. We observed a lower median proportion of lymphocytes and NK cells, and elevated percentage and number of neutrophils in patients from the 5th wave compared to the 1st. We found a reduced percentage of $CD4^+$ effector memory cells in the 1st wave group compared to the 5th wave (14.1 vs 23.2, $p < 0.05$), and a higher percentage of RTE and naïve $CD8^+$ cells in the 1st wave compared to the 5th wave ($p < 0.05$). The effector memory $CD8^+$ cells were highest in the 5th wave compared to both 1st wave and HC patients (respectively, 35.1 vs 18.1 vs 19.3%, $p < 0.05$). The 5th wave group showed significantly more differences compared to HC.

Conclusions. Our results showed a clear increase of effector cells with a simultaneous decrease in virgin T cells in the 5th COVID-19 infection. Monitoring lymphocyte subsets during infection allows assessment of the patient's immune status and of readiness of lymphocytes to respond to the immune response, and may be necessary to improve clinical outcomes.

Key words: flow cytometry, effector memory T cells, SARS-CoV-2, central memory T cells, COVID-19 waves

Background

The principal and emerging new waves of coronavirus disease 2019 (COVID-19) are primarily due to altered virus variants that are rapidly spreading worldwide.[1] They prolong the persistence of infections, causing losses in human health, life and the economy. The development of highly effective vaccines against severe acute respiratory syndrome coronavirus 2 (SARS-CoV-2) effectively reduces the risk of infection and disease development. Unfortunately, due to issues related to vaccine hesitancy, availability and distribution, COVID-19 cases cannot be entirely controlled.

The virus causing symptoms of COVID-19 is an enveloped, single-stranded RNA virus whose 5' region is rich in open reading frames and encodes proteins necessary for viral replication. The 3' region contains 5 structural proteins, namely the spike protein (S), membrane protein (M), nucleocapsid protein (N), envelope protein (E), and hemagglutinin-esterase protein (HE).[2] It is responsible for causing an infectious disease with the most common symptoms such as fever, dry cough and fatigue, shortness of breath, loss of taste or smell, and in the case of an acute course of the disease can even lead to death.[3]

The COVID-19 pandemic began in Wuhan, China, in early December 2019, then quickly spread to neighboring countries and, in the following months, appeared in most nations around the world. In this regard, the World Health Organization (WHO) on March 11, 2020 recognized the COVID-19 disease outbreak as a pandemic.[4] The first case of COVID-19 disease in Poland was detected on March 4, 2020, and as of December 2022, 6,351,408 cases of infection and 118,306 deaths have been confirmed.[5] Waves are a distinctive feature of pandemics, with seasonal variability in environmental factors affecting their duration. The start and end of COVID-19 waves were determined based on the number of identified cases of infection calculated based on the weekly incidence rate.[6,7]

The beginning of the 1st wave of COVID-19 in Poland was estimated on March 12, 2020, its duration was 109 days (until June 28) and it differed from the following waves.[8] In most people infected with the SARS-CoV-2 virus, the disease was mild, without symptoms of pneumonia and hypoxia, or in cases of moderate severity, with clinical manifestations of pneumonia, such as fever, cough and shortness of breath. Some infected patients developed severe or critical illness complicated by severe respiratory distress syndrome, sepsis or organ failure.[9] The 1st COVID-19 wave in Poland did not reveal the exact severity of the epidemic, as diagnostics were carried out only in symptomatic cases. In subsequent waves, a lower percentage of patients required hospitalization, they were younger and admitted to the ward for fewer days, with prolonged survival.[10,11] However, during the 2nd wave, twice as many cases and deaths were observed in Poland.[12] The availability of antigen and serological tests for large-scale use has contributed to this. It was found that the course of the disease in patients from the 3rd COIVID-10 wave, infected with the transformed alpha (B.1.1.7) variant, was significantly more severe than in the previous ones.[13,14] The subsequent 4th wave, comprising the next variants of SARS-CoV-2-Delta (B.1.617.2), resulted in a more severe course of the disease, being the most dangerous and having the worst results.[15,16] However, differentiation of SARS-CoV-2 viral variants was also not common in Poland.[17] Vaccination against COVID-19 was introduced at the end of December 2020, with initial availability for healthcare workers, elderly patients and persons with multiple comorbidities.[18] Despite the subsequent widespread availability of vaccines, due to high uncertainty and skepticism about the preparations, only approx. 50% vaccination coverage in Poland population was recorded.[19]

During the formation of the 5th wave, the SARS-CoV-2 transformed into BA.5 SARS-CoV-2 Omicron variant with higher infectivity but less virulence and a milder course of the disease with few clinical symptoms.[20] In Poland, the 5th COVID-19 wave began in the winter of 2021. It was the shortest of all, lasting 90 days, with the number of infected people being over 1.75 million.[8]

The 2 main pathways of immune response to pathogens are innate and acquired immunity. The innate immune response involves NK cells, complement and interferon components, and immunoglobulin A secreted in body fluids.[21] The acquired or adaptive immune response is triggered by viral replication. Intracellular viral antigens are presented to $CD8^+$ T cells in combination with MHC class I antigens, which in turn causes division and maturation of lymphocytes into both effector and memory cells. Contact with a foreign antigen turns lymphocytes into effector and central memory cells.[22] Effector T cells can directly kill virus-infected cells, while central memory cells can be activated after subsequent re-contact with the antigen and become memory effector cells or central memory cells.[23] The viral antigen-responsive $CD8^+$ T cells play a key role by identifying and killing virus-infected cells. These T cells with cytotoxic properties are active for a short time, and, after the elimination of the virus hidden in host cells, quickly disappear. Long-lived memory T cells, which activate very quickly after repeated contact with the virus, create a long-term immune response. Healthy people, not burdened with additional diseases, potentially destroy the virus after it enters their bodies and do not develop a targeted immune response.[23]

It is interesting to compare the immune status of patients from different waves of the epidemic. In particular, the evaluation of effector and memory cells may indicate the state of readiness of the patient's immune response to virus infection. Very little is known about the impact of different lymphocyte subsets on the immune response of COVID-19 patients or its consequences. We examined immunological parameters by assessing the expression of cell surface markers in lymphocyte subsets using a flow cytometer. The contribution of T cells to the establishment of long-lasting protective immunity against reinfection

in future epidemics is an important aspect of the T cell response that requires investigation. In addition, the results obtained from both groups of COVID-19 patients were compared to a healthy control (HC) group.

Objectives

This study aimed to examine the host cellular immune response, including memory and effector cell subsets, in COVID-19 patients admitted to the Department of Infectious Diseases and Allergology of the Military Institute of Medicine–National Research Institute in Warsaw in different waves of the pandemic in Poland. We focused on assessing T cell subpopulations that play a significant role in the antiviral response involving a specific immune reaction in people infected with the SARS-CoV-2 virus.

Materials and methods

Patients

The analyzed group was composed of Polish patients from 2 COVID-19 waves, the 1st wave of COVID-19 (tested from May 2020 to August 2020) and the 5th (December 2021 to April 2022). According to the WHO guidelines, patients with SARS-CoV-2 underwent real-time polymerase chain reaction (PCR) tests from nasopharyngeal swab samples. Patients positive for SARS-CoV-2 were admitted to the Department of Infectious Diseases and Allergology at the Military Institute of Medicine (Warsaw, Poland).

Inclusion criteria were as follows: adults over 18 years of age with laboratory-confirmed SARS-CoV-2 infection, meeting criteria for hospital admission for COVID-19, with an oxygen saturation of 94% or less. Additionally, based on oxygen demand, patients according to result on an ordinal scale were classified as: a hospitalized patient, not requiring supplemental oxygen but requiring medical attention (score 4) or hospitalized requiring normal oxygen supplementation (score 5) or non-invasive ventilation with high flow oxygen equipment (rated 6). Patients with acute respiratory distress syndrome (ARDS) at baseline were excluded. This 8-point scale is based on WHO recommendations modified to fit the specificity of the Polish healthcare system.

For the final analysis, we did not include any asymptomatic patients or those receiving corticosteroids, which may affect blood cell counts and possibly also lymphocyte subsets.

The 1st wave COVID-19 group consisted of 23 patients. There were 9 women and 14 men with a mean age of 55.9 ±18.2 years. The 5th COVID-19 wave group initially consisted of 66 patients, 37 women and 29 men, with a mean age of 68.5 ±18.3 years. From the 5th wave group, 7 vaccinated patients and 3 with previously confirmed SARS-CoV-2 infection were excluded, as well as 4 patients with an acute course of the disease, with ARDS at baseline. Fourteen patients died. Ultimately, the 5th COVID-19 wave study group consisted of 38 patients, among whom were 20 women and 18 men, aged 66.4 ±18.3 years. The exclusion of vaccinated patients and those previously infected with the SARS-Cov-2 virus allowed the generation of the optimal group from the 5th wave, which did not demonstrate many differences compared to the group from the 1st wave. Of note, patients from the 1st wave and the 5th wave were different people.

The treatment procedure was carried out according to current knowledge and recommendations of the Polish Society of Epidemiologists and Infectiologists.[24] The mean hospitalization was 21.5 ±16 days. Clinical characteristics of all COVID-19 patients from both groups are presented in Table 1. The HC group consisted of 20 volunteers, 18 women and 2 men, with an average age of 56 ±7.1 years.

The study was carried out by the Declaration of Helsinki, and approved by the Ethics Committee of the Military Institute of Medicine (approval No. 47/WIM/2020 dated September 16, 2020). Informed written consent for the study and publication of this work was obtained from all patients from whom samples were collected.

Materials

Peripheral blood (PB) samples were obtained from all COVID-19 patients within 24 h of admission and before antiviral and/or immunosuppressive treatment. Whole PB samples were incubated with monoclonal antibodies for 20 min at room temperature. The antibodies used are shown in Table 2. After 2 washes, the cells were analyzed for 2 h, and at least 20,000 events were collected for each sample. Data were interpreted with Cytexpert and Kaluza C v. 1.1 software (Beckman Coulter, Brea, USA), and an Infinicyt 1.8 Flow Cytometry (Cytognos, Salamanca, Spain).

The routine white blood cell count (WBC) analysis was performed on all patients using a Sysmex XN-1500 (Sysmex Corp., Kobe, Japan) hematological analyzer.

Flow cytometry analysis

Leukocyte and lymphocyte subpopulations were analyzed with multicolor flow cytometry with a monoclonal antibody panel using DxFLEX flow cytometry (Beckman Coulter). We reported the lymphocyte maturation for the $CD4^+$ and $CD8^+$ cells.[19] The following maturation populations among $CD4^+$ T cells and $CD8^+$ T cells were analyzed: RTE, naïve, effector, effector memory, and central memory cells. The phenotypes of the analyzed T cell subpopulations and all tested cells are presented in Table 2.

Statistical analyses

The analysis was performed using Statistica v. 12.0 software (TIBCO Software, Palo Alto, USA). The Shapiro–Wilk test was performed to evaluate assumptions regarding

Table 1. Characteristics of the study population with COVID-19 in different waves

Patients' characteristics		1st COVID-19 n = 23	5th COVID-19 n = 38	p < 0.05 Mann–Whitney U test
Sex: F/M, n		9/14	20/18	
Age (Me (Q1–Q3)) p-value (Shapiro–Wilk test) SW-W value		60.0 (39.0–72.0) p = 0.018 0.889	71 (52–78) p = 0.043 0.940	p = 0.040
Clinical symptoms n (%)	fever	19 (82.6%)	30 (78.9%)	p = 0.850
	cough	16 (69.6%)	25 (65.8%)	p = 0.876
	dyspnea	14 (60.9%)	5 (13.2%)	p = 0.239
Saturation (Me (Q1–Q3) p-value (Shapiro–Wilk test) SW–W value		91.0 ±7.5% p = 0.125 0.871	91.9 ±4.6% p = 0.043 0.940	p = 0.980
Conventional (passive) oxygen therapy		7 (30.4%)	29 (76.3%)	p = 0.023
Mechanical ventilation therapy		3 (13.0%)	2 (5.3%)	p = 0.987
Diseases comorbidities, n (%)	0 comorbidities	10 (43.5%)	5 (13.2%)	p = 0.098
	1 comorbidity	7 (30.4%)	15 (39.5%)	p = 0.138
	2 comorbidities	2 (8.7%)	10 (26.3%)	p = 0.068
	3 comorbidities	2 (8.7%)	5 (13.2%)	p = 0.654
	4 comorbidities	2 (8.7%)	3 (7.9%)	p = 0.980

Me – median; SW–W – Shapiro–Wilk test value.

normal distribution. The parameters compared did not meet the assumptions of normal distribution, so the non-parametric Mann–Whitney U test was used to compare the 2 groups (Table 1). Among the tested parameters (for comparison 3 groups) in Table 3 and Table 4, lymphocytes (%), neutrophils (%) naïve $CD4^+$, effector $CD8^+$ (%) and effector memory $CD8^+$ (%) met the assumptions of normality, and thus we checked the assumptions of homogeneity of variance (Brown–Forsyth test), which showed that the assumption of homogeneity of variance was not met. For these 2 parameters, Welch's analysis of variance (ANOVA) test (with Welch's correction) for independent variance estimation and Games–Howell post hoc tests were used. For other parameters where the assumption of normal distribution was not met, we used the non-parametric Kruskal–Wallis test and Dunn's post hoc test with Bonferroni correction. The results were expressed as means with SD or medians (Me) with interquartile range (Q1–Q3). Statistical significance was considered when $p < 0.05$. All analyses were performed in Prism v. 9 (GraphPad Software, La Jolla, USA).

Results

Clinical characteristics of the patients

The characteristics of the studied population with COVID-19 in different waves are provided in Table 1. There is a nonsignificant difference in the age of the patients, with those in the 5th COVID-19 wave being older than patients in the 1st COVID-19 wave (Mann–Whiteny U test, p = 0.040). The blood oxygen saturation value was similar in both waves (U-Mann–Whiteny test, p = 0.980). The percentage of symptoms, such as fever, cough and dyspnea, were similar in both groups. Patients in the 5th COVID-19 wave had a higher percentage of conventional (passive) oxygen therapy than patients in the 1st COVID-19 wave, and acute respiratory failure requiring mechanical ventilation was recorded in 2 patients from the 5th wave compared to 3 patients from the 1st wave. There were 14 deaths among patients from the 5th wave. However, after excluding vaccinated patients and patients with a severe course of disease, a uniform group of patients with mild disease severity was obtained. Finally, a higher percentage of comorbidities was found in patients from the 5th COVID-19 wave.

Basic leukocyte subpopulation

Differences between COVID-19 waves

We analyzed the leukocyte subset distribution in PB in different waves of COVID-19. Median values of the absolute number and percentage of leukocytes and lymphocyte types are presented in Table 3. There was a lower median proportion of lymphocytes and NK cells, and a significantly higher median proportion and absolute number of neutrophils in patients in the 5th COVID-19 wave compared to the 1st COVID-19 wave (Table 3).

Differences between COVID-19 and healthy control

Compared to the HC group, there were more significant differences with the 5th wave group compared to

Table 2. List of analyzed cell subpopulations with phenotype and list of antibodies

Analyzed population	Phenotype	Antibody list	Catalog No.	Clone No.
Lymphocytes	CD45$^+$bright SSC-A$^+$dim	CD45-V500	655873	2D1
Lymphocytes T	CD45$^+$bright CD3$^+$	CD45-V500 CD3-PerCP-Cy5.5	655873 332771	2D1 SK7
Lymphocytes T CD4$^+$	CD45$^+$bright CD3$^+$ CD4$^+$	CD45-V500 CD3-PerCP-Cy5.5 CD4-FITC	655873 332771 345768	2D1 SK7 SK3
Lymphocytes T CD8$^+$	CD45$^+$bright CD3$^+$ CD8$^+$	CD45-V500 CD3-PerCP-Cy5.5 CD8-APC	655873 332771 345775	2D1 SK7 SK1
Lymphocytes B	CD45$^+$bright CD19$^+$	CD45-V500 CD19-PE-Cy7	655873 341113	2D1 SJ25C1
Lymphocytes NK	CD45$^+$bright CD16$^+$ CD3$^-$	CD45-V500 CD16-APC-H7	655873 560195	2D1 3G8
Neutrophils	CD45$^+$ CD16$^+$ SSC-A$^+$	CD45-V500 CD16-APC-H7	655873 560195	2D1 3G8
Eosinophils	CD45$^+$bright SSC-A$^+$	CD45-V500	655873	2D1
Basophils	CD45$^+$dim SSC-A$^+$dim	CD45-V500	655873	2D1
Monocytes	CD45$^+$ HLA-DR$^+$	CD45-V500 HLA-DR-V450	655873 655874	2D1 L243
RTE	CD45RA$^+$ CD62L$^+$ CD31$^+$ CD3$^+$ CD45$^+$	CD45RA-APC CD62L-PE CD31-PerCP-Cy5.5 CD3-APC-H7 CD45-V500	550855 555544 566563 641415 655873	– – WM59 SK7 2D1
Naïve T cells	CD45RA$^+$ CD197$^+$ CD3$^+$ CD45$^+$	CD45RA-APC CD197-PerCP-Cy5.5 CD3-APC-H7 CD45-V500	550855 353220 641415 655873	– G043H7 SK7 2D1
Effector T cells	CD45RA$^+$ CD197$^-$ CD3$^+$ CD45$^+$	CD45RA-APC CD197-PerCP-Cy5.5 CD3-APC-H7 CD45-V500	550855 353220 641415 655873	– G043H7 SK7 2D1
Central memory T cells	CD45RO$^+$ CD197$^+$ CD3$^+$ CD45$^+$	CD45RO-PE-Cy7 CD197-PerCP-Cy5.5 CD3-APC-H7 CD45-V500	560608 353220 641415 655873	UCHL1 G043H7 SK7 2D1
Effector memory T cells	CD45RO$^+$ CD197$^-$ CD3$^+$ CD45$^+$	CD45RO-PE-Cy7 CD197-PerCP-Cy5.5 CD3-APC-H7 CD45-V500	560608 353220 641415 655873	UCHL1 G043H7 SK7 2D1
Th17	CD45RO$^+$ CD196$^+$ CD3$^+$ CD4$^+$ CD45$^+$	CD45RO-PE-Cy7 CD197-PerCP-Cy5.5 CD3-APC-H7 CD-4 FITC CD45-V500	560508 353220 641415 345768 655873	UVHL1 G043H7 SK7 SK3 2D1

RTE – recent thymic emigrants T cells.

the 1st wave group. Lymphopenia, including reduced absolute numbers relative to healthy controls, was demonstrated for both COVID-19 groups for T cells, CD4$^+$ and CD8$^+$ cells, and B cells and NK cells. A similar relationship was found for neutrophil and eosinophil numbers (Table 3). The HC group showed significantly higher percentages of lymphocytes, CD3$^+$, both CD4$^+$ and CD8$^+$ T lymphocytes, B lymphocytes and basophils compared to patients from the 5th wave group (Table 3).

T cell maturation subpopulation

Differences between COVID-19 waves

There was a significantly higher median proportion of effector memory CD4$^+$ cells in the 5th COVID-19 wave compared to the 1st (Table 4). We also observed a significantly lower median proportion of RTE CD8$^+$ cells in the 5th COVID-19 wave than in the 1st COVID-19 wave

Table 3. The median proportion of leukocytes subpopulation in peripheral blood (PB): lymphocytes, lymphocytes T ($CD4^+$, $CD8^+$), natural killer cells, granulocytes, eosinophils, basophils and monocytes in the 1st COVID-19 wave, the 5th COVID-19 wave and in healthy control

Leukocytes subpopulations	1st COVID-19 wave Me (Q1–Q3) or mean (SD)[1] A (n = 23)	5th COVID-19 wave Me (Q1–Q3) or mean (SD)[1] B (n = 38)	HC Me (Q1–Q3) or mean (SD)[1] C (n = 20)	*p < 0.050 [1]Welch's ANOVA test (with Welch's correction) for independent variance estimation [2]nonparametric Kruskal–Wallis	* p < 0.050 [1]Games–Howell post hoc [2]Dunn's post hoc test with Bonfferoni correction
Lymhocytes [%]	[1]33.6 (18.8)	[1]21.6 (12.8)	[1]39.7 (10.6)	p < 0.001[1]	A–B, B–C[1] A–B; p = 0.015 A–C; p = 0.271 B–C; p < 0.001
Lymhocytes [k/μL]	1087 (817–2420)	1154 (905–1799)	2037 (1838–2934)	p < 0.001[2]	A–C, B–C[2] A–B; p = 1.000 A–C; p = 0.004 B–C; p < 0.001
Lymphocytes T $CD3^+$ [%]	21.9 (13.8–37.5)	17.5 (10.3–22.5)	29.3 (24.0–37.2)	p < 0.001[2]	B–C[2] A–B; p = 0.154 A–C; p = 0.089 B–C; p < 0.001
Lymphocytes T $CD3^+$ [k/μL]	805 (572–1891)	897 (729– 1369)	1659 (1409–2292)	p < 0.001[2]	A–C, B–C [2] A–B; p = 1.000 A–C; p = 0.001 B–C; p < 0.001
Lymphocytes T $CD3^+$ $CD4^+$ [%]	12.3 (5.3–23.1)	9.3 (5.3–13.9)	18.6 (13.6–22.0)	p < 0.001[2]	B–C[2] A–B; p = 0.439 A–C; p = 0.073 B–C; p < 0.001
Lymphocytes T $CD3^+$ $CD4^+$ [k/μL]	526 (261–1035)	557 (450–796)	977 (756–1559)	p < 0.001[2]	A–C, B–C[2] A–B; p = 1.000 A–C; p = 0.003 B–C; p = 0.001
Lymphocytes T $CD3^+$ $CD8^+$ [%]	9.3 (3.6–12.6)	5.7 (3.1–8.1)	10.5 (7.8–13.2)	p = 0.002[2]	B–C[2] A–B; p = 0.125 A–C; p = 0.413 B–C; p < 0.001
Lymphocytes T $CD3^+$ $CD8^+$ [k/μL]	313 (160–847)	399 (206–552)	624 (456–790)	p = 0.003[2]	A–C, B–C[2] A–B; p = 1.00 A–C; p = 0.028 B–C; p = 0.003
Ratio CD4/CD8	1.6 (1.0–2.7)	1.7 (0.9–2.4)	1.8 (1.5–2.2)	p = 0.863[2]	–
Lymphocytes B $CD19^+$ [%]	2.2 (1.4–5.1	2.1 (0.8–3.7)	3.9 (3.0–5.0)	p = 0.004[2]	B–C[2] A–B; p = 0.861 A–C; p = 0.116 B–C; p = 0.003
Lymphocytes B $CD19^+$ [k/μL]	141 (77–191)	132 (58–257)	216 (190–284)	p = 0.004[2]	A–C, B–C[2] A–B; p = 1.000 A–C; p = 0.013 B–C; p = 0.007
Natural killer (NK) cells [%]	4.5 (1.5–9.1)	1.8 (0.4–3.5)	4.2 (2.8–7.0)	p < 0.001[2]	A–B, A–C, B–C[2] A–B; p = 0.003 A–C; p = 0.002 B–C; p = 0.002
Natural killer (NK) cells [k/μL]	184 (101–400)	116 (35–241)	245 (204–447)	p = 0.001[2]	B–C[2] A–B; p = 0.093 A–C; p = 0.531 B–C; p = 0.001
Neutrophils [%]	[1]55.3 (22.0)	[1]64.8 (15.8)	[1]59.4 (21.2)	*p < 0.001[1]	A–B[1] A–B; p < 0.001 A–C; p = 0.756 B–C; p = 0.817
Neutrophils [k/μL]	2704 (1556–3937)	4203 (2581–6373)	3310 (2139–4338)	p = 0.001[2]	A–B, A–C, B–C[2] A–B; p < 0.001 A–C; p < 0.001 B–C; p < 0.001
Eosinophils [%]	1.1 (0.2–2.5)	1.1 (0.6–2.9)	1.8 (1.0–3.2)	p = 0.210[2]	–
Eosinophils [k/μL]	62 (8–109)	79 (29–171)	108 (66–197)	p = 0.074[2]	–

Table 3. The median proportion of leukocytes subpopulation in peripheral blood (PB): lymphocytes, lymphocytes T (CD4+, CD8+), natural killer cells, granulocytes, eosinophils, basophils and monocytes in the 1st COVID-19 wave, the 5th COVID-19 wave and in healthy control – cont.

Leukocytes subpopulations	1st COVID-19 wave Me (Q1–Q3) or mean (SD)(1) A (n = 23)	5th COVID-19 wave Me (Q1–Q3) or mean (SD)(1) B (n = 38)	HC Me (Q1–Q3) or mean (SD)(1) C (n = 20)	*p < 0.050 (1)Welch's ANOVA test (with Welch's correction) for independent variance estimation (2)nonparametric Kruskal–Wallis	* p < 0.050 (1)Games–Howell post hoc (2)Dunn's post hoc test with Bonfferoni correction
Basophils [%]	0.3 (0.0–0.7)	0.3 (0.0–0.5)	0.5 (0.4–0.7)	p = 0.035(2)	B–C(2) A–B; p = 0.980 A–C; p = 0.233 B–C; p = 0.032
Basophils [k/μL]	14 (0–27)	16 (0–32)	31 (25–45)	p = 0.011(2)	A–B, A–C, B–C(2) A–B; p = 0.027 A– C; p = 0.027 B–C; p = 0.021
Monocytes [%]	7.2 (5.8–10.9)	9.5 (6.7–13.2)	8.2 (6.7–9.6)	p = 0.173(2)	–
Monocytes [k/μL]	388 (249–615)	615 (417–831)	449 (395–562)	p = 0.003(2)	A–B(2) A–B; p = 0.002 A–C; p = 0.382 B–C; p = 0.355

HC – healthy control; Me – median. Data expressed as median (Q1–Q3). A * marked p < 0.05 statistically significant.

Table 4. Differences in the median proportion of T lymphocyte cells in peripheral blood: recent thymic emigrants (RTE), naïve, effector, effector memory, central memory and Th17 cells between the 1st COVID-19 wave, the 5th COVID-19 wave and healthy control

Lymphocytes T subpopulations	1st COVID-19 wave Me (Q1–Q3) or mean (SD)(1) A (n = 23)	5th COVID-19 wave Me (Q1–Q3) or mean (SD) or mean (SD)(1) B (n = 38)	HC Me (Q1–Q3) or mean (SD)(1) C (n = 20)	* p < 0.050 (1)Welch's ANOVA test (with Welch's correction) for independent variance estimation (2)nonparametric Kruskal–Wallis	* p < 0.050 (1)Games–Howell post hoc (2)Dunn's post hoc test with Bonfferoni correction
RTE CD4+	19.9 (5.8–30.3)	14.2 (9.4–23.6)	31.2 (26.3–37.6)	p < 0.001(2)	A–C, B–C(2) A–B; p = 0.792 A–C; p = 0.014 B–C; p < 0.001
Naïve CD4+	41.4 (20.3)(1)	33.4 (16.9)(1)	50.0 (10.9)(1)	p < 0.001(1)	B–C(1) A–B; p = 0.365 A–C; p = 0.125 B–C; p = 0.005
Effector CD4+	2.8 (1.2–6.4)	2.6 (1.0–4.4)	1.8 (1.1–3.4)	p = 0.647(2)	–
Effector memory CD4+	14.1 (9.2–22.3)	23.2 (18.0–35.9)	12.5 (9.2–15.0)	p < 0.001(2)	A–B, B–C(2) A–B; p < 0.001 A–C; p = 1.000 B–C; p < 0.001
Central memory CD4+	35.2 (26.3–46.5)	33.4 (28.1–43.1)	33.2 (27.2–40.3)	p = 0.757(2)	–
Th17 (among CD4+)	22.5 (15.5–29.1)	21.8 (16.2–31.3)	28.8 (25.0–34.9)	p = 0.054(2)	–
RTE CD8+	28.1 (13.4–47.3)	11.7 (7.2–24.7)	39.5 (34.4–52.9)	p < 0.001((2)	A–B, B–C(2) A–B; p = 0.026 A–C; p = 0.073 B–C; p < 0.001
Naïve CD8+	22.1 (10.5–40.5)	11.8 (7.0–21.3)	42.4 (35.5–59.7)	p < 0.001(2)	A–B, A–C, B–C(2) A–B; p = 0.027 A–C; p = 0.019 B–C; p < 0.001
Effector CD8+	36.5 (23.2)(1)	39.8 (20.1)(1)	28.4 (11.8)(1)	p = 0.145(1)	–
Effector memory CD8+	20.8 (11.9)(1)	36.3 (12.9)(1)	19.6 (6.9)(1)	p < 0.00(1)	A–B, B–C(1) A–B; p < 0.001 A–C; p = 1.000 B–C; p < 0.001
Central memory CD8+	9.5 (6.6–14.5)	6.1 (3.5–12.0)	7.8 (4.1–11.4)	p = 0.242(2)	–

RTE – recent thymic emigrants; HC – healthy control; Me – median. Data expressed as median (Q1–Q3). A * marked p < 0.05 statistically significant

and naïve CD8+ cells in the 5th COVID-19 wave than in the 1st COVID-19 wave (Table 4). When we analyzed the median proportion of effector memory CD8+ cells, we noticed a significantly higher proportion in the 5th COVID-19 wave than in the 1st COVID-19 wave (Table 4). Moreover, there was a lower median proportion of central memory CD8+ cells in the 5th COVID-19 wave than in the 1st COVID-19 wave (Fig. 1, Table 4). Sample flow cytometry graphs from a selected patient from the 1st COVID-19 wave to a patient from the 5th COVID-19 wave for T cells maturation population: lymphocytes, lymphocytes T, CD4+, CD8+, naïve, effector, effector memory and central memory, Th17 and RTE cells are presented in Fig. 2 and Fig. 3.

Differences between COVID-19 and healthy control

Compared to the HC group, we found a significantly lower percentage of CD4+ RTE cells and CD8+ naïve cells in both groups of patients with COVID-19. Lower percentages of CD4+ naïve cells, CD8+ RTE cells, and higher percentages of memory effector cells of both CD4+ and CD8+ were also found in 5th-wave patients relative to the HC group (Table 4, Fig. 1).

Discussion

Despite developed immunity and vaccinations showing significant activity against various viral variants,

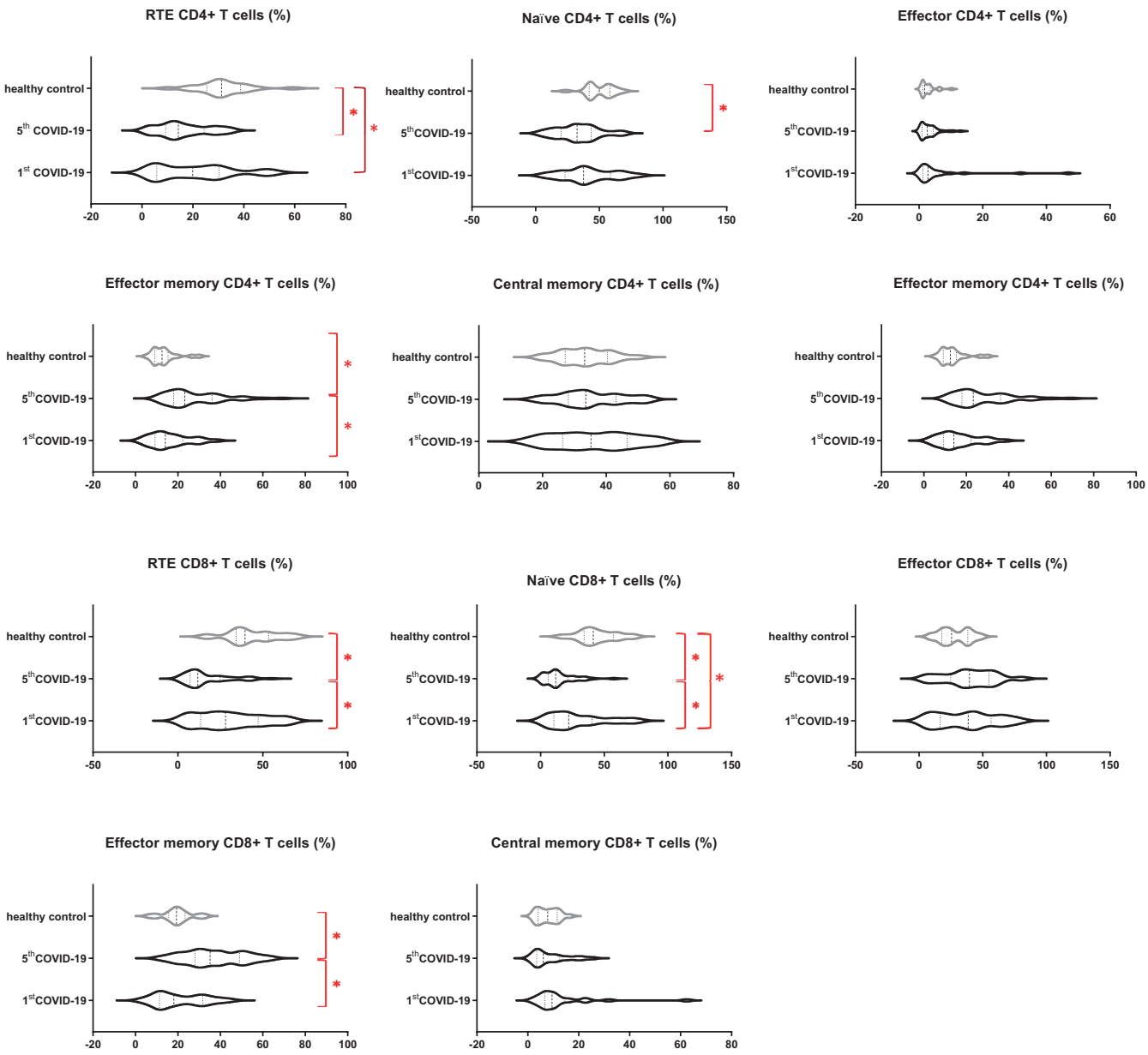

Fig. 1. The differences in the median values of T CD4+ and CD8+ lymphocytes types: Recent thymic emigrants T cells (RTE), naïve T cells, effector T cells, central memory T cells, and effector memory T cells between the 1st COVID-19 wave, 5th COVID-19 wave and healthy control. Graphs show the median values (A * marked $p < 0.05$ statistically significant)

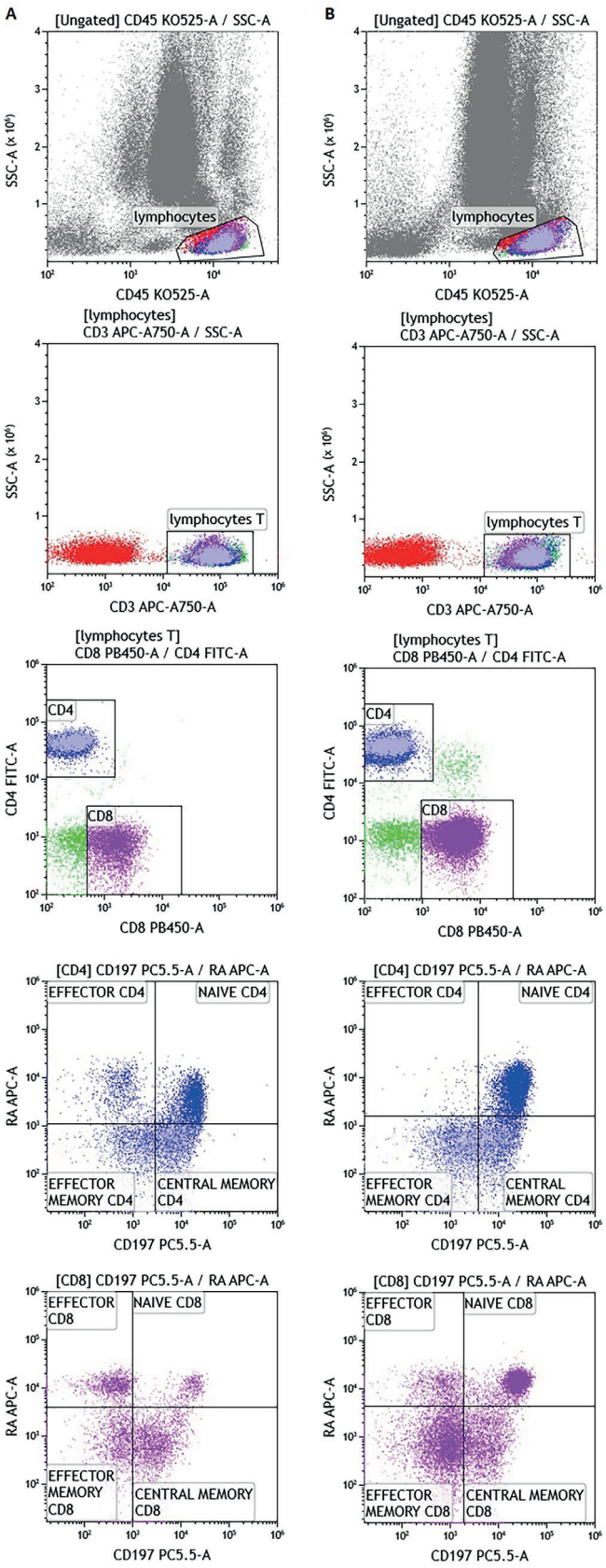

Fig. 2. Sample flow cytometry graphs from a selected patient from the 1st COVID-19 wave (A) and patient from the 5th COVID-19 wave (B) for lymphocytes, lymphocytes T, CD4+, CD8+ and T cells maturation population: naïve, effector, effector memory and central memory

SSC-A – side scatter area; RTE – recent thymic emigrants.

SARS-COV-2 still causes significantly high mortality, especially in patients with many comorbidities.[25] In our study, we presented new results comparing the clinical and immunological features of the 2 extreme waves of COVID-19 cases in Poland. We showed in our work, for the first time, the full maturation profile of T lymphocytes, from naïve cells to memory cells of patients from 2 distant waves of the COVID-19 pandemic in Poland. Our study provides characteristics of COVID-19 patients from the pandemic's 1st and 5th waves through clinical description and evaluation of leukocyte and main T-cell subpopulations. Patients from both groups showed typical symptoms of COVID-19. The group of patients from the 5th wave was associated with an elevated number of comorbidities and the amount of oxygen therapy used. The differences between the waves in the clinical picture could be due to the development of other virus variants, large-scale vaccination and greater population immunity. In the 5th wave of COVID-19, the positive group consisted mainly of elderly, unvaccinated patients with comorbidities, due to the younger infected patients not requiring hospitalization. Only a few studies have conducted comprehensive comparisons of hospitalized patients from different waves of COVID-19. According to some researchers, COVID-19 patients in the 1st wave had a more severe course of the disease than patients admitted in the 2nd wave, in which fewer patients received mechanical ventilation and experienced symptoms such as fever, cough and shortness of breath.[26] Similarly, the results of studies conducted in Spain, Japan and Iran showed a milder course of the disease during the 2nd wave.[10,27,28] There are many plausible explanations for the milder course of the disease during subsequent waves of COVID-19. The risk of infection was higher at the beginning of the pandemic, improved diagnostics and treatment could translate into the condition of hospitalized patients, and potential changes in the SARS-CoV-2 genome in subsequent waves could have an impact on the severity of the disease.[26]

It is known that lymphopenia is a characteristic feature in patients with COVID-19 and may be a basic, useful prognostic factor.[29,30] Neutrophilia is also a characteristic symptom of SARS-CoV-2 infection.[31] In our research, lymphopenia and neutrophilia were significantly higher in the 5th wave, comparing both patients from the 1st wave group and the HC group. It is known that lymphopenia, elevated neutrophil-to-lymphocyte ratio, monocyte-to-lymphocyte ratio, and elevated cytokine levels are correlated with disease severity and poor prognosis.[32,33] Charostad et al., comparing 5 waves of COVID-19, noticed the greatest increase in the number of leukocytes and the highest neutrophilia and lymphopenia in the 3rd wave, while the 1st wave had the least impact on these parameters.[34] Our data indicate that hematological parameters can serve as valuable predictive biomarkers for assessing disease status and clinical outcomes in each wave of the COVID-19

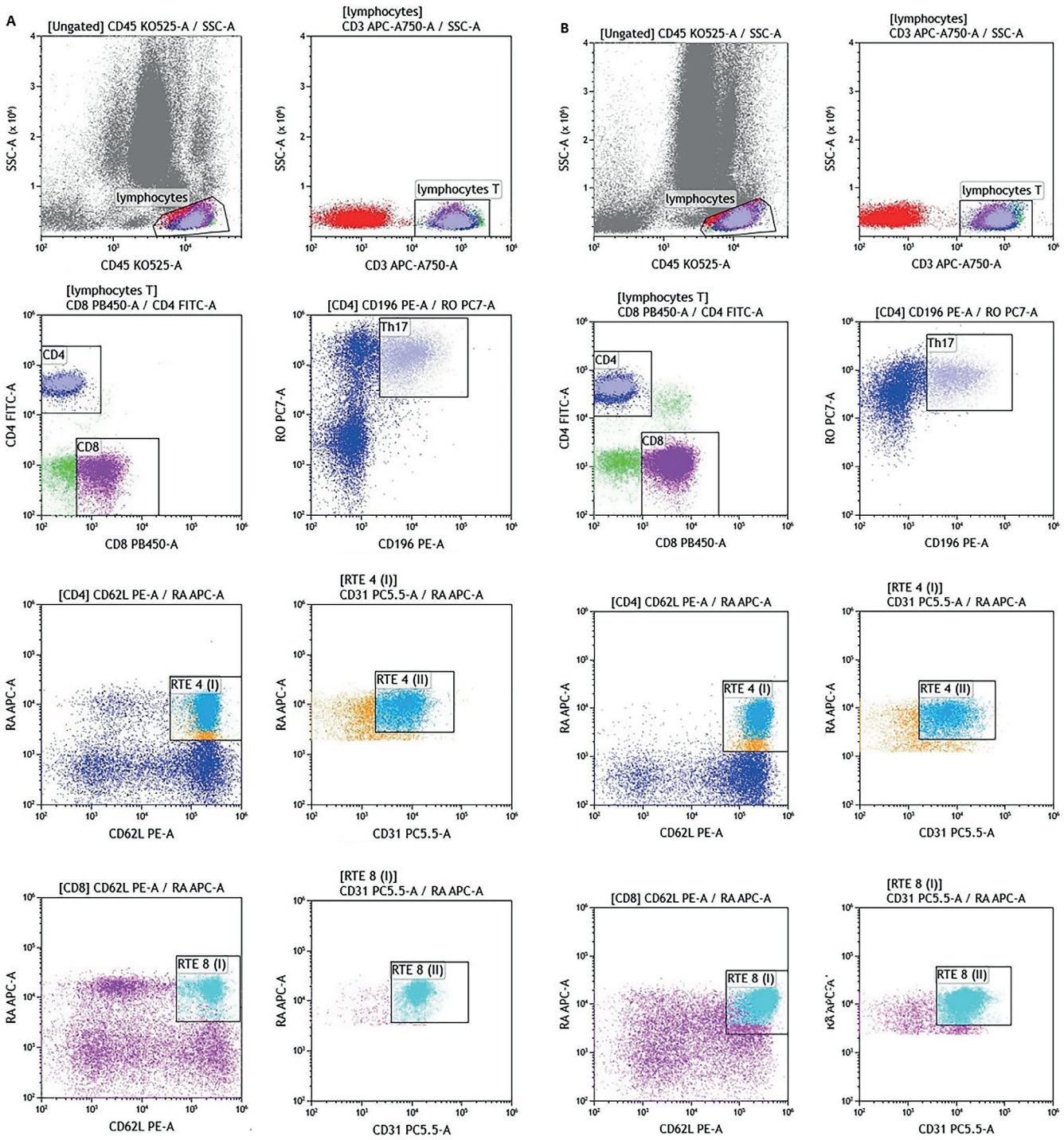

Fig. 3. Sample flow cytometry graphs from a selected patient from the 1st COVID-19 wave and a patient from the 5th COVID-19 wave for lymphocytes, lymphocytes T, CD4+, CD8+, Th17 cells and recent thymic emigrant T cells (RTE)

SSC-A – side scatter area.

pandemic and provide useful insight into the progression and prognosis of COVID-19 cases.

For a better understanding of the immune mechanisms occurring in the patients examined in this study, we analyzed the subpopulation of cells responsible for both the early and late immune response. Different types of pathogens require diverse types of immune effector cells for control. Viral infections require control of CD4+ T cells, which induce B cells to produce high-affinity antibodies that can neutralize the pathogen, and cytotoxic CD8+ T cells, which kill cells infected with the pathogen. The factor initiating the immune response is the recognition of antigens by lymphocytes, which, when stimulated, proliferate and mature into effector cells and memory cells. These cells are characterized by heterogeneity in terms of surface receptor expression, function and

location.[35] It appears that memory T cells can reduce the severity of COVID-19 infection by triggering a protective immune response.

Differentiation of T cell populations into effector and memory subsets is one of the most fundamental aspects of T cell-dependent immunity. Thus, the balance between naïve and memory T cells is crucial to maintain an effective immune response.[36] Very few reports were found comparing the composition of leukocyte and lymphocyte subsets from patients of different waves of the COVID-19 pandemic.

We showed the highest percentage of $CD8^+$ RTE cells and naïve $CD8^+$ cells in the HC group, indicating a muted immune system compared to the COVID-19 groups. In comparison, the proportion of memory effector cells was the highest in the 5th wave group of patients both in the case of $CD4^+$ and $CD8^+$ lymphocytes. The presence of effector memory cells could indicate re-contact with the antigen and residual immunological memory. Despite the lack of vaccination and confirmed infections with the SARS-Cov-2 virus, most patients from the 5th wave seem to have had contact with the virus during the first 4 waves of the pandemic.

The state of infection can also lead to the emergence of an adaptive immune response and the formation of memory cells responsible for protective immunity. Over time, the likelihood of developing immunological memory increases with subsequent exposures to the virus, either through vaccination or direct contact.

Our previous research showed an increase of T cells with immunological memory in response to COVID-19 infection. Among $CD8^+$ cells, effector cells were most abundant in COVID-19 patients. In contrast, we noted a significant growth in the proportion of $CD4^+$ central memory cells relative to the HC group. Our results indicated the development of immunological memory in patients with COVID-19 infection, without any correlation to changes in the lungs.[37,38] Netea and Li also showed more abundant effector and memory $CD8^+$ cells in COVID-19 survivors compared to healthy volunteers, highlighting their role in antiviral immunity.[39]

There was no consensus on what mechanisms might cause disease progression or inhibition. A significant body of literature has been published on the role of antibodies in COVID-19 disease, and it has been shown that $CD4^+$ T cell activity is necessary to produce antibodies against SARS-CoV-2 infection.[40] While controversy remains, it appears that the relief of COVID-19 symptoms is related to adaptive immunity and the production of memory cells. Peng et al. confirmed an association between the SARS-CoV-2-specific T cell response and recovery. The memory T cell response was shown to be greater in patients with severe disease than in those with mild COVID-19.[41] Liao et al. suggested that adaptive T cell responses are likely protective during SARS-CoV-2 infection.[42] Scalia et al. observed a decrease in most lymphocyte subsets in mild and moderate stages, a decrease in NK cells and regulatory T cells in 2nd-wave patients, and a more significant number of activated Th17 lymphocytes in all stages compared to the 1st wave. Less severe symptoms of SARS-CoV-2 infection were observed in 2nd-wave patients in advanced stages, while patients in the mild and moderate stages had a worse course compared to patients in the 1st wave. The authors suggested that in patients with mild COVID-19 at diagnosis, treatment with steroids and azithromycin appeared to blunt the immune reaction against the virus.[43] Asghar et al. found that most levels of inflammatory markers were lower in the 2nd wave, while the percentages of neutrophils and lymphocytes were higher compared to the 1st wave. Disease severity was also more predictable in the 2nd wave, which may be due to attenuation of the inflammatory response by the immediate use of immunosuppressants, antibiotics, antiviral drugs, or anticoagulants, according to treatment recommendations that were not available during the 1st wave.[44] Moreover, the course of the disease may depend on the adaptive immune response of patients. T-cell immunity plays a crucial role in controlling SARS-CoV-2, and its importance may have been relatively underestimated until now.[45] However, new data are emerging indicating that SARS-CoV-2-specific memory T cells are being produced. Long-term studies of patients who recovered from the closely related SARS virus (SARS-CoV-1) between 2002 and 2004 found that anti-SARS T cells were long-lived and remained nearly 2 decades later.[46] Therefore, the characteristics of the immune response among population groups may help develop personalized therapies for patients with severe disease.[47] Knowledge of the immune profile is also important for creating new vaccines against SARS-CoV-2, which should trigger the production of memory T cells.[46]

We proposed that memory effector $CD4^+$ and $CD8^+$ cells represent a reliable measure of immune status that may be useful for assessing recent major waves of COVID-19. Additionally, the reduced proportion of central memory $CD4^+$ cells, naive $CD8^+$ cells and RTE $CD8^+$ cells allowed for the distinguishing of patients in the last significant COVID-19 wave, which may indicate the direction of further research and comprise the next stage of diagnostics. Regular monitoring of lymphocyte subsets during SARS-Cov-2 infection will assess the patient's immune status and lymphocyte readiness for an immune response and may be essential to improve clinical outcomes.

Limitations

Our study has limitations that may introduce some potential bias. It was a study on a small group of patients, and data from a larger cohort of patients would be useful to evaluate subsequent changes in immune responses following SARS-CoV-2 infection. However, our study

provided much new information about the host immune response in COVID-19 patients that SARS-CoV-2 may act on lymphocytes, especially T cells. There has been a lack of studies assessing the virus variant in individual waves of the pandemic. Patients from only 2 waves of the pandemic were compared, although 2 extreme waves were selected, the 1st and, so far, the last (the 5th).

Conclusions

In this work, we analyzed basal peripheral leukocytes and T cell subpopulations of the maturation process and differences between COVID-19 waves compared to healthy controls. The number of characteristic changes in the maturation profile of T lymphocytes in the 5th wave group compared to the 1st wave group and the HC group indicated the switching of cell functions to effectors, ready for the immune response, and indicated the differentiation of the course of the disease depending on the wave of COVID-19.

Monitoring the memory cell population in healthy people and people at risk is very important for proper prevention or treatment. The characterization of T lymphocyte subpopulations allowed us to illustrate the phenomenon of immunological memory and readiness to effectively eliminate the virus in patients with COVID-19. The presented results allowed us to emphasize to some extent the importance of immunological memory in these patients, but further detailed studies are necessary.

Supplementary data

The Supplementary materials are available at https://doi.org/10.5281/zenodo.10803904. The package includes the following files:

Supplementary Table 1. Assessment of assumptions regarding normal distribution performed using the Shapiro–Wilk test and homogeneity of variances using the Brown–Forsythe test for the studied leukocyte subpopulations in 3 groups.

Supplementary Table 2. Assessment of assumptions regarding normal distribution performed using the Shapiro–Wilk test and homogeneity of variances using the Brown–Forsythe test for the studied lymphocytes T subpopulations in 3 groups.

Data availability

The datasets generated and/or analyzed during the current study are available from the corresponding author on reasonable request.

Consent for publication

Not applicable.

ORCID iDs

Elżbieta Rutkowska https://orcid.org/0000-0002-9727-2576
Iwona Kwiecień https://orcid.org/0000-0003-2266-971X
Agata Raniszewska https://orcid.org/0000-0003-3917-6030
Krzysztof Kłos https://orcid.org/0000-0001-9629-5680
Piotr Rzepecki https://orcid.org/0000-0003-0694-390X
Andrzej Chciałowski https://orcid.org/0000-0002-6444-4124

References

1. Dutta A. COVID-19 waves: Variant dynamics and control. *Sci Rep*. 2022;12(1):9332. doi:10.1038/s41598-022-13371-2
2. Umakanthan S, Sahu P, Ranade AV, et al. Origin, transmission, diagnosis and management of coronavirus disease 2019 (COVID-19). *Postgrad Med J*. 2020;96(1142):753–758. PMID:32563999, PMCID:PMC10016932.
3. Dixon BE, Wools-Kaloustian KK, Fadel WF, et al. Symptoms and symptom clusters associated with SARS-CoV-2 infection in community-based populations: Results from a statewide epidemiological study. *PLoS One*. 2021;16(3):e0241875. doi:10.1371/journal.pone.0241875
4. Torge D, Bernardi S, Arcangeli M, Bianchi S. Histopathological features of SARS-CoV-2 in extrapulmonary organ infection: A systematic review of literature. *Pathogens*. 2022;11(8):867. doi:10.3390/pathogens11080867
5. Barański K, Brożek G, Kowalska M, Kaleta-Pilarska A, Zejda JE. Impact of COVID-19 pandemic on total mortality in Poland. *Int J Environ Res Public Health*. 2021;18(8):4388. doi:10.3390/ijerph18084388
6. Jassat W, Mudara C, Ozougwu L, et al. Difference in mortality among individuals admitted to hospital with COVID-19 during the first and second waves in South Africa: A cohort study. *Lancet Glob Health*. 2021;9(9):e1216–e1225. doi:10.1016/S2214-109X(21)00289-8
7. De Lima Gianfelice PR, Sovek Oyarzabal R, Cunha A, Vicensi Grzybowski JM, Da Conceição Batista F, Macau EEN. The starting dates of COVID-19 multiple waves. *Chaos*. 2022;32(3):031101. doi:10.1063/5.0079904
8. Suligowski R, Ciupa T. Five waves of the COVID-19 pandemic and green–blue spaces in urban and rural areas in Poland. *Environ Res*. 2023;216:114662. doi:10.1016/j.envres.2022.114662
9. Guan WJ, Ni ZY, Hu Y, et al. Clinical characteristics of coronavirus disease 2019 in China. *N Engl J Med*. 2020;382(18):1708–1720. doi:10.1056/NEJMoa2002032
10. Saito S, Asai Y, Matsunaga N, et al. First and second COVID-19 waves in Japan: A comparison of disease severity and characteristics. *J Infect*. 2021;82(4):84–123. doi:10.1016/j.jinf.2020.10.033
11. Contou D, Fraissé M, Pajot O, Tirolien JA, Mentec H, Plantefève G. Comparison between first and second wave among critically ill COVID-19 patients admitted to a French ICU: No prognostic improvement during the second wave? *Crit Care*. 2021;25(1):3. doi:10.1186/s13054-020-03449-6
12. Śleszyński P, Czapiewski K. *Atlas Wyszehradzki/Visegrad Atlas*. Warsaw, Poland: Instytut Współpracy Polsko-Węgierskiej im. Wacława Felczaka i Polskie Towarzystwo Geograficzne; 2021. ISBN:978-83-958155-0-8.
13. Nagy É, Golopencza P, Barcs I, Ludwig E. Comparison of COVID-19 severity and mortality rates in the first four epidemic waves in Hungary in a single-center study with special regard to critically ill patients in an intensive care unit. *Trop Med Infect Dis*. 2023;8(3):153. doi:10.3390/tropicalmed8030153
14. Choi H, Chatterjee P, Hwang M, Lichtfouse E, Sharma VK, Jinadatha C. The viral phoenix: Enhanced infectivity and immunity evasion of SARS-CoV-2 variants. *Environ Chem Lett*. 2022;20(3):1539–1544. doi:10.1007/s10311-021-01318-4
15. Ong SWX, Chiew CJ, Ang LW, et al. Clinical and virological features of severe acute respiratory syndrome coronavirus 2 (SARS-CoV-2) variants of concern: A retrospective cohort study comparing B.1.1.7 (Alpha), B.1.351 (Beta), and B.1.617.2 (Delta). *Clin Infect Dis*. 2022;75(1):e1128–e1136. doi:10.1093/cid/ciab721
16. Wrenn JO, Pakala SB, Vestal G, et al. COVID-19 severity from Omicron and Delta SARS-CoV-2 variants. *Influenza Other Respir Viruses*. 2022;16(5):832–836. doi:10.1111/irv.12982
17. Włodarczyk WC. Remarks on COVID-19 pandemic in Poland. A health policy perspective [in Polish]. *Zdrowie Publiczne i Zarządzanie*. 2020;18(2):126–148. doi:10.4467/20842627OZ.20.013.12766

18. Skrzat-Klapaczyńska A, Bieńkowski C, Kowalska J, et al. The beneficial effect of the COVID-19 vaccine booster dose among healthcare workers in an infectious diseases center. *Vaccines*. 2022;10(4):552. doi:10.3390/vaccines10040552
19. Sowa P, Kiszkiel Ł, Laskowski PP, et al. COVID-19 vaccine hesitancy in Poland: Multifactorial impact trajectories. *Vaccines*. 2021;9(8):876. doi:10.3390/vaccines9080876
20. Wang C, Han J. Will the COVID-19 pandemic end with the Delta and Omicron variants? *Environ Chem Lett*. 2022;20(4):2215–2225. doi:10.1007/s10311-021-01369-7
21. Akira S, Uematsu S, Takeuchi O. Pathogen recognition and innate immunity. *Cell*. 2006;124(4):783–801. doi:10.1016/j.cell.2006.02.015
22. Fink PJ. The biology of recent thymic emigrants. *Annu Rev Immunol*. 2013;31(1):31–50. doi:10.1146/annurev-immunol-032712-100010
23. Boldt A, Borte S, Fricke S, et al. Eight color immunophenotyping of T-, B- and NK-cell subpopulations for characterization of chronic immunodeficiencies: Immunodeficiency Screening System. *Cytometry B Clin Cytom*. 2014;86(3):191–206. doi:10.1002/cytob.21162
24. Flisiak R, Horban A, Jaroszewicz J, et al. Management of SARS-CoV-2 infection: Recommendations of the Polish Association of Epidemiologists and Infectiologists as of February 23, 2022. *Pol Arch Intern Med*. 2022;132(3):16230. doi:10.20452/pamw.16230
25. El-Shabasy RM, Nayel MA, Taher MM, Abdelmonem R, Shoueir KR, Kenawy ER. Three waves changes, new variant strains, and vaccination effect against COVID-19 pandemic. *Int J Biol Macromol*. 2022;204:161–168. doi:10.1016/j.ijbiomac.2022.01.118
26. Buttenschøn HN, Lynggaard V, Sandbøl SG, Glassou EN, Haagerup A. Comparison of the clinical presentation across two waves of COVID-19: A retrospective cohort study. *BMC Infect Dis*. 2022;22(1):423. doi:10.1186/s12879-022-07413-3
27. Iftimie S, López-Azcona AF, Vallverdú I, et al. First and second waves of coronavirus disease-19: A comparative study in hospitalized patients in Reus, Spain. *PLoS One*. 2021;16(3):e0248029. doi:10.1371/journal.pone.0248029
28. Jalali SF, Ghassemzadeh M, Mouodi S, et al. Epidemiologic comparison of the first and second waves of coronavirus disease epidemics in Babol, North of Iran. *Caspian J Intern Med*. 2020;11(Suppl 1):544–550. doi:10.22088/cjim.11.0.544
29. Liu G, Jiang X, Zeng X, Pan Y, Xu H. Analysis of lymphocyte subpopulations and cytokines in COVID-19-associated pneumonia and community-acquired pneumonia. *J Immunol Res*. 2021;2021:6657894. doi:10.1155/2021/6657894
30. Tan L, Wang Q, Zhang D, et al. Lymphopenia predicts disease severity of COVID-19: A descriptive and predictive study. *Sig Transduct Target Ther*. 2020;5(1):33. doi:10.1038/s41392-020-0148-4
31. Alkhatip AAAMM, Kamel MG, Hamza MK, et al. The diagnostic and prognostic role of neutrophil-to-lymphocyte ratio in COVID-19: A systematic review and meta-analysis. *Exp Rev Mol Diagn*. 2021;21(5):505–514. doi:10.1080/14737159.2021.1915773
32. Tavakolpour S, Rakhshandehroo T, Wei EX, Rashidian M. Lymphopenia during the COVID-19 infection: What it shows and what can be learned. *Immunol Lett*. 2020;225:31–32. doi:10.1016/j.imlet.2020.06.013
33. Rutkowska E, Kwiecień I, Żabicka M, et al. Cytokines and leukocytes subpopulations profile in SARS-CoV-2 patients depending on the CT score severity. *Viruses*. 2021;13(5):880. doi:10.3390/v13050880
34. Charostad J, Rezaei Zadeh Rukerd M, Shahrokhi A, et al. Evaluation of hematological parameters alterations in different waves of COVID-19 pandemic: A cross-sectional study. *PLoS One*. 2023;18(8):e0290242. doi:10.1371/journal.pone.0290242
35. Chang JT, Wherry EJ, Goldrath AW. Molecular regulation of effector and memory T cell differentiation. *Nat Immunol*. 2014;15(12):1104–1115. doi:10.1038/ni.3031
36. Das S, Rai G, Sood V, et al. Incompetent memory immune response in severe COVID-19 patients under treatment. *Heliyon*. 2023;9(10):e20590. doi:10.1016/j.heliyon.2023.e20590
37. Lei X, Dong X, Ma R, et al. Activation and evasion of type I interferon responses by SARS-CoV-2. *Nat Commun*. 2020;11(1):3810. doi:10.1038/s41467-020-17665-9
38. Kwiecień I, Rutkowska E, Kłos K, et al. Maturation of T and B lymphocytes in the assessment of the immune status in COVID-19 patients. *Cells*. 2020;9(12):2615. doi:10.3390/cells9122615
39. Netea MG, Li Y. Immune memory in individuals with COVID-19. *Nat Cell Biol*. 2021;23(6):582–584. doi:10.1038/s41556-021-00689-8
40. Swain SL, McKinstry KK, Strutt TM. Expanding roles for $CD4^+$ T cells in immunity to viruses. *Nat Rev Immunol*. 2012;12(2):136–148. doi:10.1038/nri3152
41. Peeples L. Avoiding pitfalls in the pursuit of a COVID-19 vaccine. *Proc Natl Acad Sci U S A*. 2020;117(15):8218–8221. doi:10.1073/pnas.2005456117
42. Liao M, Liu Y, Yuan J, et al. Single-cell landscape of bronchoalveolar immune cells in patients with COVID-19. *Nat Med*. 2020;26(6):842–844. doi:10.1038/s41591-020-0901-9
43. Scalia G, Raia M, Gelzo M, et al. Cytometric analysis of patients with COVID-19: What is changed in the second wave? *J Transl Med*. 2021;19(1):403. doi:10.1186/s12967-021-03072-1
44. Asghar MS, Yasmin F, Ahsan MN, Alvi H, Taweesedt P, Surani S. Comparison of first and second waves of COVID-19 through severity markers in ICU patients of a developing country. *J Community Hosp Int Med Perspect*. 2021;11(5):576–584. doi:10.1080/20009666.2021.1949793
45. Moss P. The T cell immune response against SARS-CoV-2. *Nat Immunol*. 2022;23(2):186–193. doi:10.1038/s41590-021-01122-w
46. Jarjour NN, Masopust D, Jameson SC. T cell memory: Understanding COVID-19. *Immunity*. 2021;54(1):14–18. doi:10.1016/j.immuni.2020.12.009
47. Fischer JC, Balz V, Jazmati D, et al. Prognostic markers for the clinical course in the blood of patients with SARS-CoV-2 infection. *Eur J Med Res*. 2022;27(1):255. doi:10.1186/s40001-022-00864-z

Pulp regeneration using a peptide nanofiber artificial scaffold on animal models: A preliminary study

Ozlem Marti Akgun[1,A–F], Ayse Begum Tekinay[2,A,E], Gulistan Tansık[3,C], Ceren Yıldırım[1,B], Gunseli Guven Polat[4,E]

[1] Gulhane Dentistry Faculty, Univesity of Health Sciences, Ankara, Turkey
[2] Requalite GmbH, Gräfelfing, Germany
[3] Institute of Materials Science and Nanotechnology, Bilkent University, Ankara, Turkey
[4] Hamidiye Dentistry Faculty, Univesity of Health Sciences, İstanbul, Turkey

A – research concept and design; B – collection and/or assembly of data; C – data analysis and interpretation;
D – writing the article; E – critical revision of the article; F – final approval of the article

Advances in Clinical and Experimental Medicine, ISSN 1899–5276 (print), ISSN 2451–2680 (online) *Adv Clin Exp Med*. 2025;34(3):407–419

Address for correspondence
Ozlem Marti Akgun
E-mail: ozlemmartiakgun@gmail.com

Funding sources
None declared

Conflict of interest
None declared

Received on May 24, 2023
Reviewed on December 2, 2023
Accepted on June 4, 2024

Published online on December 5, 2024

Cite as
Akgun OM, Tekinay AB, Tansık G, Yıldırım C, Polat GG. Pulp regeneration using a peptide nanofiber artificial scaffold on animal models: A preliminary study. *Adv Clin Exp Med*. 2025;34(3):407–419. doi:10.17219/acem/189639

DOI
10.17219/acem/189639

Abstract

Background. In regenerative endodontic procedures (REPs), it is crucial to find effective materials. This study introduces glycosaminoglycan (GAG) mimetic peptide amphiphile (PA, GAG-PA) and K-PA nanofibers, synthesized to emulate sulfated GAGs, aiming to enhance tissue repair within damaged pulp – an area where standardized protocols are currently lacking.

Objectives. The objective of this study was to investigate the regenerative potential of GAG-PA nanofibers in REP.

Materials and methods. Heparan sulfate mimicking PAs was designed to develop a bioactive nanofibrous supramolecular system. The cavities on the mesial surfaces of the first upper molars of 8 rats (4 rats in the study group and 4 in the control group) were prepared, and the pulps were perforated. Then, the material was applied onto the dental pulp, and the cavities were closed with a self-curing glass ionomer cement filling material. Physiological saline was used in the control group. Thirty days after application, the teeth were extracted, and the formation of regenerative tissue sections in the pulp was evaluated using hematoxylin and eosin (H&E) staining and Masson's trichrome staining.

Results. After 30 days, H&E staining demonstrated robust tissue regeneration in the implanted region, with minimal neutrophil infiltration. Masson's trichrome staining confirmed reparative dentin formation. Quantitative analysis revealed a regeneration percentage of 85% in the study group, compared to 80% in the control group. Statistical analysis showed no significant difference in regeneration between the groups ($p > 0.05$).

Conclusions. Our comprehensive study, utilizing GAG-PA and K-PA nanofibers, demonstrated successful synthesis, characterization and formation of nanofiber networks. The in vivo experiment with rats exhibited substantial tissue regeneration with quantifiable results supporting the efficacy of the nanofiber approach. Statistical analysis confirmed the consistency between the study and control groups, emphasizing the potential of these nanofibers in endodontic tissue regeneration applications.

Key words: regenerative endodontics, dental pulp, tissue scaffolds

Background

The dental pulp is a vital soft connective tissue that has the remarkable ability to generate dentin in response to external stimuli. Furthermore, it plays a crucial role in maintaining the biological and physiological vitality of dentin, thus contributing to dental homeostasis. Dental pulp inflammation, referred to as pulpitis, is an inflammatory dental condition characterized by the degradation of dental pulp, leading to the eventual loss of its functionality. The entry of bacteria and their harmful components into the pulp triggers an inflammatory response within various host cells, such as dental pulp cells, macrophages and other immune cells.[1] Nevertheless, these actions impede the inherent self-repair mechanism of the dental pulp, resulting in prolonged inflammation that is immensely destructive and can potentially lead to tissue necrosis.[2] In the majority of cases, complete removal of the pulp tissue is performed during root canal treatment, even if a significant portion of the pulp remains healthy.[3] Unfortunately, this procedure leads to the loss of dentin, escalating the risk of tooth fractures and ultimately culminating in the extraction of the tooth. However, the possibility of extraction can be averted if the damaged pulp tissue can be regenerated.

Regenerative endodontic procedures (REP) have emerged as a viable option for addressing immature necrotic teeth with apical periodontitis, aiming to rejuvenate the necrotic pulp and facilitate root development. The absence of a standardized protocol for this treatment method has led the American Association of Endodontists (AAE) and the European Society of Endodontology (ESE) to advocate for a shared clinical guideline.[4–6] Key distinctions in these procedures typically revolve around the application of intracanal media, the method of inducing bleeding, the concentration of sodium hypochlorite, and the use of biological matrices.[6] This collaborative guideline serves as a foundation, allowing flexibility in clinical approaches while maintaining a common framework for REP.

The utilization of stem cells and/or biomaterials for dental pulp regeneration is regarded as a crucial approach to preserving tooth health. Before clinical implementation, it is essential to conduct animal studies to validate the bioavailability, safety and effectiveness of novel treatment modalities involving stem cells or biomaterials in the context of dental pulp regeneration.[7]

Synthetic biomaterials that can mimic extracellular structures have proven to be invaluable for tissue engineering and regenerative medicine applications.[8,9] Extracellular matrix (ECM) mimetic materials can recognize and control cell movements and behavior, and 3-dimensional (3D) microenvironments created using such biomaterials enable stem cells to multiply and differentiate through tailored biological signs.[10]

The biomechanical properties of synthetic polymers are critical considerations in various biomedical applications, particularly in the field of tissue engineering. Engineered to mimic the structural characteristics of natural tissues, synthetic polymers such as poly(lactic acid) (PLA), poly(glycolic acid) (PGA) and their copolymers like poly(lactic-co-glycolic acid) (PLGA) offer versatility in tailoring mechanical strength.[11] Factors such as molecular weight, crystallinity and processing methods influence the biomechanical behavior of these polymers. The mechanical strength of synthetic polymers is essential for providing structural support during tissue regeneration.[12] Additionally, the biodegradability of these polymers, where controlled degradation over time matches tissue regeneration rates, is a crucial feature. The ability to fine-tune biomechanical properties makes synthetic polymers valuable in creating scaffolds and implants that can integrate seamlessly with the biological systems they aim to support and regenerate.

In nature, proteins in the intercellular structure, known as collagen, are used by cells for mechanical support and attachment.[13] The length of a collagen fibril, which consists of aggregated polypeptides, is approx. 300 nm, and the diameter is approx. 1.5 nm. Cells can interact with collagen through integrin proteins, such as fibronectin and laminin, and move within the intercellular structure. Previous studies have shown that Arg-Gly-Asp-Ser (RGDS) on fibronectin and Ile-Lys-Val-Ala-Val peptide sequences on laminin form vital binding sites for cells to use these proteins.[14–16] These short peptide sequences have thus been placed on many synthetic polymers, allowing cells to move in environments created by these polymers. However, in general, these polymers cannot naturally degrade and do not accurately portray biological signals.

Scaffolds, 3D frameworks designed to mimic the ECM, must possess specific biomechanical characteristics for successful integration with host tissues.[17] Mechanical support is a key consideration, with properties such as compressive strength, tensile strength and modulus of elasticity crucial in maintaining structural integrity. Porosity and pore size are also vital factors, influencing nutrient and oxygen diffusion, as well as facilitating cell ingrowth.[18] Biocompatibility is essential to promote cell attachment, proliferation and differentiation, while the dynamic balance of degradation and remodeling ensures that the scaffold degrades over time, synchronizing with the natural regeneration of the tissue. The ability to modulate these biomechanical properties makes scaffolds versatile tools in regenerative medicine, providing a customizable platform for tissue repair and replacement.[19]

Ongoing research focuses on the development of synthetic or natural scaffolds.[20] Various alternative scaffolds employed for pulp regeneration, such as soluble collagen, absorbable gelatin sponge and platelet-rich plasma, have undergone examination in animal models.[21–23] However, the histological findings from these studies consistently indicate unsuccessful healing. Furthermore, a study assessing the regenerative potential of 2 lyophilized chitosan-based scaffolds (hyaluronic acid : chitosan and pectin : chitosan) reported unfavorable histological results.[24] Up to now,

cross-linked collagen sponge scaffolds have been the sole scaffolds utilized, yielding more favorable outcomes.[25]

Composed of a network of blood vessels, nerves and fibrous tissues, dental pulp contributes to the mechanical resilience of the tooth. Its ability to resist compressive forces is essential for protecting the underlying pulp tissue from external impacts and occlusal forces during biting and chewing.[26] The elasticity of dental pulp allows it to absorb and distribute mechanical stresses, acting as a shock absorber and minimizing the risk of damage to the tooth. Additionally, the pulp's regeneration plays a role in maintaining tissue health and facilitating reparative processes. Understanding the biomechanical properties of dental pulp is essential for designing dental materials and procedures that preserve pulp vitality while ensuring the overall mechanical stability of the tooth structure.[27]

The use of animal models in research on REP is necessary for several reasons. These models provide valuable insights into the efficacy, safety and mechanisms of regenerative approaches for pulp treatment. Animal models allow researchers to evaluate the potential of REP to promote pulp regeneration and repair. For example, studies in rats or dogs can assess the effectiveness of different scaffolds, growth factors or stem cell-based therapies in stimulating pulp regeneration.[28] Animal models help researchers investigate the long-term outcomes of regenerative pulp therapies. By examining histological, radiographic and functional parameters, these models provide valuable data on the success of the treatment and the quality of the regenerated pulp tissue.[29] Animal models enable researchers to evaluate the safety and biocompatibility of regenerative materials and procedures used in pulp therapy. These models help identify potential adverse effects, such as inflammation, immunological reactions or neoplastic transformations, which are critical before translating therapies to human clinical trials.[30] Animal models provide a platform to study the underlying mechanisms involved in pulp regeneration. By analyzing the cellular and molecular events occurring during the regenerative process, researchers can gain a deeper understanding of the biological pathways and factors influencing pulp tissue repair.[31] In summary, animal models are essential for evaluating the potential of REP, assessing treatment outcomes, ensuring safety and biocompatibility, and understanding the underlying mechanisms of pulp regeneration. These models play a crucial role in advancing REP and ultimately improving clinical treatments for dental pulp-related conditions.

In this study, an attempt was made to overcome some of the limitations associated with traditional scaffolds. Peptide nanofiber artificial scaffolds were introduced and evaluated as an alternative in an in vivo animal study. The purpose was to explore the potential advantages of peptide nanofiber scaffolds as an innovative approach for pulp regeneration, acknowledging the ongoing need for advancements in this field.

The hypothesis of this study posits that the application of glycosaminoglycan (GAG) mimetic peptide amphiphile (PA, GAG-PA) nanofibers as a bioactive nanofibrous supramolecular system can promote pulp regeneration in rat molars with perforated pulps. Specifically, we hypothesize that the use of heparan sulfate mimicking PAs in the treatment of pulpal injuries, when compared to a control group treated with physiological saline, will result in a statistically significant increase in the percentage of regeneration within the damaged pulp area. The evaluation of regenerative tissue sections through hematoxylin and eosin (H&E) staining and Masson's trichrome staining is expected to reveal a measurable enhancement in reparative dentin formation in the study group. However, to establish statistical significance of these observed differences, it is further hypothesized that an increase in the number of animals in future studies will be necessary.

Objectives

The present study aimed to evaluate the effect of bioactive peptide nanofibrous hydrogels, which can create an artificial 3D environment, on the differentiation of dental pulp stem cells into odontoblasts and vascular nerve cells for pulp regeneration in animal models.

Materials and methods

Materials

The acbr (Karlsruhe, Germany) or Nova-Biochem (London, UK) supplied all the amino acids, such as lauric acid, 4-(2',4'-dimethoxyphenyl-Fmoc-aminomethyl)-phenoxyacetamido-norleucyl-MBHA resin (Rink amide MBHA resin), diisopropylethylamine (DIEA), and 2-(1H-benzotriazol-1-yl)-1,1,3,3 tetramethyluroniumhexafluorophosphate (HBTU). Thermo Fisher Scientific (Waltham, USA) and Sigma-Aldrich (Darmstadt, Germany) provided the remaining chemicals used in this study.

Synthesis, characterization and purification of peptide amphiphile molecules

The Lauryl-Val-Val-Ala-Gly-Lys-Am (K-PA) and Lauryl-Val-Val-Ala-Gly-Glu-Gly-Asp (Lys-p-sulfobenzoate)-Ser-Am (GAG-PA) peptides were synthesized using a previously published procedure.[32] The Fmoc solid-phase peptide synthesis method was employed for their synthesis.

The synthesized peptide amphiphiles were subjected to liquid chromatography–mass spectrometry (LC–MS) analysis to determine their identity and purity. For LC–MS analysis, an Agilent 6530 Q-TOF instrument with an electrospray ionization (ESI) source and either a Zorbax Extend-C18 2.1×50 mm column (Agilent, Santa Clara, USA) (for basic conditions) or a Zorbax SB-C8 4.6×100 mm column (for acidic conditions) was employed to obtain

Table 1. The statistical values related to the regenerated area and the mean color intensity

Statistics	Regenerated area		Mean color intensity	
	serum	gel	serum	gel
median	85.86	92.1	45.06	68.04
SD	NaN	12.05	NaN	13.23
Minimum	85.86	71.43	45.06	54.79
Maximum	85.86	92.48	45.06	81.26
U	1		0	
z	–0.45		–1.34	
asymptotic p	0.655		0.18	
exact p	1		0.5	
r	0.22		0.67	

SD – standard deviation; NaN – not a number.

mass spectra. The mobile phase consisted of a gradient of water (with 0.1% formic acid or 0.1% ammonium hydroxide (NH_4OH) and acetonitrile (with 0.1% formic acid or 0.1% NH_4OH).

To purify the peptides, an Agilent preparative reverse-phase HPLC system with either a Zorbax Extend-C18 21.2×150 mm column (for basic conditions) or a Zorbax SB-C8 21.2×150 mm column (for acidic conditions) was utilized. The mobile phase employed a gradient of water (with 0.1% trifluoroacetic acid (TFA) or 0.1% NH_4OH) and acetonitrile (with 0.1% TFA or 0.1% NH_4OH). For the K-PA peptide, a 0.1 M hydrochloric acid (HCl) solution was used to remove residual TFA, followed by lyophilization. The details can be found in Table 1.

Visualization of peptide amphiphile nanofiber network using scanning electron microscopy

The morphology of nanofiber networks formed by peptide amphiphile molecules was examined using scanning electron microscopy (SEM) (FEI Quanta 200 FEG SEM; FEI Company, Hillsboro, USA). To prepare the samples, GAG-PA and K-PA solutions (10 mM) were mixed at a 1:3 ratio in a final volume of 60 µL on a silicon wafer, allowing for the stabilization of all net charges. After 15 min of gelation, the samples underwent sequential dehydration using ethanol concentrations of 20%, 40%, 60%, 80%, and 100% v/v. Subsequently, an Autosamdri-815B critical point dryer (Tousimis, Rockville, USA) was used for drying the samples. A thin coating of 4-nm gold-palladium (Au-Pd) was applied to the dried samples, and imaging was conducted using an FEI Quanta 200 FEG SEM (FEI Company) operating in high vacuum mode with a 5 keV beam energy.

Characterization of nanofiber secondary structures through circular dichroism analysis

To conduct circular dichroism (CD) measurements, samples were prepared by mixing 3×10^{-2} mM GAG-PA and 9×10^{-2} mM K-PA. The CD measurements were carried out using a JASCO J815 CD spectrometer (JASCO, Tokyo, Japan) at room temperature (21–22°C), covering a wavelength range of 300–190 nm. The data interval and data pitch were set at 0.1 nm with a scanning speed of 100 nm/min. Each measurement was performed in triplicate. The digital integration time (DIT) for CD measurements was set to 1 s, the bandwidth was set at 1 nm, and the sensitivity was set to the standard value.

Preparation of scaffolds

A bioactive nanofibrous supramolecular system was developed using peptide amphiphiles that mimic heparan sulfate (GAG-PAs) (Fig. 1,2). The GAG-PA and K-PA molecules were dissolved in double-distilled water (ddH_2O) at a concentration of 10 mM and subjected to sterilization under UV light for 1 h. To stabilize all net charges, the samples were prepared by mixing GAG-PA and K-PA solutions at a volume ratio of 1:3.

Ethics statement

The Animal Research Ethics Committee of Gülhane Military Medical Academy (GMMA; Ankara, Turkey) approved the clinical protocol on March 6, 2012, with reference No. 187. The experimental animals were provided by the GMMA within the project number AR-2012/55.

Animal model

Animal pilot studies related to REP are generally conducted on small animal models, and rats are commonly used. In this context, 8 female Sprague Dawley rats, weighing approx. 200 g each, were employed for the study when they reached 6 weeks of age. Our study was planned with 8 rats as it is a preliminary investigation. These rats were housed under standard conditions, with a temperature of 23°C and a regular light/dark schedule, and provided with unrestricted access to food and water. The cages were equipped with appropriate bedding material for comfort, and regular cleaning was performed to maintain hygienic conditions. All necessary measures were taken to ensure the wellbeing and ethical treatment of the rats throughout the experimental period. The overall health status of the rats used in the study was assessed through regular monitoring and evaluation, following established protocols used in similar studies. The rats were observed daily for any signs of distress, abnormal behavior or physical abnormalities. Body weight measurements were recorded periodically to monitor their growth and overall condition. Additionally, clinical parameters such as coat appearance, activity level and food and water intake were assessed to ensure their wellbeing. Any rats showing signs of illness or discomfort were promptly evaluated by a veterinarian, and appropriate measures were taken to address their

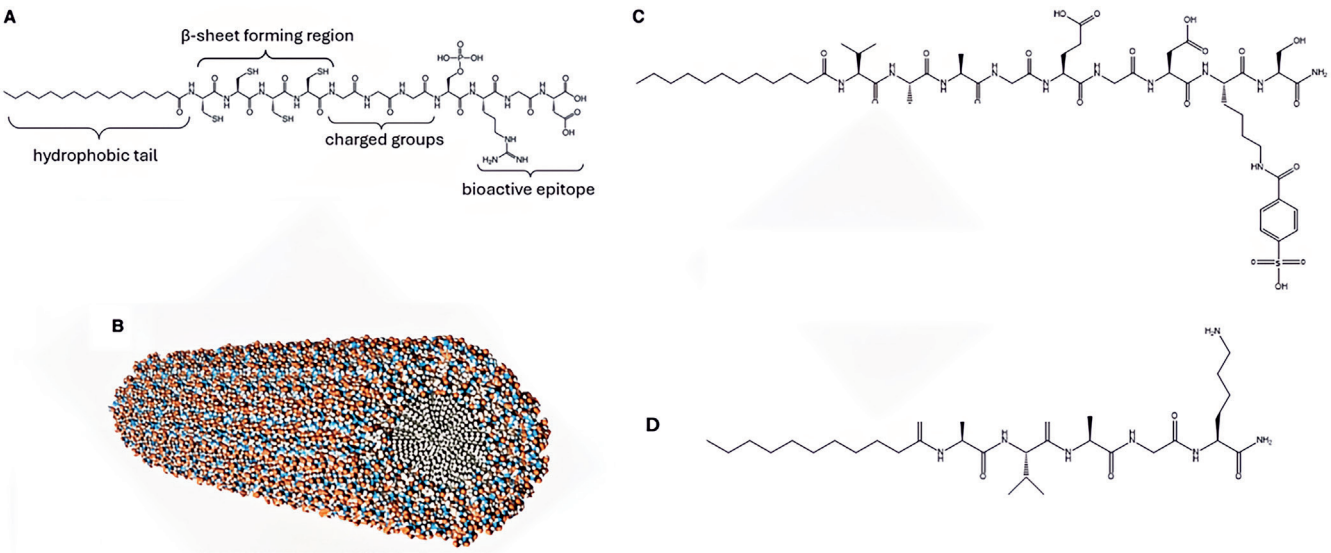

Fig. 1. A. Chemical composition of PA; B. Illustration depicting the self-assembly of PA molecules forming a cylindrical micelle. Chemical structures of (C) negatively charged GAG-PA and (D) K-PA

PA – peptide amphiphile; GAG-PA – glycosaminoglycan mimetic peptide amphiphile; K-PA – positively charged peptide amphiphile.

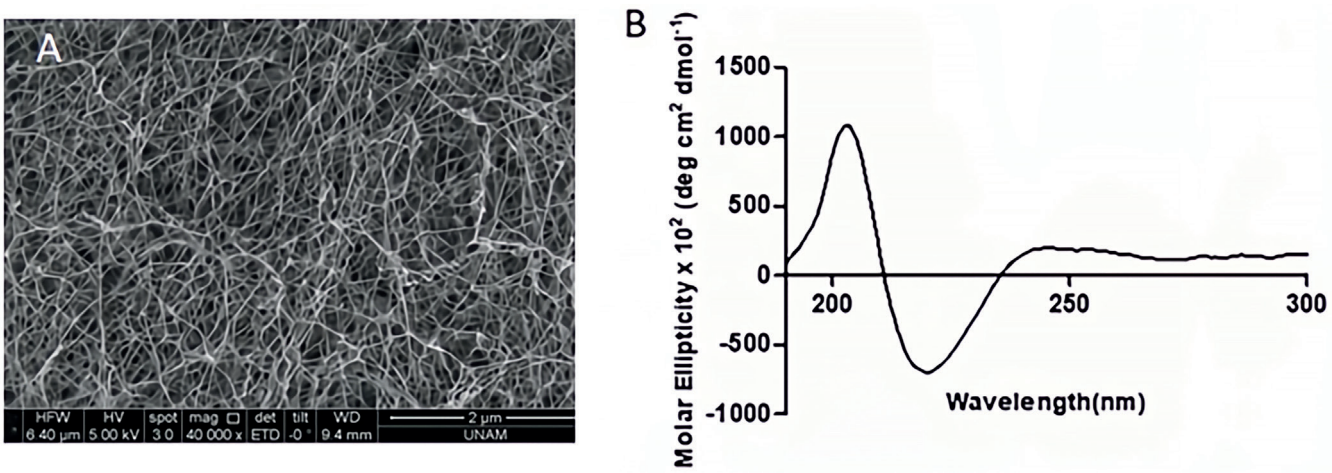

Fig. 2. A. SEM image of nanofibrous networks formed by GAG-PA/K-PA; B. CD spectra of GAG-PA

SEM – scanning electron microscope; GAG-PA – glycosaminoglycan mimetic peptide amphiphile; K-PA – positively charged peptide amphiphile; CD – circular dichroism.

health needs. An animal care technician provided daily care to the animals, maintained their living environment, and monitored their health and wellbeing.

Application procedure

To induce a pulp defect, the rats were administered intraperitoneal (ip.) injections of 2% xylazine and 10% ketamine for anesthesia. A total of 8 rats were included in the experiment and divided equally into 2 groups: a study group and a control group, with 4 rats assigned to each group. Gingival tissue and maxillary molars were disinfected using 2.5% hydrogen peroxide (LabChem, Zelienople, USA), and the mesial surface of the molars was additionally disinfected with 2.5% sodium hypochlorite (Clinix, London, UK). Cavities were prepared on the mesial surfaces of the first upper molars in all 8 rats, and the pulps were perforated with the aid of a No.1/2 round bur (Meisinger, Neuss, Germany). Working length (WL), i.e., the size of the exposed region, was equal to the diameter of the bur (0.6 mm), determined with paper points. The exposed region underwent a thorough rinsing procedure utilizing a solution comprising 0.5% sodium hypochlorite (Clinix) and 15% ethylenediaminetetraacetic acid (EDTA; Saver, Tekirdag, Turkey). In the study group, peptide amphiphiles (PAs) were applied to the dental pulp, and the cavities were sealed with a self-curing glass ionomer cement filling material (Riva Self Cure; SDI Ltd., Bayswater, Australia). In the control group, physiological saline (Deva, Istanbul, Turkey) was injected into the created defect area. Thirty days afer application, the rats were euthanized by employing a solution of 3% paraformaldehyde and 0.2%

glutaraldehyde. The teeth were subsequently extracted through surgical means and immersed in a 3% paraformaldehyde solution for 24 h. Subsequently, the tooth samples underwent demineralization using 10% EDTA and were sectioned with a Leica microtome (Leica Camera AG, Wetzlar, Germany) into 5-µm thick slices. The sections underwent deparaffinization using xylene, followed by rehydration through a sequence of ethanol solutions. Finally, the sections were stained with H&E. The slides were analyzed using the ImageJ software (National Institutes of Health (NIH), Bethesda, USA) at ×5 objective magnification to calculate the percentage of pink area in defined sites for each sample.

For Masson's trichrome staining, paraffin-embedded sections on slides were fixed in Bouin's solution, a fixative commonly used to preserve tissue morphology. The slides were then subjected to a series of staining steps to visualize specific tissue components. Initially, the slides were incubated in Weigert's iron hematoxylin solution, which selectively stained the nuclei of cells in a dark black color. Subsequently, the slides were exposed to Biebrich scarlet-acid fuchsin, resulting in the staining of collagen fibers in a vibrant red hue. Finally, aniline blue was applied to the slides, causing the collagen fibers to appear as a distinct blue color. Throughout the staining process, extensive washing steps were performed to ensure proper removal of excess dye and optimization of staining specificity. This staining protocol enabled the clear differentiation of collagen fibers (blue) from the cell nuclei (black). In addition to H&E staining, Masson's staining was performed to assess the presence of regenerative tissue sections within the pulp samples, providing valuable insights into the regenerative capacity of the treated tissues.

Statistical analyses

Statistical analyses were performed using IBM SPSS v. 24.0 (IBM Corp., Armonk, USA). The percentages of regeneration and mean color intensity of regenerated areas in rats of the study and control groups were analyzed statistically using the Mann–Whitney U test. A p-value of less than 0.05 was deemed to be statistically significant.

Results

In this study, GAG-PA and K-PA molecules were synthesized through solid-phase peptide synthesis to mimic sulfated GAGs and induce nanofiber formation. The GAG-PA was designed with functional groups such as sulfonate, hydroxyl and carboxylate to mimic GAGs. The K-PA, a positively charged molecule, was combined with GAG-PA to facilitate nanofiber formation through electrostatic interactions. The peptide amphiphiles that were synthesized underwent characterization through LC–MS analysis and subsequent purification using preparative HPLC. Scanning electron microscopy images revealed the formation of porous nanofiber networks when GAG-PA and K-PA were mixed. Circular dichroism spectrum analysis indicated a predominant β-sheet secondary structure in the self-assembled peptide amphiphile nanofibers. To assess the regeneration of tissue sections in the damaged pulp, H&E staining and Masson's trichrome staining were performed. The degree of tissue regeneration in the affected area was evaluated using these staining techniques (Fig. 3).

We carefully adhered to the requirement of providing the average baseline characteristics of the animals (e.g., age, weight, gender, microbiological status) at the beginning of the experiment. By diligently documenting these parameters, we ensured the transparency and validity of our research findings. The age and weight information allowed us to assess any potential age-related or weight-related effects on the outcomes of the experiment. We also recorded the gender of the animals to account for any gender-specific variations or influences. Furthermore, including the microbiological status provided crucial insights into the overall health and potential microbial factors that might impact the experimental results. All in all, our study respected and met the essential guideline of providing the average baseline characteristics of the animals, thereby contributing to the rigor and comprehensiveness of our research.

After 30 days, the implanted region demonstrated tissue regeneration that resembled pulp, characterized by the absence of noticeable neutrophil infiltration. The regeneration percentage in the damaged area was evaluated using H&E staining (Fig. 4). Additionally, Masson's trichrome staining confirmed the formation of reparative dentin (Fig. 5). These observations were made in both the study and control groups at the 30-day mark. However, statistical analysis revealed no significant difference between the 2 groups ($p > 0.05$). The statistical values and plots for the regenerated area and mean color intensity are provided in Table 1 and Fig. 6. Figure 6 presents the plots for the regenerated area and mean color intensity. Plot A displays the bar plots representing the mean regenerated area (%) for the serum and gel groups, with error bars indicating the standard deviation (SD) of the mean. In Plot B, a box-and-whisker plot shows the distribution of the regenerated area (%) for the serum and gel groups. For the serum group, the 1st quartile (Q1), the median and the 3rd quartile (Q3) were 85.86%. For the gel group, Q1 was 81.77%, the median was 92.10% and Q3 was 92.29%. Plot C features bar plots representing the mean color intensity (%) for the serum and gel groups, with error bars indicating the SD of the mean. Similarly, Plot D shows a box-and-whisker plot for the distribution of mean color intensity (%) for the serum and gel groups. For the serum group, Q1, the median and Q3 were 45.06%. For the gel group, Q1, the median, and Q3 were 61.42%, 68.04% and 74.65%, respectively.

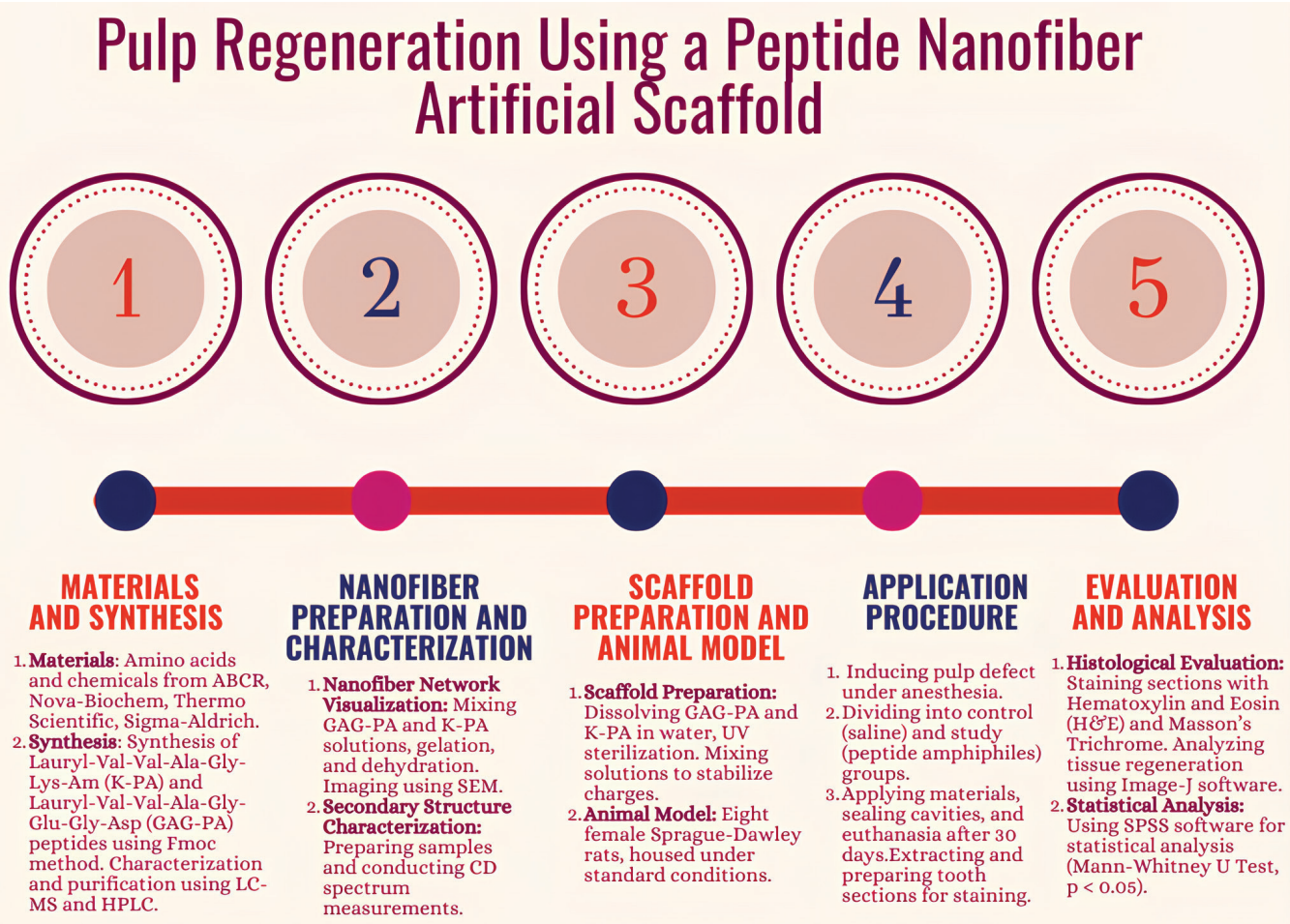

Fig. 3. Diagram of tissue regeneration evaluation after 30 days

GAG-PA – glycosaminoglycan mimetic peptide amphiphile; K-PA – positively charged peptide amphiphile; LC-MS – liquid chromatography–mass spectrometry; HPLC – high-performance liquid chromatography; SEM – scanning electron microscope; CD – circular dichroism; H&E – hematoxylin and eosin.

Discussion

In this research, dynamic nanostructures were produced by utilizing hydrogen bonding between peptide sequences and utilized in the field of dental pulp tissue engineering for pulpotomized rat molars. Over 30 days, the previously pulpotomized area of the pulp was successfully replenished with regenerated tissue, demonstrating an absence of inflammation. These findings strongly suggest that hydrogel scaffolds incorporating GAG-PA nanofibers play a significant role in promoting dental pulp regeneration.

In the present study, PA nanofibers were injected into the pulp tissue of rats, and regenerated tissue was observed in the pulpotomized region. Cordeiro et al.[33] conducted a study wherein dental pulp stem cells were seeded onto poly L-lactide acid (PLLA) scaffolds positioned within the pulp-chamber space of human tooth slices, which were subsequently implanted subcutaneously in mice. The resulting tissue exhibited a comparable architecture and cellularity to dental pulp tissue, although it did not fill the entire pulp space. Ito et al.[7] presented a protocol for in vivo pulp tissue engineering in pulpotomized rat teeth involving rat bone marrow mesenchymal stem cells (RBMMSCs), preformed biodegradable scaffolds and hydrogels. Consistent with our findings, the implantation of RBMMSCs, along with preformed scaffolds and hydrogels, resulted in pulp tissue regeneration within pulpotomized pulp chambers in rats.

Previous studies have shown that nanostructures consisting of certain peptides can be used for cell therapy.[34–38] For example, when the RGDS signal in fibronectin binds cells in a network formed by nanostructures, the cells can live in the artificial matrix.[39,40] This study was conducted in collaboration with the Ulusal Nanoteknoloji Araştırma Merkezi (UNAM)-National Nanotechnology Research Center (Ankara, Turkey), which synthesizes these nanostructures.

Inflammation of dental pulp tissue with the progression of dental caries causes severe pain, which can be relieved by root canal treatment. Teeth that have undergone root canal treatment cannot renew themselves, and their life is shortened. Therefore, problems related to the dental pulp are important for endodontists and pedodontists. Pulp regeneration to revive dentine-producing odontoblasts and produce new capillaries and nerve cells can be an effective alternative method for endodontic therapies.

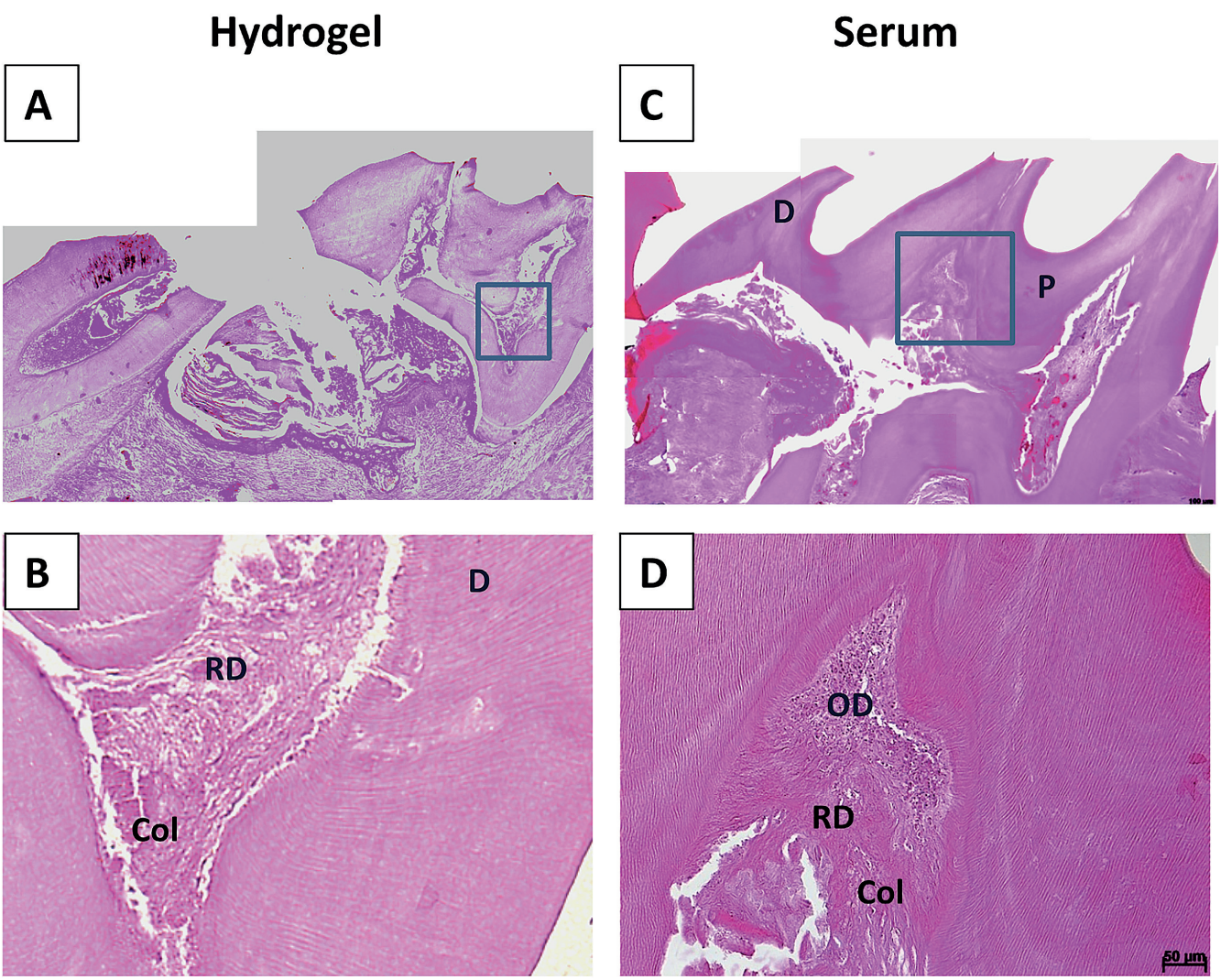

Fig. 4. Hematoxylin and eosin (H&E) staining. Hydrogel/serum was injected into the rat's molar tooth, and the rat was sacrificed after 4 weeks of injection. A,B. Hydrogel injection; C,D. Serum injection

D – dentin; P – pulp; DS – defect site; Col – collagen; RD – reparative dentin; OD – odontoblasts.

Within the scope of tissue engineering studies, dental pulp tissue production is of great importance in REP. We believe that the bioactive intercellular scaffold consisting of peptides generated in this study, when applied together with growth factors, may induce dental tissue formation in the region where it is applied.

In the literature, favorable outcomes of regenerative treatment procedures are frequently discussed. However, a systematic review conducted in 2022 revealed a lack of robust evidence supporting the effectiveness of regeneration procedures in necrotic immature teeth.[17] The development of a healthy dentin-pulp complex is not solely dependent on the survival of stem cells from the apical papilla (SCAPs). It also requires the presence of epithelial cells derived from Hertwig's epithelial root sheath (HERS) and their interaction with epithelial rests of Malassez (ERM). Hertwig's epithelial root sheath functions as a barrier between dental follicles and dental papilla cells, and it has regulatory properties that determine the shape, number and dimensions of roots.[6,41] Normal and healthy development of the dentin-pulp complex necessitates the survival of HERS, ERM and SCAP. Therefore, defining regeneration procedures is crucial. Additionally, in human and animal studies targeting endodontic regeneration, it is accepted that internal periodontal tissues regenerate more significantly than pulp tissue formation in root canals. This is attributed to the formation of bone-like tissue, periodontal ligament and cementum in place of dentin walls, as reported in histological examinations.[6,24]

To improve the effectiveness of biomaterials and regenerative drugs in cell therapy, it is necessary to support the vital activities of the cells in the early stages, and the biomaterial should later disappear through biological destruction, preventing the development of natural tissue.[42] The matrix consists of synthetic biomaterials and provides mechanical support to the cells and can carry proteins, biological signals, nutrients, and various genes, which increases its utility. In previous studies,

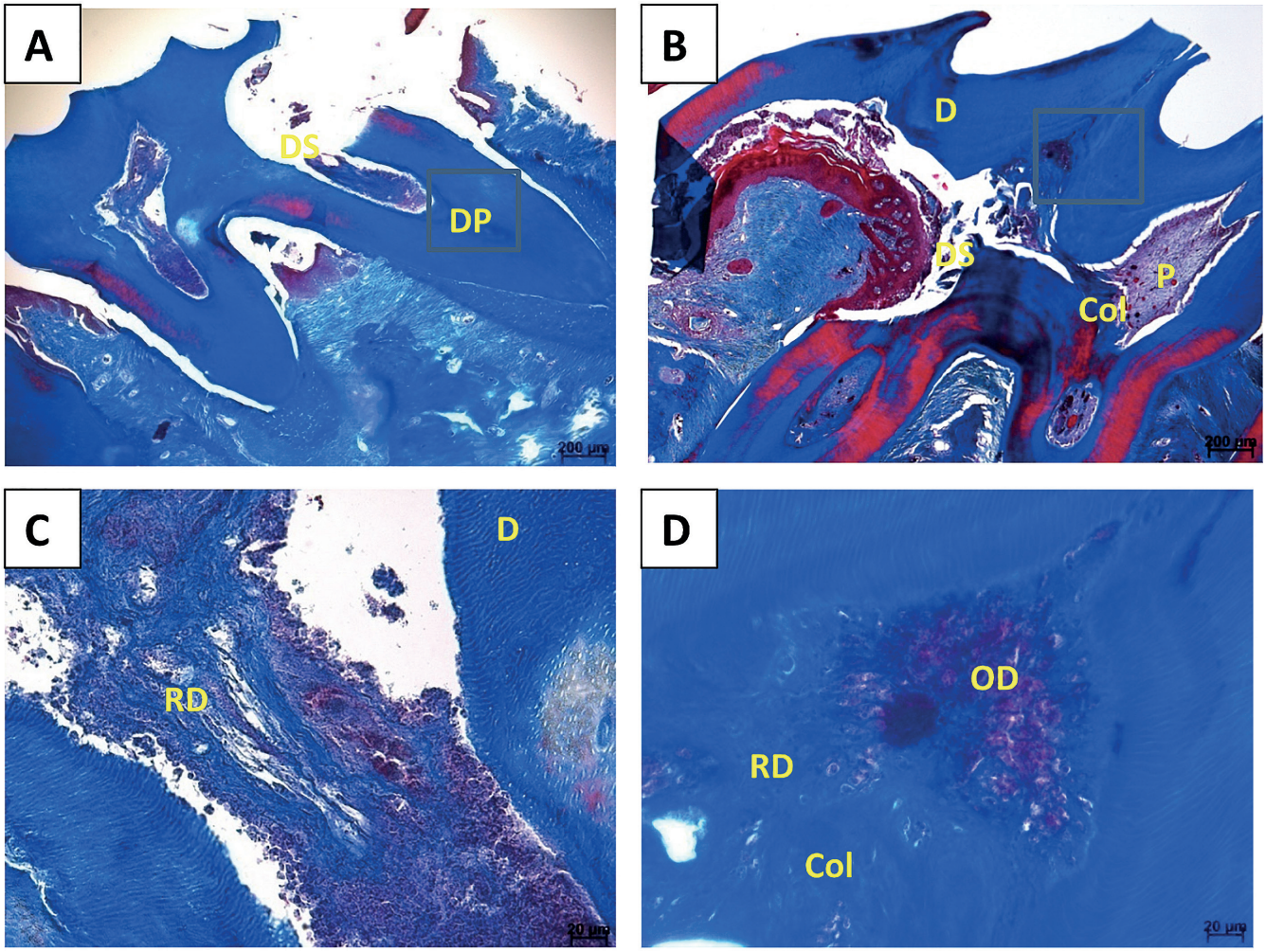

Fig. 5. Masson's trichrome staining. Hydrogel/serum was injected into the rat's molar tooth, and the rat was sacrificed after 4 weeks of injection. A,C. Collagen deposition and reparative dentin formation in the hydrogel group; B,D. Collagen organization and odontoblast alignment in the serum group

D – dentin; P – pulp; DP – damaged pulp; DS – defect site; Col – collagen; RD – reparative dentin; OD – odontoblasts.

the development of multipurpose biomaterials with some programmable collectible molecules made it possible for cells to survive outside their natural environment in bioactive matrices consisting of dynamic, natural and chemical intermediates.[43] Intense efforts are being made in the field of tissue engineering and regenerative medicine to develop materials that contain peptide signals and can form complex supramolecular nanostructures. Bioactive peptide sequences can be used to mimic the natural cell environment in the matrices of such molecules.[44]

Based on the results of our study, although no difference was observed between the control and study groups, we believe a significant difference could be observed with an increase in the number of samples. In addition, the regeneration without any inflammation in the samples in the study group was considered a success.

The biomechanical properties of dental pulp and scaffolds are integral considerations in advancing regenerative dentistry and dental tissue engineering. Dental pulp, situated within the pulp chamber, exhibits essential characteristics such as compressive strength, crucial for withstanding occlusal forces during biting and chewing, and elasticity, which enables it to act as a shock absorber, protecting the underlying tissues.[45] The vasculature within dental pulp contributes significantly to tissue vitality and regenerative potential. In parallel, the biomechanical properties of scaffolds play a pivotal role in dental tissue engineering. Scaffolds must offer structural integrity to support tissue regeneration, be biocompatible to facilitate cell interactions, and possess controlled degradation characteristics to align with the pace of tissue healing.[46] Additionally, the design of scaffolds should include appropriate porosity and permeability to allow for nutrient and oxygen diffusion, fostering cell ingrowth. Achieving a biomechanical match between scaffolds and native dental tissues is paramount for successful outcomes in regenerative dentistry applications, ensuring optimal support for tissue regeneration and functional restoration.[47]

The materials developed in this study can be examined for therapeutic potential in humans. The injectable structure of the scaffold may be used for treating dental problems. Thus, further studies are needed for the development

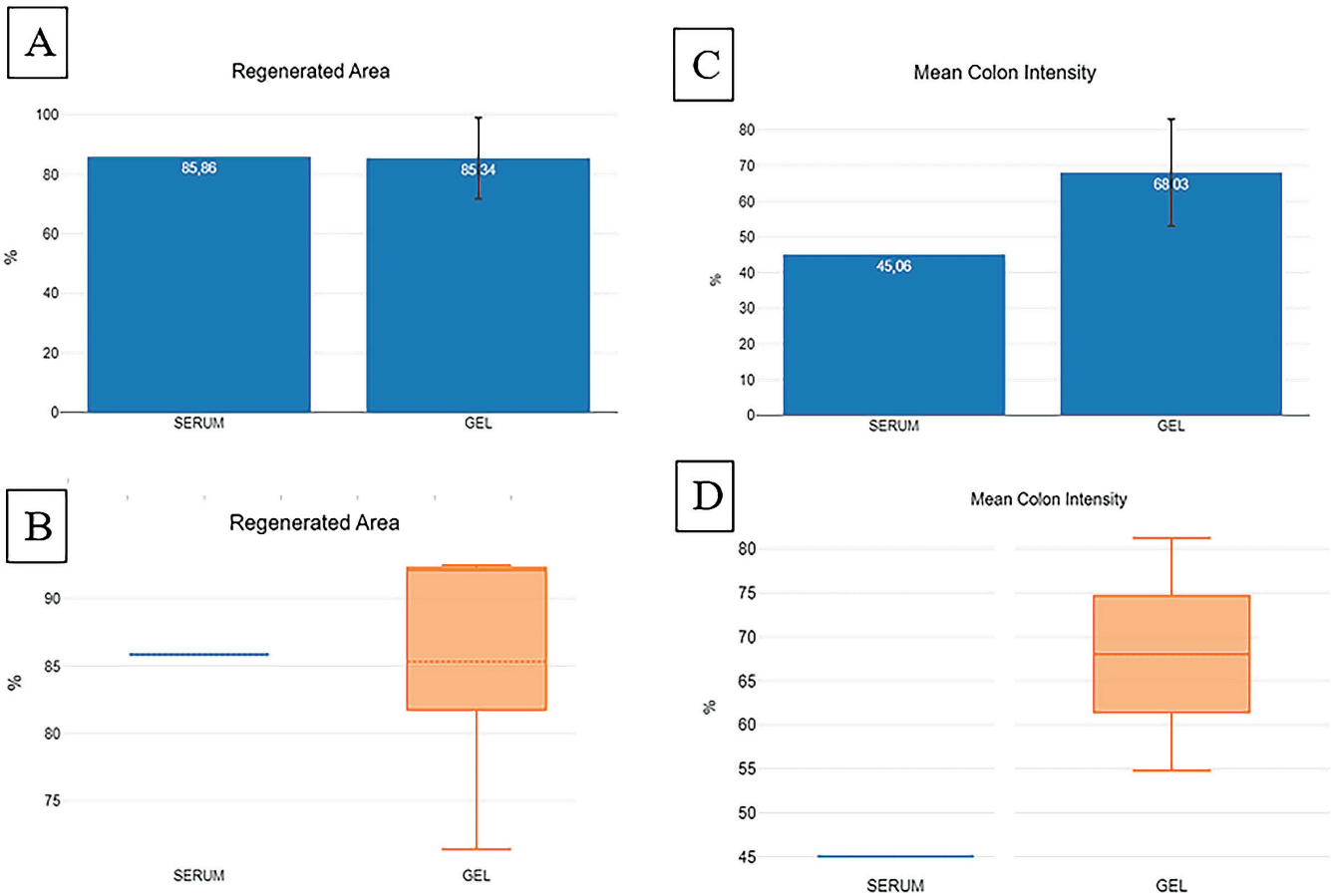

Fig. 6. Plots for the regenerated area and mean color intensity. The box represents the interquartile range (Q1 to Q3), the line inside the box indicates the median, and the whiskers extend to the minimum and maximum values excluding outliers. A. Bar plot representing the mean regenerated area (%) for serum and gel groups, with error bars indicating standard deviation (SD); B. Box-and-whisker plot showing the distribution of regenerated area (%) for serum and gel groups; C. Bar plot for mean color intensity (%) with error bars indicating SD; D. Box-and-whisker plot depicting the distribution of mean color intensity (%) for serum and gel groups, detailing interquartile range (IQR), median, and outlier data points

and production of biomaterials that have the characteristics of controlled aggregation, the transmission of biological signals to cells, imitation of the natural cell environment, and synergistic effects with biological factors.

Several studies have emphasized the benefits of using animal models in REP. Animal models allow for controlled experiments, providing insights into biological processes and potential therapeutic outcomes. For example, a study by Nakashima et al.[43] highlighted the ability of an animal model to accurately simulate pulpal regeneration and evaluate the effectiveness of novel biomaterials. However, it is crucial to acknowledge the limitations associated with animal models. Variability in anatomy, physiology and immune responses can exist between animals and humans, affecting the translatability of findings. Previous studies, such as Piglionico et al.,[44] have emphasized the importance of considering these differences when interpreting results from animal studies and applying them to human REP.

Dental pulp regeneration is a dynamic process involving the proliferation and differentiation of various cell types, along with the deposition of extracellular matrix components such as dentin. The 30-day experimental duration captured critical early events in the regenerative process, including the inflammatory response, cell migration and initial matrix deposition.[45] This timeframe strikes a balance between obtaining meaningful data on the effectiveness of GAG-PA nanofibers in guiding pulp regeneration and minimizing potential ethical concerns related to prolonged experimental periods for laboratory animals. While the study successfully observed reparative dentin formation, the acknowledgment of a lack of statistically significant differences between the study and control groups suggests that a longer observation period or an increased number of animals may be necessary to capture more advanced stages of regeneration and detect significant treatment effects. The researchers chose a 30-day duration as an initial exploration, recognizing the potential for further investigations with refined methodologies and extended timelines to elucidate the full scope of the regenerative outcomes.

In this study, rat teeth were used due to their similarities to human teeth in terms of size, structure and biological properties. These similarities make rat teeth a valuable model for studying the efficacy and safety of biomaterials in REP. Also, rats are commonly used in scientific research due to their abundance, ease of breeding and short reproductive cycle. Additionally, ethical considerations

come into play, as using rats as an alternative to human teeth helps minimize potential harm and discomfort to human subjects. Conducting experiments on rat teeth is relatively cost-effective and practical compared to using human teeth. Rat teeth can be obtained at a lower cost and in larger quantities, allowing for more extensive experimentation and analysis. Ethical guidelines and regulations often require initial testing on animals before moving to human trials. By using rat teeth, researchers can comply with these regulations and gather essential preliminary data before considering human clinical trials.

To apply the results of this manuscript to humans, further studies should be conducted on larger animal models that more closely resemble human dental anatomy and physiology. While the current study utilized rats, which are a common choice for initial investigations due to their ease of handling and cost-effectiveness, translating these findings to the human context requires studies on larger animals with dental structures more akin to humans. Animal models such as non-human primates are often preferred for dental research because they share similarities in tooth structure, size and dental pulp characteristics with humans. Conducting studies on these larger animals would provide a more representative evaluation of the effectiveness of GAG-PA nanofibers in guiding pulp regeneration, helping to bridge the gap between preclinical experiments and potential human applications. Additionally, increasing the sample size and diversity in animal models can contribute to a more robust statistical analysis, addressing the observed limitations in the current study and enhancing the reliability of the results for potential clinical relevance in humans.

The clinical or radiographic outcomes of REP remain somewhat unpredictable. However, in vivo studies of scaffolds lead to clinical studies.[20,25,41] The findings of our study will inform future research, which will aim to identify the relative efficacy of different scaffolds. Various materials that will provide different functionalities to scaffolds continue to be produced. Examples include antimicrobial peptides (AMPs) such as LL37 peptides and various nanoscale scaffolds.[46,48] However, AMPs have limited therapeutic effects due to their short residence time in the circulatory system and their sensitivity to proteases. These limitations are major obstacles to the success of AMPs.[46,47] In contrast, nanoscale scaffolds, hydrogels and various scaffolds can be added to AMP-based materials to increase the therapeutic efficacy of the material.[48] It is possible that nanoscale scaffolds and antimicrobial proteins such as LL37 peptides may explain their activity on regeneration. Further pioneering studies similar to our study are needed to elucidate this issue.

Limitations

Our study encountered certain limitations, including the utilization of rat teeth instead of human teeth and the relatively small sample size. Animal models serve as indispensable tools for researchers to attain a comprehensive understanding of diseases, advance the development of effective treatments and explore innovative ideas, concepts and technologies. These animal models play a vital role in conferring scientific validity to their investigations. When evaluating various therapeutic approaches in the domain of REP, reliable animal models simulating pulpal defects assume significant importance. While the structural and compositional differences between rat incisors and human teeth are considerable, the similarities in structural characteristics, such as the pulp chamber, pulp tissue, root, and apical delta with minor apical foramen, make rat and human molars more comparable. Furthermore, the use of rats in REP research proves advantageous due to the lower costs and efforts associated with housing, feeding, and care compared to larger animals. Additionally, most of the antibodies necessary for cellular and molecular biological techniques are specifically available for rats.

Conclusions

In this study, reparative dentin formation was observed in both groups, but without a significant difference between the groups. To obtain a significant difference, the number of animals used must be increased. Moreover, the PA-based nanomaterials used in this study were non-toxic to the dental tissue and were digested by the enzyme in dental tissue over time. Bioactive signals were presented to the sensing proteins effectively and functionally using the wide reaction surface features of the nanostructures. Our findings indicate that these biomaterials can be used to produce molecules for application in the regeneration of dental tissue and dental pulp, thus leading to improved quality of human life.

Data availability

The datasets generated and/or analyzed during the current study are available from the corresponding author on reasonable request.

Consent for publication

Not applicable.

ORCID iDs

Ozlem Marti Akgun https://orcid.org/0000-0003-1180-1391
Ayse Begum Tekinay https://orcid.org/0000-0002-4453-814X
Gulistan Tansık https://orcid.org/0000-0003-2867-7286
Ceren Yıldırım https://orcid.org/0000-0002-8360-6926
Gunseli Guven Polat https://orcid.org/0000-0003-1228-1260

References

1. Cooper PR, Chicca IJ, Holder MJ, Milward MR. Inflammation and regeneration in the dentin-pulp complex: Net gain or net loss? *J Endod*. 2017;43(Suppl 9):S87–S94. doi:10.1016/j.joen.2017.06.011

2. Xue D, Gong Z, Zhu F, Qiu Y, Li X. Simvastatin increases cell viability and suppresses the expression of cytokines and vascular endothelial growth factorin inflamed human dental pulp stem cells in vitro. *Adv Clin Exp Med*. 2018;27(12):1615–1623. doi:10.17219/acem/75776
3. Barthel C, Rosenkranz B, Leuenberg A, Roulet J. Pulp capping of carious exposures: Treatment outcome after 5 and 10 years. A retrospective study. *J Endod*. 2000;26(9):525–528. doi:10.1097/00004770-200009000-00010
4. Galler KM, Krastl G, Simon S, et al. European Society of Endodontology position statement: Revitalization procedures. *Int Endodontic J*. 2016;49(8):717–723. doi:10.1111/iej.12629
5. American Association of Endodontists (AAE). Considerations for Regenerative Procedures (Revised January 4, 2018) . Chicago, USA: American Association of Endodontists (AAE); 2018. https://www.aae.org/specialty/clinical-resources/guide-clinical-endodontics. Accessed October 15, 2023.
6. Palma PJ, Martins J, Diogo P, et al. Does apical papilla survive and develop in apical periodontitis presence after regenerative endodontic procedures? *Appl Sci*. 2019;9(19):3942. doi:10.3390/app9193942
7. Ito T, Kaneko T, Sueyama Y, Kaneko R, Okiji T. Dental pulp tissue engineering of pulpotomized rat molars with bone marrow mesenchymal stem cells. *Odontology*. 2017;105(4):392–397. doi:10.1007/s10266-016-0283-0
8. Chen FM, Liu X. Advancing biomaterials of human origin for tissue engineering. *Prog Polym Sci*. 2016;53:86–168. doi:10.1016/j.progpolymsci.2015.02.004
9. Dzobo K, Thomford NE, Senthebane DA, et al. Advances in regenerative medicine and tissue engineering: Innovation and transformation of medicine. *Stem Cells Int*. 2018;2018:2495848. doi:10.1155/2018/2495848
10. Luo Y. Three-dimensional scaffolds. In:Lanza R, Vacanti JP, Langer R, Atala A, eds. *Principles of Tissue Engineering*. 5th ed. Cambridge, USA: Academic Press; 2020:343–360. doi:10.1016/B978-0-12-818422-6.00020-4
11. Henke M, Tessmar J, Göpferich A. Biomimetic polymers (for biomedical applications). In: Moeller M, Matyjaszewski K, eds.*Polymer Science: A Comprehensive Reference*. Amsterdam, the Netherlands–New York, USA: Elsevier; 2012:339–361. doi:10.1016/B978-0-444-53349-4.00222-3
12. Al-Shalawi FD, Mohamed Ariff AH, Jung DW, et al. Biomaterials as implants in the orthopedic field for regenerative medicine: Metal versus synthetic polymers. *Polymers (Basel)*. 2023;15(12):2601. doi:10.3390/polym15122601
13. Shoulders MD, Raines RT. Collagen structure and stability. *Annu Rev Biochem*. 2009;78(1):929–958. doi:10.1146/annurev.biochem.77.032207.120833
14. Hosoyama K, Lazurko C, Muñoz M, McTiernan CD, Alarcon EI. Peptide-based functional biomaterials for soft-tissue repair. *Front Bioeng Biotechnol*. 2019;7:205. doi:10.3389/fbioe.2019.00205
15. Ortega-Velázquez R, Ez-Marqués MLD, Ruiz-Torres MP, González-Rubio M, Rodrí Guez-Puyol M, Rodrí Guez Puyol D. Arg-Gly-Asp-Ser peptide stimulates transforming growth factor-β1 transcription and secretion through integrin activation. *FASEB J*. 2003;17(11):1529–1531. doi:10.1096/fj.02-0785fje
16. Klimek K, Ginalska G. Proteins and peptides as important modifiers of the polymer scaffolds for tissue engineering applications: A review. *Polymers (Basel)*. 2020;12(4):844. doi:10.3390/polym12040844
17. Suamte L, Tirkey A, Barman J, Jayasekhar Babu P. Various manufacturing methods and ideal properties of scaffolds for tissue engineering applications. *Smart Mater Manufact*. 2023;1:100011. doi:10.1016/j.smmf.2022.100011
18. Vivanco J, Aiyangar A, Araneda A, Ploeg HL. Mechanical characterization of injection-molded macro porous bioceramic bone scaffolds. *J Mech Behav Biomed Mater*. 2012;9:137–152. doi:10.1016/j.jmbbm.2012.02.003
19. Shafiee A, Ahmadi H, Taheri B, et al. Appropriate scaffold selection for CNS tissue engineering. *Avicenna J Med Biotechnol*. 2020;12(4):203–220. PMID:33014312. PMCID:PMC7502166.
20. Thibodeau B, Teixeira F, Yamauchi M, Caplan DJ, Trope M. Pulp revascularization of immature dog teeth with apical periodontitis. *J Endod*. 2007;33(6):680–689. doi:10.1016/j.joen.2007.03.001
21. Zhu X, Zhang C, Huang GTJ, Cheung GSP, Dissanayaka WL, Zhu W. Transplantation of dental pulp stem cells and platelet-rich plasma for pulp regeneration. *J Endod*. 2012;38(12):1604–1609. doi:10.1016/j.joen.2012.09.001
22. Wang Y, Zhao Y, Jia W, Yang J, Ge L. Preliminary study on dental pulp stem cell-mediated pulp regeneration in canine immature permanent teeth. *J Endod*. 2013;39(2):195–201. doi:10.1016/j.joen.2012.10.002
23. Yamauchi N, Nagaoka H, Yamauchi S, Teixeira FB, Miguez P, Yamauchi M. Immunohistological characterization of newly formed tissues after regenerative procedure in immature dog teeth. *J Endod*. 2011;37(12):1636–1641. doi:10.1016/j.joen.2011.08.025
24. Palma PJ, Ramos JC, Martins JB, et al. Histologic evaluation of regenerative endodontic procedures with the use of chitosan scaffolds in immature dog teeth with apical periodontitis. *J Endod*. 2017;43(8):1279–1287. doi:10.1016/j.joen.2017.03.005
25. Coimbra P, Alves P, Valente TAM, Santos R, Correia IJ, Ferreira P. Sodium hyaluronate/chitosan polyelectrolyte complex scaffolds for dental pulp regeneration: Synthesis and characterization. *Int J Biol Macromol*. 2011;49(4):573–579. doi:10.1016/j.ijbiomac.2011.06.011
26. Demarco FF, Conde MCM, Cavalcanti BN, Casagrande L, Sakai VT, Nör JE. Dental pulp tissue engineering. *Braz Dent J*. 2011;22(1):3–13. doi:10.1590/S0103-64402011000100001
27. Zhang W, Yelick PC. Vital pulp therapy: Current progress of dental pulp regeneration and revascularization. *Int J Dent*. 2010;2010:856087. doi:10.1155/2010/856087
28. Choi K, Oshida Y, Platt JA, Cochran MA, Matis BA, Yi K. Microtensile bond strength of glass ionomer cements to artificially created carious dentin. *Oper Dent*. 2006;31(5):590–597. doi:10.2341/05-108
29. Murray PE, Garcia-Godoy F, Hargreaves KM. Regenerative endodontics: A review of current status and a call for action. *J Endod*. 2007;33(4):377–390. doi:10.1016/j.joen.2006.09.013
30. Nahsan FPS, Mondelli RFL, Franco EB, et al. Clinical strategies for esthetic excellence in anterior tooth restorations: Understanding color and composite resin selection. *J Appl Oral Sci*. 2012;20(2):151–156. doi:10.1590/S1678-77572012000200005
31. Dohan DM, Choukroun J, Diss A, et al. Platelet-rich fibrin (PRF): A second-generation platelet concentrate. Part II: Platelet-related biologic features. *Oral Surg Oral Med Oral Pathol Oral Radiol Endodontol*. 2006;101(3):e45–e50. doi:10.1016/j.tripleo.2005.07.009
32. Tansik G, Kilic E, Beter M, et al. A glycosaminoglycan mimetic peptide nanofiber gel as an osteoinductive scaffold. *Biomater Sci*. 2016;4(9):1328–1339. doi:10.1039/C6BM00179C
33. Cordeiro MM, Dong Z, Kaneko T, et al. Dental pulp tissue engineering with stem cells from exfoliated deciduous teeth. *J Endod*. 2008;34(8):962–969. doi:10.1016/j.joen.2008.04.009
34. Gessner I, Neundorf I. Nanoparticles modified with cell-penetrating peptides: Conjugation mechanisms, physicochemical properties, and application in cancer diagnosis and therapy. *Int J Mol Sci*. 2020;21(7):2536. doi:10.3390/ijms21072536
35. Habibi N, Kamaly N, Memic A, Shafiee H. Self-assembled peptide-based nanostructures: Smart nanomaterials toward targeted drug delivery. *Nano Today*. 2016;11(1):41–60. doi:10.1016/j.nantod.2016.02.004
36. Perán M, García MA, López-Ruiz E, et al. Functionalized nanostructures with application in regenerative medicine. *Int J Mol Sci*. 2012;13(3):3847–3886. doi:10.3390/ijms13033847
37. Yasa IC, Gunduz N, Kilinc M, Guler MO, Tekinay AB. Basal lamina mimetic nanofibrous peptide networks for skeletal myogenesis. *Sci Rep*. 2015;5(1):16460. doi:10.1038/srep16460
38. Dolatshahi-Pirouz A, Jensen T, Kraft DC, et al. Fibronectin adsorption, cell adhesion, and proliferation on nanostructured tantalum surfaces. *ACS Nano*. 2010;4(5):2874–2882. doi:10.1021/nn9017872
39. Bhat S, Kumar A. Biomaterials in regenerative medicine. *J Postgrad Med Educ Res*. 2012;46(2):81–89. doi:10.5005/jp-journals-10028-1018
40. Ahmed S, Chauhan VM, Ghaemmaghami AM, Aylott JW. New generation of bioreactors that advance extracellular matrix modelling and tissue engineering. *Biotechnol Lett*. 2019;41(1):1–25. doi:10.1007/s10529-018-2611-7
41. Xiong J, Mrozik K, Gronthos S, Bartold PM. Epithelial cell rests of malassez contain unique stem cell populations capable of undergoing epithelial–mesenchymal transition. *Stem Cells Dev*. 2012;21(11):2012–2025. doi:10.1089/scd.2011.0471
42. Arslan E, Garip IC, Gulseren G, Tekinay AB, Guler MO. Bioactive supramolecular peptide nanofibers for regenerative medicine. *Adv Healthc Mater*. 2014;3(9):1357–1376. doi:10.1002/adhm.201300491

43. Nakashima M, Iohara K, Bottino MC, Fouad AF, Nör JE, Huang GTJ. Animal models for stem cell-based pulp regeneration: Foundation for human clinical applications. *Tissue Eng Part B Rev*. 2019;25(2): 100–113. doi:10.1089/ten.teb.2018.0194
44. Piglionico SS, Pons C, Romieu O, Cuisinier F, Levallois B, Panayotov IV. In vitro, ex vivo, and in vivo models for dental pulp regeneration. *J Mater Sci Mater Med*. 2023;34(4):15. doi:10.1007/s10856-023-06718-2
45. Yu C, Abbott P. An overview of the dental pulp: Its functions and responses to injury. *Aust Dent J*. 2007;52(1 Suppl):S4–S16. doi:10.1111/j.1834-7819.2007.tb00525.x
46. Rai A, Ferrão R, Palma P, et al. Antimicrobial peptide-based materials: Opportunities and challenges. *J Mater Chem B*. 2022;10(14):2384–2429. doi:10.1039/D1TB02617H
47. Comune M, Rai A, Palma P, TondaTuro C, Ferreira L. Antimicrobial and pro-angiogenic properties of soluble and nanoparticle-immobilized LL37 peptides. *Biomater Sci*. 2021;9(24):8153–8159. doi:10.1039/D1BM01034D
48. Diogo P, Amparo F. Faustino M, Palma PJ, Rai A, Graça Neves M, Miguel Santos J. May carriers at nanoscale improve the endodontic's future? *Adv Drug Deliv Rev*. 2023;195:114731. doi:10.1016/j.addr.2023.114731

Effectiveness of gua sha with Masanggoubang oil in rats with chronic soft tissue injury

Min Zhu[1,A,C,D], Dong Zhao[2,B], Chunxia Lu[3,B], Jin Cui[2,3,E,F]

[1] Acupuncture and Tuina College, Chengdu University of Traditional Chinese Medicine, China
[2] Acupuncture and Tuina College, Guizhou University of Traditional Chinese Medicine, Guiyang, China
[3] Department of Acupuncture-Moxibustion, First Affiliated Hospital of Guizhou University of Traditional Chinese Medicine, Guiyang, China

A – research concept and design; B – collection and/or assembly of data; C – data analysis and interpretation;
D – writing the article; E – critical revision of the article; F – final approval of the article

Advances in Clinical and Experimental Medicine, ISSN 1899–5276 (print), ISSN 2451–2680 (online) *Adv Clin Exp Med*. 2025;34(3):421–432

Address for correspondence
Jin Cui
E-mail: 516260179@qq.com

Funding sources
This study was supported by the Miao Medical Collaborative Innovation Research Center of Guizhou Province (grant No. QJK-2022-024) and the Guizhou Provincial Administration of Traditional Chinese Medicine (grant No. QZYY-2023-051). The funding bodies had no influence on the design of the study, data collection, analysis, interpretation, or manuscript writing.

Conflict of interest
None declared

Received on October 12, 2023
Reviewed on November 18, 2023
Accepted on April 5, 2024

Published online on January 27, 2025

Cite as
Zhu M, Zhao D, Lu C, Cui J. Effectiveness of gua sha with Masanggoubang oil in rats with chronic soft tissue injury. *Adv Clin Exp Med*. 2025;34(3):421–432. doi:10.17219/acem/186865

DOI
10.17219/acem/186865

Abstract

Background. Chronic soft tissue injury is characterized by sterile inflammation and pain. Gua sha with Masanggoubang oil (GSMO) treatment has been found to possess anti-inflammatory and analgesic effects.

Objectives. To explore the mechanism of GSMO in chronic soft tissue injuries.

Materials and methods. Fifty male rats were randomly divided into 5 groups (n = 10): 1) control group; 2) chronic soft tissue injury model group; 3) GSMO group; 4) inunction with Masanggoubang oil (IMO) group; and 5) ua sha with tea oil (GSTO) group. The control group and model group received no treatment, while the GSTO group and GSMO group received gua sha therapy with tea oil or Masanggoubang oil on the injured sites. The rats in the IMO group were treated with Masanggoubang oil inunction on the injured sites once every other day, 4 times in total. All animals were sacrificed 48 h after the last treatment. Muscle tissue sections from the injured sites of the rats were stained with hematoxylin & eosin (H&E) staining to observe pathological changes. The protein levels of tumor necrosis factor alpha (TNF-α), interleukin 1β (IL-1β), interleukin 6 (IL-6), inducible nitric oxide synthase (iNOS), and β-endorphin (β-EP) in the rats' skin, serum, and muscle were determined using enzyme-linked immunosorbent assay (ELISA).

Results. Gua sha with Masanggoubang oil treatment alleviated necrosis and the denaturation of muscle fibers at the injured sites, reduced connective tissue proliferation and scar tissue generation, downregulated the levels of TNF-α, IL-6 and iNOS in the skin and TNF-α, IL-1β, IL-6, and iNOS in the muscle and serum, and upregulated β-EP levels in the muscle.

Conclusions. Gua sha with Masanggoubang oil treatment significantly improved the inflammatory response in rats with chronic soft tissue injury, which may be associated with a reduction of M1 macrophage polarization in the peripheral blood and local tissues. Additionally, the combination of gua sha therapy and Masanggoubang oil may have a synergistic effect in treating chronic soft tissue injuries.

Key words: gua sha with Masanggoubang oil, chronic soft tissue injury, M1 macrophage polarization, TNF-α, β-EP

Background

Chronic soft tissue injuries involve microcirculatory disorders and sterile inflammation caused by prolonged chronic stress, characterized by swelling, pain, limb dysfunction, and even disability in severe cases. The incidence reaches approx. 90% in adults,[1] severely impacting the patient's physical and mental health as well as their quality of life.[2] Due to its high incidence and difficulty in eradication, it is listed among the top 3 most challenging diseases by the World Health Organization (WHO).[3] The mechanisms of pain and limb dysfunction in chronic soft tissue injuries remain unclear, but modern medicine associates it with local microcirculatory disorders, compression of nerve endings and inflammatory responses.[4] Recently, there has been a notable surge in attention to M1 macrophage polarization concerning the inflammatory mechanisms of soft tissue injuries.[5,6] M1 macrophages stimulate the inflammatory response through the release of pro-inflammatory cytokines, including interleukin 6 (IL-6), interleukin 1β (IL-1β), tumor necrosis factor alpha (TNF-α), and inducible nitric oxide synthase (iNOS). This process heightens the sensitivity of the peripheral and central nervous systems, ultimately leading to hyperalgesia.[7,8] Tumor necrosis factor alpha plays a pivotal role as an inflammatory mediator, instigating the release of a cascade of other pro-inflammatory cytokines, such as IL-1β and IL-6.[9] The expression level of iNOS in skeletal muscles correlates with the magnitude of inflammatory damage.[10] Beta-endorphin (β-EP), an endogenous opioid peptide secreted by immune cells and exhibiting characteristic opioid-like effects, acts on opioid receptors in primary afferent neurons, obstructing pain transmission and eliciting an analgesic effect.[11] Previous studies have identified potential correlations between levels of TNF-α, IL-6, IL-1β, iNOS, and β-EP and soft tissue injuries.[11–13] Traditional Western medical approaches to chronic soft tissue injuries commonly involve a prescription for nonsteroidal anti-inflammatory drugs. Nevertheless, this therapeutic approach manifests obvious adverse effects, including hepatorenal damage and gastrointestinal reactions, while failing to impede the progression of the disease.

In traditional Chinese medicine (TCM), chronic soft tissue injuries are considered tendon and muscle injuries resulting from qi (circulating life force) stagnation, blood stasis, and an obstruction of meridians (paths through which qi flows). The therapeutic strategy is directed towards alleviating pain by promoting blood circulation, resolving blood stasis and improving qi flow. Gua sha, a TCM therapeutic modality extensively applied in Asia, demonstrates notable efficacy in the management of chronic pain. Its mechanism involves the stimulation of acupuncture points (acupoints) and meridians based on the meridians and acupoints theory. In the course of gua sha therapy, a tool such as a buffalo horn or coin is used to scrape the body's surface, often in conjunction with massage oil or water. This intentional scraping of the skin produces sha (therapeutic petechiae), engendering new biological effects. Gua sha functions to stimulate meridians, promote blood circulation, remove blood stasis, balance yin and yang (complementary and at the same time opposing forces that interact to form a dynamic system), and regulate the intestines.[14] From an anatomical perspective, yin and yang are linked to various anatomical regions of the body. Specifically, yin is linked to the inferior portions of the body, including the pelvis and lower extremities, while yang is associated with the superior regions of the body, such as the upper extremities, head and neck, and the back. A previous study proposed that gua sha demonstrates its effects in stimulating cutaneous telangiectasia, activating the serotonergic, noradrenergic and opioid systems,[15] elevating 5-hydroxytryptamine, mast cells, $CD4^+$, $CD8^+$, and IL-6 levels in local skin tissues, and reducing IL-1, prostaglandin E2 and phospholipase A2 expression. These mechanisms collectively contribute to pain relief,[16–20] toxin elimination, heightened antioxidant activity, and upregulated immune functions involved in regulating the circulatory, nervous, immune, and other systems, notably the musculoskeletal system.[21,22]

Gua sha with Masanggoubang oil (GSMO) is a characteristic external therapeutic technique within Chinese Miao medicine (a branch of TCM practiced by Miao ethnic group in China). This scraping medium is produced by blending Masanggoubang, a Miao herb derived from the root of *Astilbe chinensis*, with tea oil. Researchers have shown that Masanggoubang contains flavonoids, with *Astilbe* being the main component. These flavonoids exhibit anti-inflammatory, analgesic, circulatory, and decongestant properties.[23,24] A study has confirmed that *Astilbe* mediates anti-inflammatory functions by downregulating the expression of proteins such as nitric oxide (NO), prostaglandin E2, iNOS, and cyclooxygenase-2, along with modulating the mRNA expression of IL-6 and TNF-α through its impact on the NF-κB pathway.[25] Furthermore, studies published in 2020 have demonstrated that oral administration of *Astilbe* improved inflammation and slowed down the progression of osteoarthritis in rats by regulating the NF-κB, PI3K/AKT and TLR4/MD-2 pathways.[26–28] Similarly, the external application of Masanggoubang has been found to improve clinical symptoms and enhance the quality of life in patients with knee osteoarthritis and rheumatic arthritis.[29,30] Huang and Xia[31] discovered that GSMO mitigated limitations in shoulder joint activity and deltoid muscle atrophy in patients recovering from cervical spine surgery. Another randomized, multicenter, parallel-controlled clinical trial published in 2017 found that GSMO not only alleviated neck and shoulder pain but also improved symptoms of upper limb numbness in patients with cervical spondylotic radiculopathy. Moreover, the efficacy of this intervention was observed to surpass that of gua sha with tea oil (GSTO).[32] Furthermore, an independent

study in 2018 substantiated the differences in clinical effectiveness in patients with chronic soft tissue injuries when employing scraping with varying concentrations of Masanggoubang oil. This study shed light on the impact of the scraping medium on clinical outcomes.[33] Additionally, another study has reported that the external application of Masanggoubang oil does not cause skin irritation or allergic reactions.[34] This finding further reinforces the evidence of its efficacy and safety. However, the precise mechanisms underlying its action on chronic soft tissue injuries remain undetermined. Therefore, the objective of this study was to elucidate the effect and mechanism of GSMO therapy on chronic soft tissue injuries, ultimately aiming to advance its clinical application.

Objectives

Generally, chronic soft tissue injuries correlate with elevated levels of IL-1β, IL-6, TNF-α, and iNOS. Both gua sha and Masanggoubang have demonstrated anti-inflammatory and analgesic effects. Consequently, we hypothesized that GSMO therapy holds the potential to mitigate chronic soft tissue injury by regulating the expression of inflammatory and pain-related cytokines. To investigate this, this study aimed to identify the potential mechanism of GSMO in rats with chronic soft tissue injuries by evaluating the expression levels of TNF-α, IL-1β, IL-6, iNOS, and β-EP in skin, muscle and serum samples, along with a meticulous examination of histopathological changes in skin and muscle tissues.

Materials and methods

Animals

Fifty male Sprague Dawley rats, 8 weeks old and weighing 280 ±10 g, were included in this study. The rats were housed under standard laboratory conditions, with a temperature maintained at 22 ±2°C and humidity ranging from 50% to 60%. A 12-h light/dark cycle was followed, and the rats were given unrestricted access to a standard diet (18% protein, 4% fat, 5% crude fiber, 7.6% amino acids, etc.) and water. All animal experiments followed the guidelines of the Ethics Committee for Animal Experiments of the Guizhou University of Traditional Chinese Medicine (Guiyang, China) (approval No. 20160003).

Chemicals, drugs, and instruments

High-dose Masanggoubang oil (Masanggoubang/tea oil: 1.54 g/mL, homemade),[33] urethane (Sinopharm Chemical Reagent Co., Ltd., Beijing, China), tea oil (Guizhou Malinghe Plant Oil Co., Ltd., Xingyi, China), a scraping board (Suzhou Medical Products Co., Ltd., Suzhou, China), distilled water, formalin solution (Shenzhen Xigene Biotechnology Co., Ltd., Shenzhen, China), paraffin (Sinopharm Chemical Reagent Co., Ltd., Beijing, China), hematoxylin & eosin (H&E) staining kits, and 8% sodium sulfide hair remover (Guizhou Weiboxin Biotechnology Co., Ltd., Guiyang, China) were used in the experiments. Interleukin 1 beta, IL-6, TNF-α, iNOS, and β-EP enzyme-linked immunosorbent assay (ELISA) kits were purchased from Wuhan Huamei Biospes Co. (Wuhan, China). Scales; a homemade fixator, syringes, latex gloves, a centrifuge, a homogenizer, a slicer, an oven, and a computerized image acquisition and analysis system (Olympus DP70 (Olympus Corp., Tokyo, Japan) photographic system and Olympus BX51 microscope (Olympus Corp.) were also used in the experiments.

Modelling

Following a 1-week adaptation phase, a cohort of 50 rats was selected and divided into 5 different groups using the random number table method. Each group consisted of 10 rats and was designated as the control group, the model group, the GSMO group, the GSTO group, and the inunction with Masanggoubang oil (IMO) group. In the model group, the rats' right hind thigh underwent initial hair removal, followed by mechanical modeling as per the methodology established by Kami et al.,[35] which involves positioning the rats' right hind limb in knee extension with the ankle maintained at 90° of dorsiflexion. Subsequently, trauma was induced by dropping a weight (335 g) on the gastrocnemius muscle from a height of 80 cm. The weight carried 1.57 J of kinetic energy upon striking the muscle. The impact area was approx. 1 cm^2, resulting in discernible swelling following 3 consecutive strikes. While scattered bleeding spots were observed, no lesions formed, and the rats displayed a noticeable limp. The model showed a success rate of 100% based on anatomical and histological verification. In the absence of any intervention, the animals naturally progressed to develop a chronic soft tissue injury model after 2 weeks of normal feeding.

Treatment

The untreated control and model groups received no intervention. In the case of the remaining 3 groups, a designated individual immobilized the rats while a second person applied tea oil or Masanggoubang oil to the injured sites using a buffalo horn scraper. This procedure lasted 5 min, performed at an approx. rate of 70 repetitions per min until the appearance of sha on the skin. This treatment regimen was administered once every other day until sha disappeared, totaling 4 sessions. In the IMO group, 1 person immobilized the rats while another applied Masanggoubang oil to the injured soft tissue once every other day, amounting to a total of 4 applications.

Sample preparation

Tissue and serum cytokine sample preparation

Serum cytokine samples were prepared 48 h after the last treatment (until sha disappeared). To ensure consistency, all animals underwent a 12-h fasting period prior to anesthesia induction. For anesthesia, the rats were intraperitoneally (ip.) injected with 20% urethane at a dosage of 0.8 mL per 100 g of body weight. Subsequently, 5 mL of blood was collected from the abdominal aorta while the rats were under anesthesia. The collected samples were allowed to stand at room temperature for 1 h before being centrifuged at 3,500 rpm/min for 15 min. The supernatant was then collected and stored at –20°C for later use.

Muscle tissue samples were prepared 48 h after the last treatment (until sha disappeared). The rats were euthanized by cervical dislocation, and local muscle tissues were isolated. Blood was rinsed with pre-cooled normal saline at 4°C, and the samples were blotted dry with filter paper. The tissues were weighed and homogenized to a concentration of 10%. Subsequently, the homogenized samples were subjected to centrifugation at 5,000 rpm/min for 10 min at 4°C. The resulting supernatant was collected and stored at –20°C for later use.

Histopathological section sample preparation

Forty-eight hours after the last treatment, all the rats were euthanized by the cervical dislocation method after the sha had faded. The local muscle tissues were then separated, fixed and individually preserved in a formalin solution.

Sample testing

Tumor necrosis factor alpha, IL-1β, IL-6, iNOS, and β-EP levels in the skin, muscle and serum samples were determined with ELISA according to the kits' instructions.[36,37]

Paraffin-embedded tissue sections were prepared as follows. The muscle tissues were cut separately along the injury site. They were then rinsed in saline solutions, dehydrated, embedded in paraffin, and sectioned. Subsequently, the sections were stained with H&E to generate pathological sections for observing the pathological changes.

Statistical analyses

All data were analyzed using IBM SPSS Statistics for Windows v. 24 (IBM Corp., Armonk, USA). Due to the small number of observations in the group ($n \leq 10$), the assumption of normality of distribution for parametric tests was not checked, and a nonparametric test was used. Results were expressed as median and quartiles. The Kruskal–Wallis test was used. The Mann–Whitney–Wilcoxon U test for rank sums for independent samples was employed for post hoc comparisons of each group with the control group, and a post hoc Dunn's test was used for comparisons of the individual groups. A significance level of $\alpha = 0.05$ was adopted. A Bonferroni correction of multiple comparisons with a significance level of $\alpha = 0.01$ was applied to the Kruskal–Wallis test and Man–Whitney–Wilcoxon test for the rank sums of independent samples. No correction for multiple comparisons of significance level was applied to the post hoc Dunn's test.

Results

All 50 rats were included in the analysis.

Histopathological findings

Histopathological findings in skin samples

The results of H&E staining showed that in the model group, the stratum corneum exhibited a strip-like and uniform distribution, with tightly arranged cells involved in the formation of the stratum corneum. In comparison to the model group, both the GSTO group and GSMO group showed a loosely arranged stratum corneum with increased intercellular spaces, indicating that the physical stimulation of gua sha enlarges the interstitial spaces in the skin tissue of the applied area (Fig. 1).

Histopathological findings of muscle samples

Hematoxylin and eosin staining also revealed that in the model group, the local muscle tissues in the injured area exhibited irregular cell arrangement, muscle fiber degeneration, necrosis, and dead muscle fibers, along with the proliferation of connective tissue. In comparison to the model, IMO and GSTO groups, the pathological changes in muscle tissues were less pronounced in the GSMO group, suggesting that GSMO significantly improves the degree of soft tissue damage (Fig. 2).

Levels of TNF-α, IL-1β, IL-6, iNOS, and β-EP in skin tissue

The ELISA results indicated a noteworthy elevation in skin levels of TNF-α (post hoc Dunn's test: $p < 0.001$), IL-1β (post hoc Dunn's test: $p = 0.008$), IL-6 (post hoc Dunn's test: $p = 0.001$), and iNOS (post hoc Dunn's test: $p = 0.002$) in the model group compared to the control group, but no statistically significant difference was observed in the level of β-EP.

After treatment, a notable reduction in the levels of TNF-α (post hoc Dunn's test: $p < 0.001$, $p = 0.012$, respectively), IL-6 (post hoc Dunn's test: $p < 0.001$, $p = 0.005$, respectively) and iNOS (post hoc Dunn's test: $p < 0.001$, $p = 0.024$, respectively) were observed in the skin tissues of the GSMO and

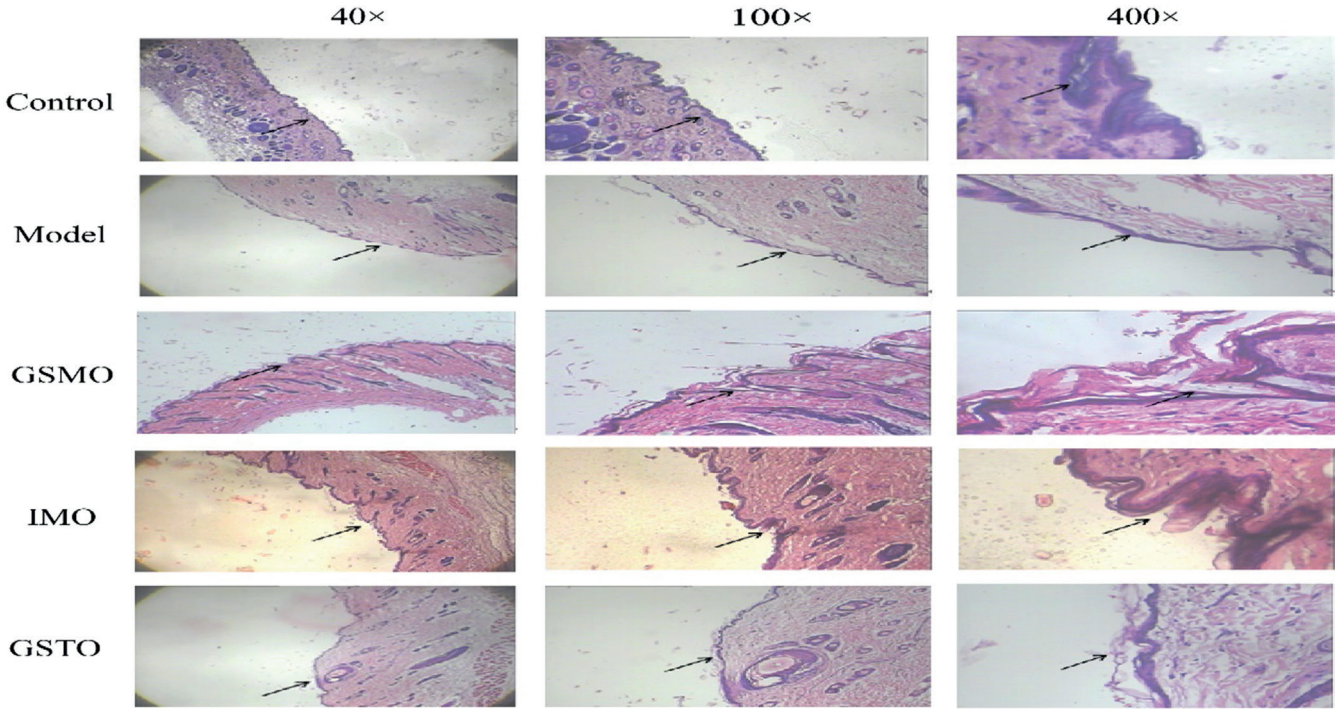

Fig. 1. The results of hematoxylin & eosin (H&E) staining indicated that GSMO effectively improved the histological morphology of skin tissue in rats with chronic soft tissue injury (n = 6 per group)

GSMO – gua sha with Masanggoubang oil; GSTO – gua sha with tea oil; IMO – inunction with Masanggoubang oil.

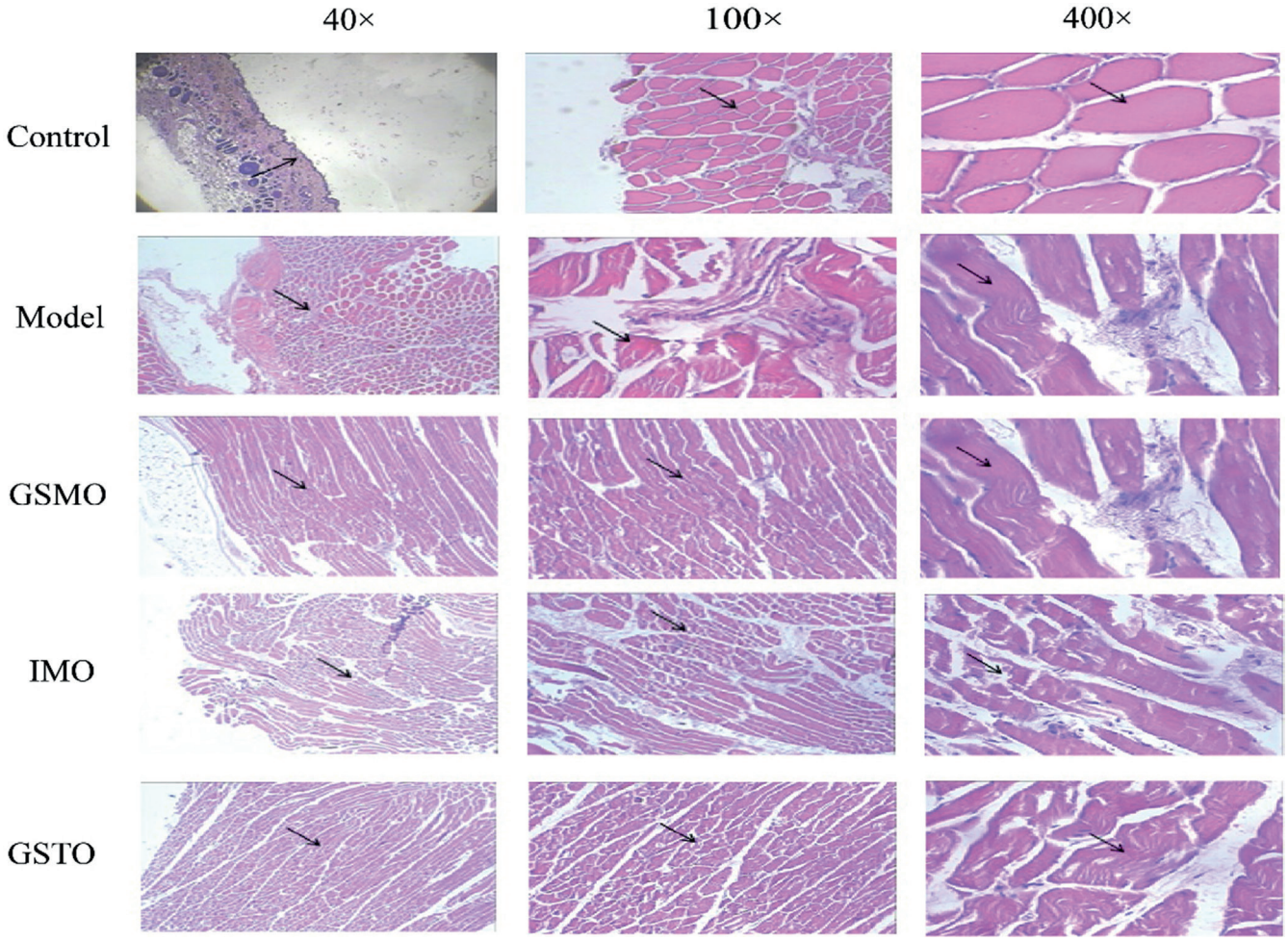

Fig. 2. The results of hematoxylin & eosin (H&E) staining demonstrated that GSMO improved the histological morphology of muscle tissue in rats with chronic soft tissue injury (n = 6 per group)

GSMO – gua sha with Masanggoubang oil; GSTO – gua sha with tea oil; IMO – inunction with Masanggoubang oil.

IMO groups compared to the model group. Conversely, no significant disparity was evident in the GSTO group. Additionally, the levels of TNF-α (post hoc Dunn's test: $p = 0.004$) significantly decreased in the skin tissues of the GSMO group in comparison to the GSTO group, while no significant variance was noted in the IMO group. Furthermore, these cytokine levels displayed no discernible differences between the GSMO and IMO groups. Moreover, in comparison to the control group, the GSMO group exhibited no significant differences in skin levels of TNF-α, IL-1β, IL-6, and iNOS. Similarly, the IMO group showed no significant differences in skin levels of TNF-α, IL-6 and iNOS when compared to the control group. Likewise, the GSTO group exhibited no significant differences in skin levels of IL-6 and iNOS in comparison to the control group (Table 1, Fig. 3).

Levels of TNF-α, IL-1β, IL-6, iNOS, and β-EP in muscle tissue

The ELISA results revealed markedly higher levels of TNF-α (post hoc Dunn's test: $p < 0.001$), IL-1β (post hoc Dunn's test: $p = 0.001$), IL-6 (post hoc Dunn's test: $p = 0.001$), and iNOS (post hoc Dunn's test: $p < 0.001$) in the muscle tissues of the model group compared to the control group. Conversely, β-EP (post hoc Dunn's test: $p < 0.001$) exhibited a significant decrease.

Following the intervention, the GSMO group demonstrated a notable reduction in muscle levels of TNF-α (post hoc Dunn's test: $p < 0.001$), IL-1β (post hoc Dunn's test: $p = 0.003$), IL-6 (post hoc Dunn's test: $p = 0.013$), and iNOS (post hoc Dunn's test: $p < 0.001$) compared to the model group. Additionally, a significant increase in β-EP (post hoc Dunn's test: $p = 0.014$) was observed. Conversely, the IMO group and GSTO groups did not exhibit significant differences in muscle levels of TNF-α, IL-1β, IL-6, iNOS, and β-EP. Furthermore, comparing the GSMO group to the GSTO group, significant differences were observed in TNF-α (post hoc Dunn's test: $p = 0.002$), IL-1β (post hoc Dunn's test: $p = 0.018$) and β-EP (post hoc Dunn's test: $p = 0.018$) levels. Similarly, the GSMO group revealed significant variances in TNF-α (post hoc Dunn's test: $p = 0.017$), IL-1β (post hoc Dunn's test: $p = 0.034$), iNOS (post hoc Dunn's test: $p = 0.040$), and β-EP (post hoc Dunn's test: $p = 0.019$) levels compared to the IMO group. Nevertheless, no significant differences were found in these cytokine levels between the GSTO and IMO groups. Furthermore, the GSMO group exhibited no significant differences in these cytokine levels compared to the control group (Table 2, Fig. 4A–E)

Levels of TNF-α, IL-1β, IL-6, iNOS, and β-EP in serum

The ELISA results unveiled notably elevated levels of IL-1β (post hoc Dunn's test: $p < 0.001$) and iNOS (post hoc Dunn's test: $p = 0.003$) in the serum of the model group compared to the control group.

After treatment, in comparison to the model group, the GSMO group demonstrated a significant decrease in serum levels of TNF-α (post hoc Dunn's test: $p = 0.019$), IL-1β (post hoc Dunn's test: $p = 0.015$), IL-6 (post hoc Dunn's test: $p = 0.004$), and iNOS (post hoc Dunn's test: $p = 0.001$). Additionally, both the IMO and GSTO groups exhibited a significant reduction in serum levels of iNOS (post hoc Dunn's test: $p = 0.003$, $p < 0.001$, respectively) when compared to the model group. When compared with the GSTO group, the GSMO group demonstrated an increased level of β-EP (post hoc Dunn's test: $p = 0.001$). However, no significant differences were observed in these cytokine levels between the GSTO and IMO groups. Notably, the GSMO group displayed remarkable differences in IL-6 (post hoc Dunn's test: $p = 0.002$) and β-EP (post hoc Dunn's test: $p = 0.015$) levels compared to the IMO group. Furthermore, compared to the control group, a notable reduction in the levels of IL-6 (post hoc Dunn's test: $p = 0.001$) was observed in the serum of the GSMO group, while no significant differences were observed in TNF-α, IL-1β, iNOS, and β-EP levels in the GSMO group when compared to the control group. Similarly, no significant differences in the levels of TNF-α, IL-6 and iNOS were observed in the serum of the IMO and GSTO groups compared to the control group (Table 3, Fig. 5A–E).

Discussion

Chronic soft tissue injuries refer to a traumatic syndrome in which soft tissues or skeletal muscles are subjected to a direct or indirect force or prolonged chronic strain, characterized by aseptic inflammation and resulting in soft tissue spasms and scarring.[2] Gua sha with Masanggoubang oil therapy is known as one of the distinctive external therapies in the traditional Miao medicine for its anti-inflammatory and analgesic effects.[38] Its efficacy and safety in the treatment of chronic soft tissue injuries have been extensively confirmed.[23,32,34] However, its underlying mechanism of action remains unclear. Therefore, this study explores the therapeutic effects of GSMO on rats with chronic soft tissue injuries and identifies its potential mechanisms of action.

This study found that GSMO can alleviate soft tissue necrosis, degeneration and scar tissue proliferation at the injury site, mitigate inflammatory responses, downregulate TNF-α, IL-6 and iNOS levels in the skin tissues, as well as TNF-α, IL-1β, IL-6, and iNOS levels in muscle and serum, and upregulate β-EP levels in the muscles of rats with chronic soft tissue injuries.

Chronic soft tissue injuries primarily manifest as inflammatory responses and pain. In recent years, there has been increasing attention on the role of M1 macrophage polarization in inflammatory diseases.[5,6] M1 macrophages promote inflammation by densely releasing pro-inflammatory

Table 1. TNF-α, IL-1β, IL-6, iNOS, and β-EP skin levels in rats with chronic soft tissue injury (median (Q1–Q3))

Group		TNF-α [pg/mL]	IL-1β [pg/mL]	IL-6 [pg/mL]	iNOS [IU/mL]	β-EP [pg/mL]
Control (n = 10)		26.72 (18.38–37.74)	1045.52 (788.74–1611.62)	1.76 (1.39–3.41)	7.58 (5.33–11.58)	29.98 (21.90–44.74)
Model (n = 10)		100.91 (79.37–147.45)$^{\$\$\$}$	3243.58 (2233.56–11157.35)$^{\$\$}$	6.59 (5.05–7.27)$^{\$\$}$	17.08 (14.45–32.81)$^{\$\$}$	20.70 (13.56–42.41)
GSMO (n = 10)		21.08 (16.10–31.82)***&&	2171.46 (2012.14–2264.05)	1.45 (0.72–2.63)***	6.82 (4.01–10.56)***	25.02 (17.33–43.02)
IMO (n = 10)		37.17 (29.09–49.45)*	3480.24 (2947.88–5542.41)$^{\$\$}$	2.47 (1.83–3.10)**	8.93 (6.93–11.71)*	19.95 (11.22–24.79)
GSTO (n = 10)		74.55 (47.85–99.46)$^{\$}$	3871.68 (2626.87–5476.69)$^{\$\$}$	4.64 (2.73–5.31)	10.20 (8.93–14.49)	16.92 (8.42–28.54)
H		32.33	23.09	27.04	21.86	7.40
df		4	4	4	4	4
p-value		<0.001	<0.001	<0.001	<0.001	0.116
post hoc test p-values	control vs model	<0.001	0.008	0.001	0.002	>0.999
	control vs GSMO	>0.999	>0.999	>0.999	>0.999	>0.999
	control vs IMO	>0.999	0.002	>0.999	>0.999	0.384
	control vs GSTO	0.035	0.002	0.363	0.703	0.167
	model vs GSMO	<0.001	0.429	<0.001	<0.001	>0.999
	model vs IMO	0.012	>0.999	0.005	0.024	>0.999
	model vs GSTO	>0.999	>0.999	0.582	0.592	>0.999
	GSTO vs GSMO	0.004	0.154	0.083	0.261	>0.999
	GSTO vs IMO	0.461	>0.999	>0.999	>0.999	>0.999
	GSMO vs IMO	>0.999	0.135	>0.999	>0.999	>0.999

$^{\$}p < 0.05$, $^{\$\$}p < 0.01$, $^{\$\$\$}p < 0.001$, compared with the control group; *p < 0.05, **p < 0.01, ***p < 0.001, compared with the model group; $^{\&\&}p < 0.01$, compared with the GSTO group. β-EP – β-endorphin; df – degrees of freedom; GSMO – gua sha with Masanggoubang oil; GSTO – gua sha with tea oil; H – the value of the test statistic for the Kruskal–Wallis test; IL-1β – interleukin 1β; IL-6 – interleukin 6; IMO – inunction with Masanggoubang oil; iNOS – inducible nitric oxide synthase; TNF-α – tumor necrosis factor alpha. Statistical analysis was performed using the Kruskal–Wallis test, which was preferably employed for the statistical analysis of TNF-α, IL-1β, IL-6, iNOS, and β-EP. The post hoc Dunn's test was subsequently applied.

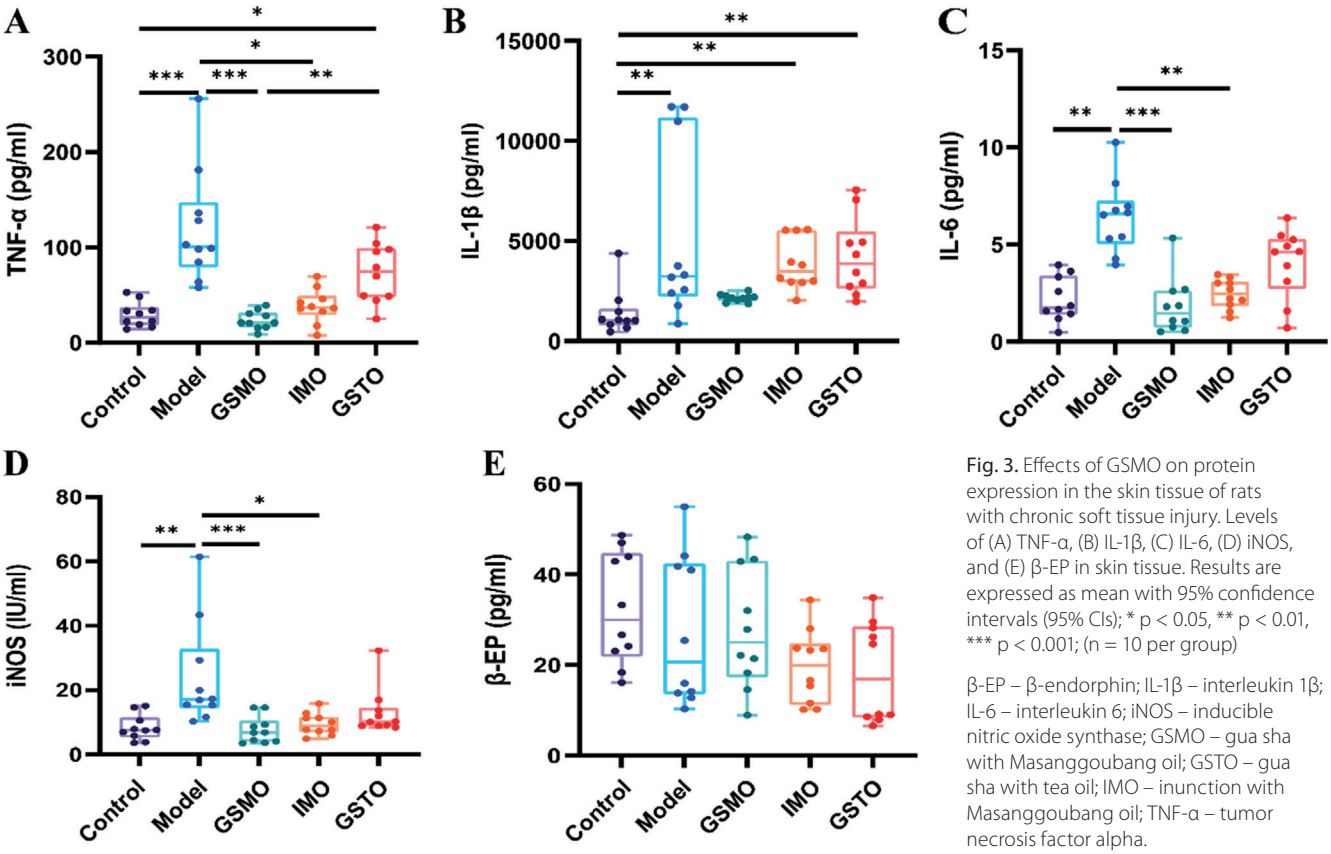

Fig. 3. Effects of GSMO on protein expression in the skin tissue of rats with chronic soft tissue injury. Levels of (A) TNF-α, (B) IL-1β, (C) IL-6, (D) iNOS, and (E) β-EP in skin tissue. Results are expressed as mean with 95% confidence intervals (95% CIs); * p < 0.05, ** p < 0.01, *** p < 0.001; (n = 10 per group)

β-EP – β-endorphin; IL-1β – interleukin 1β; IL-6 – interleukin 6; iNOS – inducible nitric oxide synthase; GSMO – gua sha with Masanggoubang oil; GSTO – gua sha with tea oil; IMO – inunction with Masanggoubang oil; TNF-α – tumor necrosis factor alpha.

Table 2. TNF-α, IL-1β, IL-6, iNOS, and β-EP muscle levels in rats with chronic soft tissue injury (median (Q1–Q3))

Group		TNF-α [pg/mL]	IL-1β [pg/mL]	IL-6 [pg/mL]	iNOS [IU/mL]	β-EP [pg/mL]
Control (n = 10)		86.63 (63.59–101.90)	615.94 (540.36–708.99)	3.37 (2.08–4.31)	5.34 (5.05–5.82)	165.14 (123.43–247.06)
Model (n = 10)		176.26 (140.59–221.29)$^{\$\$\$}$	1530.93 (976.65–1956.43)$^{\$\$}$	6.88 (4.92–9.94)$^{\$\$}$	23.57 (19.93–27.94)$^{\$\$\$}$	43.90 (22.92–47.29)$^{\$\$\$}$
GSMO (n = 10)		85.42 (66.84–90.46)$^{***\&\&\#}$	694.70 (464.89–772.08)$^{**\&\#}$	3.85 (2.84–5.51)*	7.19 (6.73–8.21)$^{***\#}$	77.60 (72.29–126.84)$^{*\&\#}$
IMO (n = 10)		142.00 (116.19–162.83)$^{\$}$	1144.91 (849.32–1522.11)$^{\$}$	6.14 (4.04–8.57)$^{\$}$	18.62 (14.64–21.98)$^{\$\$\$}$	38.41 (31.50–47.40)$^{\$\$\$}$
GSTO (n = 10)		156.31 (133.84–172.58)$^{\$\$}$	1169.40 (935.46–1436.34)$^{\$\$}$	6.36 (4.99–8.00)$^{\$\$}$	11.68 (9.66–13.99)$^{\$}$	35.59 (23.64–53.33)$^{\$\$\$}$
H		33.18	28.42	23.36	40.30	35.14
df		4	4	4	4	4
p-value		<0.001	<0.001	<0.001	<0.001	<0.001
Post hoc test p-values	control vs model	<0.001	0.001	0.001	<0.001	<0.001
	control vs GSMO	>0.999	>0.999	>0.999	>0.999	>0.999
	control vs IMO	0.038	0.011	0.043	<0.001	<0.001
	control vs GSTO	0.004	0.006	0.009	0.012	<0.001
	model vs GSMO	<0.001	0.003	0.013	<0.001	0.014
	model vs IMO	>0.999	>0.999	>0.999	>0.999	>0.999
	model vs GSTO	>0.999	>0.999	>0.999	0.167	>0.999
	GSTO vs GSMO	0.002	0.018	0.097	0.960	0.018
	GSTO vs IMO	>0.999	>0.999	>0.999	>0.999	>0.999
	GSMO vs IMO	0.017	0.034	0.330	0.040	0.019

$^{\$}$ p < 0.05, $^{\$\$}$p < 0.01, $^{\$\$\$}$p < 0.001, compared with the control group; *p < 0.05, **p < 0.01, ***p < 0.001, compared with the model group; $^{\&}$p < 0.05, $^{\&\&}$p < 0.01, compared with the GSTO group; $^{\#}$p < 0.05, compared with the IMO group. β-EP – β-endorphin; df – degrees of freedom; GSMO – gua sha with Masanggoubang oil; GSTO – gua sha with tea oil; H – the value of the test statistic for the Kruskal–Wallis test; IL-1β – interleukin 1β; IL-6 – interleukin 6; IMO – inunction with Masanggoubang oil; iNOS – inducible nitric oxide synthase; TNF-α – tumor necrosis factor alpha. Statistical analysis was performed using the Kruskal–Wallis test, which was preferably employed for statistical analysis of TNF-α, IL-1β, IL-6, iNOS, and β-EP. The post hoc Dunn's test was subsequently applied.

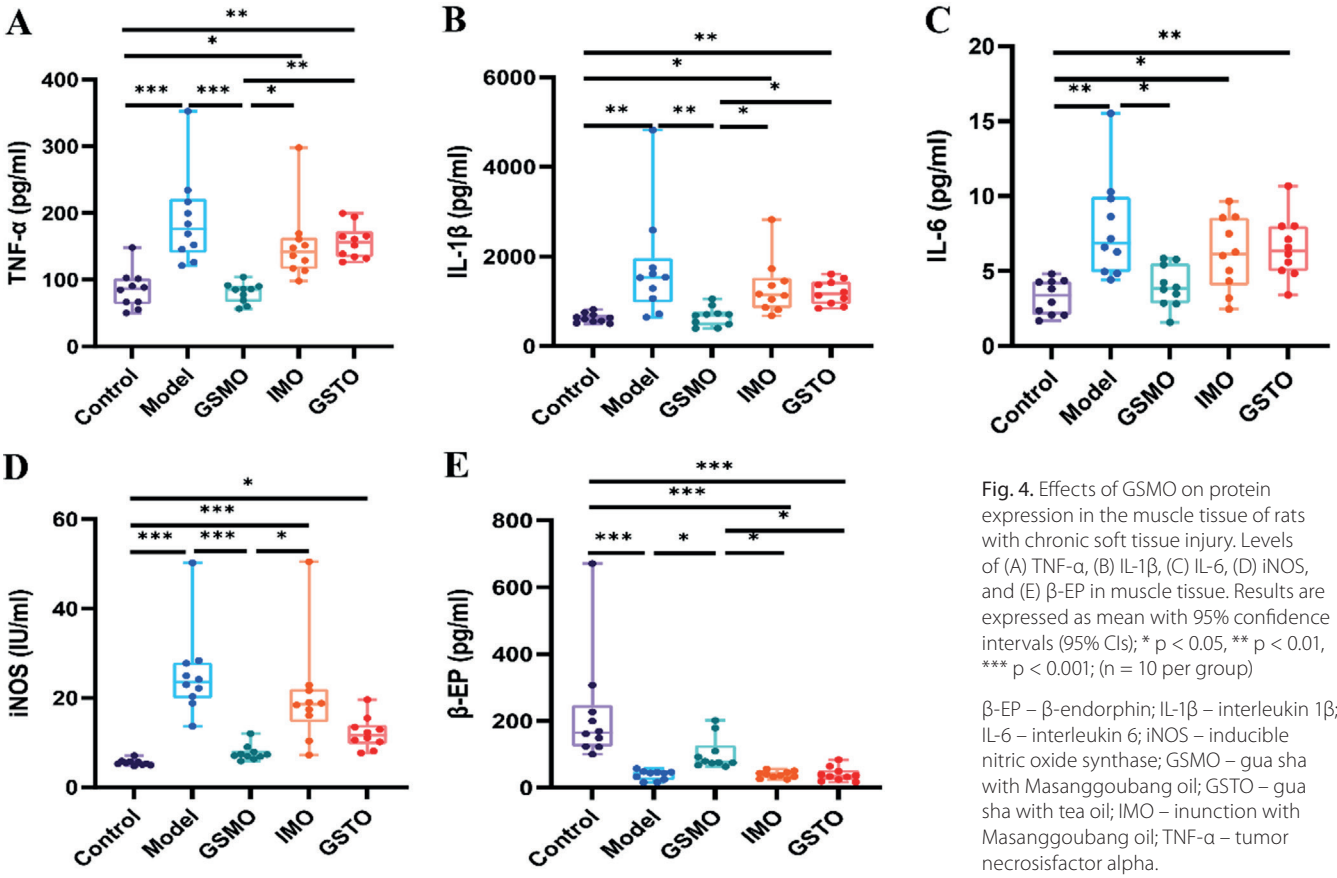

Fig. 4. Effects of GSMO on protein expression in the muscle tissue of rats with chronic soft tissue injury. Levels of (A) TNF-α, (B) IL-1β, (C) IL-6, (D) iNOS, and (E) β-EP in muscle tissue. Results are expressed as mean with 95% confidence intervals (95% CIs); * p < 0.05, ** p < 0.01, *** p < 0.001; (n = 10 per group)

β-EP – β-endorphin; IL-1β – interleukin 1β; IL-6 – interleukin 6; iNOS – inducible nitric oxide synthase; GSMO – gua sha with Masanggoubang oil; GSTO – gua sha with tea oil; IMO – inunction with Masanggoubang oil; TNF-α – tumor necrosisfactor alpha.

Table 3. TNF-α, IL-1β, IL-6, iNOS, and β-EP serum levels in rats with chronic soft tissue injury (median (Q1–Q3))

Group		TNF-α [pg/mL]	IL-1β [pg/mL]	IL-6 [pg/ml]	iNOS [IU/mL]	β-EP [pg/mL]
Control (n = 10)		1.81 (0.81–2.79)	56.86 (51.90–62.46)	7.63 (5.77–8.02)	0.14 (0.06–0.25)	2196.08 (2139.87–2250.16)
Model (n = 10)		2.73 (2.39–3.00)	86.22 (74.14–88.61)$^{\$\$\$}$	6.76 (5.13–7.93)	1.36 (1.22–1.57)$^{\$\$}$	1996.75 (1546.24–2139.77)
GSMO (n = 10)		1.28 (0.73–1.68)*	65.17 (59.95–72.19)*	4.38 (3.12–4.78)$^{\$\$}$**$^{\#\#}$	0.14 (0.06–0.19)**	2183.28 (2047.14–2226.38)$^{\&\&\#}$
IMO (n = 10)		1.87 (0.85–3.57)	81.40 (77.58–86.49)$^{\$\$}$	6.46 (6.14–8.55)	0.18 (0.04–0.39)**	1336.49 (638.66–1936.04)$^{\$\$}$
GSTO (n = 10)		1.13 (0.73–2.88)	82.74 (80.69–84.42)$^{\$\$\$}$	6.26 (5.13–7.16)	0.12 (0.07–0.13)***	940.62 (615.36–1720.98)$^{\$\$\$}$
H		10.59	32.20	20.52	24.29	29.92
df		4	4	4	4	4
p-value		0.032	<0.001	<0.001	<0.001	<0.001
Post hoc test p-values	control vs model	0.551	<0.001	>0.999	0.003	0.306
	control vs GSMO	>0.999	>0.999	0.001	>0.999	>0.999
	control vs IMO	>0.999	0.001	>0.999	>0.999	0.003
	control vs GSTO	>0.999	<0.001	>0.999	>0.999	<0.001
	model vs GSMO	0.019	0.015	0.004	0.001	0.915
	model vs IMO	>0.999	>0.999	>0.999	0.003	>0.999
	model vs GSTO	0.209	>0.999	>0.999	<0.001	0.223
	GSTO vs. GSMO	>0.999	0.052	0.056	>0.999	0.001
	GSTO vs. IMO	>0.999	>0.999	>0.999	>0.999	>0.999
	GSMO vs. IMO	>0.999	0.059	0.002	>0.999	0.015

$^{\$\$}p < 0.01$, $^{\$\$\$}p < 0.001$, compared with the control group; *p < 0.05, **p < 0.01, **p < 0.001, compared with the model group; $^{\&\&}p < 0.01$, compared with the GSTO group; $^{\#}p < 0.05$, $^{\#\#}p < 0.01$, compared with the IMO group. β-EP – β-endorphin; df – degrees of freedom; GSMO – gua sha with Masanggoubang oil; GSTO – gua sha with tea oil; H – the value of the test statistic for the Kruskal–Wallis test; IL-1β – interleukin 1β; IL-6 – interleukin 6; IMO – inunction with Masanggoubang oil; iNOS – inducible nitric oxide synthase; TNF-α – tumor necrosis factor alpha. Statistical analysis was performed using the Kruskal–Wallis test, which was preferably for the statistical analysis of TNF-α, IL-1β, IL-6, iNOS, and β-EP. The post hoc Dunn's test was subsequently applied.

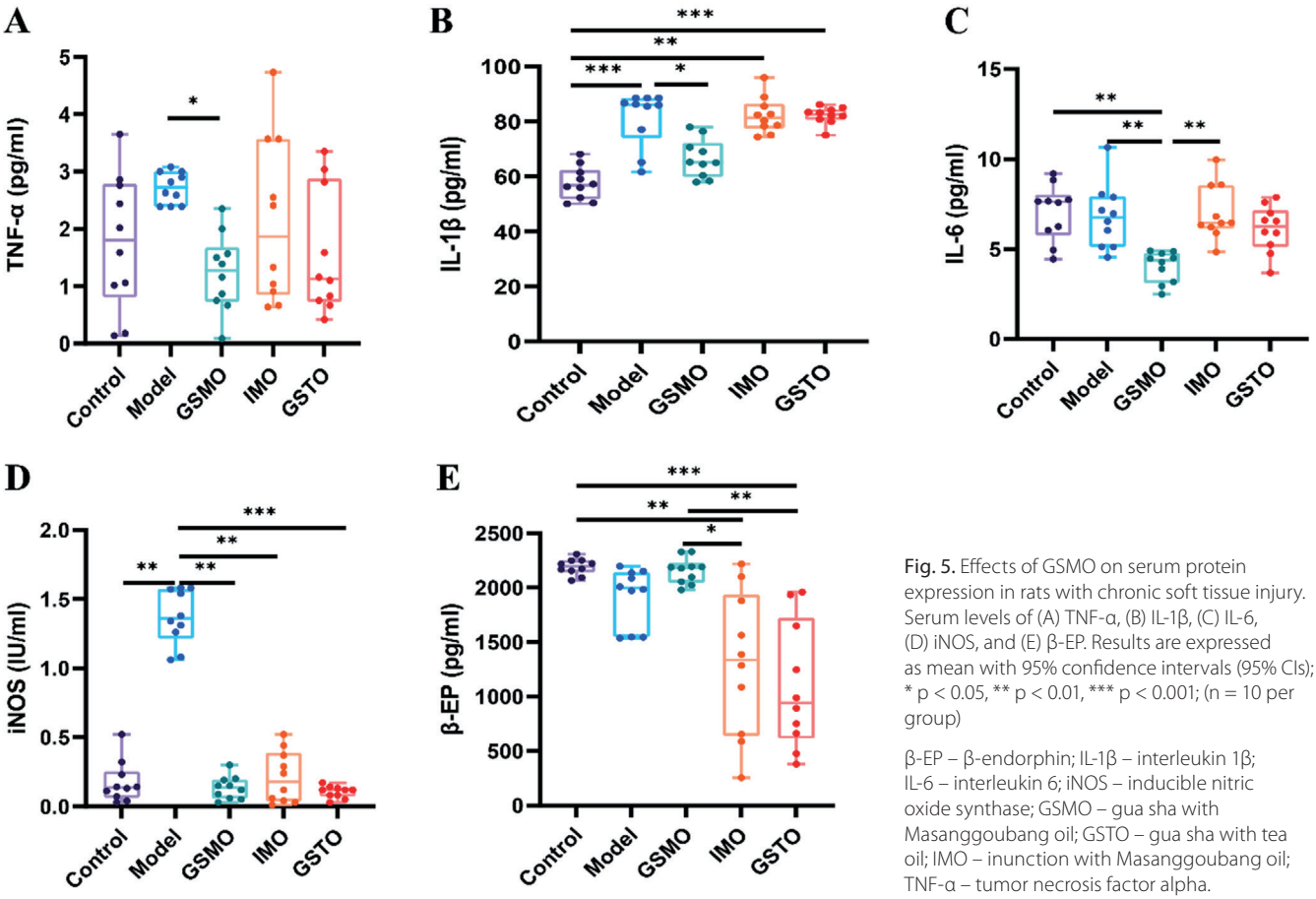

Fig. 5. Effects of GSMO on serum protein expression in rats with chronic soft tissue injury. Serum levels of (A) TNF-α, (B) IL-1β, (C) IL-6, (D) iNOS, and (E) β-EP. Results are expressed as mean with 95% confidence intervals (95% CIs); * p < 0.05, ** p < 0.01, *** p < 0.001; (n = 10 per group)

β-EP – β-endorphin; IL-1β – interleukin 1β; IL-6 – interleukin 6; iNOS – inducible nitric oxide synthase; GSMO – gua sha with Masanggoubang oil; GSTO – gua sha with tea oil; IMO – inunction with Masanggoubang oil; TNF-α – tumor necrosis factor alpha.

factors such as IL-6, IL-1β and TNF-α. High expression of iNOS catalyzes the production of the neurotransmitter NO, thereby increasing the sensitivity of the peripheral and central nervous systems and inducing pain hypersensitivity.[7,8] Among these, TNF-α is an important mediator in the inflammatory response, inducing a cascade of IL-6 and IL-1β release, thereby increasing inflammation.[9] Simultaneously, a decrease in TNF-α is closely associated with the improvement of limb disabilities.[20] Previous studies have found macrophage polarization to play a crucial role in suppressing soft tissue inflammation and promoting tissue repair and regeneration.[39,40] Yang et al.[12] discovered that gua sha therapy improves pain perception and the inflammatory response in chronic soft tissue injuries by downregulating the expression of TNF-α, IL-1β and IL-6 in the serum, which is consistent with our findings. Bai found that electroacupuncture alleviates inflammation in rats with myofascial injuries by downregulating iNOS levels.[41] We observed that the levels of serum and muscle iNOS were downregulated in the GSMO group, which is consistent with the literature. Beta-EP is an important endogenous opioid neuropeptide that exerts powerful analgesic effects by inhibiting pain transmission pathways.[42] Peripheral and central opioid receptors participate in the analgesic effects during the early stages of inflammation.[43] He and Zhou[13] found that tuina (a hands-on body treatment that uses Chinese Daoist principles to bring the 8 principles of TCM into balance) massage alleviates pain symptoms by upregulating serum β-EP levels in patients with lumbar disc herniations. Our research shows that the GSMO group exhibited upregulated muscle β-EP levels, which may promote blood circulation in the body to facilitate the exchange of β-EP from serum to tissues and enhance local analgesic effects.[44] This finding is consistent with the literature.

Similarly, this study found that IMO and GSTO therapies also improved the inflammatory response to varying degrees in rats with chronic soft tissue injuries. Our experimental results revealed decreased TNF-α, IL-6 and iNOS levels in the skin tissues at the injury site, as well as serum iNOS levels in the IMO group. In the GSTO group, the serum iNOS levels also decreased. The observed improvements in the IMO group can be attributed to the active ingredients in Masanggoubang oil penetrating the dermis of the damaged area and exerting anti-inflammatory effects to some extent.[38] Gua sha with tea oil partially alleviated the inflammatory response in the injured soft tissues by improving local blood circulation and facilitating the metabolism of inflammatory factors.[44]

Furthermore, this study found that GSMO, IMO and GSTO therapies all improved the inflammatory response in rats with chronic soft tissue injuries to varying degrees. Among them, GSMO therapy was superior to IMO and GSTO therapies alone, revealing a synergistic effect of combining gua sha therapy and Masanggoubang oil. The scraping medium was identified as an important factor influencing the efficacy of gua sha therapy. Compared to IMO, GSMO significantly improved muscle TNF-α, IL-1β, iNOS, and β-EP levels. This may be attributed to gua sha therapy's ability to expand the interstitial space, facilitating the deep absorption of active ingredients from Masanggoubang oil into the muscle layer. Compared to GSTO, GSMO significantly improved skin TNF-α levels, muscle TNF-α, IL-1β and β-EP levels, as well as serum β-EP levels, possibly due to the combined effect of gua sha therapy and Masanggoubang oil, which may enhance the anti-inflammatory action and significantly improve soft tissue inflammation.

Limitations

We found that GSMO can upregulate muscle β-EP levels in rats with chronic soft tissue injuries. Therefore, we speculate that GSMO may also alleviate pain in rats with chronic soft tissue injuries. However, we only tested 1 pain factor, so further evaluation of its analgesic effectiveness should include pain threshold measurement scores and other serum pain substances such as substance P and neuropeptide Y.[45,46] Additionally, the underlying mechanisms of GSMO for chronic soft tissue injuries remain unclear. It would be beneficial to explore the relevant signaling pathways of scraping therapy using gene chip technology and further clarify its mechanism of action by combining immunological techniques and proteomics. Moreover, future studies should consider extending the observation period to investigate the long-term effects of GSMO. Furthermore, conducting comparative efficacy studies between GSMO and prescription drugs would provide a comprehensive evaluation of its therapeutic effects on chronic soft tissue injuries.

Conclusions

Our results indicate that GSMO can alleviate the inflammatory response in rats with chronic soft tissue injuries, which may be related to the inhibition of M1 macrophage polarization. Additionally, we found that the combination of gua sha therapy and Masanggoubang oil has a synergistic effect in treating chronic soft tissue injuries. Therefore, this study may provide valuable insights into the clinical treatment of chronic soft tissue injuries. In summary, GSMO demonstrates a favorable therapeutic effect of chronic soft tissue injuries, significantly improving the inflammatory response in rats with chronic soft tissue injuries. The mechanism behind this improvement may be associated with the reduction of M1 macrophage polarization in the peripheral blood and local tissues. Gua sha with Masanggoubang oil shows promise as an effective method for the treatment of chronic soft tissue injuries, and our research provides scientific evidence supporting its use in this context.

Supplementary data

The Supplementary materials are available at https://doi.org/10.5281/zenodo.10889055. The package includes the following files:

Supplementary Table 1. Comparative analysis of TNF-α, IL-1β, IL-6, iNOS, and β-EP skin levels compared control group to the other 4 groups.

Supplementary Table 2. Comparative analysis of TNF-α, IL-1β, IL-6, iNOS, and β-EP muscle levels compared control group to the other 4 groups.

Supplementary Table 3. Comparative analysis of TNF-α, IL-1β, IL-6, iNOS, and β-EP serum levels compared control group to the other 4 groups.

Data availability

The datasets generated and/or analyzed during the current study are available from the corresponding author on reasonable request.

Consent for publication

Not applicable.

ORCID iDs

Min Zhu https://orcid.org/0000-0002-4937-5191
Dong Zhao https://orcid.org/0009-0000-9636-9037
Chunxia Lu https://orcid.org/0009-0006-8030-8671
Jin Cui https://orcid.org/0000-0002-0106-2620

References

1. Liang D, Hu S, Chen JY. A multicentric study of low-intensity focused ultrasound in the treatment of soft-tissue injury induced pain [in Chinese]. *Chinese Journal of Pain Medicine*. 2020;26(1):48–52. http://doi.med.wanfangdata.com.cn/10.3969/j.issn.1006-9852.2020.01.009. Accessed October 15, 2023.
2. Yan JX, Liao X, Tang LZ, et al. Carbon arc lamp therapy enhances the repair potential of chronic soft tissue injury in rats compared with the ability of photobiomodulation therapy. *Photobiomodul Photomed Laser Surg*. 2021;39(5):311–320. doi:10.1089/photob.2020.4885
3. Xu JG, Cui JJ, Dong NN, Cao YY. High-power spectral instrument for chronic soft tissue injury [in Chinese]. *Optics and Precision Engineering*. 2021;29(2):278–285. doi:10.37188/OPE.20212902.0278
4. Song YX, Liu J. Effect of acupotomy on the serum levels of TNF-a, IL-1β and IL-6 in patients with chronic soft tissue injury [in Chinese]. *Shaanxi Medical Journal*. 2017;46(17):2056–2058. http://doi.med.wanfangdata.com.cn/10.3969/j.issn.0253-9926.2017.17.007. Accessed October 15, 2023.
5. Wan L, Liu J, Huang C, Wang K, Zhu Z, Li F. A novel pharmaceutical preparation of *Tripterygium wilfordii* Hook. f. regulates macrophage polarization to alleviate inflammation in rheumatoid arthritis. *J Pharm Pharmacol*. 2023;75(11):1442–1457. doi:10.1093/jpp/rgad078
6. Deng J, Golub LM, Lee HM, et al. A novel modified-curcumin 2.24 resolves inflammation by promoting M2 macrophage polarization. *Sci Rep*. 2023;13(1):15513. doi:10.1038/s41598-023-42848-x
7. Raoof R, Martin Gil C, Lafeber FPJG, et al. Dorsal root ganglia macrophages maintain osteoarthritis pain. *J Neurosci*. 2021;41(39):8249–8261. doi:10.1523/JNEUROSCI.1787-20.2021
8. Wang SZ, Zhu QX, Chen JX. Anti-inflammation and analgesic effect of isoimperatorin on the polarization of macrophage M1 via NF-KB and JAK1/STAT1 signaling pathway [in Chinese]. *Central South Pharmacy*. 2023;21(8):1985–1990. http://doi.med.wanfangdata.com.cn/10.7539/j.issn.1672-2981.2023.08.002. Accessed October 15, 2023.
9. De Magalhães SF, Manzo LP, De Faria FM, et al. Inflammatory pain in peripheral tissue depends on the activation of the TNF-α type 1 receptor in the primary afferent neuron. *Eur J Neurosci*. 2021;53(2):376–389. doi:10.1111/ejn.14985
10. Dong J. Effect of Qingbai powder on nitric oxide synthase system and nitric oxide expression in skeletal muscle of a rat model of chronic soft tissue injury ([n Chinese]. *Chinese Journal of Tissue Engineering Research*. 2011;15(37):6963–6966. http://doi.med.wanfangdata.com.cn/10.3969/j.issn.1673-8225.2011.37.029. Accessed October 15, 2023.
11. Tao S, Wang X, Liao C, et al. The efficacy of moxibustion on the serum levels of CXCL1 and β-EP in patients with rheumatoid arthritis. *Pain Res Manag*. 2021;2021:7466313. doi:10.1155/2021/7466313
12. Yang M, Zhang H, Yue R, Shi Q, Bian Y. Gua sha attenuates thermal hyperalgesia and decreases proinflammatory cytokine expression in serum in rats with lumbar disc herniation induced by autologous nucleus pulposus. *J Tradit Chin Med*. 2018;38(5):698–704. PMID:32185986.
13. He X, Zhou R. Clinical observation of abdominal massage combined with Chinese herbal medicine in the treatment of lumbar disc herniation (cold-damp obstruction syndrome) [in Chinese]. *Journal of Emergency in Traditional Chinese Medicine*. 2018;27(1):137–139. https://doi.org/10.3969/j.issn.1004-745X.2018.01.045. Accessed October 15, 2023.
14. Wu XX, Zhang J, Ding Z. Effect of gua sha therapy on the immune functions of the skin and the body in healthy individuals [in Chinese]. *Journal of Nanjing University of Traditional Chinese Medicine*. 2019;35(1):58–62. Accessed October 15, 2023.
15. Lee MS, Choi TY, Kim JI, Choi SM. Using guasha to treat musculoskeletal pain: A systematic review of controlled clinical trials. *Chin Med*. 2010;5(1):5. doi:10.1186/1749-8546-5-5
16. Yang KW, Yang JS, Xu DS. A comparative study on the changes of rat skin morphology,5-hydroxy-tryptamine and mast cell expression with different guasha intensity [in Chinese]. *Journal of Basic Chinese Medicine*. 2021;27(4):587–591.
17. Wang YY, Chen H, Zhang HB. Effects of guasha therapy on skin tissue morphology and the expression of GCS, SP and SOD of the human body [in Chinese]. *China Journal of Traditional Chinese Medicine and Pharmacy*. 2019;34(7):3204–3208. http://kns.cnki.net/KCMS/detail/detail.aspx?dbcode=CJFD&filename=BXYY201907105. Accessed October 15, 2023.
18. Yang H, Wang GY, Chen XX. Effect of Tongyang scraping therapy on inflammatory cytokines and immune function in rats with lumbar disc herniation [in Chinese]. *Chinese Journal of Gerontology*. 2018;38(10):2477–2479. http://doi.med.wanfangdata.com.cn/10.3969/j.issn.1005-9202.2018.10.069. Accessed October 15, 2023.
19. Wang YY, Chen H, Zhang H.B. Effects of guasha therapy on antioxidation and immunity functions of healthy human body [in Chinese]. *Chinese Journal of Information on Traditional Chinese Medicine*. 2018;25(12):32–34. http://doi.med.wanfangdata.com.cn/10.3969/j.issn.1005-5304.2018.12.009. Accessed October 15, 2023.
20. Yuen JWM, Tsang WWN, Tse SHM, et al. The effects of gua sha on symptoms and inflammatory biomarkers associated with chronic low back pain: A randomized active-controlled crossover pilot study in elderly. *Complement Ther Med*. 2017;32:25–32. doi:10.1016/j.ctim.2017.03.010
21. Wang YY, Ji J, Yang KW. Study on scraping along meridians [in Chinese]. *Journal of Basic Chinese Medicine*. 2021;27(3):527–530.
22. Yang M, Yue RZ, Zhang Q. Analysis of clinical disease spectrum of single scraping therapy based on bibliometrics [in Chinese]. *Chinese Nursing Research*. 2019;33(8):1320–1324.
23. Lu CX, Zhao D, Cui J. Advance in Masanggoubang [in Chinese]. *Chinese Journal of Ethnomedicine and Ethnopharmacy*. 2016;25(16):42–43. http://doi.med.wanfangdata.com.cn/10.3969/j.issn.1007-8517.2016.16.zgmzmjyyzz201616014. Accessed October 15, 2023.
24. Li YQ, Yuan TT, Mao FY. Research progress on pharmacological activity and plant source of astilbin [in Chinese]. *China Pharmacy*. 2017;28(19):2718–2723.
25. Gil TY, Jin BR, Hong CH, Park JH, An HJ. *Astilbe Chinensis* ethanol extract suppresses inflammation in macrophages via NF-κB pathway. *BMC Complement Med Ther*. 2020;20(1):302. doi:10.1186/s12906-020-03073-5
26. Yang M, Chen C, Wang K, Chen Y, Xia J. Astilbin influences the progression of osteoarthritis in rats by down-regulation of PGE-2 expression via the NF-κB pathway. *Ann Transl Med*. 2020;8(12):766–766. doi:10.21037/atm-20-4485

27. Chen C, Yang M, Chen Y, et al. Astilbin-induced inhibition of the PI3K/AKT signaling pathway decelerates the progression of osteoarthritis. *Exp Ther Med*. 2020;20(4):3078–3083. doi:10.3892/etm.2020.9048
28. Sun S, Yan Z, Shui X, et al. Astilbin prevents osteoarthritis development through the TLR4/MD-2 pathway. *J Cell Mol Med*. 2020;24(22):13104–13114. doi:10.1111/jcmm.15915
29. Li BJ, Xia JF, Long MH. Observation of the therapeutic efficacy of Miao medicine, Mashanggoubang spray, in the treatment of knee osteoarthritis [in Chinese]. *Journal of Medicine & Pharmacy of Chinese Minorities*. 2017;23(12):14–16. http://doi.med.wanfangdata.com.cn/10.3969/j.issn.1006-6810.2017.12.007. Accessed October 15, 2023.
30. Xia JF, Zhu GQ, Lv C. Observation of the therapeutic efficacy of Miao medicine, Mashanggoubang wine decoctions, in the treatment of 34 cases of rheumatoid arthritis [in Chinese]. *Chinese Journal of Ethnomedicine and Ethnopharmacy*. 2012;21(2):7. http://doi.med.wanfangdata.com.cn/10.3969/j.issn.1007-8517.2012.02.006. Accessed October 15, 2023.
31. Huang H, Xia JF. Clinical study on the treatment of postoperative patients with cervical spine by gua sha with Masanggoubang oil [in Chinese]. *Journal of Guiyang College of Traditional Chinese Medicine*. 2011;33(2):63–64. http://doi.med.wanfangdata.com.cn/10.3969/j.issn.1002-1108.2011.02-33. Accessed October 15, 2023.
32. Xia JF, Cui J, Lv C. Gua sha with Masanggoubang oil for cervical spondylotic radiculopathy: A randomized multicenter parallel controlled study [in Chinese]. *China Journal of Traditional Chinese Medicine*. 2017;32(6):2808–2811. Accessed October 15, 2023.
33. Zhao D. Evaluation of the clinical efficacy of gua sha treatment of chronic soft tissue injury with Masanggougang oil and study of the mechanism of Gua Sha treatment [master's thesis, in Chinese]. *Guiyang College of Traditional Chinese Medicine*; 2018.
34. Zhang X, Tian ZH. The study on acute toxicity and oil safety of Masanggoubang [in Chinese]. *Journal of Medicine and Pharmacy of Chinese Minorities*. 2012;18(8):53–55. http://doi.med.wanfangdata.com.cn/10.3969/j.issn.1006-6810.2012.08.029. Accessed October 15, 2023
35. Kami K, Masuhara M, Kashiba H, Kawai Y, Noguchi K, Senba E. Changes of vinculin and extracellular matrix components following blunt trauma to rat skeletal muscle. *Med Sci Sports Exerc*. 1993;25(7):832–840. doi:10.1249/00005768-199307000-00012
36. Ding Q, Fang H, Jin P, et al. Pretreating mesenchymal stem cells with IL-6 regulates the inflammatory response of DSS-induced ulcerative colitis in rats. *Transpl Immunol*. 2023;76:101765. doi:10.1016/j.trim.2022.101765
37. Chen Z, Hu L, Liao Y, et al. Different processed products of curcumae radix regulate pain-related substances in a rat model of qi stagnation and blood stasis. *Front Pharmacol*. 2020;11:242. doi:10.3389/fphar.2020.00242
38. Dai CY, Dai CH. Review of pharmacological action and application of lucidum [in Chinese]. *Shanghai Medical & Pharmaceutical Journal*. 2021;42(5):69–72. Accessed October 15, 2023.
39. Ye J, Xie C, Wang C, et al. Promoting musculoskeletal system soft tissue regeneration by biomaterial-mediated modulation of macrophage polarization. *Bioact Mater*. 2021;6(11):4096–4109. doi:10.1016/j.bioactmat.2021.04.017
40. Oyaizu T, Enomoto M, Yamamoto N, et al. Hyperbaric oxygen reduces inflammation, oxygenates injured muscle, and regenerates skeletal muscle via macrophage and satellite cell activation. *Sci Rep*. 2018;8(1):1288. doi:10.1038/s41598-018-19670-x
41. Bai YZ. The effect of electroacupuncture at the Weizhong acupoint on the regulation mechanism of microglia in the injured lumbar multifidus muscle of rats [doctoral thesis] [in Chinese]. Beijing, China: Beijing University of Traditional Chinese Medicine; 2019. Accessed October 15, 2023.
42. Wu T, Wang D, Zhang X, Li J, Yuan B. Comparison of pain relief and limb function improvement after extracorporeal shock wave therapy and thermomagnetic therapy in the treatment of low back pain. *Pak J Med Sci*. 2022;39(1):268–273. doi:10.12669/pjms.39.1.6668
43. Wei HT. Effects of anesthetic soup on the local tissue after acute soft tissue in rats and the beta-endocrine in the lower cavity of the brain [master's thesis] [in Chinese]. Chengdu, China: Chengdu Sport University; 2017.
44. Nielsen A, Knoblauch NTM, Dobos GJ, Michalsen A, Kaptchuk TJ. The effect of gua sha treatment on the microcirculation of surface tissue: A pilot study in healthy subjects. *Explore (NY)*. 2007;3(5):456–466. doi:10.1016/j.explore.2007.06.001
45. Zhang HY, Yang M, Yue RZ. Effects of Gua Sha therapy on inflammatory factors of DRG and serum pain substances in a lumbar disc herniation rat model [in Chinese]. *Lishizhen Medicine and Materia Medica Research*. 2017;28(2):500–503. http://doi.med.wanfangdata.com.cn/10.3969/j.issn.1008-0805.2017.02.090. Accessed October 15, 2023.
46. Yang W, Deng HM, Guo QP. Experimental study and mechanism research of 701 Diedazhentonggao on acute and chronic soft tissue injury in rabbit [in Chinese]. *Journal of Chinese Medicinal Materials*. 2014;37(7):1222–1229. Accessed October 15, 2023.

Development and validation of the antibody-dependent cellular phagocytosis-based signature: A prognostic risk model of gastric cancer

*Qing Zheng[1,D–F], *Zhenqi Gong[1,B], Baizhi Li[1,A–D], Huaiming Wang[1,A–C], Shaoxiong Lin[2,F]

[1] Department of Gastrointestinal Surgery, The First Affiliated Hospital of Shantou University Medical College, China
[2] Department of Otolaryngology, The First Affiliated Hospital of Shantou University Medical College, China

A – research concept and design; B – collection and/or assembly of data; C – data analysis and interpretation;
D – writing the article; E – critical revision of the article; F – final approval of the article

Advances in Clinical and Experimental Medicine, ISSN 1899–5276 (print), ISSN 2451–2680 (online) *Adv Clin Exp Med*. 2025;34(3):433–446

Address for correspondence
Huaiming Wang
E-mail: 17f1hmwang@stu.edu.cn

Funding sources
This work was supported by grants from Guangdong Basic and Applied Basic Research Foundation (grant No. 2021A1515220075), Shantou Science and Technology Bureau (grant No. 2006241552607), "Dengfeng Project" for the construction of high-level hospitals in Guangdong Province – the First Affiliated Hospital of Shantou University Medical College Supporting Funding (grant No. 202003–17), and Guangdong province Medical ReseFundGrant (grant No. A2022419).

Conflict of interest
None declared

*Qing Zheng and Zhenqi Gong contributed equally to this work.

Received on February 24, 2023
Reviewed on March 28, 2024
Accepted on June 11, 2024

Published online on November 18, 2024

Cite as
Zheng Q, Gong Z, Li B, Wang H, Lin S. Development and validation of the antibody-dependent cellular phagocytosis-based signature: A prognostic risk model of gastric cancer. *Adv Clin Exp Med*. 2025;34(3):433–446. doi:10.17219/acem/189914

DOI
10.17219/acem/189914

Abstract

Background. Accumulating evidence has supported the effect of antibody-dependent cellular phagocytosis (ADCP) on the tumor microenvironment (TME) and cancer therapy. However, an ADCP-based signature to predict the prognosis of gastric cancer (GC) has not been established.

Objectives. We aimed to develop an ADCP-based signature to improve the prognosis prediction of GC.

Materials and methods. Antibody-dependent cellular phagocytosis genes that exhibited a differential expression were characterized, followed by the construction and validation of the ADCP-based signature. The potential association between the ADCP-based signature and TME was explored, and the features of the signature genes were investigated. Finally, a predictive nomogram was established based on the ADCP-based signature.

Results. Four ADCP-related genes, *MKNK2*, *VCAN*, *LRAT*, and *GNGB*, were identified to construct the ADCP-based signature, and a high ADCP score predicted an unfavorable prognosis in GC patients ($p < 0.05$). The ADCP-based signature was significantly associated with immune cells, immune checkpoints and immune signaling pathways ($p < 0.05$). Gastric cancer patients with high ADCP scores benefited less from immunotherapy compared to those with low ADCP scores. A nomogram including age, stage and risk score of the ADCP-based signature was constructed to predict the 1-, 3- and 5-year survival probabilities, with an area under the curve (AUC) of 0.669, 0.675 and 0.685, respectively.

Conclusions. The ADCP-based signature may serve as a new option for prognosis prediction and the personalized treatment of GC patients.

Key words: bioinformatics analysis, gastric cancer, tumor microenvironment, prognostic signature, antibody-dependent cellular phagocytosis

Background

Gastric cancer (GC) was the 5th most diagnosed cancer and the 4th most common cause of cancer death in 2020.[1] The incidence and mortality of GC have been reduced in recent years as a result of the prevention and treatment of *Helicobacter pylori* and Epstein–Barr virus (EBV) infections.[2,3] However, the prognosis of GC patients continues to be unsatisfactory due to the impact of locally advanced and distant metastases.[4,5]

Immunotherapy is a promising treatment strategy, but only a fraction of GC patients benefit from it.[6] Also, the immunosuppressive microenvironment of tumors severely reduces the effectiveness of immunotherapy. Therefore, there is a strong need for precise immunotherapy and accurate efficacy prediction using immune-based biomarkers.

Antibody-dependent cellular phagocytosis (ADCP) is the mechanism that leads to the internalization and degradation of target cells through the activation of Fcγ receptors on the surface of macrophages to induce phagocytosis.[7] It has been shown that the ADCP process can influence the evolution of the tumor microenvironment (TME). A previous study has found that rituximab results in the upregulation of multiple Fcγ receptors on macrophages, which correlates with their phagocytic response.[8] In addition, anti-KIT antibodies have been observed to inhibit the growth of gastrointestinal stromal tumors by inducing the phagocytosis of macrophages.[9] These studies suggest that ADCP may regulate the progression of different cancers. Hence, it is valuable to examine the role of ADCP-related genes in the progression of GC, as well as establish a relevant prognostic model for the treatment of GC.

In the present research, we conducted bioinformatics approaches to construct and validate an ADCP-based prognostic signature by employing The Cancer Genome Atlas (TCGA) database and the Gene Expression Omnibus (GEO) database. We further explored the role of the ADCP-based signature in the immune microenvironment. Our study can effectively predict the prognosis of GC patients and may provide new perspectives for the treatment of GC.

Objectives

We aimed to develop a robust ADCP-based signature to improve the predicted prognosis of GC.

Methods

Data collection and processing

RNA-seq data and clinical information on TCGA-STAD were downloaded from the UCSC-Xena platform (https://toil.xenahubs.net), which contained 32 normal tissue samples and 375 tumor tissue samples. The dataset GSE66229 with 300 tumor tissue samples was downloaded from the GEO database for subsequent model validation analysis. A total of 3,405 genes were obtained by downloading ADCP-related genes (Supplementary Table 1) from a study by Kamber et al.[10] and matching them with the above expression profiles. Our workflow is presented in Fig. 1.

Protein–protein interaction network and functional enrichment analysis

The differential expression analysis of ADCP genes was carried out using the R package DESeq2 (v. 1.36.0, https://www.bioconductor.org/packages/release/bioc/html/DESeq2.html). A false discovery rate (FDR) less than 0.05 and a |log2FoldChange| >1 were selected as the threshold for screening differentially expressed genes. The interaction relationship of the differentially expressed genes was analyzed using the Search Tool for the Retrieval of Interacting Genes/Proteins (STRING) database (https://cn.string-db.org/) and imported into Cytoscape (v. 3.9.1) to map the protein-protein interaction (PPI) network. Gene Ontology (GO; http://www.geneontology.org) and Kyoto Encyclopedia of Genes and Genomes (KEGG; http://www.genome.ad.jp/kegg) functional enrichment analysis was conducted using the ClusterProfiler package (v. 4.4.4, https://bioconductor.org/packages/release/bioc/html/clusterProfiler.html).[11]

Construction and verification of the ADCP-based signature

The 2 datasets from TCGA and GEO were log2-transformed and normalized to obey the same distribution, thus eliminating the effect from different batches. Tumor samples from TCGA-STAD were segregated into a training set and a test set with a 6:4 random split. Samples with survival times less than 30 days were filtered, and a total of 342 tumor tissue samples were finally included. In the training set samples, the differentially expressed genes and the survival information of the samples were merged to identify genes strongly related to the overall prognosis for survival using univariate Cox regression analysis performed with the survival package (v. 3.4-0, https://github.com/therneau/survival).[12] The genes were further screened using a 10-fold cross-validation analysis using the executed least absolute shrinkage and selection operator (LASSO) Cox regression model employing the glmnet package (v. 2.0-18, httRiskscore://cran.r-project.org/web/packages/glmnet/index.html).[13] Next, multivariable regression was conducted to further filter the genes. Relying on the gene regression prognostic coefficients and the expression levels of genes in the training set samples, a risk score model was developed; it was derived as follows:

$$\text{risk score} = \Sigma\ (\text{Expi} \times \text{Coefi});$$

Expi and Coefi represent the expression levels and LASSO regression coefficients of prognostic genes.

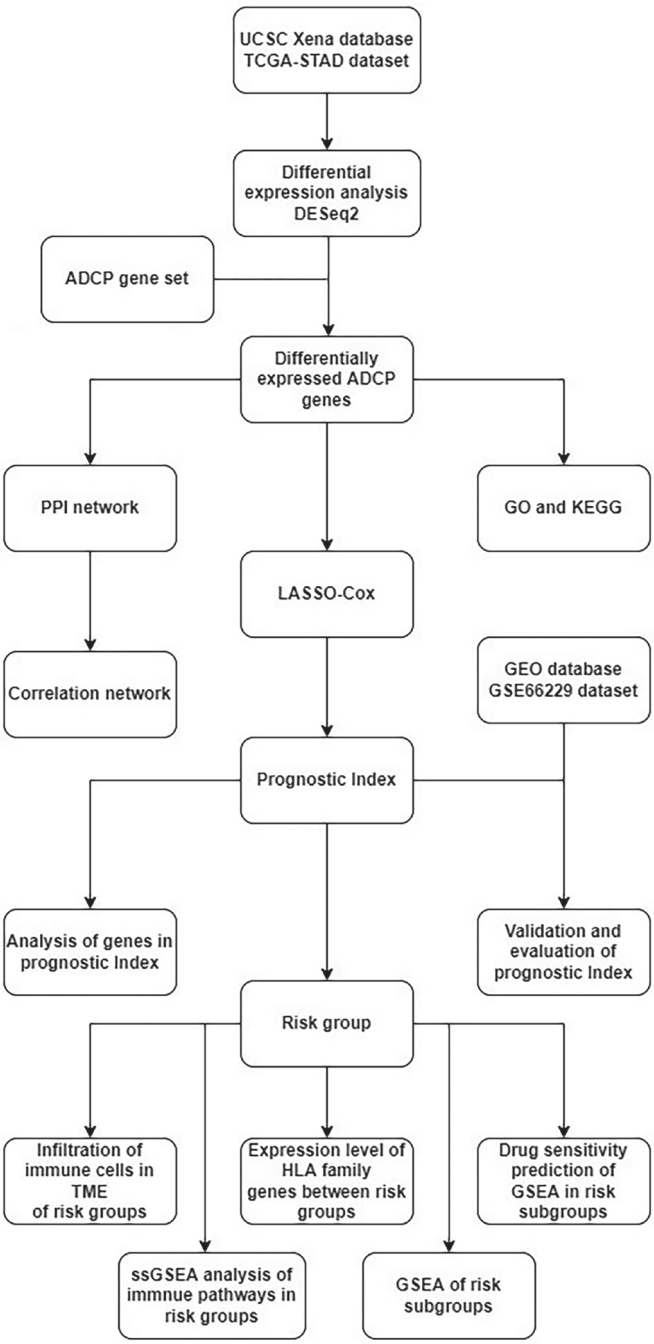

Fig. 1. Study flowchart. Transcriptome data and clinical data were downloaded from TCGA and UCSC Xena. Differential expression analyses were conducted on ADCP-related genes. Protein–protein interaction network and functional enrichment analyses were performed on differentially expressed ADCP-related genes. Four key genes were identified using uni- and multivariable Cox regression as well as the LASSO method to construct an ADCP-based signature. The predictive performance of the ADCP-based signature was validated using GSE66229 from the GEO database. The immune-infiltrating cells, immune pathways and drug sensitivity were explored in risk subgroups defined by the ADCP-based signature

TCGA – The Cancer Genome Atlas; UCSC – University of California Santa Cruz; ADCP – antibody-dependent cellular phagocytosis; PPI – protein-protein interaction; LASSO – Least Absolute Shrinkage and Selection Operator; GEO – Gene Expression Omnibus; STAD – stomach adenocarcinoma; GO – Gene Ontology; KEGG – Kyoto Encyclopedia of Genes and Genomes; TME – tumor microenvironment; HLA – human leukocyte antigen; GSEA – Gene Set Enrichment Analysis; ssGSEA – single-sample Gene Set Enrichment Analysis.

To inspect the correctness of the model, the risk score of each sample from the test set of TCGA and the external validation set of GEO was calculated using the same regression coefficients according to the risk score calculation formula. The samples from the 2 aforementioned validation sets were differentiated based on the median risk score as the cutoff. The overall survival (OS) of each group was assessed using Kaplan–Meier curves. We then plotted the 1-, 3- and 5-year receiver operating characteristic (ROC) curves using the R package survival ROC (v. 1.0.3, https://cran.rstudio.com/web/packages/survivalROC/index.html) and calculated the 1-, 3- and 5-year area under the curve (AUC) values, respectively.

Prognostic characterization of genes in the model and construction of ceRNA networks

We used the TCGA-STAD dataset for survival analysis of the ADCP-related genes in the signature. The multiMiR package was used to predict gene-associated microRNAs (miRNAs) in the model. Starbase was then used to predict lncRNAs that interact with miRNAs, and the CHEA3 database (https://maayanlab.cloud/chea3) was used to predict transcription factors (TFs) of the model genes. All results were imported into Cytoscape (https://cytoscape.org) to construct a competitive endogenous RNA (ceRNA) network.

Characteristics of the TME and GSEA in different subgroups

To further examine the immune microenvironment in high- and low-risk groups, Estimation of STromal and Immune cells in MAlignant Tumours using Expression data (ESTIMATE),[14] Cell-type Identification by Estimating Relative Subsets of RNA Transcripts (CIBERSORT),[15]as well as single-sample gene set enrichment analysis (ssGSEA) algorithms were utilized to obtain TME scores and immune cell scores. Moreover, we extracted immune gene-related pathways through the immport database (https://www.immport.org/home). To assess immune pathway variations between high- and low-risk groups, the ssGSEA algorithm was used to calculate the immune pathway scores of cancer samples. We also captured expression data of human leukocyte antigen (HLA) family genes and immune checkpoint-associated genes to analyze their differential expression in high- and low-risk groups. Gene Set Enrichment Analysis (GSEA) was performed using the ClusterProfiler package (v. 3.18.0)[11] to observe significant pathways enriched in the high- and low-risk groups.

Drug sensitivity and immunotherapy efficacy prediction

The sensitivity of patients to chemotherapeutic agents was evaluated using Genomics of Drug Sensitivity in Cancer

(GDSC; https://www.cancerrxgene.org).[16] The R software package pRRophetic (v. 0.5, https://github.com/paulgeeleher/pRRophetic) was used to determine half-maximal inhibitory concentrations (IC50). We evaluated the differential in drug sensitivity between high- and low-risk groups. The Tumor Immune Dysfunction and Exclusion (TIDE) method was used to predict the benefit of immune checkpoint inhibitor (ICI) treatment in patients with GC.

Construction of nomogram

Clinical risk models were constructed using univariate and multivariate Cox regression analyses. Next, clinical risk values were calculated for all samples of TCGA-STAD. The prognosis was assessed using Kaplan–Meier curve analysis, and to test the clinical risk model, ROC curves were generated. The calibration curve analysis of the model was assessed using the R package rms (v. 6.3-0, https://hbiostat.org/r/rms). Using the R package dcurves (v. 0.3.0, https://github.com/ddsjoberg/dcurves), decision curve analysis (DCA) decision curves were produced to evaluate the clinical risk model.

Statistical analyses

All analyses were conducted in R v. 4.2.1 (R Foundation for Statistical Computing, Vienna, Austria), and a p-value of 0.05 or less was deemed statistically significant. Univariate and multivariate Cox regression analyses were performed to identify genes and clinical parameters significantly associated with the OS prognosis. Schoenfeld residual plots (conducted by the ggcoxzph function of the survival R package) were used to assess the proportional hazards assumption, which determines whether the effect of the variable on the hazard function is constant over time. The log-rank test was used to compare the differences in survival distributions. A Wilcoxon test was used to compare the differences in medians between samples. The key R-script used in this study can be found in the Supplementary materials.

Results

Differentially expressed ADCP genes and their function in GC

The TCGA dataset was used to obtain the differential expression matrix of GC, which was intersected with ADCP-related genes to obtain 531 differentially expressed ADCP-related genes (238 of them were upregulated and 293 were downregulated, Fig. 2A, Supplementary Table 2). The most significantly up- and downregulated genes were plotted as a heat map (Fig. 2B), with a total of 20 included. These 531 differentially expressed ADCP-related genes were mapped into a PPI network (Fig. 2C, Supplementary Table 7) through the STRING database. Gene Ontology (Fig. 2D, Supplementary Table 3) and KEGG analysis (Fig. 2E, Supplementary Table 4) were used to explore the functions of the 531 genes. Functional investigation of differentially expressed ADCP-related genes revealed that they were involved in the p53 signaling pathway, PI3K/Akt signaling pathway, calcium signaling pathway, and platinum drug resistance (Fig. 2E), which suggested the possible role of ADCP genes in cancer progression and metastasis.

Development and validation of ADCP-based signature

Based on the above 531 differential genes, univariate Cox regression was applied using the TCGA-STAD training set to detect 7 prognosis genes (*ADAMTS12*, *MKNK2*, *VCAN*, *MMP1*, *CLDN9*, *LRAT*, and *GNG8*; Fig. 3A, Supplementary Table 5). The results of the proportional hazards assumption can be found in Supplementary Fig. 1. To further screen the prognostic markers of GC, LASSO regression was employed to identify the prognostic genes acquired from the above univariate Cox regression. The optimal λ was obtained when the partial likelihood of deviance reached the minimum value (Fig. 3B,C). Four prognosis-associated genes (*MKNK2*, *VCAN*, *LRAT*, and *GNGB*; Fig. 3D, Supplementary Table 6) were available to construct ADCP-related gene signatures after performing multivariate Cox regression. Based on the median risk score, the samples from the training set were separated into a high-risk group (risk score >median risk score) and a low-risk group (risk score ≤median risk score). The ROC curve was plotted to display the 1-, 3- and 5-year AUC for the training set. Validation of the model was conducted in the TCGA test set and the GEO external validation set, indicating a good predictive performance of the model (Fig. 3E). The prognosis differed significantly between the 2 groups, with patients in the high-risk score group presenting a poorer prognosis. In the TCGA-STAD training cohort of 206 GC patients, those with high-risk scores (50%) had a shorter OS (p = 5e-07) than those with low-risk scores (50%). High-risk patients (52.941%) had a shorter OS than low-risk patients (47.059%) across all 136 GC patients in the TCGA-STAD test cohorts (p = 0.003; Fig. 3F). To identify whether or not the ADCP-based signature was reliable, the accuracy of the ADCP-based signature was evaluated using the GEO external validation cohort, with a total of 300 GC patients participating in this study. As seen in Fig. 3F, high-risk patients (49%) had a shorter OS than the low-risk group (51%) (p = 5e-05). The prognostic information of the 4 genes in the signature was demonstrated using a Kaplan–Meier curve, while 3 genes showed significant prognostic value in GC. Between the MKNK2 subgroups, no OS differences were observed (log-rank test, p = 0.151, Fig. 4A). In the VCAN high-expression group, GC patients were found to have a lower survival probability

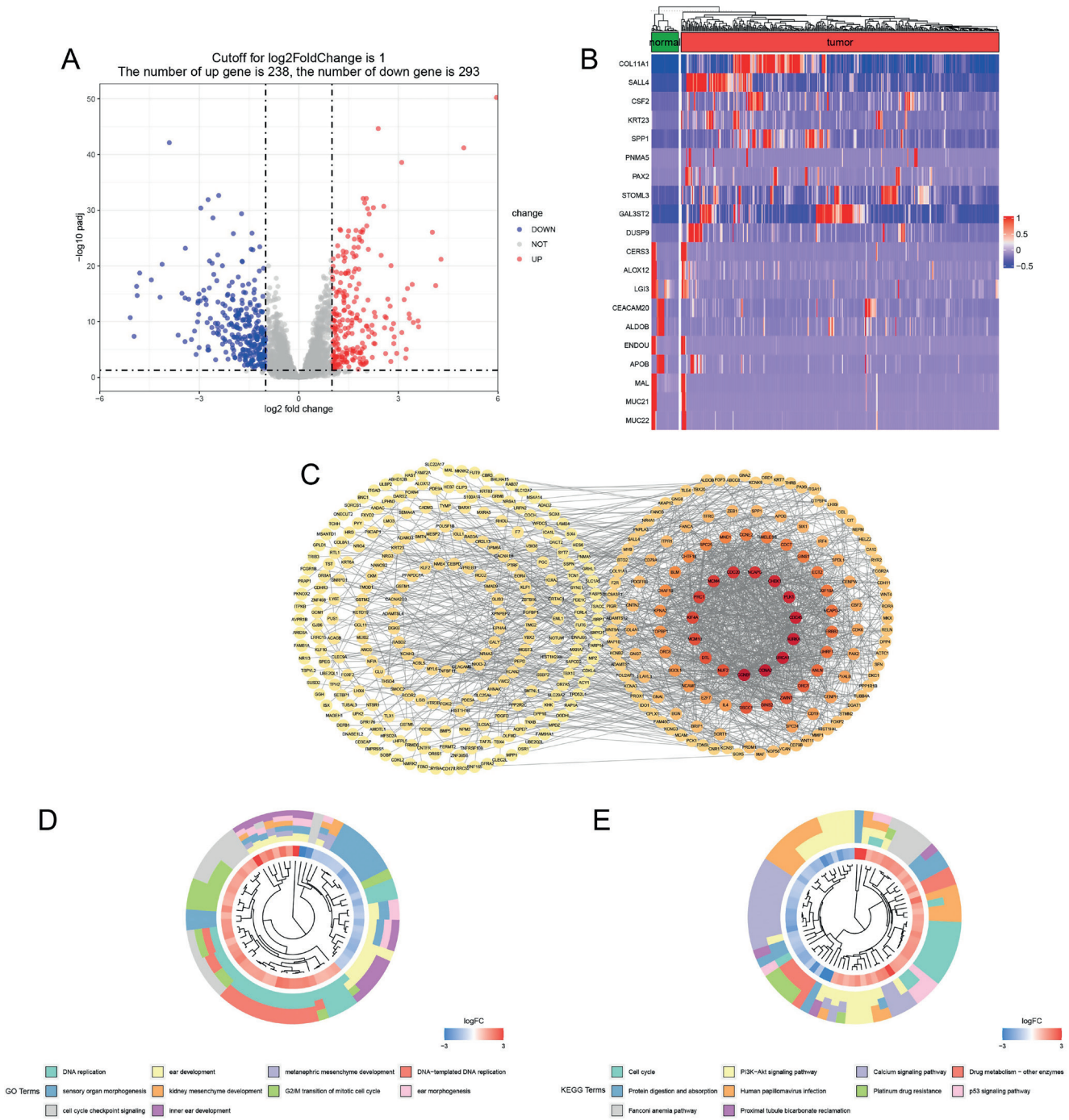

Fig. 2. Identification and characterization of differentially expressed ADCP-related genes. A. A volcano plot representing the 531 differentially expressed ADCP genes (238 of them were upregulated and 293 were downregulated) with a threshold of FDR less than 0.05 and a |log2FC| > 1; B. A heat map containing the 20 most significantly up-and downregulatedADCP genes between normal and tumor samples; C. The PPI network of 531 differentially expressed ADCP-related genes; D–E. GO (D) and KEGG (E) and analysis exploring the functions of the 531 genes

ADCP – antibody-dependent cellular phagocytosis; PPI – protein–protein interaction; FDR – false discovery rate; FC – fold change; GO – Gene Ontology; KEGG – Kyoto Encyclopedia of Genes and Genomes.

(log-rank test, p = 0.027, Fig. 4B). Also, in the LRAT high-expression group, GC patients had a significantly lower OS (log-rank test, p = 0.01, Fig. 4C). The high *GNG8* expression group indicated a more favorable prognosis (log-rank test, p = 0.011, Fig. 4D). Based on the 4 genes, 61 miRNAs were predicted using multiR, and 52 lncRNAs were further predicted with starbase (http://starbase.sysu.edu.cn), followed by the TFs of genes predicted with the CHEA3 database, and the top 10 TFs of meanRank were selected. Genes, miRNAs, lncRNAs, TFs, and interactions between them were imported into Cytoscape to map the ceRNA-TF network.

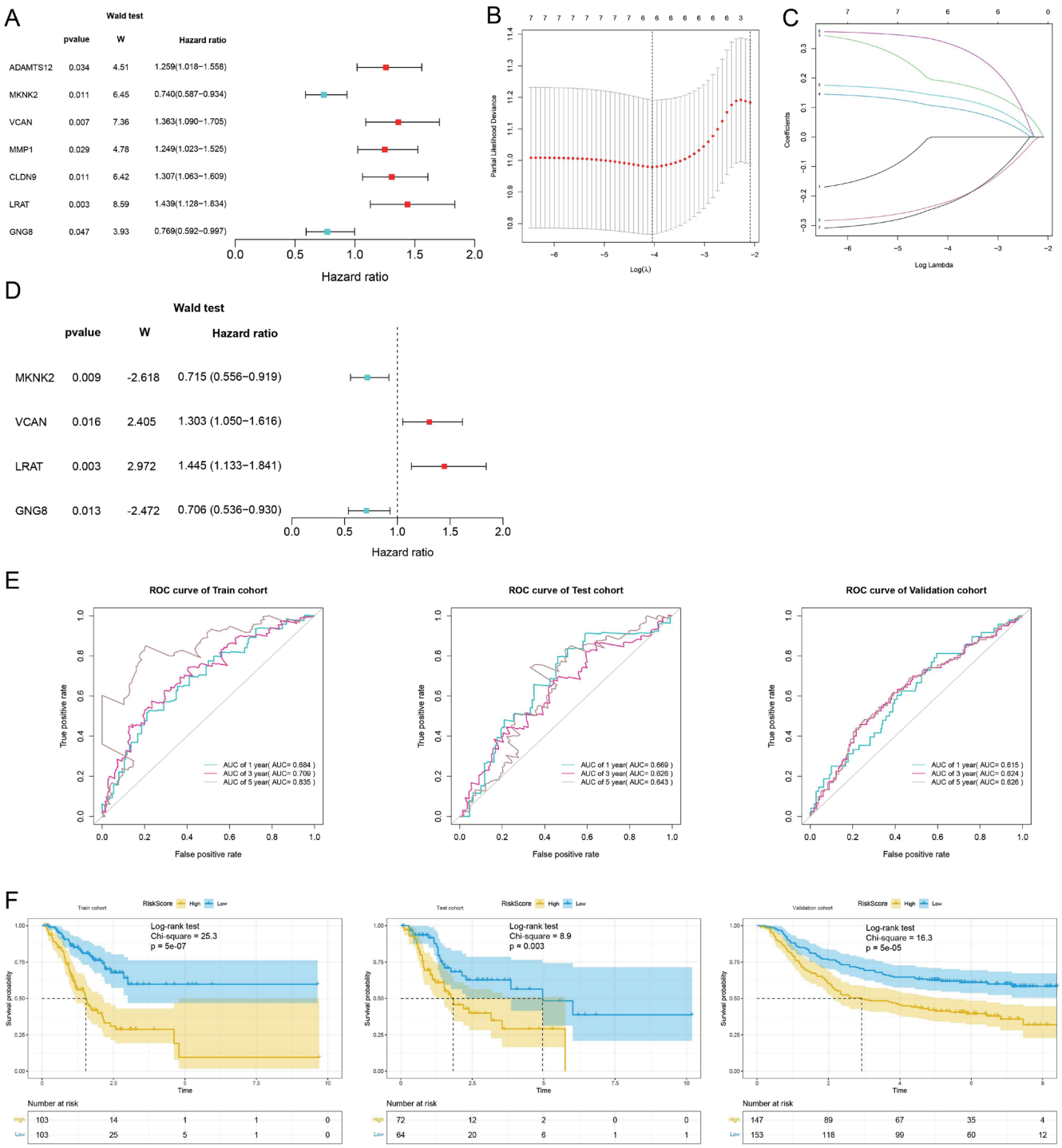

Fig. 3. Construction and validation of an ADCP-based signature. A. Univariate Cox regression analysis identified 7 ADCP-related genes with prognostic value (*ADAMTS12*, *MKNK2*, *VCAN*, *MMP1*, *CLDN9*, *LRAT*, and *GNG8*); B. Selection of the tuning parameter (λ) in the least absolute shrinkage and selection operator (LASSO) regression with a 10-fold cross-validation as the minimum criteria; C. LASSO coefficient profiles for clinical features and 6 non-zero coefficients were selected; D. Four genes (*MKNK2*, *VCAN*, *LRAT*, and *GNG8*) were selected by multivariate Cox regression analysis; E. Receiver operating characteristic (ROC) curves to display the 1-, 3- and 5-year area under the curve (AUC) in the train cohort, test cohort and validation cohort; F. Survival differences between low- and high-risk groups in the training cohort (log-rank test, p = 5e-07), test cohort (log-rank test, p = 0.003) and validation cohort (log-rank test, p = 5e-05)

ADCP – antibody-dependent cellular phagocytosis; ADAMTS12 – a disintegrin and metalloproteinase with thrombospondin motifs 12; MKNK2 – threonine kinase 2/MAP kinase interacting serine; VCAN – versican; MMP1 – matrix metallopeptidase 1; CLDN9 – claudin 9; LRAT – lecithin retinol acyltransferase; GNG8 – G protein subunit gamma 8.

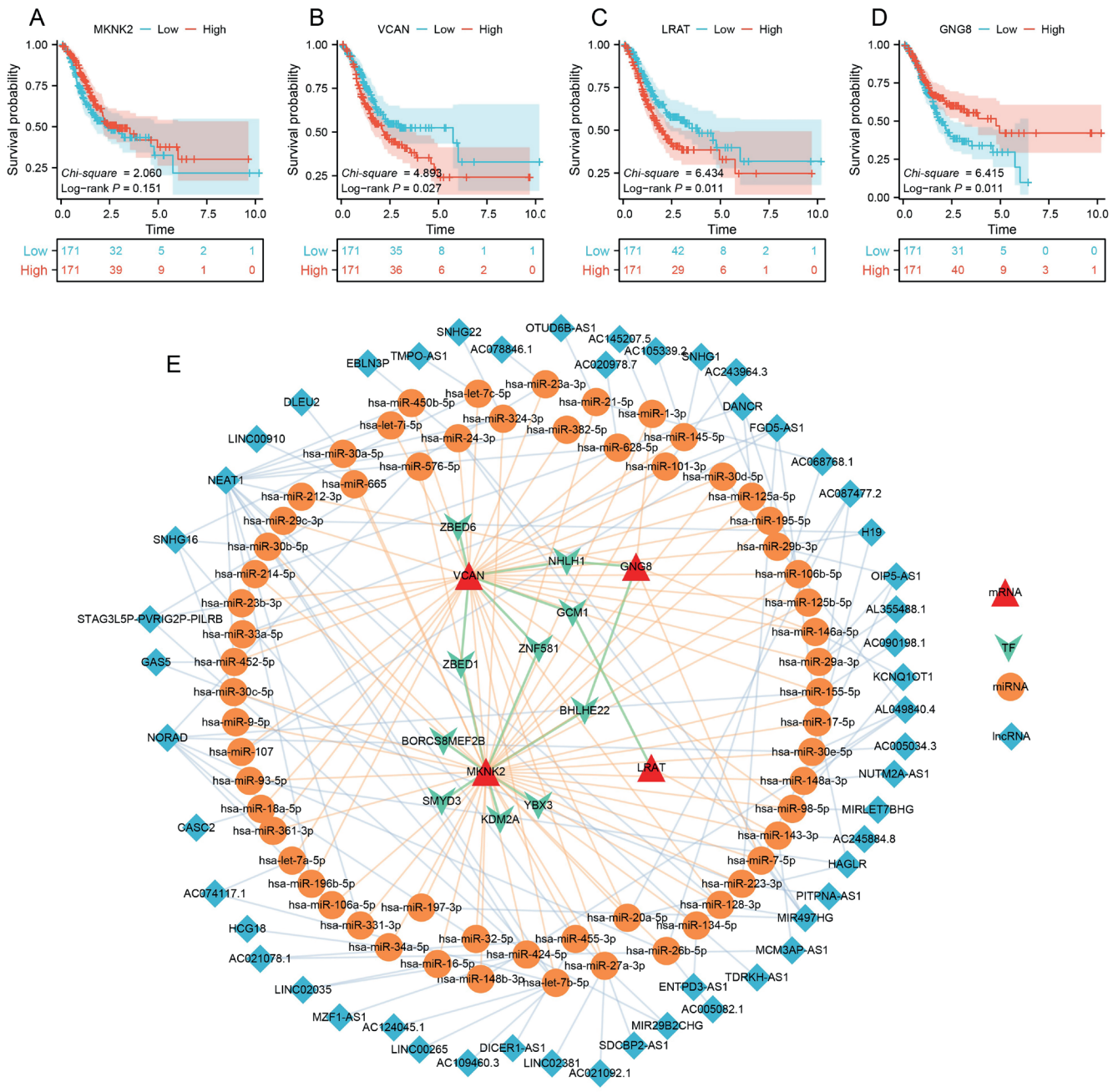

Fig. 4. Survival estimation and PPI network of the signature genes. A–D. Survival differences between low- and high-expression groups of MKNK2 (A) (log-rank test, p = 0.151), VCAN (B) (log-rank test, p = 0.027), LRAT (C) (log-rank test, p = 0.011) and GNG8 (D) (log-rank test, p = 0.011); E. ceRNA-TF network based on the selected genes, miRNAs, lncRNAs, and transcription factors

PPI – protein–protein interaction; MKNK2 – threonine kinase 2/MAP kinase interacting serine; VCAN – versican; LRAT – lecithin retinol acyltransferase; GNG8 – G protein subunit gamma 8; ceRNA – competing endogenous ribonucleic acid; TF – transcription factors; miRNA – microRNA; lncRNA – long non-coding ribonucleic acid.

ADCP-based signature in TME

To gain further insight into the involvement of ADCP-based signature in TME, we used the CIBERSORT (Fig. 5A), ssGSEA (Fig. 5B) and ESTIMATE (Fig. 5C) algorithms to explore the immune infiltration in subgroups. A higher percentage of M2 macrophages was observed in the high-risk score group from the result of CIBERSORT, while T cells CD8$^+$ accounted for a smaller percentage compared to the low-risk score group (Fig. 5A, Supplementary Table 8). The ssGSEA algorithm showed a higher percentage of regulatory T cells (Tregs), as well as a lower percentage of activated CD8$^+$ T cells and activated B cells in the high-risk group (Fig. 5B, Supplementary Table 9). The ESTIMATE algorithm also confirmed the differences in immune infiltration between the high- and low-risk groups (Fig. 5C). In the following work, we analyzed the connection between signature genes and immune cells. As shown in Fig. 5D, VCAN had a significant correlation

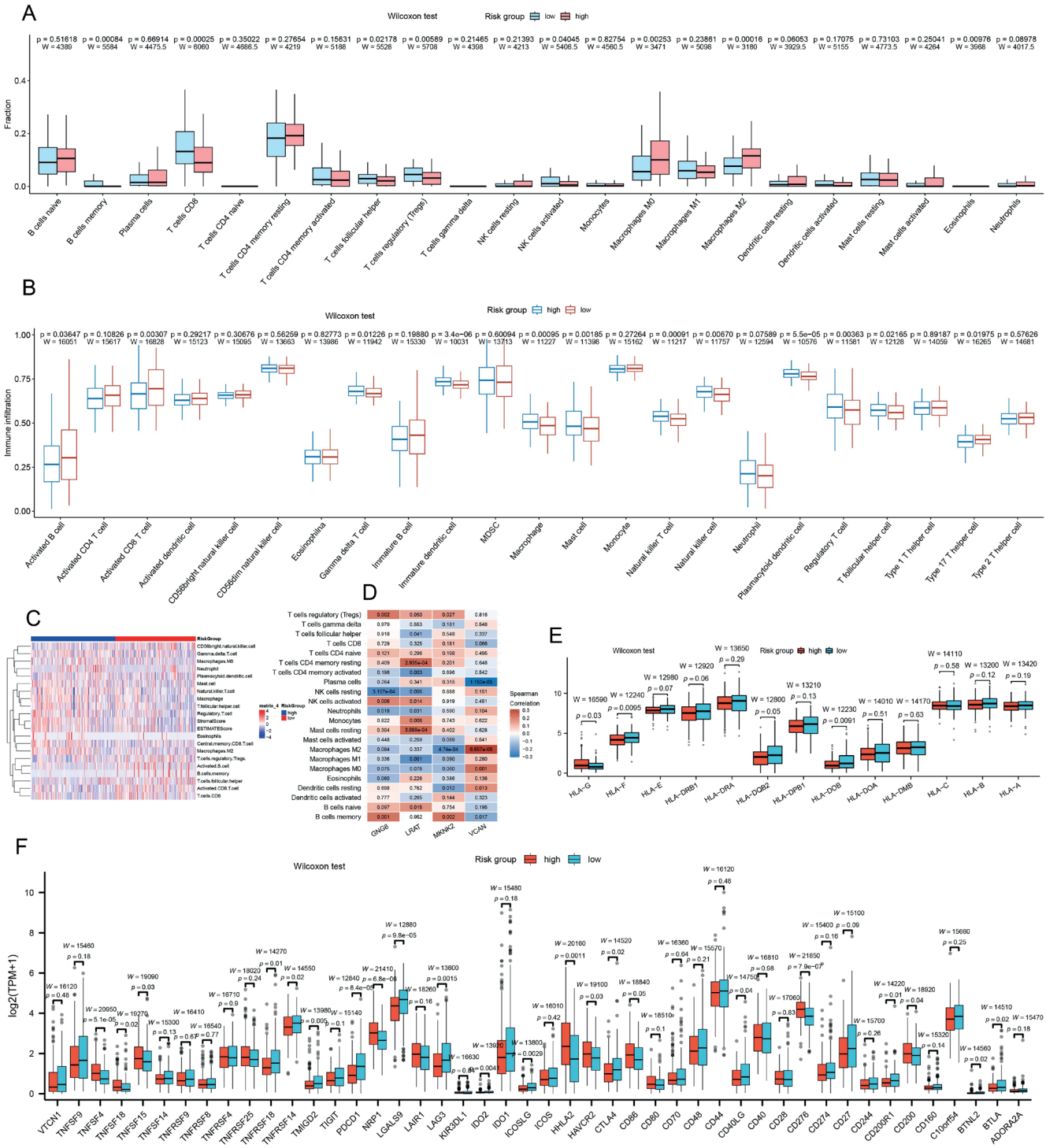

Fig. 5. Immune cell infiltration and immunomodulators of the ADCP-based signature. A,B. Differences in the abundance of immune cell infiltration in high- and low-risk groups using CIBERSORT (A) and ssGSEA (B) algorithms; C. Heat map of immune infiltration between high- and low-risk groups using the CIBERSORT and ESTIMATE algorithms; D. Heat map of the correlation between model genes and differential immune cells using CIBERSORT; E. Differences in the expression of HLA family genes between high- and low-risk groups; F. Differences in the expression of immune checkpoints between high- and low-risk groups

ADCP – antibody-dependent cellular phagocytosis; CIBERSORT – Cell-type Identification by Estimating Relative Subsets of RNA Transcripts; ESTIMATE – Estimation of STromal and Immune cells in MAlignant Tumours using Expression data; ssGSEA – single-sample Gene Set Enrichment Analysis; HLA – human leukocyte antigen.

with M2 macrophages. GNG8 was positively correlated with Tregs and was negatively correlated with activated natural killer cells (Supplementary Table 10). Surprisingly, HLA gene expression and immune checkpoint gene expression varied significantly across the 2 risk groups (Fig. 5E,F, Supplementary Tables 11,12).

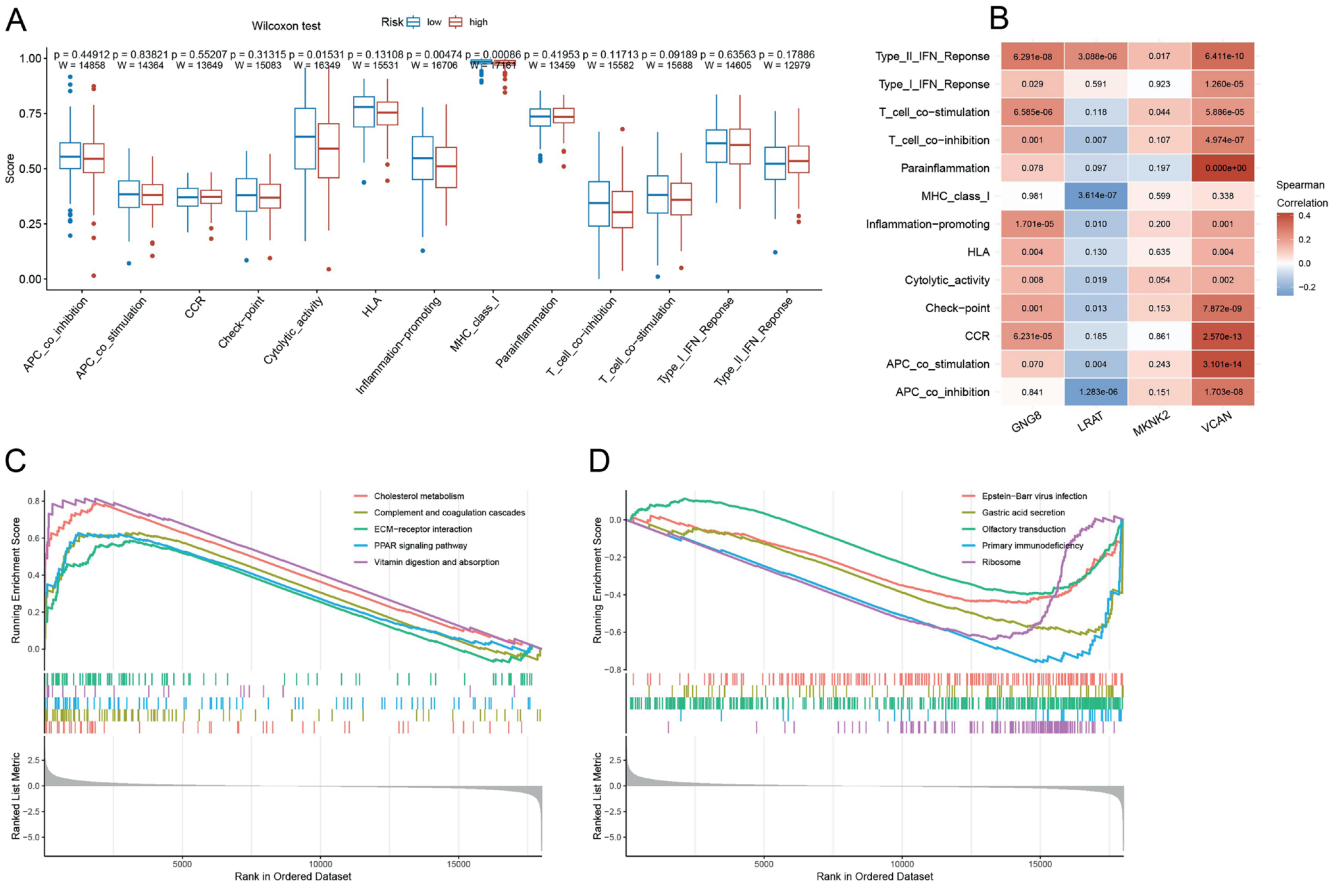

Fig. 6. Immune pathways of the ADCP-based signature. A. Box plots presenting the differences in immune pathway enrichment scores between high- and low-risk groups using ssGSEA; B. Heat map of the correlation between model gene expression and immune pathways using ssGSEA; C,D. High- (C) and low-risk (D) and groups significantly enriched in the different pathways using GSEA

ADCP – antibody-dependent cellular phagocytosis; ssGSEA – single-sample Gene Set Enrichment Analysis; GSEA – Gene Set Enrichment Analysis.

To further characterize the effect of the ADCP-based signature on the TME, we examined the variations of immune pathways between the subgroups. The ssGSEA method was used to provide an estimated value for each cancer sample's immune pathway, which is presented in Fig. 6A and Supplementary Table 13. The association of 4 key genes in the signature with immune-related pathways was also explored (Fig. 6B, Supplementary Table 14). A comparative study of significantly enriched pathways between subgroups was accomplished using GSEA, and the 5 most strongly associated pathways were selected for presentation (Fig. 6C,D, Supplementary Table 15).

Drug sensitivity and immunotherapy efficacy prediction

As shown in Fig. 7A, patients with high-risk scores exhibited a higher TIDE scoring. Nine compounds with sensitization differences in the high- and low-risk groups were illustrated. In the high-risk group of ADCP-based signatures, the IC50 of GNF.2, Z.LLNle.CHO, AP.24534, imatinib, NSC.87877, NVP.TAE684, pazopanib, X17.AAG, and PHA.665752 were significantly lower when compared with the low-risk group (Fig. 7B).

Construction of nomogram

Univariate Cox analysis of the risk score and clinical parameters (age, gender, stage, and grade) demonstrated that age, stage, and risk scores could serve as prognostic factors for GC patients (Supplementary Fig. 2). With additional multivariate Cox regression analysis, a clinical risk model consisting of 3 independent prognostic factors: age, stage and risk score (Fig. 8A) was finally constructed as a nomogram (Fig. 8B). The Kaplan–Meier curve demonstrated that patients with high nomogram scores have a more unfavorable prognosis (Fig. 8C; log-rank test, p = 1.77e-06). The AUC values for 1, 3 and 5 years shown in the ROC curves (Fig. 8D) were 0.669, 0.675 and 0.685, respectively. Calibration curves (Fig. 8E), as well as DCA curves (Fig. 8F), were evaluated for the nomogram, implying it has a good level of predictive accuracy.

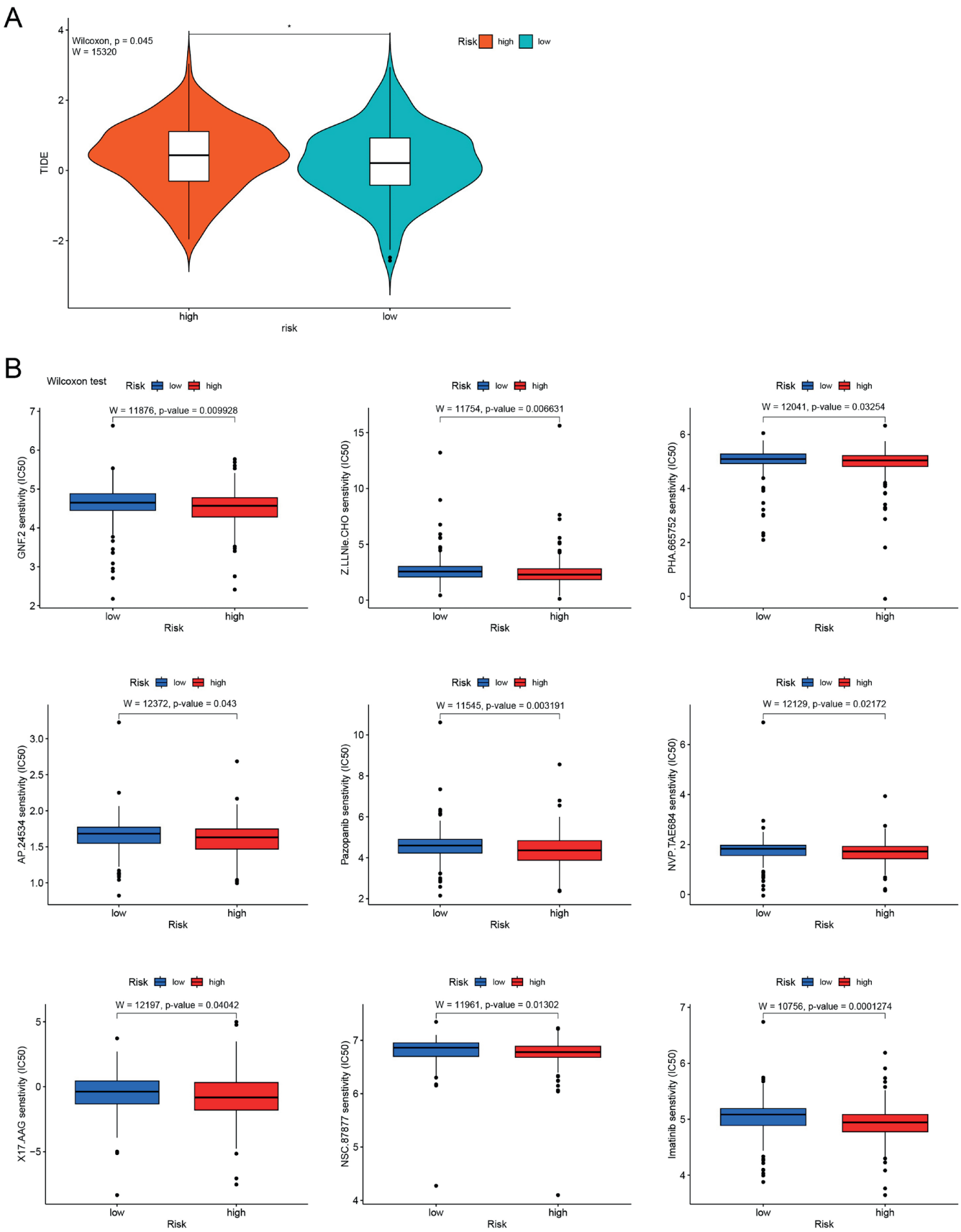

Fig. 7. Analyses of drug sensitivity and immunotherapy responses between subgroups. A. The TIDE score was more enriched in the high-risk group; B. The pRRophetic algorithm showed 9 compounds that are more effective for high-risk patients

TIDE – Tumor Immune Dysfunction and Exclusion.

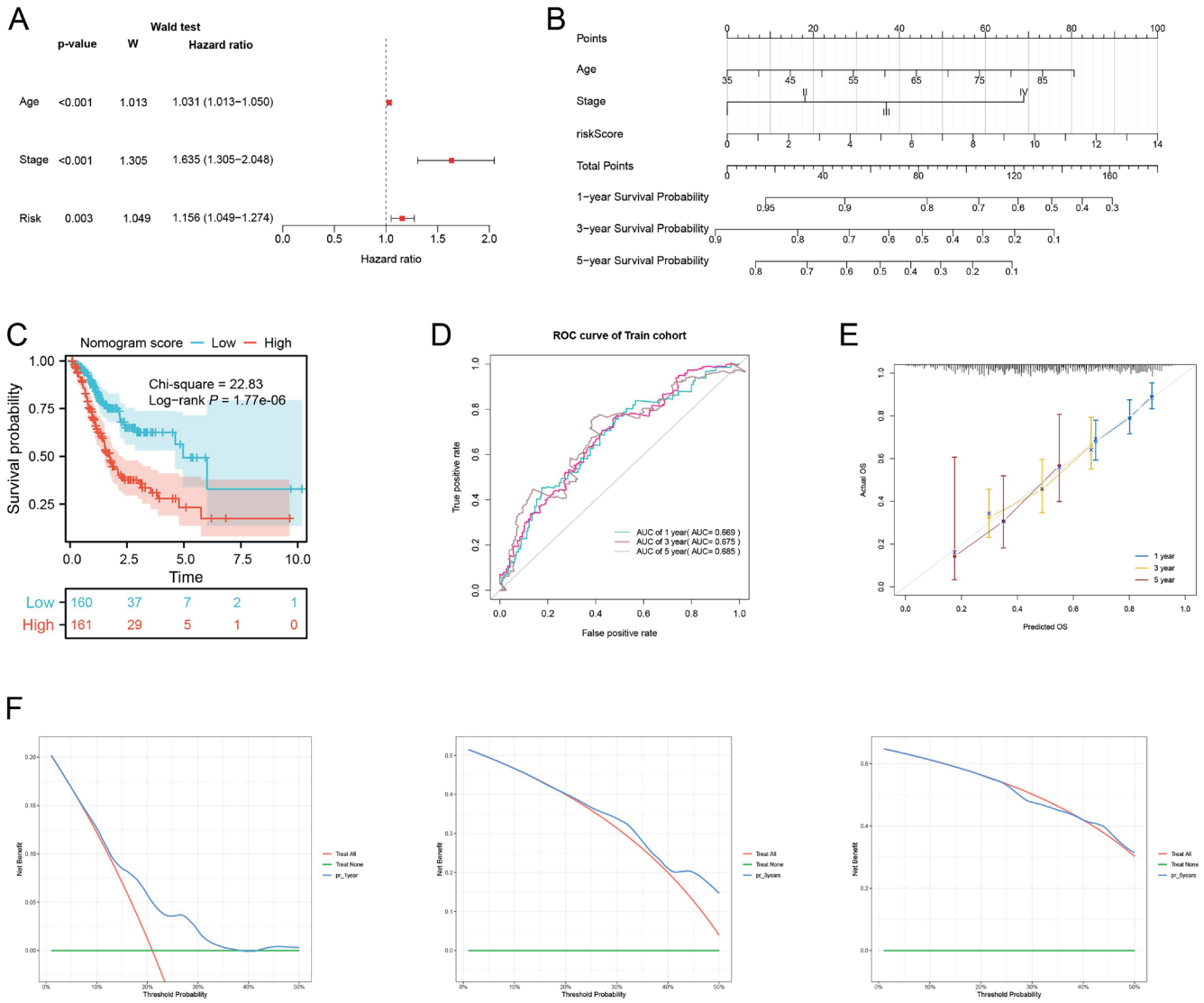

Fig. 8. Construction of nomogram. A. Multivariate Cox analysis revealed 3 independent prognostic factors (age, stage and risk score); B. A predictive nomogram based on age, stage and risk score; C. Overall survival estimation of nomogram score subgroups (log-rank test, p = 1.77e-06); D. ROC curves showed that the 1-, 3- and 5-year AUC reached 0.669, 0.675 and 0.685 in the TCGA train cohort, respectively; E. The 1-, 3- and 5-year calibration curves of the nomogram; F. The 1-, 3- and 5-year DCA decision curves of the nomogram.

ROC – receiver operating characteristic; AUC – area under the curve; TCGA – The Cancer Genome Atlas; DCA – decision curve analysis

Discussion

Due to the heterogeneity of GC, the survival durations among patients exhibits huge variation, which covers a range from 5 months to 10 years.[17,18] Patients with early-stage localized GC have a 5-year OS rate above 60%, while in those diagnosed with distant metastasis, it is lower than 5%.[19] Encouragingly, the exploration of reliable biomarkers through bioinformatics has demonstrated remarkable potential in clinical applications. It was recognized that prognostic signatures derived from multiple genes exhibited a significant role in the survival prediction of malignancies. We built an ADCP-based prognostic signature incorporating TCGA data and verified its practicability using the GEO dataset, as well as researching its characteristics with TME. The signature correlates with multiple immune cells and immune checkpoints. Additionally, differential drug sensitivities and immune efficacies were detected in the subgroups.

The 4 genes in the ADCP-based signature (*MKNK2*, *VCAN*, *LRAT*, and *GNGB*) have been reported in association with the progression of cancer. As in previous studies, *MKNK2* (threonine kinase 2/MAP kinase interacting serine) has been considered an oncogene, which acts as a mediator of various cellular processes to promote the development of prostate cancer and gliomas.[20,21] Furthermore, it has been discovered that *MKNK2* can be targeted by miR-125b, leading to the progression of breast cancer.[22] A previous study also demonstrated that *MKNK2* contributes to the enhancement of chemoresistance of ovarian cancer by inhibiting autophagy through miR-125b.[23] Versican (VCAN) accumulates in tumor cells and

mesenchyme as a protein and is regulated by cytokines. In cancer research, it has been proven that VCAN is involved in the progression of GC. Moreover, VCAN has been recognized as an independent prognostic predictor of GC.[24] Lecithin retinol acyltransferase (LRAT) converts retinol to retinyl esters, regulating cell growth and differentiation.[25] Researchers have demonstrated a significant loss of LRAT expression in invasive bladder cancer, correlating with an increasing tumor stage.[26] G protein subunit gamma 8 (GNG8) participates in chemokine signaling that controls leukocyte migration across the endothelium, which may have a potential implication for the TME.[27]

As research on the TME deepens, the development of new immunotherapy regimens targeting the TME is becoming a major field of interest for cancer treatment. Given that the characteristics of the TME can influence the efficacy of immunotherapy, we focused on the role of ADCP signatures in the TME. The high-risk group of ADCP signatures exhibited a lower probability of survival, resulting from the suppression of the TME. As an important component of the TME, M2 macrophages can secrete undesirable cytokines, thus promoting tumor angiogenesis and tumor metastasis, which is detrimental to patient prognosis. A larger percentage of M2 macrophages was found in the high-risk group, while CD8 T cells, the main contributor that kills tumor cells, displayed a significant proportional decline. Interestingly, there are differential infiltrations of Tregs between the high- and low-risk groups. Tregs are key immune cells with immunosuppressive abilities in the TME, which exert effects through mechanisms such as secreting cytokines, limiting the activation of $CD4^+$ helper T cells and $CD8^+$ cytotoxic T cells, and regulating antigen-presenting cell (APC) functions.[28–33] This hinders GC patients from benefiting from ICI therapy. Targeting Tregs holds great potential for reshaping the GC immune microenvironment, enhancing anti-tumor immune responses and improving the OS rate of GC patients. This study stratified GC patients based on ADCP-related genes at the transcriptomic level and also stratified the abundance of Tregs. For GC patients with high Treg activity, traditional ICIs may not be sufficient to fully activate anti-tumor immune responses. In this case, adopting additional strategies to inhibit Treg activities becomes an effective supplementary approach.

Our functional enrichment analysis further suggested that the ADCP model regulates the TME through multiple immune pathways and has a strong immune characteristic. Considering high-risk patients may not benefit as much from immunotherapy, we screened for sensitive and effective compounds for high-risk patients and found that they are more sensitive to pazopanib and imatinib. Notably, imatinib and pazopanib are both tyrosine kinase inhibitors. In addition to the 2 targeted drugs, some chemical drugs were also identified; however, most are limited to cellular experiments. Moreover, traditional cancer chemotherapy based on chemical drugs is prone to drug resistance and toxic side effects. As an improved form of chemotherapy, metronomic chemotherapy involves administering low doses of drugs continuously without long breaks, which can help avoid these 2 drawbacks. More than 10 years ago, Chinese scholars demonstrated the efficacy and good tolerability of metronomic capecitabine for palliative treatment of advanced GC patients after fluoropyrimidine-based chemotherapy.[34] Furthermore, the good tolerability and potential durable anti-tumor activity of metronomic capecitabine in patients with hepatocellular carcinoma undergoing sorafenib treatment was also confirmed.[35] Mechanistically, metronomic chemotherapy works by inhibiting tumor angiogenesis and inducing immunogenic cell death (ICD), thereby regulating vascular–immune crosstalk.[36] As a result, the combination of metronomic chemotherapy with ICIs has shown synergistic therapeutic effects in preclinical and clinical studies. Especially for high-risk patients, the combination of both may be an effective approach. Unfortunately, metronomic chemotherapy is currently used as a palliative standard care tool. Utilizing bioinformatic methods to identify biomarkers can benefit metronomic chemotherapy and may expand the role of metronomic chemotherapy in cancer therapy.

To more accurately exploit the predictive ability of the ADCP signature, we combined univariate and multivariate analysis with Cox regression and eventually constructed a nomogram selecting age, stage and risk scores. This nomogram visualized the logistic regression model to facilitate rapid clinical judgment on the prognosis of GC patients. The AUC curve demonstrated that the model predicted the prognosis of GC patients with reliable accuracy. The calibration curve illustrates that the predicted probability of patient survival is in good agreement with the actual probability, and its clinical application can be attempted.

Limitations

Despite the fact that this research made some contributions, it did have several shortcomings. First, although our work evaluated high sample sizes of GC cohorts to construct a well-validated prognostic signature, the use of diverse platforms might generate sampling bias, which may induce some ambiguity in the assessments of gene expression. Second, the underlying mechanisms by which the 4 genes (*MKNK2*, *VCAN*, *LRAT*, and *GNGB*) that were combined into the ADCP signature in our investigation contributed to GC progression, and the unfavorable outcome still remains unexplained; additional in-depth research into their biological functions might generate fresh targets and therapeutic strategies. Third, recognizing that these cohorts are merely retrospective, more prospective clinical studies are necessary to confirm our results. In particular, future research needs to evaluate the predictive function of the ADCP signature throughout

both prognosis and the responsiveness to different kinds of treatment interventions. Finally, the accuracy of CIBERSORT and ssGSEA is limited by the representativeness of the training data and the assumptions of the algorithms themselves, leading to biases in assessing the levels of immune cell infiltration. These 2 algorithms mainly focus on the composition and proportion of immunocytes, with limited evaluation of their functional states. This calls for the adoption of more validated algorithms to analyze immunocytes and to compare algorithm performance through methods like cross-validation. Additionally, integrating multi-omics data, including gene expression, proteomics and metabolomics data, is essential for inferring the functional states of immune cells.

Conclusions

We identified 4 prognosis-associated genes that were related to OS and the TME in GC by also constructing a model with strong predictive effects. To the best of our knowledge, this report is the first effort to develop a prognostic signature of ADCP-related genes for GC. Our study offers a novel option for the diagnosis and prediction of GC and may contribute new biomarkers for the treatment of GC.

Ethical approval

This article does not contain any studies with human participants or animals performed by any of the authors. Therefore, no ethical approval or consent was required. No administrative permission and/or licenses were acquired for this study to access the original data used in this research.

Supplementary data

The Supplementary materials are available at https://doi.org/10.5281/zenodo.11065549. The package includes the following files:

Supplementary Fig. 1. Proportional hazards assumption based on Schoenfeld's global and individual test. (A–D) The p-values of the Schoenfeld's global test are all greater than 0.05 in gene selection using univariate Cox regression (A) and multivariate Cox regression (B), selection of ADCP-based signature and clinical features using univariate cox regression (C), and multivariate Cox regression (D).

Supplementary Fig. 2. Selection of ADCP-based signature and clinical parameters using univariate Cox regression.

Supplementary Table 1. Antibody-dependent cellular phagocytosis-related genes.

Supplementary Table 2. 531 differentially expressed antibody-dependent cellular phagocytosis-related genes.

Supplementary Table 3. Results of GO.

Supplementary Table 4. Results of KEGG.

Supplementary Table 5. Selection of antibody-dependent cellular phagocytosis-related genes with prognostic value using univariate Cox regression analysis.

Supplementary Table 6. Selection of antibody-dependent cellular phagocytosis-related genes with prognostic value using multivariate Cox regression analysis.

Supplementary Table 7. Node information of protein-protein interactions.

Supplementary Table 8. Wilcoxon test results of immunocyte infiltration between risk subgroups using CIBERSORT.

Supplementary Table 9. Wilcoxon test results of immunocyte infiltration between risk subgroups using ssGSEA.

Supplementary Table 10. Spearman correlation results of immunocyte infiltration and signature genes using CIBERSORT.

Supplementary Table 11. Wilcoxon test results of HLA gene expression between risk subgroups.

Supplementary Table 12. Wilcoxon test results of immune checkpoint expression between risk subgroups.

Supplementary Table 13. Wilcoxon test results of immune pathways between risk subgroups using ssGSEA.

Supplementary Table 14. Spearman correlation results of immune pathways and signature genes using ssGSEA.

Supplementary Table 15. GSEA results between risk subgroups.

Data availability

The datasets generated and/or analyzed during the current study are available from the corresponding author on reasonable request.

Consent for publication

Not applicable.

ORCID iDs

Qing Zheng https://orcid.org/0000-0002-3199-2861
Zhenqi Gong https://orcid.org/0000-0003-3369-3061
Huaiming Wang https://orcid.org/0000-0002-8461-0388

References

1. Boorjian S, Tickoo SK, Mongan NP, et al. Reduced lecithin. *Clin Cancer Res*. 2004;10(10):3429–3437. doi:10.1158/1078-0432.CCR-03-0756
2. Campbell C, Rudensky A. Roles of regulatory T cells in tissue pathophysiology and metabolism. *Cell Metab*. 2020;31(1):18–25. doi:10.1016/j.cmet.2019.09.010
3. Chen W, Zheng R, Baade PD, et al. Cancer statistics in China, 2015. *CA Cancer J Clin*. 2016;66(2):115–132. doi:10.3322/caac.21338
4. Cuadrado E, Van Den Biggelaar M, De Kivit S, et al. Proteomic analyses of human regulatory T cells reveal adaptations in signaling pathways that protect cellular identity. *Immunity*. 2018;48(5):1046–1059.e6. doi:10.1016/j.immuni.2018.04.008
5. Edris B, Willingham SB, Weiskopf K, et al. Anti-KIT monoclonal antibody inhibits imatinib-resistant gastrointestinal stromal tumor growth. *Proc Natl Acad Sci U S A*. 2013;110(9):3501–3506. doi:10.1073/pnas.1222893110

6. Friedman J, Hastie T, Tibshirani R, et al. LASSO and elastic-net regularized generalized linear models. Pasadena, USA: Stanford University; 2023. https://glmnet.stanford.edu. Accessed January 6, 2023.
7. Gao JP, Xu W, Liu WT, Yan M, Zhu ZG. Tumor heterogeneity of gastric cancer: From the perspective of tumor-initiating cell. *World J Gastroenterol*. 2018;24(24):2567–2581. doi:10.3748/wjg.v24.i24.2567
8. Geeleher P, Cox N, Huang RS. pRRophetic: An R Package for prediction of clinical chemotherapeutic response from tumor gene expression levels. *PLoS One*. 2014;9(9):e107468. doi:10.1371/journal.pone.0107468
9. Granito A, Marinelli S, Terzi E, et al. Metronomic capecitabine as second-line treatment in hepatocellular carcinoma after sorafenib failure. *Digest Liver Dis*. 2015;47(6):518–522. doi:10.1016/j.dld.2015.03.010
10. Kamber RA, Nishiga Y, Morton B, et al. Inter-cellular CRISPR screens reveal regulators of cancer cell phagocytosis. *Nature*. 2021;597(7877):549–554. doi:10.1038/s41586-021-03879-4
11. He S, Shen J, Hong L, Niu L, Niu D. Capecitabine "metronomic" chemotherapy for palliative treatment of elderly patients with advanced gastric cancer after fluoropyrimidine-based chemotherapy. *Med Oncol*. 2012;29(1):100–106. doi:10.1007/s12032-010-9791-x
12. Kamen L, Myneni S, Langsdorf C, et al. A novel method for determining antibody-dependent cellular phagocytosis. *J Immunol Methods*. 2019;468:55–60. doi:10.1016/j.jim.2019.03.001
13. Leidi M, Gotti E, Bologna L, et al. M2 macrophages phagocytose rituximab-opsonized leukemic targets more efficiently than M1 cells in vitro. *J Immunol*. 2009;182(7):4415–4422. doi:10.4049/jimmunol.0713732
14. Li MO, Rudensky AY. T cell receptor signalling in the control of regulatory T cell differentiation and function. *Nat Rev Immunol*. 2016;16(4):220–233. doi:10.1038/nri.2016.26
15. Li W, Han F, Fu M, Wang Z. High expression of VCAN is an independent predictor of poor prognosis in gastric cancer. *J Int Med Res*. 2020;48(1):030006051989127. doi:10.1177/0300060519891271
16. Liu B, Sun Y, Tang M, et al. The miR-361-3p increases enzalutamide (Enz) sensitivity via targeting the ARv7 and MKNK2 to better suppress the Enz-resistant prostate cancer. *Cell Death Dis*. 2020;11(9):807. doi:10.1038/s41419-020-02932-w
17. Mogilevsky M, Shimshon O, Kumar S, et al. Modulation of *MKNK2* alternative splicing by splice-switching oligonucleotides as a novel approach for glioblastoma treatment. *Nucl Acids Res*. 2018;46(21):11396–11404. doi:10.1093/nar/gky921
18. Muraro E, Vinante L, Fratta E, et al. Metronomic chemotherapy: Antitumor pathways and combination with immune checkpoint inhibitors. *Cancers (Basel)*. 2023;15(9):2471. doi:10.3390/cancers15092471
19. Newman AM, Liu CL, Green MR, et al. Robust enumeration of cell subsets from tissue expression profiles. *Nat Methods*. 2015;12(5):453–457. doi:10.1038/nmeth.3337
20. Newton R, Priyadharshini B, Turka LA. Immunometabolism of regulatory T cells. *Nat Immunol*. 2016;17(6):618–625. doi:10.1038/ni.3466
21. Sakaguchi S, Mikami N, Wing JB, Tanaka A, Ichiyama K, Ohkura N. Regulatory T cells and human disease. *Annu Rev Immunol*. 2020;38(1):541–566. doi:10.1146/annurev-immunol-042718-041717
22. Shah MA, Ajani JA. Gastric cancer: An enigmatic and heterogeneous disease. *JAMA*. 2010;303(17):1753. doi:10.1001/jama.2010.553
23. Sheren-Manoff M, Shin SJ, Su D, Bok D, Rando RR, Gudas LJ. Reduced lecithin:retinol acyltransferase expression in human breast cancer. *Int J Oncol*. 2006;29(5):1193–1199. PMID:17016651.
24. Sillé FCM, Thomas R, Smith MT, Conde L, Skibola CF. Post-GWAS functional characterization of susceptibility variants for chronic lymphocytic leukemia. *PLoS One*. 2012;7(1):e29632. doi:10.1371/journal.pone.0029632
25. Smyth EC, Nilsson M, Grabsch HI, Van Grieken NC, Lordick F. Gastric cancer. *Lancet*. 2020;396(10251):635–648. doi:10.1016/S0140-6736(20)31288-5
26. Sung H, Ferlay J, Siegel RL, et al. Global cancer statistics 2020: GLOBOCAN estimates of incidence and mortality worldwide for 36 cancers in 185 countries. *CA Cancer J Clin*. 2021;71(3):209–249. doi:10.3322/caac.21660
27. Therneau T, Lumley T. Package Survival: A package for Survival Analysis in R. R Package. Version 2, 38. Comprehensive R Archive Network (CRAN); 2024. https://vps.fmvz.usp.br/CRAN/web/packages/survival/survival.pdf. Accessed January 6, 2023.
28. Van Cutsem E, Sagaert X, Topal B, Haustermans K, Prenen H. Gastric cancer. *Lancet*. 2016;388(10060):2654–2664. doi:10.1016/S0140-6736(16)30354-3
29. Van Der Veeken J, Gonzalez AJ, Cho H, et al. Memory of inflammation in regulatory T cells. *Cell*. 2016;166(4):977–990. doi:10.1016/j.cell.2016.07.006
29. Wang J, Da C, Su Y, Song R, Bai Z. MKNK2 enhances chemoresistance of ovarian cancer by suppressing autophagy via miR-125b. *Biochem Biophys Res Commun*. 2021;556:31–38. doi:10.1016/j.bbrc.2021.02.084
31. Wang Y, Zhang X, Ding J, Chao Z, Dress A, Lai L. MKNK2 is a valid target of miR-125b in breast cancer. *Gene Reports*. 2016;5:92–97. doi:10.1016/j.genrep.2016.09.008
32. Wu T, Hu E, Xu S, et al. clusterProfiler 4.0: A universal enrichment tool for interpreting omics data. *Innovation (Camb)*. 2021;2(3):100141. doi:10.1016/j.xinn.2021.100141
33. Yoshihara K, Shahmoradgoli M, Martínez E, et al. Inferring tumour purity and stromal and immune cell admixture from expression data. *Nat Commun*. 2013;4(1):2612. doi:10.1038/ncomms3612
34. Yuan L, Xu ZY, Ruan SM, Mo S, Qin JJ, Cheng XD. Long non-coding RNAs towards precision medicine in gastric cancer: Early diagnosis, treatment, and drug resistance. *Mol Cancer*. 2020;19(1):96. doi:10.1186/s12943-020-01219-0
35. Zhao Q, Cao L, Guan L, et al. Immunotherapy for gastric cancer: Dilemmas and prospect. *Brief Funct Genomics*. 2019;18(2):107–112. doi:10.1093/bfgp/ely019
36. Zong L, Abe M, Seto Y, Ji J. The challenge of screening for early gastric cancer in China. *Lancet*. 2016;388(10060):2606. doi:10.1016/S0140-6736(16)32226-7

Advantages and limitations of nanostructures for biomedical applications

Szymon Roszkowski[A–F], Zofia Durczynska[C,E,F]

Division of Biochemistry and Biogerontology, Collegium Medicum, Nicolaus Copernicus University, Toruń, Poland

A – research concept and design; B – collection and/or assembly of data; C – data analysis and interpretation;
D – writing the article; E – critical revision of the article; F – final approval of the article

Advances in Clinical and Experimental Medicine, ISSN 1899–5276 (print), ISSN 2451–2680 (online) *Adv Clin Exp Med*. 2025;34(3):447–456

Address for correspondence
Szymon Roszkowski
E-mail: szymonr@cm.umk.pl

Funding sources
None declared

Conflict of interest
None declared

Received on October 7, 2023
Reviewed on February 5, 2024
Accepted on April 5, 2024

Published online on June 11, 2024

Abstract

This review examines recent progress in developing nanoscale drug delivery systems for biomedical applications. Key nanocarriers, including inorganic nanoparticles, dendrimers, protein nanoparticles, polymeric micelles, liposomes, carbon nanotubes (CNTs), quantum dots (QDs), and biopolymeric nanoparticles, were summarized. Compared with free drugs, the tunable physicochemical properties of these materials allow for the encapsulation of therapeutics and improved pharmacokinetics. However, limitations such as toxicity, poor biodegradability, lack of controlled release, and low encapsulation efficiency remain. Inorganic nanoparticles exhibit issues with accumulation and toxicity. Dendrimers require complex syntheses and demonstrations of long-term safety. Protein nanoparticles suffer from low drug loading and stability. Polymeric micelles have stability and tumor penetration limitations. Liposomes exhibit low encapsulation efficiency and rapid clearance. Carbon nanotubes demonstrate toxicity and poor aqueous solubility. Quantum dots contain heavy metals, leading to toxicity. Biopolymeric nanoparticles have low stability and control over release kinetics. Strategies such as surface engineering with polymers and ligands aim to enhance nanoparticle targeting and biocompatibility. The combination of nanostructures in hybrid systems aims to synergize benefits while mitigating individual limitations. Stimulus-responsive and multifunctional nanoparticles enable triggered release and imaging capabilities. Overall, continued research into novel bioinspired designs, smart responsiveness and hybrid approaches is critical to fully realize the clinical potential of engineered nanomedicines for advanced drug delivery applications.

Key words: drug delivery, nanoparticles, nanomedicine, targeted delivery, clinical translation

Cite as
Roszkowski S, Durczynska Z. Advantages and limitations of nanostructures for biomedical applications. *Adv Clin Exp Med*. 2025;34(3):447–456. doi:10.17219/acem/186846

DOI
10.17219/acem/186846

Introduction

Modern encapsulation methods demonstrate an advantage over conventional methods of delivering biologically active substances to the target site.[1] Nanostructures are materials with at least 1 dimension in the 1–100 nm range. Their small size imparts novel optical, electronic and chemical properties compared to those of bulk materials. This has generated great interest in using nanostructures for biomedical applications such as drug delivery, bioimaging and biosensing.[2,3] However, the unique properties of nanostructures can also lead to toxicity, making it critical to consider both advantages and limitations during development.[4,5]

Nanocapsules (NCs) can target and enter select tissues at the molecular level. They provide a high absorption rate, increased cellular uptake, and precise and targeted delivery of substances to target cells without interacting with the environment.[6] In addition, nanoencapsulation of drugs results in improved absorption of poorly soluble drugs, reduces drug toxicity and minimizes or suppresses resistance resulting from physiological barriers in the body.[7]

Over the past few decades, nanostructures of various shapes and sizes have been developed for encapsulating many substances, including inorganic nanoparticles, dendrimers, protein nanoparticles, polymeric micelles, liposomes, carbon nanotubes (CNTs), quantum dots (QDs), and biopolymeric nanoparticles. Table 1 summarizes the advantages and disadvantages of these nanoparticles.[8] Figure 1 summarizes main classes of nanoparticles and their properties.

The current solution to the limitations of using each of these nanostructures individually is to use a combination of different nanostructures, resulting in a hybrid nanocapsule.[9,10] On the other hand, protein nanoparticles have attracted great interest in the field of nanotechnology due to their excellent biodegradability, low toxicity, water solubility, and high similarity to the components of the extracellular matrix.[11,12] The surface of protein nanoparticles can be chemically functionalized by adding directing ligands, such as peptides, antibodies, vitamins, hormones, or enzymes.

Table 1. Advantages and drawbacks of nanostructures[8]

Nanostructure	Advantages	Drawbacks
Inorganic nanoparticles	facile synthesis easy surface functionalization good stability versatility exceptional optical and electronic properties	nonbiodegradable toxicity coating required
Dendrimers	synthesis of well-defined structures high chemical and biological stability efficacy, purity and long shelf life high surface area, loading capacity and targeting biodegradable and biocompatible	complex synthetic route low yield and difficulties in obtaining higher generations
Protein nanoparticles	low toxicity biodegradability good mechanical properties versatility	chemical modifications of their surface are usually required to yield stimulus-responsive nanomedicines low drug loading efficiency
Polymeric micelles	efficient carrier system for hydrophilic drugs biodegradable and biocompatible self-assembling potential targeting functional modification low toxicity	short circulation times in blood-specific cytotoxicity need of surface modifications
Liposomes	amphiphilic structures easy surface functionalization biocompatibility	conventional liposomes: instability insufficient drug loading faster drug release shorter circulation times in blood
Carbon nanotubes	quasi-1D nanostructure easy surface functionalization exceptional surface area and cell membrane penetrability efficient loading remarkable optical and electronic properties	poor solubility in many solvents including water low biodegradability toxicity
Quantum dots	good solubility in water after surface modification strong fluorescence intensity	nonbiodegradable cytotoxicity to lung cells induction of oxidative stress
Biopolymeric nanoparticles	isolated from different natural resources (abundance) excellent geometrical dimensions high specific surface area good mechanical and barrier properties lack of toxicity biodegradable and biocompatible	hydrophobic materials poor encapsulation efficiency of medicines resistance against enzymatic degradation

These ligands accurately identify cells and tissues, promoting and improving the targeting mechanism.[13,14]

Objectives

This review summarizes the current knowledge on major nanostructure classes for biomedical applications and discusses their advantages and limitations for drug delivery, bioimaging and biosensing. We discuss key challenges related to toxicity, stability, pharmacokinetics, and accumulation that need to be addressed to enable the clinical translation of nanostructures. Our study highlights promising strategies for improving biocompatibility and innovative stimulus-responsive approaches that could optimize nanostructures for biomedicine.

Inorganic nanoparticles

Inorganic nanoparticles such as gold, iron oxide and silica nanoparticles have been widely studied for biomedical applications due to their unique properties and relative ease of synthesis.[15] Gold nanoparticles exhibit strong surface plasmon resonance, allowing for enhanced contrast in imaging modalities such as computed tomography (CT), photoacoustic imaging and multiphoton microscopy.[16] The inert nature of these materials also makes them useful for surface-enhanced Raman spectroscopy sensing.[17] Iron oxide nanoparticles demonstrate superparamagnetism, enabling their use as T2 contrast agents for magnetic resonance imaging (MRI) and magnetic particle imaging.[18] Mesoporous silica nanoparticles have high surface areas and pore volumes, permitting high payloads of imaging agents and therapeutics.[19]

However, toxicity concerns remain a significant barrier to the clinical translation of many nanomaterials.[20] Factors influencing toxicity include composition, size, shape, surface charge, and coating.[21] Inorganic nanoparticles tend to accumulate in organs such as the liver and spleen.[22] Iron oxide nanomaterials could alter iron homeostasis.[23] Silica nanoparticles have been associated with liver enzyme release.[24] Strategies, such as surface coating with proteins or polymers (e.g., polyethylene glycol (PEG); PEGylation), are being explored to improve biocompatibility.[25] The need for surface modification also complicates regulatory approval.[26] There are still open questions regarding the long-term safety, metabolism and excretion of nanoparticles.[27] Their non-biodegradable nature may lead to potential accumulation and unintended effects.[28] Overall, a thorough evaluation of nanoparticle toxicity through both in vitro and in vivo studies across multiple models is necessary to enable successful clinical translation.[29]

Dendrimers

Dendrimers are highly branched polymeric nanostructures with definable compositions and monodisperse size distributions.[30] Their stability, high loading capacity and modifiable surfaces are beneficial for drug and gene delivery.[31,32] For example, polyamidoamine (PAMAM) dendrimers have been extensively studied for use in siRNA and drug delivery due to their cationic surface charge, which allows electrostatic complexation with nucleic acids.[33] Strategies such as PEGylation or acetylation have been used to reduce cytotoxicity.[34] Drawbacks include complex syntheses, especially for higher generations, and the need to demonstrate long-term safety.[35] Toxicity has been linked to cationic charge and immunostimulation, although neutral and anionic dendrimers appear safer.[36] Additional studies focused on metabolism and excretion over months or years are still needed.[37] Overall, dendrimers are a versatile platform that shows promise for drug and gene delivery, but further studies are needed to establish clinical translatability.[38]

Protein nanoparticles

Nanoparticles fabricated from proteins such as albumin have good biocompatibility and biodegradability.[39] As natural materials, they are generally nontoxic and do not elicit unwanted immunological responses.[40] Albumin is particularly attractive due to the presence of numerous functional groups, which enable modifications as well as high thermal and aqueous solution stability.[41] Albumin nanoparticles can transport drugs via both encapsulation in the core and absorption on the surface.[42] They have been applied for the delivery of anticancer compounds, including paclitaxel, doxorubicin and methotrexate.[43–45]

However, under physiological conditions, albumin undergoes relatively rapid enzymatic degradation and breakdown, which can limit controlled drug release.[46] Therefore, it is important to modify the surface of these carriers to impart desired stimuli-responsive release properties.[47] For example, researchers have developed a new drug delivery system based on amine-functionalized mesoporous silica (SBA-15) loaded with bovine serum albumin (BSA), which was subsequently coated with a thin layer of poly(acrylic acid) (PAA). It was found that BSA is released from such a system at a higher pH of 7.4 rather than at a lower pH of 1.2. This finding suggested that this approach may be useful for the release of protein or drugs in environments with higher pH values, such as the small intestine or colon.[48] The proposed drug carrier utilizes electrostatic interactions between the protein and the silica nanoparticles and regulates drug release through changes in the pH of the environment. Therefore, these findings highlight the prospect of targeted delivery of protein drugs to specific organs of the gastrointestinal tract. Another strategy of targeted delivery is crosslinking albumin using aldehydes, which enhances its stability and allows for the conjugation of ligands recognized by cancer cells.[49]

For some hydrophobic drugs, a low loading efficiency of less than 10% into albumin nanoparticles has been

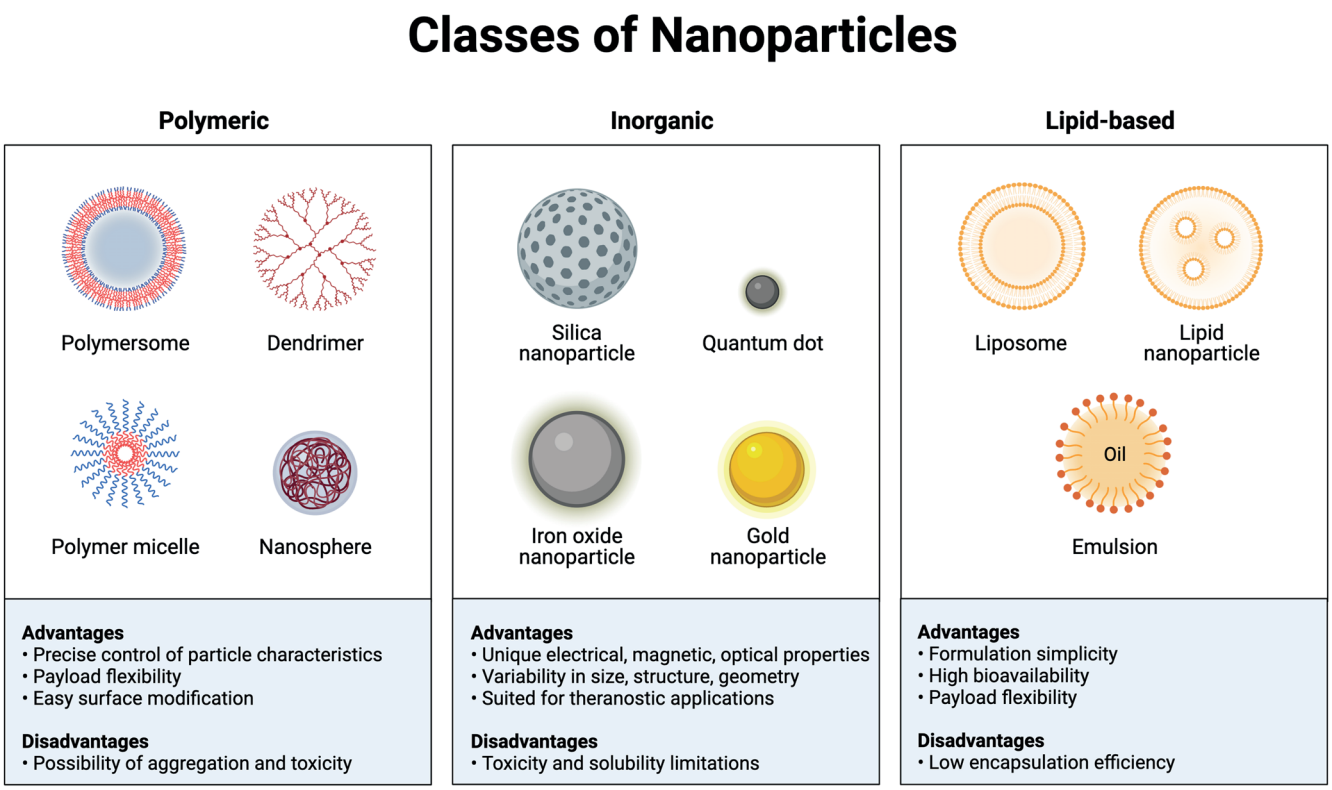

Fig. 1. Main classes of nanoparticles and their properties. The sizes given are the most common diameter ranges of these nanoparticles. However, these are approximate values because the dimensions of actual nanoparticles depend on many factors, such as the method of their synthesis or the materials used

demonstrated.[50] This may require surface modification with amphiphilic substances or solvent saturation techniques.[51] Other limitations include a potentially overly slow release of active compounds, as well as difficulties with scalability and standardization of manufacturing processes.[52]

The main methods for preparing albumin nanoparticles include desolvation, self-assembly, thermal gelation, spray-drying, emulsification, double emulsification, nanoparticle albumin-bound (Nab)-technology, and pH coacervation.[51] The resulting carriers differ in size, morphology and surface properties depending on the production conditions. For example, high temperature and pH lead to the aggregation and formation of larger particles.[50] In addition to albumin, other proteins, such as gelatin, are used. Gelatin can ionize and form complexes with nucleic acids.[52] However, the surface properties of these materials are inferior to those of albumin and their stability is lower.

Despite certain challenges, protein nanoparticles constitute a promising therapeutic platform, and further research into improving their pharmacokinetic and pharmacodynamic properties is warranted.[53] For instance, the modification of albumin with PEG can increase the plasma circulation time and tumor accumulation via the enhanced permeability and retention (EPR) effect.[54] Conjugation with targeting ligands enables active targeting of cancer cells.[45] Novel approaches also include using albumin in hybrid nanostructures together with lipids, polymers, or CNTs.[55] These systems combine the advantages of different materials and may enhance therapeutic performance.

In summary, protein nanoparticles, especially albumin-based nanoparticles, demonstrate several promising properties as anticancer drug carriers. One successful example of protein nanoparticles already used in clinical practice is albumin-bound paclitaxel nanoparticles, which are sold under the name Abraxane®. This drug was obtained through high-pressure homogenization of a drug and bovine albumin solution, resulting in nanoparticles approx. 130 nm in size that are easy to administer intravenously. The production of Abraxane could be easily scaled up to an industrial level without loss of stability or therapeutic activity. Therefore, methods such as simple pressure homogenization used in Abraxane constitute a promising strategy for the development of other albumin-based formulations. Nevertheless, there is still a need to optimize advanced protein nanostructures in terms of pharmacokinetic properties and drug release profiles.

Polymeric micelles

Polymeric micelles formed through the self-assembly of amphiphilic block copolymers have emerged as promising carriers for delivering hydrophobic drugs such as anticancer agents.[56] The core-shell nanostructure comprises an inner hydrophobic domain stabilized by a hydrophilic

outer layer, allowing encapsulation of water-insoluble drugs within the core. Polymeric micelles can enhance the solubility, bioavailability and tumor-targeting potential of hydrophobic therapeutics.[57] Common polymers investigated include PEG, poly(epsilon-caprolactone) (PCL) and poly(lactic acid) (PLA) due to their biocompatibility and biodegradability. Polyethylene glycol results in an outer brush-like "stealth" layer that inhibits protein adsorption and opsonization, thereby increasing circulation time.[58]

A key advantage of polymeric micelles is their ability to accumulate in tumors through the EPR effect from leaky tumor vasculature and poor lymphatic drainage.[56] Passive targeting of tumors has been demonstrated with various micelle formulations.[59] Active targeting can also be achieved by attaching targeting ligands to recognize receptors overexpressed on cancer cells.[6] However, limitations exist, such as a lack of adequate tumor penetration into poorly permeable tumors and toxicity concerns.[60]

Stability is a major issue affecting polymeric micelle drug carriers. Upon dilution, micelles can dissociate below the critical micelle concentration, interact with cells/proteins or undergo changes in temperature, pH or ionic strength.[59] This can lead to premature drug release during circulation. Strategies to improve stability include core crosslinking, increasing polymer hydrophobicity, introducing hydrogen bonding, and shell crosslinking.[61] Shell crosslinking with disulfide bonds can provide redox-responsive release intracellularly.[62]

Controlling the rate of drug release remains a key challenge. Drug release from polymeric micelles relies on diffusion and polymer erosion mechanisms. Diffusion-controlled release can be too slow, while erosion-dominated release decreases control.[62] Tuning polymer properties, such as molecular weight and copolymer block ratios, modulates degradation.[61] The introduction of stimuli-responsive components triggers release in response to changes in pH, temperature or enzymatic activity.[63]

Another major limitation is the systemic toxicity of polymers and degradation products. Polymers need to be safely eliminated from the body. Polymer cytotoxicity has been associated with effects on membranes, protein binding, mitochondria, and the induction of apoptosis. Strategies to reduce toxicity include utilizing biodegradable and biocompatible polymers, limiting molecular weights, and optimizing micelle stability to prevent premature release.[64] Extensive in vitro and in vivo testing is critical.[65,66]

While polymeric micelles offer versatility in design and tunable properties for cancer therapy, key challenges in stability, drug release kinetics, tumor penetration, and toxicity must still be overcome for clinical translation.[67,68] Further optimization of polymeric micelle systems through novel bioinspired designs and stimulus-responsive approaches continues to be an active area of pharmaceutical research.[69,70]

Liposomes

Liposomes are biocompatible vesicles composed of phospholipid bilayers that can encapsulate both hydrophilic and hydrophobic drugs.[71] The tunable surface chemistry and composition of these materials make them versatile drug carriers.[72,73] Conventional liposomes constructed from phospholipids such as phosphatidylcholine have been extensively investigated for the delivery of anticancer agents, antibiotics, peptides, proteins, and nucleic acids.[74,75] Hydrophobic drugs can be incorporated into the lipid bilayer, while hydrophilic drugs can be entrapped in the aqueous core.[76]

However, conventional liposomes have significant limitations, including poor stability, short circulation half-lives and low encapsulation efficiency. Liposomes are prone to aggregation, fusion, lipid oxidation, and enzymatic degradation.[77] Upon intravenous administration, liposomes are rapidly cleared by the mononuclear phagocyte system, limiting bioavailability.[78] Strategies to overcome these issues include the use of a cholesterol formulation to strengthen membranes, PEGylation to provide a steric barrier against opsonization, and charge modulation to increase stability.[79]

Another key challenge is the low encapsulation efficiency of conventional formulations for hydrophilic drugs. Remote loading approaches have been developed to actively load preformed liposomes using an ionic or pH gradient. Active loading provides high-efficiency encapsulation but requires an optimized lipid composition and consideration of drug ionization. Alternative methods using new drug encapsulation methodologies, such as the use of genetically engineered elastin-like recombinamers and supercritical fluid techniques, could lead to more precise drug delivery systems.[80]

Controlling the release rate of encapsulated drugs also remains an issue. Conventional liposomes exhibit burst release and limited ability to provide sustained, localized delivery. Stimulus-responsive liposomes engineered to be thermosensitive, pH sensitive or degrade enzymatically allow for triggered release.[78] Localized delivery can also be achieved using liposomes embedded within hydrogel matrices.[81]

Overall, liposomal drug carriers have progressed significantly with innovations in formulation, stimulus responsiveness and surface functionality. However, the stability, encapsulation efficiency, sustained release, and therapeutic efficacy of these materials must continue to be enhanced for clinical translation.[82] Further advances in liposome technology through multicomponent systems and synergistic delivery with external triggers show promise for cancer therapy.[83]

Carbon nanotubes

Carbon nanotubes have emerged as promising nanocarriers for drug delivery due to their high aspect ratio, ultrahigh surface area and ability to penetrate cells. Both

single-walled CNTs (SWCNTs) and multi-walled CNTs (MWCNTs) have been explored for biomedical applications. The needle-like shape of these cells allows for the piercing of cell membranes, enabling penetration of the cytoplasm and nucleus.[84] This approach facilitates the delivery of therapeutics such as small molecule chemotherapeutics, proteins, peptides, and nucleic acids into hard-to-access cells. Carbon nanotubes also have a very high drug-loading capacity due to their extensive surface area. Drugs can be loaded inside CNTs, in the interstitial spaces between nanotubes in bundles or attached to the external surface.[85]

However, concerns about CNT toxicity have hindered its clinical translation. Toxicity is influenced by structural factors such as length, diameter, surface chemistry, and degree of aggregation. Longer CNTs appear more toxic due to frustrating phagocytosis, where immune cells cannot fully engulf lengthy nanotubes.[86] Chemical functionalization of CNT surfaces with -COOH groups reduces toxicity compared to that of pristine nanotubes.[87] PEGylation is another strategy for decreasing immunogenicity and increasing biocompatibility. Carbon nanotubes have also demonstrated dose-dependent toxicity to vital organs such as the lungs, liver and kidneys after intravenous administration.[88]

Another major limitation of CNTs is their non-biodegradable nature, which can lead to long-term accumulation in the body.[89] To date, attempts have been made to develop biodegradable CNTs using techniques such as oxidation cutting, polymer coating and nucleic acid hybridization, but with only partial degradation.[90] Carbon nanotube aggregation and poor solubility in aqueous solutions also pose challenges.[91] Ultrasonication and the use of surfactants such as sodium dodecyl sulfate improve dispersibility but may inadvertently increase toxicity.[89] An alternative method for dispersing CNTs is their noncovalent functionalization with amphiphilic polymers or DNA; however, maintaining the stability of CNTs in a biological environment remains a challenge.[92]

A promising strategy to improve the biocompatibility and solubility of CNTs while decreasing their systemic toxicity is encapsulation of CNTs in micelles, liposomes or hydrogel particles.[93] Although CNTs have great potential as nanocarriers for drugs, overcoming key limitations related to their toxicity, degradability and solubility is necessary. Possible solutions include engineering new hybrid structures that combine CNTs with organic and polymeric materials. This approach allows the unique properties of CNTs to be exploited for drug delivery and release.[94]

Quantum dots

Quantum dots are semiconductor nanocrystals that possess unique optical properties derived from quantum confinement effects.[95] By tuning the QD size and composition, the fluorescence emission can be precisely controlled from the visible to near-infrared range.[96] This has enabled widespread exploration of QDs for biomedical imaging both in vitro and in vivo.[97] Compared with organic dyes and fluorescent proteins, QDs have greater brightness, greater stability against photobleaching, and narrower emission spectra. These advantages have led to QD applications in immunofluorescence assays, targeted cancer cell imaging, lymph node mapping, and multifunctional nanoparticles.[98]

However, the toxicity of QDs remains a major concern hindering clinical translation. Most QDs contain heavy metal components such as cadmium that are known to be cytotoxic.[99] Metal release through QD oxidation or degradation is a primary toxicity mechanism.[100] Quantum dots can also induce reactive oxygen species (ROS) formation, leading to oxidative stress and inflammation.[101] Coating strategies using inert shells and polymers aim to prevent direct QD exposure, but stability and potential leaching issues persist. The coating thickness and charge affect cellular interactions and toxicity profiles. Furthermore, there are remaining questions regarding the long-term accumulation, metabolism and excretion of QDs in vivo.[102]

A key limitation of QDs is their non-biodegradable nature. Attempts have been made to develop biodegradable QDs using less toxic elements such as indium, zinc and silicon.[103] Combining QDs with organic polymers and biomolecules is another approach to impart biodegradability.[104] However, maintaining the optical properties of QDs after biodegradation remains challenging. Engineering smaller QDs less than 5 nm in diameter may enable renal clearance and prevent bioaccumulation.[105] However, ultrasmall QDs sacrifice brightness and tend to be less stable.

The solubility and dispersion of QDs in biological environments also require optimization. Quantum dot surface modification with hydrophilic ligands, polymers, silica shells, and amphiphilic coatings enhances water solubility.[106] Conjugation to proteins, peptides and DNA improves colloidal stability and biocompatibility.[107] Incorporating QDs into larger nanocarriers such as liposomes may help overcome limitations related to their toxicity and solubility.[108] However, maintenance of fluorescence and prevention of leaching needs to be demonstrated.

Overall, despite their advantageous optical properties, QDs still have significant unresolved issues associated with the toxicity of heavy metals they contain, lack of biodegradability, oxidative effects, and colloidal stability. Before fully harnessing their potential in biomedicine, advanced engineering approaches are necessary to address these key challenges.[99,109]

Biopolymeric nanoparticles

Nanoparticles fabricated from natural biopolymers have attracted increasing interest as drug delivery systems due to their biocompatibility, biodegradability and abundance in nature. Chitosan, alginate, gelatin, and albumin are

among the most extensively explored materials.[110] Chitosan is derived from chitin found in crustacean shells and has mucoadhesive properties useful for mucosal delivery.[111] The alginate obtained from seaweed contains carboxyl groups that enable crosslinking for hydrogel particle formation.[112] Gelatin is derived from collagen and has excellent cell adhesion potential and low antigenicity. The serum albumin concentration is known to be derived from serum and has versatile drug-binding abilities.[113] These biopolymers are generally regarded as safe and have low toxicity.

However, biopolymeric nanoparticles, especially those containing hydrophobic drugs, have limitations, including poor encapsulation efficiency.[110] The porous structures of these materials allow rapid diffusion and burst release of payloads. Chemical or ionic crosslinking is often required to reinforce structures, control swelling and enable sustained release.[114] However, excessive crosslinking can improperly retard drug release. Biopolymers also tend to have low stability against enzymatic degradation, limiting their circulation time. Shell hardening techniques such as polyelectrolyte coating provide some protection.[115]

Another challenge is scaling up biopolymeric nanoparticle production while maintaining consistent physicochemical properties between batches. Variables such as polymer source, purification methods and crosslinking affect reproducibility.[110] The storage stability over the shelf life also needs to be demonstrated. Sterilization methods can impact drug release characteristics and particle integrity.[116]

Furthermore, compared with synthetic polymers, most biopolymers lack functional groups for facile surface modification and ligand conjugation. This restricts opportunities for active targeting. The intrinsic immunogenicity of some biopolymers, such as chitosan, may also cause concerns.[117]

In summary, biopolymeric nanoparticles offer the advantages of biocompatibility, sustainability and tunable properties that provide versatility in drug delivery design. However, continued research to improve the encapsulation efficiency, colloidal and enzymatic stability, scale-up processes, and reproducible manufacturing is needed to fully harness the potential of these materials.

Limitations

While this review provides a broad overview of nanostructures for biomedical applications, it has certain limitations that should be acknowledged. First, the focus was on summarizing key nanostructure classes without comprehensive coverage of all existing and emerging nanostructures. However, certain novel systems, such as protein-polymer hybrids, DNA origami and lipid-polymer assemblies, have not been discussed in depth. Second, the review was limited to nanostructures for drug delivery, bioimaging and biosensing, while excluding other biomedical areas such as tissue engineering, biomarkers and nanostructured surfaces. Furthermore, only selected key references were cited for each nanostructure type and application due to space constraints. The examples highlighted specific advantages and challenges but did not capture all ongoing research or clinical developments related to nanostructures.

Conclusions

Nanotechnology has enabled the engineering of nanoparticles with tremendous potential for targeted drug delivery and controlled release. Key advancements have been made in the field of inorganic nanoparticles, dendrimers, protein nanoparticles, polymeric micelles, liposomes, CNTs, QDs, and biopolymeric nanoparticles. Each platform offers unique advantages but also limitations that must be mitigated. Surface modification strategies, including PEGylation and ligand bioconjugation, can enhance nanoparticle biocompatibility, stability and active targeting abilities. Stimulus-responsive engineered nanoparticles enable triggered release in response to tumor microenvironment cues. The combination of nanostructures in multifunctional hybrid systems aims to synergize benefits while compensating for individual drawbacks. However, issues related to scale-up manufacturing, storage stability, pharmacokinetics, tumor penetration, and clinical toxicity remain barriers to translation. Overall, continued interdisciplinary research across chemistry, materials science, biology, and medicine focused on bioinspired designs, multifunctionality and novel responsiveness mechanisms is critical to fully realize the clinical potential of engineered nanoparticles for advanced drug delivery.

ORCID iDs

Szymon Roszkowski https://orcid.org/0000-0003-2575-0863
Zofia Durczyńska https://orcid.org/0009-0007-7857-9226

References

1. Farokhzad OC, Langer R. Impact of nanotechnology on drug delivery. *ACS Nano*. 2009;3(1):16–20. doi:10.1021/nn900002m
2. Suk JS, Xu Q, Kim N, Hanes J, Ensign LM. PEGylation as a strategy for improving nanoparticle-based drug and gene delivery. *Adv Drug Deliv Rev*. 2016;99:28–51. doi:10.1016/j.addr.2015.09.012
3. Ertas YN, Abedi Dorcheh K, Akbari A, Jabbari E. Nanoparticles for targeted drug delivery to cancer stem cells: A review of recent advances. *Nanomaterials*. 2021;11(7):1755. doi:10.3390/nano11071755
4. Ventola CL. Progress in nanomedicine: Approved and investigational nanodrugs. *P T*. 2017;42(12):742–755. PMID:29234213. PMCID: PMC5720487.
5. Forest V. Experimental and computational nanotoxicology: Complementary approaches for nanomaterial hazard assessment. *Nanomaterials*. 2022;12(8):1346. doi:10.3390/nano12081346
6. Senapati S, Mahanta AK, Kumar S, Maiti P. Controlled drug delivery vehicles for cancer treatment and their performance. *Sig Transduct Target Ther*. 2018;3(1):7. doi:10.1038/s41392-017-0004-3
7. De Jong. Drug delivery and nanoparticles: Applications and hazards. *Int J Nanomed*. 2008;3(2):133–139. doi:10.2147/IJN.S596
8. Montané X, Bajek A, Roszkowski K, et al. Encapsulation for cancer therapy. *Molecules*. 2020;25(7):1605. doi:10.3390/molecules25071605
9. Wang Y, Zhao Q, Han N, et al. Mesoporous silica nanoparticles in drug delivery and biomedical applications. *Nanomed Nanotechnol Biol Med*. 2015;11(2):313–327. doi:10.1016/j.nano.2014.09.014

10. Song X, Feng L, Liang C, Yang K, Liu Z. Ultrasound triggered tumor oxygenation with oxygen-shuttle nanoperfluorocarbon to overcome hypoxia-associated resistance in cancer therapies. *Nano Lett*. 2016; 16(10):6145–6153. doi:10.1021/acs.nanolett.6b02365
11. Nel AE, Mädler L, Velegol D, et al. Understanding biophysicochemical interactions at the nano–bio interface. *Nature Mater*. 2009;8(7): 543–557. doi:10.1038/nmat2442
12. Hong S, Choi DW, Kim HN, Park CG, Lee W, Park HH. Protein-based nanoparticles as drug delivery systems. *Pharmaceutics*. 2020;12(7):604. doi:10.3390/pharmaceutics12070604
13. Veselov VV, Nosyrev AE, Jicsinszky L, Alyautdin RN, Cravotto G. Targeted delivery methods for anticancer drugs. *Cancers (Basel)*. 2022; 14(3):622. doi:10.3390/cancers14030622
14. Thomas TP, Huang B, Choi SK, et al. Polyvalent dendrimer-methotrexate as a folate receptor-targeted cancer therapeutic. *Mol Pharm*. 2012;9(9):2669–2676. doi:10.1021/mp3002232
15. Parveen S, Misra R, Sahoo SK. Nanoparticles: A boon to drug delivery, therapeutics, diagnostics and imaging. *Nanomed Nanotechnol Biol Med*. 2012;8(2):147–166. doi:10.1016/j.nano.2011.05.016
16. Jokerst JV, Cole AJ, Van De Sompel D, Gambhir SS. Gold nanorods for ovarian cancer detection with photoacoustic imaging and resection guidance via Raman imaging in living mice. *ACS Nano*. 2012;6(11):10366–10377. doi:10.1021/nn304347g
17. Zeng Y, Ananth R, Dill TJ, et al. Metasurface-enhanced Raman spectroscopy (mSERS) for oriented molecular sensing. *ACS Appl Mater Interfaces*. 2022;14(28):32598–32607. doi:10.1021/acsami.2c01656
18. Fernández-Barahona I, Muñoz-Hernando M, Ruiz-Cabello J, Herranz F, Pellico J. Iron oxide nanoparticles: An alternative for positive contrast in magnetic resonance imaging. *Inorganics*. 2020;8(4):28. doi:10.3390/inorganics8040028
19. Slowing I, Viveroescoto J, Wu C, Lin V. Mesoporous silica nanoparticles as controlled release drug delivery and gene transfection carriers. *Adv Drug Deliv Rev*. 2008;60(11):1278–1288. doi:10.1016/j.addr.2008.03.012
20. Fröhlich E. The role of surface charge in cellular uptake and cytotoxicity of medical nanoparticles. *Int J Nanomed*. 2012;7:5577–5591. doi:10.2147/IJN.S36111
21. Albanese A, Tang PS, Chan WCW. The effect of nanoparticle size, shape, and surface chemistry on biological systems. *Annu Rev Biomed Eng*. 2012;14(1):1–16. doi:10.1146/annurev-bioeng-071811-150124
22. Zhang XD, Wu, Shen, et al. Size-dependent in vivo toxicity of PEG-coated gold nanoparticles. *Int J Nanomed*. 2011;6:2071–2081. doi:10.2147/IJN.S21657
23. Singh N, Jenkins GJS, Asadi R, Doak SH. Potential toxicity of superparamagnetic iron oxide nanoparticles (SPION). *Nano Rev*. 2010;1(1):5358. doi:10.3402/nano.v1i0.5358
24. Napierska D, Thomassen LC, Lison D, Martens JA, Hoet PH. The nanosilica hazard: Another variable entity. *Part Fibre Toxicol*. 2010;7(1):39. doi:10.1186/1743-8977-7-39
25. Torres-Obreque KM, Meneguetti GP, Muso-Cachumba JJ, et al. Building better biobetters: From fundamentals to industrial application. *Drug Discov Today*. 2022;27(1):65–81. doi:10.1016/j.drudis.2021.08.009
26. Ratner BD, Hoffman AS, McArthur SL. Physicochemical surface modification of materials used in medicine. In: Wagner W, Zhang G, Sakiyama-Elbert S, Yaszemski M, eds. *Biomaterials Science*. Cambridge, USA: Academic Press; 2020:487–505. doi:10.1016/B978-0-12-816137-1.00033-7
27. Yang ST, Luo J, Zhou Q, Wang H. Pharmacokinetics, metabolism and toxicity of carbon nanotubes for biomedical purposes. *Theranostics*. 2012;2(3):271–282. doi:10.7150/thno.3618
28. Kalia VC, Singh Patel SK, Shanmugam R, Lee JK. Polyhydroxyalkanoates: Trends and advances toward biotechnological applications. *Bioresour Technol*. 2021;326:124737. doi:10.1016/j.biortech.2021.124737
29. Dobrovolskaia MA. Pre-clinical immunotoxicity studies of nanotechnology-formulated drugs: Challenges, considerations and strategy. *J Control Release*. 2015;220:571–583. doi:10.1016/j.jconrel.2015.08.056
30. Nan W, Zhang C, Wang H, Chen H, Ji S. Direct modification of extracellular vesicles and its applications for cancer therapy: A mini-review. *Front Chem*. 2022;10:910341. doi:10.3389/fchem.2022.910341
31. Paris JL, Vallet-Regí M. Mesoporous silica nanoparticles for co-delivery of drugs and nucleic acids in oncology: A review. *Pharmaceutics*. 2020;12(6):526. doi:10.3390/pharmaceutics12060526
32. Carvalho AM, Cordeiro RA, Faneca H. Silica-based gene delivery systems: from design to therapeutic applications. *Pharmaceutics*. 2020; 12(7):649. doi:10.3390/pharmaceutics12070649
33. Zhou J, Wu J, Hafdi N, Behr JP, Erbacher P, Peng L. PAMAM dendrimers for efficient siRNA delivery and potent gene silencing. *Chem Commun (Camb)*. 2006;22:2362. doi:10.1039/b601381c
34. El-Shafie S, Fahmy SA, Ziko L, Elzahed N, Shoeib T, Kakarougkas A. Encapsulation of nedaplatin in novel PEGylated liposomes increases its cytotoxicity and genotoxicity against A549 and U2OS human cancer cells. *Pharmaceutics*. 2020;12(9):863. doi:10.3390/pharmaceutics12090863
35. Svenson S. Dendrimers as versatile platform in drug delivery applications. *Eur J Pharm Biopharm*. 2009;71(3):445–462. doi:10.1016/j.ejpb.2008.09.023
36. Jain K, Kesharwani P, Gupta U, Jain NK. Dendrimer toxicity: Let's meet the challenge. *Int J Pharm*. 2010;394(1–2):122–142. doi:10.1016/j.ijpharm.2010.04.027
37. Kaminskas LM, Boyd BJ, Porter CJ. Dendrimer pharmacokinetics: The effect of size, structure and surface characteristics on ADME properties [erratum in: *Nanomedicine (Lond)*. 2012;7(1):167–168. PMID:21955077]. *Nanomedicine*. 2011;6(6):1063–1084. doi:10.2217/nnm.11.67
38. Bober Z, Bartusik-Aebisher D, Aebisher D. Application of dendrimers in anticancer diagnostics and therapy. *Molecules*. 2022;27(10):3237. doi:10.3390/molecules27103237
39. Abdelhamid MAA, Ki MR, Abd El-Hafeez AA, Son RG, Pack SP. Tailored functionalized protein nanocarriers for cancer therapy: Recent developments and prospects. *Pharmaceutics*. 2023;15(1):168. doi:10.3390/pharmaceutics15010168
40. Elzoghby AO, Samy WM, Elgindy NA. Protein-based nanocarriers as promising drug and gene delivery systems. *J Control Release*. 2012; 161(1):38–49. doi:10.1016/j.jconrel.2012.04.036
41. Kratz F. Albumin as a drug carrier: Design of prodrugs, drug conjugates and nanoparticles. *J Control Release*. 2008;132(3):171–183. doi:10.1016/j.jconrel.2008.05.010
42. Desai N. Challenges in development of nanoparticle-based therapeutics. *AAPS J*. 2012;14(2):282–295. doi:10.1208/s12248-012-9339-4
43. Hawkins MJ, Soon-Shiong P, Desai N. Protein nanoparticles as drug carriers in clinical medicine. *Adv Drug Deliv Rev*. 2008;60(8):876–885. doi:10.1016/j.addr.2007.08.044
44. Vonarbourg A, Passirani C, Desigaux L, et al. The encapsulation of DNA molecules within biomimetic lipid nanocapsules. *Biomaterials*. 2009;30(18):3197–3204. doi:10.1016/j.biomaterials.2009.03.009
45. Chu KS, Schorzman AN, Finniss MC, et al. Nanoparticle drug loading as a design parameter to improve docetaxel pharmacokinetics and efficacy. *Biomaterials*. 2013;34(33):8424–8429. doi:10.1016/j.biomaterials.2013.07.038
46. Yang Z, Zhang N, Ma T, Liu L, Zhao L, Xie H. Engineered bovine serum albumin-based nanoparticles with pH-sensitivity for doxorubicin delivery and controlled release. *Drug Deliv*. 2020;27(1):1156–1164. doi:10.1080/10717544.2020.1797243
47. Hu Q, Sun W, Wang C, Gu Z. Recent advances of cocktail chemotherapy by combination drug delivery systems. *Adv Drug Deliv Rev*. 2016;98:19–34. doi:10.1016/j.addr.2015.10.022
48. Song SW, Hidajat K, Kawi S. pH-Controllable drug release using hydrogel encapsulated mesoporous silica. *Chem Commun (Camb)*. 2007; (42):4396. doi:10.1039/b707626f
49. Li L, Yang J, Soodvilai S, Wang J, Opanasopit P, Kopeček J. Drug-free albumin-triggered sensitization of cancer cells to anticancer drugs. *J Control Release*. 2019;293:84–93. doi:10.1016/j.jconrel.2018.11.015
50. Hao L, Zhou Q, Piao Y, Zhou Z, Tang J, Shen Y. Albumin-binding prodrugs via reversible iminoboronate forming nanoparticles for cancer drug delivery. *J Control Release*. 2021;330:362–371. doi:10.1016/j.jconrel.2020.12.035
51. Meng R, Zhu H, Wang Z, Hao S, Wang B. Preparation of drug-loaded albumin nanoparticles and its application in cancer therapy. Pugazhendhi A, ed. *J Nanomater*. 2022;2022:1137145. doi:10.1155/2022/3052175
52. Margulis-Goshen K, Magdassi S. Formation of simvastatin nanoparticles from microemulsion. *Nanomed Nanotechnol Biol Med*. 2009; 5(3):274–281. doi:10.1016/j.nano.2008.11.004

53. Kreuter J, Hekmatara T, Dreis S, Vogel T, Gelperina S, Langer K. Covalent attachment of apolipoprotein A-I and apolipoprotein B-100 to albumin nanoparticles enables drug transport into the brain. *J Control Release*. 2007;118(1):54–58. doi:10.1016/j.jconrel.2006.12.012
54. Lee JH, Nan A. Combination drug delivery approaches in metastatic breast cancer. *J Drug Deliv*. 2012;2012:915375. doi:10.1155/2012/915375
55. Ghorbanizamani F, Moulahoum H, Zihnioglu F, Timur S. Nanohybrid carriers: The yin–yang equilibrium between natural and synthetic in biomedicine. *Biomater Sci*. 2020;8(12):3237–3247. doi:10.1039/D0BM00401D
56. Maeda H, Nakamura H, Fang J. The EPR effect for macromolecular drug delivery to solid tumors: Improvement of tumor uptake, lowering of systemic toxicity, and distinct tumor imaging in vivo. *Adv Drug Deliv Rev*. 2013;65(1):71–79. doi:10.1016/j.addr.2012.10.002
57. Gong J, Chen M, Zheng Y, Wang S, Wang Y. Polymeric micelles drug delivery system in oncology. *J Control Release*. 2012;159(3):312–323. doi:10.1016/j.jconrel.2011.12.012
58. Otsuka H, Nagasaki Y, Kataoka K. PEGylated nanoparticles for biological and pharmaceutical applications. *Adv Drug Deliv Rev*. 2003; 55(3):403–419. doi:10.1016/S0169-409X(02)00226-0
59. Danquah MK, Zhang XA, Mahato RI. Extravasation of polymeric nanomedicines across tumor vasculature. *Adv Drug Deliv Rev*. 2011;63(8): 623–639. doi:10.1016/j.addr.2010.11.005
60. Xu X, Ho W, Zhang X, Bertrand N, Farokhzad O. Cancer nanomedicine: From targeted delivery to combination therapy. *Trends Mol Med*. 2015;21(4):223–232. doi:10.1016/j.molmed.2015.01.001
61. Gaucher G, Dufresne MH, Sant VP, Kang N, Maysinger D, Leroux JC. Block copolymer micelles: Preparation, characterization and application in drug delivery. *J Control Release*. 2005;109(1–3):169–188. doi:10.1016/j.jconrel.2005.09.034
62. Mura S, Nicolas J, Couvreur P. Stimuli-responsive nanocarriers for drug delivery. *Nature Mater*. 2013;12(11):991–1003. doi:10.1038/nmat3776
63. Jackson AW, Chennamaneni LR, Thoniyot P. Main-chain degradable, pH-responsive and covalently cross-linked nanoparticles via a one-step RAFT-based radical ring-opening terpolymerization. *Eur Polym J*. 2020;122:109391. doi:10.1016/j.eurpolymj.2019.109391
64. Idrees H, Zaidi SZJ, Sabir A, Khan RU, Zhang X, Hassan S.U. A review of biodegradable natural polymer-based nanoparticles for drug delivery applications. *Nanomaterials*. 2020;10(10):1970. doi:10.3390/nano10101970
65. Haque FM, Ishibashi JSA, Lidston CAL, et al. Defining the macromolecules of tomorrow through synergistic sustainable polymer research. *Chem Rev*. 2022;122(6):6322–6373. doi:10.1021/acs.chemrev.1c00173
66. Asadi N, Del Bakhshayesh AR, Davaran S, Akbarzadeh A. Common biocompatible polymeric materials for tissue engineering and regenerative medicine. *Mater Chem Phys*. 2020;242:122528. doi:10.1016/j.matchemphys.2019.122528
67. Kotta S, Aldawsari HM, Badr-Eldin SM, Nair AB, Yt K. Progress in polymeric micelles for drug delivery applications. *Pharmaceutics*. 2022; 14(8):1636. doi:10.3390/pharmaceutics14081636
68. Xie L, Liu R, Chen X, He M, Zhang Y, Chen S. Micelles based on lysine, histidine, or arginine: Designing structures for enhanced drug delivery. *Front Bioeng Biotechnol*. 2021;9:744657. doi:10.3389/fbioe.2021.744657
69. Das SS, Bharadwaj P, Bilal M, et al. Stimuli-responsive polymeric nanocarriers for drug delivery, imaging, and theragnosis. *Polymers (Basel)*. 2020;12(6):1397. doi:10.3390/polym12061397
70. Hwang D, Ramsey JD, Kabanov AV. Polymeric micelles for the delivery of poorly soluble drugs: From nanoformulation to clinical approval. *Adv Drug Deliv Rev*. 2020;156:80–118. doi:10.1016/j.addr.2020.09.009
71. Saraf S, Jain A, Tiwari A, Verma A, Panda PK, Jain SK. Advances in liposomal drug delivery to cancer: An overview. *J Drug Deliv Sci Technol*. 2020;56:101549. doi:10.1016/j.jddst.2020.101549
72. Fathi S, Oyelere AK. Liposomal drug delivery systems for targeted cancer therapy: Is active targeting the best choice? *Future Med Chem*. 2016;8(17):2091–2112. doi:10.4155/fmc-2016-0135
73. Jahromi LP, Fuhrmann G. Bacterial extracellular vesicles: Understanding biology promotes applications as nanopharmaceuticals. *Adv Drug Deliv Rev*. 2021;173:125–140. doi:10.1016/j.addr.2021.03.012
74. Guimarães D, Cavaco-Paulo A, Nogueira E. Design of liposomes as drug delivery system for therapeutic applications. *Int J Pharm*. 2021; 601:120571. doi:10.1016/j.ijpharm.2021.120571
75. Wang S, Chen Y, Guo J, Huang Q. Liposomes for tumor targeted therapy: A review. *Int J Mol Sci*. 2023;24(3):2643. doi:10.3390/ijms24032643
76. Zhigaltsev IV, Cullis PR. Morphological behavior of liposomes and lipid nanoparticles. *Langmuir*. 2023;39(9):3185–3193. doi:10.1021/acs.langmuir.2c02794
77. Gbian DL, Omri A. Lipid-based drug delivery systems for diseases managements. *Biomedicines*. 2022;10(9):2137. doi:10.3390/biomedicines10092137
78. Eroğlu İ, İbrahim M. Liposome–ligand conjugates: A review on the current state of art. *J Drug Target*. 2020;28(3):225–244. doi:10.1080/1061186X.2019.1648479
79. Kim EM, Jeong HJ. Liposomes: Biomedical applications. *Chonnam Med J*. 2021;57(1):27. doi:10.4068/cmj.2021.57.1.27
80. Vallejo R, Gonzalez-Valdivieso J, Santos M, Rodriguez-Rojo S, Arias FJ. Production of elastin-like recombinamer-based nanoparticles for docetaxel encapsulation and use as smart drug-delivery systems using a supercritical anti-solvent process. *J Industr Eng Chem*. 2021;93:361–374. doi:10.1016/j.jiec.2020.10.013
81. Antimisiaris SG, Marazioti A, Kannavou M, et al. Overcoming barriers by local drug delivery with liposomes. *Adv Drug Deliv Rev*. 2021; 174:53–86. doi:10.1016/j.addr.2021.01.019
82. Cardoso BD, Cardoso VF, Lanceros-Méndez S, Castanheira EMS. Solid magnetoliposomes as multi-stimuli-responsive systems for controlled release of doxorubicin: Assessment of lipid formulations. *Biomedicines*. 2022;10(5):1207. doi:10.3390/biomedicines10051207
83. Pande S. Liposomes for drug delivery: Review of vesicular composition, factors affecting drug release and drug loading in liposomes. *Artif Cells Nanomed Biotechnol*. 2023;51(1):428–440. doi:10.1080/21691401.2023.2247036
84. Bianco A, Kostarelos K, Prato M. Applications of carbon nanotubes in drug delivery. *Curr Opin Chem Biol*. 2005;9(6):674–679. doi:10.1016/j.cbpa.2005.10.005
85. Liu Z, Chen K, Davis C, et al. Drug delivery with carbon nanotubes for in vivo cancer treatment. *Cancer Res*. 2008;68(16):6652–6660. doi:10.1158/0008-5472.CAN-08-1468
86. Bianco A, Kostarelos K, Prato M. Making carbon nanotubes biocompatible and biodegradable. *Chem Commun (Camb)*. 2011;47(37):10182. doi:10.1039/c1cc13011k
87. Bhattacharya K, Andón FT, El-Sayed R, Fadeel B. Mechanisms of carbon nanotube-induced toxicity: Focus on pulmonary inflammation. *Adv Drug Deliv Rev*. 2013;65(15):2087–2097. doi:10.1016/j.addr.2013.05.012
88. Madani SY, Mandel A, Seifalian AM. A concise review of carbon nanotube's toxicology. *Nano Rev*. 2013;4(1):21521. doi:10.3402/nano.v4i0.21521
89. Prajapati SK, Malaiya A, Kesharwani P, Soni D, Jain A. Biomedical applications and toxicities of carbon nanotubes. *Drug Chem Toxicol*. 2022;45(1):435–450. doi:10.1080/01480545.2019.1709492
90. Meskher H, Ragdi T, Thakur AK, et al. A review on CNTs-based electrochemical sensors and biosensors: Unique properties and potential applications [published online as ahead of print on February 1, 2023]. *Crit Rev Anal Chem*. 2023. doi:10.1080/10408347.2023.2171277
91. Klumpp C, Kostarelos K, Prato M, Bianco A. Functionalized carbon nanotubes as emerging nanovectors for the delivery of therapeutics. *Biochim Biophys Acta*. 2006;1758(3):404–412. doi:10.1016/j.bbamem.2005.10.008
92. Podesta JE, Al-Jamal KT, Herrero MA, et al. Antitumor activity and prolonged survival by carbon-nanotube-mediated therapeutic siRNA silencing in a human lung xenograft model. *Small*. 2009;5(10): 1176–1185. doi:10.1002/smll.200801572
93. Bura C, Mocan T, Grapa C, Mocan L. Carbon nanotubes-based assays for cancer detection and screening. *Pharmaceutics*. 2022;14(4):781. doi:10.3390/pharmaceutics14040781
94. Bhirde AA, Patel V, Gavard J, et al. Targeted killing of cancer cells in vivo and in vitro with EGF-directed carbon nanotube-based drug delivery. *ACS Nano*. 2009;3(2):307–316. doi:10.1021/nn800551s
95. Michalet X, Pinaud FF, Bentolila LA, et al. Quantum dots for live cells, in vivo imaging, and diagnostics. *Science*. 2005;307(5709):538–544. doi:10.1126/science.1104274
96. Resch-Genger U, Grabolle M, Cavaliere-Jaricot S, Nitschke R, Nann T. Quantum dots versus organic dyes as fluorescent labels. *Nat Methods*. 2008;5(9):763–775. doi:10.1038/nmeth.1248
97. Gao X, Cui Y, Levenson RM, Chung LWK, Nie S. In vivo cancer targeting and imaging with semiconductor quantum dots. *Nat Biotechnol*. 2004;22(8):969–976. doi:10.1038/nbt994

98. Yaghini E, Seifalian AM, MacRobert AJ. Quantum dots and their potential biomedical applications in photosensitization for photodynamic therapy. *Nanomedicine*. 2009;4(3):353–363. doi:10.2217/nnm.09.9
99. Liu N, Tang M. Toxicity of different types of quantum dots to mammalian cells in vitro: An update review. *J Hazard Mater*. 2020;399:122606. doi:10.1016/j.jhazmat.2020.122606
100. Dussert F, Sarret G, Wegner KD, et al. Physico-chemical transformation and toxicity of multi-shell InP quantum dots under simulated sunlight irradiation, in an environmentally realistic scenario. *Nanomaterials*. 2022;12(20):3703. doi:10.3390/nano12203703
101. Lovrić J, Bazzi HS, Cuie Y, Fortin GRA, Winnik FM, Maysinger D. Differences in subcellular distribution and toxicity of green and red emitting CdTe quantum dots. *J Mol Med*. 2005;83(5):377–385. doi:10.1007/s00109-004-0629-x
102. Clift MJD, Rothen-Rutishauser B, Brown DM, et al. The impact of different nanoparticle surface chemistry and size on uptake and toxicity in a murine macrophage cell line. *Toxicol Appl Pharmacol*. 2008;232(3):418–427. doi:10.1016/j.taap.2008.06.009
103. He X, Ma N. An overview of recent advances in quantum dots for biomedical applications. *Colloids Surf B Biointerfaces*. 2014;124:118–131. doi:10.1016/j.colsurfb.2014.06.002
104. Susumu K, Uyeda HT, Medintz IL, Pons T, Delehanty JB, Mattoussi H. Enhancing the stability and biological functionalities of quantum dots via compact multifunctional ligands. *J Am Chem Soc*. 2007;129(45):13987–13996. doi:10.1021/ja0749744
105. Min J, Zhang Y, Zhou Y, et al. Size engineering of trap effects in oxidized and hydroxylated ZnSe quantum dots. *Nano Lett*. 2022;22(9):3604–3611. doi:10.1021/acs.nanolett.2c00118
106. Medintz IL, Uyeda HT, Goldman ER, Mattoussi H. Quantum dot bioconjugates for imaging, labelling and sensing. *Nature Mater*. 2005;4(6):435–446. doi:10.1038/nmat1390
107. Dennis AM, Rhee WJ, Sotto D, Dublin SN, Bao G. Quantum dot–fluorescent protein FRET probes for sensing intracellular pH. *ACS Nano*. 2012;6(4):2917–2924. doi:10.1021/nn2038077
108. Souza SO, Lira RB, Cunha CRA, Santos BS, Fontes A, Pereira G. Methods for intracellular delivery of quantum dots. *Top Curr Chem (Cham)*. 2021;379(1):1. doi:10.1007/s41061-020-00313-7
109. Kays JC, Saeboe AM, Toufanian R, Kurant DE, Dennis AM. Shell-free copper indium sulfide quantum dots induce toxicity in vitro and in vivo. *Nano Lett*. 2020;20(3):1980–1991. doi:10.1021/acs.nanolett.9b05259
110. Kumari A, Yadav SK, Yadav SC. Biodegradable polymeric nanoparticles based drug delivery systems. *Colloids Surf B Biointerfaces*. 2010;75(1):1–18. doi:10.1016/j.colsurfb.2009.09.001
111. Moura LIF, Dias AMA, Carvalho E, De Sousa HC. Recent advances on the development of wound dressings for diabetic foot ulcer treatment: A review. *Acta Biomater*. 2013;9(7):7093–7114. doi:10.1016/j.actbio.2013.03.033
112. Lee KY, Mooney DJ. Alginate: Properties and biomedical applications. *Prog Polym Sci*. 2012;37(1):106–126. doi:10.1016/j.progpolymsci.2011.06.003
113. Young S, Wong M, Tabata Y, Mikos AG. Gelatin as a delivery vehicle for the controlled release of bioactive molecules. *J Control Release*. 2005;109(1–3):256–274. doi:10.1016/j.jconrel.2005.09.023
114. Sultana Y, Mall S, Maurya DP, Kumar D, Das M. Preparation and in vitro characterization of diltiazem hydrochloride loaded alginate microspheres. *Pharm Dev Technol*. 2009;14(3):321–331. doi:10.1080/10837450802626304
115. Rivera-Gil P, De Koker S, De Geest BG, Parak WJ. Intracellular processing of proteins mediated by biodegradable polyelectrolyte capsules. *Nano Lett*. 2009;9(12):4398–4402. doi:10.1021/nl902697j
116. Jafarzadeh S, Mohammadi Nafchi A, Salehabadi A, Oladzad-Abbasabadi N, Jafari SM. Application of bio-nanocomposite films and edible coatings for extending the shelf life of fresh fruits and vegetables. *Adv Coll Interface Sci*. 2021;291:102405. doi:10.1016/j.cis.2021.102405
117. Petroni S, Tagliaro I, Antonini C, et al. Chitosan-based biomaterials: Insights into chemistry, properties, devices, and their biomedical applications. *Marine Drugs*. 2023;21(3):147. doi:10.3390/md21030147

Prognostic factors associated with worse outcomes in patients with GBS: A systematic review

Marta Grelowska[1,B–D], Katarzyna Logoń[1,B–D], Edyta Dziadkowiak[2,A,D–F]

[1] Student Scientific Association of Neurology, Wroclaw Medical University, Poland
[2] Department of Neurology, Wroclaw Medical University, Poland

A – research concept and design; B – collection and/or assembly of data; C – data analysis and interpretation;
D – writing the article; E – critical revision of the article; F – final approval of the article

Advances in Clinical and Experimental Medicine, ISSN 1899–5276 (print), ISSN 2451–2680 (online) *Adv Clin Exp Med*. 2025;34(3):457–467

Address for correspondence
Edyta Dziadkowiak
E-mail: edyta.dziadkowiak@umw.edu.pl

Funding sources
None declared

Conflict of interest
None declared

Received on November 30, 2023
Reviewed on March 23, 2024
Accepted on April 8, 2024

Published online on October 2, 2024

Abstract

Guillain–Barré syndrome (GBS) is an autoimmune polyradiculoneuropathy with diverse clinical subtypes, characterized by rapidly evolving motor weakness, sensory disturbances and areflexia. The global prevalence of GBS has been steadily increasing, with regional disparities. Mortality rates vary but remain elevated in patients requiring mechanical ventilation. This systematic review aimed to evaluate the predictive risk factors for the severity of the disease and poor short- and long-term outcomes of GBS. The literature search was conducted using the PubMed database by 2 independently working researchers. After a screening process of studies published before November 2023, a total of 109 articles were selected. Original articles, systematic and narrative reviews, meta-analyses, and editorials were selected based on their clinical relevance. The exclusion criteria included patients under 18 years of age, pregnant women and articles in languages other than English and Polish. Long-lasting GBS complications included pain, fatigue and persistent neurological deficits, affecting patients for years after recovery. Identifying the appropriate therapeutic methods, risk factors and prognoses of GBS at an early stage is crucial. Various risk factors for death and poor functional outcomes were found, regarding patient characteristics, the clinical course of GBS, laboratory and neurographic results, as well as treatment methods.

Key words: treatment outcome, risk factors, prognosis, Guillain–Barré syndrome

Cite as
Grelowska M, Logoń K, Dziadkowiak E. Prognostic factors associated with worse outcomes in patients with GBS: A systematic review. *Adv Clin Exp Med*. 2025;34(3):457–467. doi:10.17219/acem/186949

DOI
10.17219/acem/186949

Introduction

Guillain–Barré syndrome (GBS) is an autoimmune inflammatory polyradiculoneuropathy affecting peripheral nerves.[1] It is characterized by rapidly evolving ascending motor weakness, areflexia and sensory disturbances that develop within 4 weeks.[2] Guillain–Barré syndrome often follows infections, but it can also occur after vaccinations, surgeries or during pregnancy.[3] The main variants of GBS include acute inflammatory demyelinating polyradiculoneuropathy (AIDP), acute motor axonal neuropathy (AMAN), acute motor and sensory axonal neuropathy (AMSAN), and Miller–Fisher syndrome (MFS).[2] Acute inflammatory demyelinating polyradiculoneuropathy manifests as a sensorimotor form that can co-occur with cranial nerve deficits and autonomic dysfunction. Acute motor axonal neuropathy is a pure motor form in which the cranial nerves are intact. Acute motor and sensory axonal neuropathy (AMSAN) is a condition that shares similarities with the AMAN pattern, but it additionally affects sensory nerves.[4] Miller–Fisher syndrome is less common and is characterized by ataxia, ophthalmoplegia and areflexia.[5]

The age-standardized prevalence of GBS is the highest in high-income Asia Pacific and North American countries, especially Japan and Singapore. East Asia and Oceania have the lowest GBS prevalence rates.[6] The AIDP type is significantly more common in Europe and North America, while AMAN occurs more frequently in East Asia.[5]

The prevalence of GBS has continued to increase globally over the years. In 1990, the global prevalence per 100,000 persons was 3.6%, and in 2019 it reached 9.5%.[6] In a 2009 study, the global incidence of GBS was estimated between 1.1 and 1.8 cases per 100,000 persons/year.[7] In the recent 2021 meta-analysis, the incidence of GBS among the cohort studies was higher and varied from 0.30 to 6.08 cases per 100,000 persons and 0.42 to 6.58 cases per 100,000 person-years.[8] Guillain–Barré syndrome is slightly more frequent in men than in women and its incidence tends to increase with age.[9]

The mortality rates of GBS vary significantly between studies and range between 1–18%.[10–12] They remain higher (12–20%) in patients requiring endotracheal intubation and mechanical ventilation (MV).[13,14]

Guillain–Barré syndrome is associated with long-lasting complications, such as pain, fatigue, disability, and impaired psychosocial functioning.[15] Persistence of moderate-to-severe pain was reported in different studies after 1 or 2 years in over 1/3 of patients.[16,17] Patients, after recovering from GBS, still report neurological deficits. Many studies described deficits in ambulation and sensation occurring 1 year after illness onset.[18,19] Motor and sensory disturbances were reported quite commonly even 10 years later.[20] In a study by Durand et al., after 6 months, almost 1/3 of patients had a disability grade ≥2 (Plasma Exchange/Sandoglobulin Guillain–Barré Syndrome Trial Group, 1998: 0 = healthy, no signs or symptoms of Guillain–Barré syndrome; 1 = minor symptoms or signs and able to run; 2 = able to walk 5 m across an open space without assistance; 3 = able to walk 5 m across an open space with the help of 1 person and waist-level walking-frame, stick, or sticks; 4 = chairbound/bedbound: unable to walk as in 3; 5 = requiring assisted ventilation (for at least part of day or night); 6 = dead).[21] In another study, at 3–5 years after GBS onset, 20% of patients had a disability grade of 2 and 10% had a disability grade of 3.[22] In a recent long-term study, approx. 10% of patients exhibited disability by the end of the study period. Of these, 5% demonstrated moderate disability, while 5.2% exhibited severe disability.[23]

The outcomes of GBS differ between the GBS subtypes. A study by Zhang et al. found that the prognosis of AMAN patients was poorer than that of AIDP patients,[24] which was confirmed in a 2020 study where AMAN was found to be an independent predictor of an unfavorable outcome.[25] A recent 2022 study reported worse outcomes in patients with AMAN and AMSAN compared to those with AIDP.[26] Patients with MFS usually have a good natural recovery, and almost no residual deficits were left at follow-up, regardless of the treatment.[27]

The pathophysiology of GBS is based on the phenomenon of molecular mimicry. Depending on the site on the nerve cell where the antibody attack occurs, GBS assumes a specific clinical form. The autoimmune process is usually initiated by an infection. Figure 1 shows these processes in a clinical form.

The figures were drawn with Procreate v. 5.3.3 (Savage Interactive, Hobart, Australia). Parts of the Fig. 1 were made using pictures from Servier Medical Art, which is licensed under a Creative Commons Attribution 3.0 Unported License (https://creativecommons.org/licenses/by/3.0/). The diagnosis and management of GBS should be based on guidelines published in 2023 by van Doorn et al.[28] The diagnosis is established regarding the patient's history and neurological, electrophysiological and cerebrospinal fluid (CSF) examinations. An alternative diagnosis for the weakness must be excluded.[29,30] Guillain–Barré syndrome should be taken into account in patients who have rapidly progressive symmetric motor weakness of the legs and/or arms in the absence of other apparent causes, especially if there is a history of recent diarrhea or respiratory infection.[28] Patients with the classic sensorimotor form present with distal paresthesias or sensory loss, ascending weakness, and a loss of reflexes. Symptoms develop within no more than 4 weeks and in most patients within 2 weeks.[28,30,31] Cerebrospinal fluid analysis is valuable and usually shows an elevated protein level and a normal cell count, known as albuminocytologic dissociation.[32] In standard conduction velocity tests, prolongation of distal latencies, slowing of conduction velocities mostly in motor fibers, and prolongation or absence of F-waves are observed.[33]

Electrodiagnostic studies are also helpful in differentiating between the 4 subtypes of classical GBS: AIDP, AMAN, AMSAN, and MFS.[34] The criterion for the diagnosis

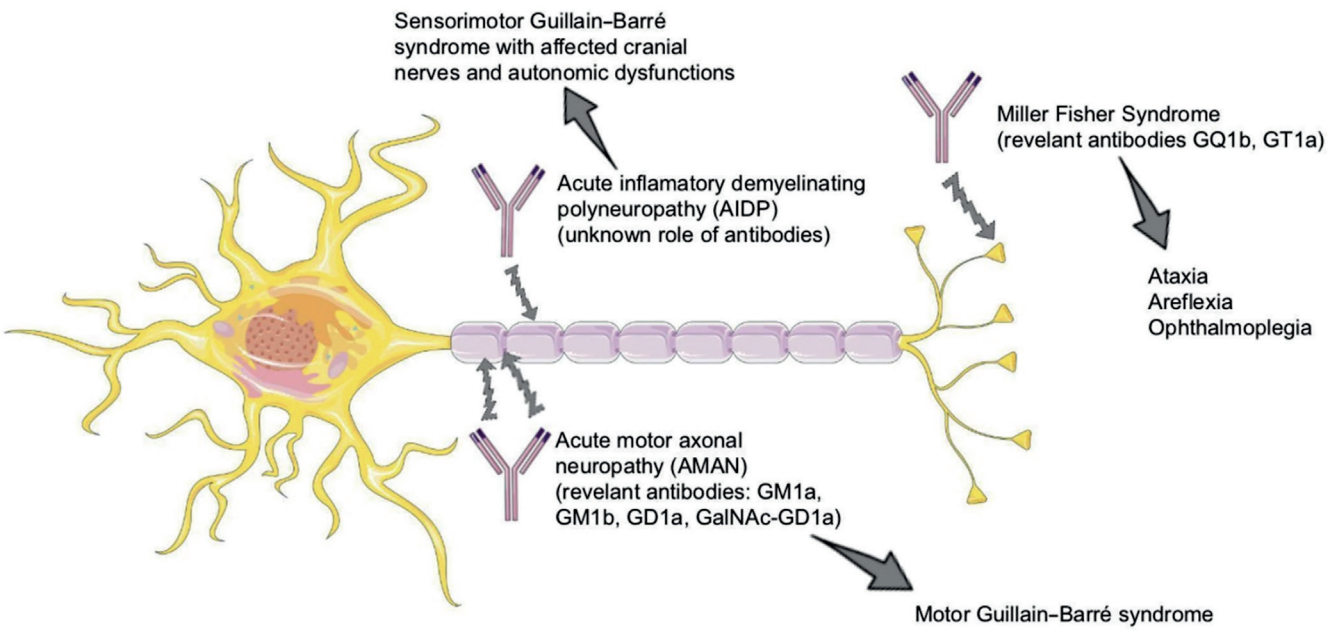

Fig. 1. Pathomechanism of GBS subtypes

of AIDP is the electrophysiological confirmation of a decrease in the conduction velocity of 2 or more motor nerves, suggesting an immune-mediated demyelinating process involving the membrane of Schwann cells or myelin.[35] Acute motor axonal neuropathy is distinguished from AIDP due to the occurrence of axonal involvement without demyelination. The diagnosis of AMAN is based on the finding of reversible conduction failure due to axonal conduction block at the nodes of Ranvier or the motor nerve terminal without axonal degeneration or extensive axonal degeneration.[28] There are also rarer types of GBS, such as AMSAN and MFS. The first of them concerns changes, the basis of which lies in the axonal degeneration of both motor and sensory fibers. The latter is characterized by a characteristic triad of clinical symptoms, which includes ophthalmoplegia, ataxia and areflexia, which is closely related to the presence of specific antibodies against ganglioside GQ1b.[36]

It is currently believed that the best effects in GBS therapy are achieved through the use of intravenous immunoglobulin (IVIG) 0.4 g/kg within 2 weeks of the onset of symptoms for 5 days.[37] Good results are also achieved by performing plasmapheresis in the amount of 4–6 treatments. The key variable influencing the effectiveness of therapy is the time of initiation of therapy, which should be started as soon as possible, up to 12 h after the onset of symptoms.[38]

Objectives

This study aimed to undertake a new review of the up-to-date literature concerning the risk factors regarding patient characteristics, the course of GBS, and laboratory and neurographic test results. The efficacy of the possible treatments was also discussed.

Materials and methods

A review of scientific articles published in the PubMed database between 1981 and 2023 was performed. Data were collected in September 2023 by 2 independently working researchers. The following filters were used in the PubMed database: ((GBS) OR (Guillain–Barré syndrome)) AND (long-term) AND ((disability) OR (outcomes) OR (mortality)), ((GBS) AND (risk factors)) and ((GBS) AND (predictors)) for a total of 1,384 results. Of these, 944 articles were removed after reviewing the title or abstract, since they were unrelated to the topic of the research. The exclusion criteria were patients under 18 years of age and pregnant women. Conference abstracts and articles in languages other than English and Polish were excluded as well. Ultimately, 73 articles were qualified for analysis. Additionally, 36 papers were used that did not appear in the automatic search but were considered relevant. The summary of the results for unfavorable outcomes is provided in Table 1. The summary of the studies mentioned in this review is provided in Table 2.[39–92] Figure 2 depicts the Preferred Reporting Items for Systematic Reviews and Meta-Analyses (PRISMA) chart of evaluated studies. All figures and tables were prepared manually Servier Medical Art and Procreate software.

Risk factors: Patient characteristics

Risk factors for death regarding patient characteristics are older age and pre-existing comorbidities, such as organ dysfunction (including cardiac and pulmonary disease), diabetes mellitus and coronary artery disease.[39–41] In a study by Dhar et al., advanced age was the strongest predictor of poor outcomes.[40,42] Van den Berg et al. found

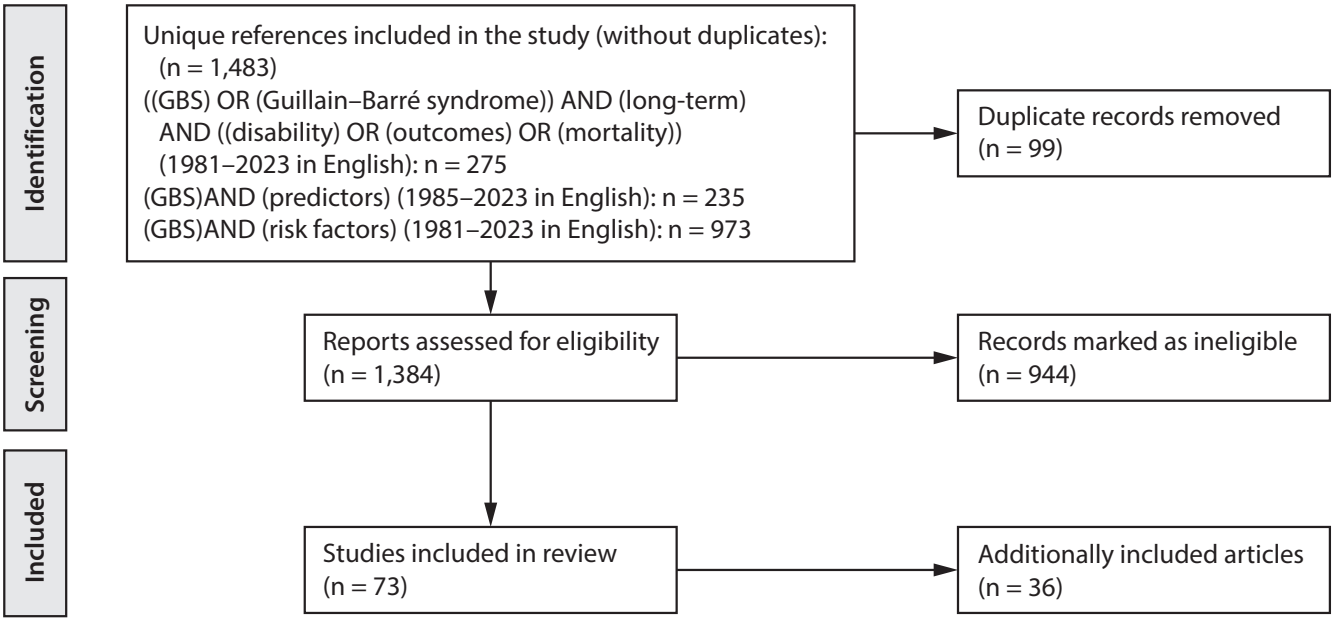

Fig. 2. Identification of studies via database and registers

Table 1. Overview of prognostic factors for death and disability in Guillain–Barré syndrome

Type	Prognostic factor
Demographic	older age pre-existing comorbidity: pulmonary disease, cardiac disease, dyslipidemia, diabetes recent history of surgery
Clinical	higher severity of weakness at entry mechanical ventilation lack of mechanical ventilation when needed increased delay from onset of weakness to entry voiding difficulty longer time to peak disability autonomic dysfunction bulbar nerve involvement papilledema neck flexor weakness the type of the antecedent disorder: gastroenteritis pulmonary infection long duration stay in hospital chief complaint: weakness
Laboratory	presence of anti-GD1a/GD1b and/or anti-GD1b/GT1b antibodies hyponatremia low serum albumin levels higher neutrophil/lymphocyte ratio (NLR) and elevated C-reactive protein (CRP) elevated protein levels elevated neurofilament light protein (NFL) lower folate levels higher fasting blood glucose (FPG) levels increased cerebrospinal fluid total protein (CSF-TP) higher protein-to-albumin ratio (CAR) elevated CRP
Neurographic	markedly attenuated compound muscle action potentials inexcitable motor nerves denervation changes lack of electrical activity in the quadriceps femoris muscle on the 10th day lower deltoid muscle strength decreased intraepidermal nerve fiber density (IENFD)

that 73% of the deceased patients had a history of pulmonary or cardiac disease.[43] This is consistent with other studies, in which mortality was significantly associated with underlying cardiopulmonary diseases.[13,44] A recent 2022 study found a correlation between dyslipidemia and the severity of GBS.[45] Furthermore, the recent history of surgery is associated with an unfavorable short-term prognosis and disease severity.[41]

Risk factors: Clinical course of the disease

Several risk factors for death and poor functional outcome regarding the clinical course of GBS were found, including the severity of weakness at entry, MV, delay from onset of weakness to entry, voiding difficulties, and time to peak disability.[43,46,47,93] The time between onset of disease and death is highly variable. In a study by van den Berg et al., the median time was 76 days (ranging from 23–152 days). Sixty-seven percent of patients died in the recovery phase, 20% in the acute progressive phase and 13% during the plateau phase.[43] The severity of the disease is usually assessed using the Medical Research Council (MRC) sum score or GBS disability score.[94,95] In a recent 2023 study, the best predictor of clinical rating scores using the Hughes Disability Scale (HDS) and Overall Neuropathy Limitation Scale (ONLS) was a low MRCSS on the 10th day of treatment.[48] A study of Bangladeshi patients revealed that MV and the absence of ventilator support when it was required were risk factors for death. The unavailability of MV for patients with acute respiratory failure was identified as the most important risk factor that accounted for 20% of deaths.[49] The need for MV is correlated with longer hospital stay and and reduced rate of recovery up to 1 year after the onset of disease.[50]

Table 2. A summary of the studies mentioned in a review

Author	Year of study	Number of patients	Type of study	Estimated factor
Shangab et al.[39]	2020	82 GBS patients	retrospective study	older age, requirement for MV, axonal type of nerve injury, severity of weakness at entry
Dhar et al.[40]	2008	77 GBS patients	retrospective study	advanced age, prolonged MV, ICU complications (mostly pneumonia)
Wen et al.[41]	2021	155 GBS patients	retrospective study	recent history of surgery, older age, cranial nerve impairment, elevated levels of liver enzymes, lower MRC score, requirement for MV, pneumonia
Zhang et al.[42]	2017	535 GBS patients	retrospective study	older age, lower MRC score at nadir
van den Berg et al.[43]	2013	527 GBS patients	prospective study	older age, severity of weakness at entry, requirement for MV, delay from onset of weakness to entry, longer time to peak disability
Serrano and Rabinstein[44]	2010	85 patients admitted to the intensive care unit with acute neuromuscular respiratory failure	retrospective study	older age, longer MV, longer ICU stay
Ding et al.[45]	2022	147 GBS patients and 153 healthy individuals	case–control study	dyslipidemia
González-Suárez et al.[46]	2013	106 GBS cases	retrospective study	older age, severe deficits at onset, injured cranial nerves, requiring MV, axonal lesion patterns
Park et al.[47]	2016	47 GBS patients	retrospective study	older age, severity at admission, voiding difficulty, MV
Khedr et al.[48]	2023	62 GBS patients	prospective study	older age, the presence of an antecedent event particularly diarrhea, low MRC score at the 10th day, elevated CRP, hyponatremia, cytoalbuminous dissociation
Ishaque et al.[49]	2017	407 GBS patients	prospective study	lack of MV when it was required, autonomic dysfunction, bulbar nerve involvement, MV, longer progressive phase
Shangab and Al-Kaylani[50]	2021	82 GBS patients	retrospective study	need for MV
Verma et al.[51]	2013	90 GBS patients	prospective study	autonomic dysfunction, neck flexor weakness, MV requirement, lower MRC score on admission, axonal pattern on electrophysiological assessment
Paul et al.[52]	2012	138 GBS patients	retrospective and prospective study	presence of bulbar weakness
Beghi et al.[53]	1996	297 GBS patients	multicentre prospective study	older age, antecedent gastroenteritis, electrophysiological signs of axonopathy, latency to nadir
Walgaard et al.[54]	2011	397 GBS patients	prospective study	older age, preceding diarrhea, low MRC score at admission and at 1 week
Kobori et al.[55]	2017	4,132 GBS patients	retrospective study	coexisting cytomegalovirus, herpes simplex virus infections on admission
Di et al.[56]	2023	62 GBS patients	retrospective study	pneumonia, hyponatremia, hypoalbuminemia
Nasiri et al.[57]	2018	57 GBS patients	retrospective study	autonomic dysfunction
Alloush et al.[58]	2019	20 GBS patients	analytical observational study	need for MV, longer stay at the hospital
Wang et al.[59]	2017	523 GBS patients	retrospective study	chief complaint of weakness
Kaida et al.[60]	2007	234 GBS patients	retrospective study	ganglioside complexes (GSCs)
Lardone et al.[61]	2010	34 GBS patients	prospective study	specificity of anti-GM1 antibodies
Koga et al.[62]	2003	134 GBS patients	retrospective study	IgG1 and IgG3 subclass of anti-GM1 antibody
Bech et al.[63]	1997	17 GBS patients	prospective study	IgM anti-GM1 antibodies
Wu et al.[64]	2012	1,590 GBS patients	meta-analysis	TNF-α 308A allele
Safa et al.[65]	2020	669 GBS patients	literature review	a.o. TNF-α 308A allele
Tunç[66]	2019	81 GBS patients	retrospective study	decreased albumin and sodium levels, increased CSF protein levels, higher age, elevated NLR, higher CRP levels
Sipilä et al.[67]	2017	69 GBS patients	retrospective study	low plasma sodium level
Saifudheen et al.[68]	2011	50 GBS patients	retrospective study	age >50, ventilatory support, hyponatremia, and bulbar weakness

Table 2. A summary of the studies mentioned in a review – cont.

Author	Year of study	Number of patients	Type of study	Estimated factor
Wang et al.[69]	2015	55 GBS patients	prospective study	hyponatremia
Rumalla et al.[70]	2017	54,778 GBS patients	multicentre retrospective study	hyponatremia
Ozdemir[71]	2016	62 GBS patients	retrospective study	albumin levels, NLR and PLR
Jahan et al.[72]	2023	140 GBS patients	prospective study	elevated NLR
Sun et al.[73]	2023	136 GBS patients	retrospective study	elevated NLR
Ning et al.[74]	2021	426 GBS patients	retrospective study	NLR and PLR
Ning et al.[75]	2021	200 GBS patients	retrospective study	CAR and CRP levels
Sahin et al.[76]	2017	24 GBS patients	retrospective study	CSF protein level; NLR
Gonzalez-Quevedo et al.[77]	2009	53 GBS patients	prospective study	B-CSFB dysfunction
Bourque et al.[78]	2020	173 GBS patients	retrospective study	CSF-TP values
Bae et al.[79]	2016	85 GBS patients	prospective study	chronic inflammation and nerve ischaemia in diabetes mellitus
Wang et al.[80]	2015	304 GBS patients	prospective study	higher level of fasting plasma glucose (FPG)
Peric et al.[81]	2017	257 GBS patients	retrospective study	presence of diabetes mellitus independently of age
Gao et al.[82]	2018	112 GBS patients	retrospective study	serum folate levels
Petzold et al.[83]	2006	23 GBS patients	prospective study	high CSF NfH levels
Axelsson et al.[84]	2018	18 GBS patients	pilot study	high NFL in CSF
Martín-Aguilar et al.[85]	2020	98 + 24 samples of GBS patients	prospective study	increased sNfL levels
López-Hernández et al.[86]	2022	153 GBS patients	ambispective cohort study	deltoid muscle strength
Sundar et al.[87]	2005	46 GBS patients	retrospective study	abnormal H reflex and F waves
Miller et al.[88]	1988	60 GBS patients	prospective study	mean compound muscle action potential amplitude
Ruts et al.[89]	2012	32 GBS patients	prospective study	intraepidermal nerve fiber density (IENFD)
Grimm et al.[90]	2016	27 GBS patients	prospective study	ultrasonographic detection of cervical spinal nerve and vagus nerve enlargement
França et al.[91]	2005	18 GBS patients	retrospective study	elderly age is associated with complications after plasmapheresis
Wang et al.[92]	2017	186 GBS patients	retrospective study	no correlation between treatment options and long-term improvement

MRC – Medical Research Council; MV – mechanical ventilation; NLR – neutrophil-to-lymphocyte ratio; PLR – platelet-to-lymphocyte ratio; CAR – C-reactive protein-to-albumin ratio; CRP – C-reactive protein; CSF – cerebrospinal fluid; NLR – neutrophil/lymphocyte ratio; CSF-TP – CSF total protein; B-CSFB – blood-CSF barrier; CSF NfH – cerebrospinal fluid neurofilament; NLP – neurofilament light protein; sNfL – serum neurofilament light chain.

The probability of developing respiratory insufficiency within the 1st week can be assessed with the Erasmus GBS Respiratory Insufficiency Score (EGRIS).[96] It employs time between the onset of weakness and admission, facial and/or bulbar weakness, and MRC scores to divide patients into 3 groups according to their risk. In 2023, Luijten et al. published a modified EGRIS, which requires less information for a prediction, can be used at multiple time points, and is used in less severe cases.[97] The inability to walk unaided at 4 and 26 weeks in GBS patients can be predicted using the modified Erasmus GBS Outcome Score (mEGOS).[98]

Autonomic dysfunction, bulbar nerve involvement, papilledema, and neck flexor weakness have also been identified as factors associated with adverse outcomes in GBS patients.[48,49,51] Bulbar palsy and neck flexor weakness are often correlated with respiratory compromise and the need for MV.[51,52] Durand et al. reported that bulbar palsy was present in 38% of ventilated patients and in 10% of non-ventilated patients,[21] while Paul et al. found bulbar involvement in 92.5% of ventilated patients compared to 28.2% of non-ventilated patients.[52]

The Italian Guillain–Barré Study Group observed that the type of antecedent disorder influenced the chances of clinical recovery. Patients who experienced gastroenteritis prior to the onset of symptoms took the longest time to achieve clinical recovery, with an average duration of 292 days, whereas those with an upper respiratory infection averaged 193 days, and patients with influenza took an average of 123 days to recover.[53] This was later confirmed in studies by van Koningsveld et al., Walgaard et al. and Khedr et al., in which preceding diarrhea was an unfavorable factor for recovery at 3 and 6 months.[48,54,99] Moreover, coexisting cytomegalovirus (CMV) and herpes simplex virus (HSV) infections on admission may correlate with a higher risk of respiratory failure.[55]

The study by Dhar et al. stated that for the occurrence of severe complications, the risk difference did not reach statistical significance in terms of final recovery. However, serious ICU complications were associated with a longer time to recover.[40] A recent 2023 study found that pulmonary infections can be used as an independent predictor for a poor early prognosis in patients with GBS.[56]

A prolonged hospital stay was found to be significantly associated with a poorer prognosis. This may be attributed to the higher incidence of complications commonly associated with prolonged hospital stays, including pneumonia, sepsis and respiratory distress syndrome (RDS).[58,58]

Wang et al. found that the chief complaints of GBS patients could be clinic predictors of disease severity, the need for MV and short-term outcomes. Patients presenting with weakness as a main complaint were more likely to experience a severe disease progression and have a worse short-term outcome, while a chief complaint of numbness and cranial nerve involvement was a promising predictor.[59]

In a study conducted by Lopez–Hernandez et al., the AMAN subtype was found to be a predictor of worse short-term outcomes.[25]

Risk factors: Laboratory tests

For the clinician, the most important factor is the susceptibility of the GBS variant to standard treatment regimens. A direct predictor of therapeutic problems is the need for MV. Patients who showed the presence of anti-GD1a/GD1b and/or anti-GD1b/GT1b antibodies were most likely to have GBS with impaired spontaneous breathing.[60] The presence of antibodies against ganglioside complexes (GSCs) also determines the occurrence of symptoms such as ophthalmoplegia and lower cranial nerve deficits.[60] Gangliosides such as GD1a may interact with GM1 in cell membranes to regulate the binding and biological activity of some anti-GM1 antibodies. However, studies have shown that the high specificity of anti-GM1 antibodies in GBS is a factor defining the disease severity.[61] It is worth paying attention to the presence of anti-GM1 antibodies (immunoglobulin g; IgG) in patients with GBS due to the selection of treatment. Intravenous immunoglobulins have been proven to be more effective than plasmapheresis in patients with these antibodies.[62] Studies also show that monitoring anti-GM1 IgM levels can predict clinical status and recovery in patients with GBS.[63]

Despite the relatively small number of available studies, it should be remembered that the presence of the tumor necrosis factor alpha (TNF-α) 308A allele may be a moderate risk factor for GBS.[64] Additionally, it has been noted that GBS patients show abnormal expression of immune-related genes. Identification of GBS risk alleles may help identify risk groups, avoid triggers and design personalized therapeutic approaches.[65]

Moreover, researchers are using serum C3 complement levels as a biomarker in GBS. Higher C3 levels are associated with longer hospitalizations and more frequent treatment-related fluctuations. These patients also presented lower MRCSS and higher GBS disability scores (GBSDS). The clinical severity of GBS occurs with longitudinal change in C3 levels.[100]

Other important parameters that will indicate difficulties in treatment are sodium, albumin, neutrophil/lymphocyte ratio (NLR), C-reactive protein (CRP), and protein concentrations in the CSF.[48,66] Hyponatremia occurs during more severe GBS episodes but is not directly correlated with or directly specific to them. Its occurrence is probably related to the disturbance of body homeostasis.[66–68] However, analyses have proven a relationship between the results of the HDS and the ONLS and sodium concentrations in patients with a poor prognosis.[48,67,69] Sodium levels should be monitored, especially in patients with other risk factors, as they can directly affect outcomes.[70]

Low serum albumin levels accompanied more severe forms of GBS. Researchers believe that their level is a protective factor. Serum albumin plays a strong antioxidant role by inhibiting free hydroxyl radicals that are produced in the process of inflammation, demyelination and axonal damage. Therefore, it was found to be beneficial to administer human albumin in patients with GBS and hypoalbuminemia.[55,66]

Neutrophil/lymphocyte ratio and CPR are considered non-specific parameters of blood tests. However, they can confirm the diagnosis, and at the end of the 1st month of the disease, their levels have a prognostic value for a more severe course.[66,71,72] Neutrophil/lymphocyte ratio can be considered an independent risk factor for GBS.[73,74]

According to studies, a CRP >5 and protein-to-albumin ratio (CAR) >0.21 are independently associated with the occurrence of respiratory failure in patients with GBS, while a CRP >5 and CAR >0.19 predict poorer short-term outcomes in patients with GBS. The researchers suggest measuring the CAR on admission as it may be a better predictor of complications such as risk of respiratory failture than only CRP results.[75]

Elevated protein levels in the CSF are detected during inflammation of the nervous system. It has been noted that the lower the protein values at the beginning of a GBS episode, the better the prognosis.[76] High values may indicate destruction of the blood–nerve barrier.[77] It has been observed that there are higher absolute values of CSF total protein (CSF-TP) in classic sensorimotor GBS and local GBS compared to MFS and motor GBS. However, due to the weak correlation of CSF-TP and disability in GBS, it cannot be used as a factor for the modification of treatment plans.[78]

Diabetes exacerbates the clinical and electrophysiological symptoms of GBS and affects long-term disability due to the presence of chronic low-grade inflammation (elevated inflammatory markers: CRP, TNF-α and interleukin 6; IL-6).[79] Higher fasting blood glucose (FPG) levels on admission were associated with a poorer short-term

prognosis as measured using the MRCSSs and GBS disability scale at discharge. However, the development of disability is not related to blood HbA1c or CSF glucose concentrations.[80] Additionally, some diabetic patients may have pre-existing nerve damage, which exacerbates the reduced rate of nerve regeneration. It is also noted that patients with GBS and diabetes are more likely to develop the axonal form of the disease, and the electrophysiological changes in these patients are more pronounced.[81]

A significant relationship was demonstrated between folate deficiency at the time of admission and the duration of GBS progression. The exact role is unclear, but it is known that folate is essential for peripheral nerves, and its deficiency is associated with axonal sensory polyneuropathy.[82]

Long-term symptoms of GBS are caused by axonal damage. The presence of elevated levels of neurofilaments (NfH), a biomarker indicative of axonal damage, has been demonstrated to possess prognostic value in the context of GBS. Additionally, CSF NfH levels correlated with F scores and MRCSSs. These were higher in patients with neurophysiological features of axonal degeneration. The cutoff point for poorer motor and functional outcomes was defined as >0.73 ng/mL of NfH in the CSF.[83] Additionally, research shows that neurofilament light protein (NFL) should be included as an early indicator of patients requiring extensive medical and rehabilitation interventions for the long term. Patients who are severely disabled at the onset of GBS but have low concentrations of NFL in their CSF are considered to have a significantly greater chance of recovery.[84,85]

Risk factors: Neurographic tests

Neurophysiological tests can be successfully used to establish the initial diagnosis. Attempts to use them to determine the prognosis raises many doubts. There is no shortage of voices claiming that the lack of electrical excitability of the motor nerves and the lack of electrical activity in the quadriceps femoris muscle on the 10th day after the onset of the disease are independent factors for a more severe course and more difficult treatment.[101] However, more recent studies have shown that the diagnostic value of neurophysiological methods increases in proportion to the time since the onset of the disease.[102] Besides the quadriceps femoris muscle, deltoid muscle strength may also have a predictive value.[86]

Studies show that patients with markedly attenuated compound muscle action potentials (CMAPs), inexcitable motor nerves, and denervation changes on electromyography will be required to undergo MV. Nevertheless, the most prevalent abnormalities observed in both patients requiring and not requiring ventilation are abnormal H reflexes and F waves.[87,88]

Another predictive factor was found to be the intraepidermal nerve fiber density (IENFD), which correlates (decreases early and stays low for a long time) with pain intensity in the acute phase and may predict long-term disability.[89] In USG, there can be detected vagus nerve or cervical spinal nerve hypertrophy and regression of these changes within 6 months indicates a better prognosis.[90]

Risk factors: Treatment course

In the treatment of GBS, it is important to use IVIGs or plasmapheresis, which, according to researchers, maximizes survival potential.[103,104] There are also no significant differences between the use of plasma exchange and IVIG. Nevertheless, control using the ONLS indicates the advantage of treatment with IVIG.[48,91] Long-standing improvements may not be directly related to IVIG treatment but are caused by self-limitations. Despite this, studies prove that this treatment had a long-term effect on both mild and moderate-to-severe GBS.[92] It also does not seem that more intensive treatment has a significant impact on improvement in patients with advanced degrees of disability. Studies have shown that patients unable to walk on their own did not show improvement after an additional course of immunotherapy.[105]

Limitations

This systematic review has several limitations. First, only articles in English and Polish were included. No searches were made for scientific reports in other languages. Furthermore, the simultaneous appearance of some conditions or diagnostic test results and GBS episodes can be coincidental. Moreover, the heterogeneity of patients makes it difficult to combine and interpret the results, limiting conclusions. It was not possible to fully verify this data due to insufficient information about the patients.

Conclusions

This review of the literature focused on identifying prognostic factors associated with a worse outcome in patients with GBS. Scales to identify patients at high risk of mortality have also been developed to assess the course of GBS. Knowledge of these prognostic factors may, in the future, make it possible to modify the current treatment regimens for these patients.

ORCID iDs

Marta Grelowska https://orcid.org/0009-0001-6634-512X
Katarzyna Logoń https://orcid.org/0000-0002-9038-2940
Edyta Dziadkowiak https://orcid.org/0000-0002-9618-9308

References

1. Arcila-Londono X, Lewis R. Guillain–Barré syndrome. *Semin Neurol*. 2012;32(3):179–186. doi:10.1055/s-0032-1329196
2. Dimachkie MM, Barohn RJ. Guillain–Barré syndrome and variants. *Neurol Clin*. 2013;31(2):491–510. doi:10.1016/j.ncl.2013.01.005

3. Walling AD, Dickson G. Guillain–Barré syndrome. *Am Fam Physician*. 2013;87(3):191–197. PMID:23418763.
4. Van Den Berg B, Walgaard C, Drenthen J, Fokke C, Jacobs BC, Van Doorn PA. Guillain–Barré syndrome: Pathogenesis, diagnosis, treatment and prognosis. *Nat Rev Neurol*. 2014;10(8):469–482. doi:10.1038/nrneurol.2014.121
5. Kuwabara S. Guillain–Barré syndrome: Epidemiology, pathophysiology and management. *Drugs*. 2004;64(6):597–610. doi:10.2165/00003495-200464060-00003
6. Bragazzi NL, Kolahi AA, Nejadghaderi SA, et al. Global, regional, and national burden of Guillain–Barré syndrome and its underlying causes from 1990 to 2019. *J Neuroinflammation*. 2021;18(1):264. doi:10.1186/s12974-021-02319-4
7. McGrogan A, Madle GC, Seaman HE, De Vries CS. The epidemiology of Guillain–Barré syndrome worldwide. *Neuroepidemiology*. 2009;32(2):150–163. doi:10.1159/000184748
8. Wachira VK, Farinasso CM, Silva RB, Peixoto HM, De Oliveira MRF. Incidence of Guillain–Barré syndrome in the world between 1985 and 2020: A systematic review. *Glob Epidemiol*. 2023;5:100098. doi:10.1016/j.gloepi.2023.100098
9. Sejvar JJ, Baughman AL, Wise M, Morgan OW. Population incidence of Guillain–Barré syndrome: A systematic review and meta-analysis. *Neuroepidemiology*. 2011;36(2):123–133. doi:10.1159/000324710
10. Levison LS, Thomsen RW, Andersen H. Increased mortality following Guillain–Barré syndrome: A population-based cohort study. *Eur J Neurol*. 2022;29(4):1145–1154. doi:10.1111/ene.15204
11. Fragiel M, Miró Ò, Llorens P, et al. Incidence, clinical, risk factors and outcomes of Guillain–Barré in Covid-19. *Ann Neurol*. 2021;89(3):598–603. doi:10.1002/ana.25987
12. Palaiodimou L, Stefanou M, Katsanos AH, et al. Prevalence, clinical characteristics and outcomes of Guillain–Barré syndrome spectrum associated with COVID-19: A systematic review and meta-analysis. *Eur J Neurol*. 2021;28(10):3517–3529. doi:10.1111/ene.14860
13. Lawn ND, Wijdicks EFM. Fatal Guillain–Barré syndrome. *Neurology*. 1999;52(3):635–635. doi:10.1212/WNL.52.3.635
14. Alshekhlee A, Hussain Z, Sultan B, Katirji B. Guillain–Barré syndrome: Incidence and mortality rates in US hospitals. *Neurology*. 2008;70(18):1608–1613. doi:10.1212/01.wnl.0000310983.38724.d4
15. Khan F, Pallant JF, Ng L, Bhasker A. Factors associated with long-term functional outcomes and psychological sequelae in Guillain–Barré syndrome. *J Neurol*. 2010;257(12):2024–2031. doi:10.1007/s00415-010-5653-x
16. Ruts L, Drenthen J, Jongen JLM, et al. Pain in Guillain–Barré syndrome: A long-term follow-up study. *Neurology*. 2010;75(16):1439–1447. doi:10.1212/WNL.0b013e3181f88345
17. Forsberg A, Press R, Einarsson U, De Pedro-Cuesta J, Widén Holmqvist L. Impairment in Guillain–Barré syndrome during the first 2 years after onset: A prospective study. *J Neurol Sci*. 2004;227(1):131–138. doi:10.1016/j.jns.2004.09.021
18. Meythaler JM. Rehabilitation of Guillain–Barré syndrome. *Arch Phys Med Rehabil*. 1997;78(8):872–879. doi:10.1016/S0003-9993(97)90203-3
19. Bernsen RAJAM, De Jager AEJ, Van Der Meche FGA, Suurmeijer TPBM. How Guillain–Barré patients experience their functioning after 1 year. *Acta Neurol Scand*. 2005;112(1):51–56. doi:10.1111/j.1600-0404.2005.00429.x
20. Forsberg A, Press R, Holmqvist LW. Residual disability 10 years after falling ill in Guillain–Barré syndrome: A prospective follow-up study. *J Neurol Sci*. 2012;317(1–2):74–79. doi:10.1016/j.jns.2012.02.026
21. Durand MC, Porcher R, Orlikowski D, et al. Clinical and electrophysiological predictors of respiratory failure in Guillain–Barré syndrome: A prospective study. *Lancet Neurol*. 2006;5(12):1021–1028. doi:10.1016/S1474-4422(06)70603-2
22. Bersano A, Carpo M, Allaria S, Franciotta D, Citterio A, Nobile-Orazio E. Long term disability and social status change after Guillain–Barré syndrome. *J Neurol*. 2006;253(2):214–218. doi:10.1007/s00415-005-0958-x
23. Yi SW, Lee JH, Hong JM, Choi YC, Park HJ. Incidence, disability, and mortality in patients with Guillain–Barré syndrome in Korea: A nationwide population-based study. *J Clin Neurol*. 2022;18(1):48. doi:10.3988/jcn.2022.18.1.48
24. Zhang G, Li Q, Zhang R, Wei X, Wang J, Qin X. Subtypes and prognosis of Guillain–Barré syndrome in Southwest China. *PLoS One*. 2015;10(7):e0133520. doi:10.1371/journal.pone.0133520
25. López-Hernández JC, Colunga-Lozano LE, Garcia-Trejo S, et al. Electrophysiological subtypes and associated prognosis factors of Mexican adults diagnosed with Guillain–Barré syndrome: A single center experience. *J Clin Neurosci*. 2020;80:292–297. doi:10.1016/j.jocn.2020.04.059
26. Kiraz M, Yılgör A, Milanlıoğlu A, Çilingir V, Çağaç A, Özkan S. Clinical subtypes, seasonality, and short-term prognosis of Guillain–Barré syndrome in an Eastern city of Turkey. *NeuroAsia*. 2022;27(4):937–944. doi:10.54029/2022wak
27. Bai HX, Wang Z, Tan L, Xiao B, Goldstein JM, Yang L. The effectiveness of immunomodulating treatment on Miller–Fisher syndrome: A retrospective analysis of 65 Chinese patients. *J Peripher Nerv Syst*. 2013;18(2):195–196. doi:10.1111/jns5.12030
28. Van Doorn PA, Van den Bergh PYK, Hadden RDM, et al. European Academy of Neurology/Peripheral Nerve Society Guideline on diagnosis and treatment of Guillain–Barré syndrome. *Eur J Neurol*. 2023;30(12):3646–3674. doi:10.1111/ene.16073
29. Asbury AK, Cornblath DR. Assessment of current diagnostic criteria for Guillain–Barré syndrome. *Ann Neurol*. 1990;27(Suppl 1):S21–S24. doi:10.1002/ana.410270707
30. Sejvar JJ, Kohl KS, Gidudu J, et al. Guillain–Barré syndrome and Fisher syndrome: Case definitions and guidelines for collection, analysis, and presentation of immunization safety data. *Vaccine*. 2011;29(3):599–612. doi:10.1016/j.vaccine.2010.06.003
31. Nomura K. Guillain–Barré syndrome: Clinical features, immune mechanisms, and therapies [in Japanese]. *Rinsho Shinkeigaku*. 1996;36(12):1367–1369. PMID:9128414.
32. Guillain G, Barré JA, Strohl A. Radiculoneuritis syndrome with hyperalbuminosis of cerebrospinal fluid without cellular reaction: Notes on clinical features and graphs of tendon reflexes (1916) [in French]. *Ann Med Interne (Paris)*. 1999;150(1):24–32. PMID:10400560.
33. Vucic S, Cairns KD, Black KR, Tick Chong PS, Cros D. Neurophysiologic findings in early acute inflammatory demyelinating polyradiculoneuropathy. *Clin Neurophysiol*. 2004;115(10):2329–2335. doi:10.1016/j.clinph.2004.05.009
34. Rajabally YA, Durand MC, Mitchell J, Orlikowski D, Nicolas G. Electrophysiological diagnosis of Guillain–Barré syndrome subtype: Could a single study suffice? *J Neurol Neurosurg Psychiatry*. 2015;86(1):115–119. doi:10.1136/jnnp-2014-307815
35. Prineas JW. Pathology of the Guillain–Barré syndrome. *Ann Neurol*. 1981;9(Suppl 1):6–19. doi:10.1002/ana.410090704
36. Yuki N, Taki T, Takahashi M, et al. Molecular mimicry between GQ_{1b} ganglioside and lipopolysaccharides of *Campylobacter jejuni* isolated from patients with Fisher's syndrome. *Ann Neurol*. 1994;36(5):791–793. doi:10.1002/ana.410360517
37. Hughes RA, Swan AV, Van Doorn PA. Intravenous immunoglobulin for Guillain–Barré syndrome. *Cochrane Database Syst Rev*. 2014;2014(9):CD002063. doi:10.1002/14651858.CD002063.pub6
38. Chevret S, Hughes RA, Annane D. Plasma exchange for Guillain–Barré syndrome. *Cochrane Database Syst Rev*. 2017;2017(2):CD001798. doi:10.1002/14651858.CD001798.pub3
39. Shangab M, Al Kaylani M. Clinical course and predictors of poor functional outcome in Guillain–Barré syndrome: A retrospective study. *Dubai Med J*. 2020;3(3):93–98. doi:10.1159/000510443
40. Dhar R, Stitt L, Hahn AF. The morbidity and outcome of patients with Guillain–Barré syndrome admitted to the intensive care unit. *J Neurol Sci*. 2008;264(1–2):121–128. doi:10.1016/j.jns.2007.08.005
41. Wen P, Wang L, Liu H, et al. Risk factors for the severity of Guillain–Barré syndrome and predictors of short-term prognosis of severe Guillain–Barré syndrome. *Sci Rep*. 2021;11(1):11578. doi:10.1038/s41598-021-91132-3
42. Zhang B, Wu X, Shen D, et al. The clinical characteristics and short-term prognosis in elderly patients with Guillain–Barré syndrome. *Medicine (Baltimore)*. 2017;96(1):e5848. doi:10.1097/MD.0000000000005848
43. Van Den Berg B, Bunschoten C, Van Doorn PA, Jacobs BC. Mortality in Guillain–Barré syndrome. *Neurology*. 2013;80(18):1650–1654. doi:10.1212/WNL.0b013e3182904fcc
44. Cabrera Serrano M, Rabinstein AA. Causes and outcomes of acute neuromuscular respiratory failure. *Arch Neurol*. 2010;67(9):1089–1094. doi:10.1001/archneurol.2010.207
45. Ding Y, Wang L, Sun J, et al. Remnant cholesterol and dyslipidemia are risk factors for Guillain–Barré syndrome and severe Guillain–Barré syndrome by promoting monocyte activation. *Front Immunol*. 2022;13:946825. doi:10.3389/fimmu.2022.946825

46. González-Suárez I, Sanz-Gallego I, Rodríguez De Rivera FJ, Arpa J. Guillain–Barré syndrome: Natural history and prognostic factors. A retrospective review of 106 cases. *BMC Neurol*. 2013;13(1):95. doi:10.1186/1471-2377-13-95
47. Park SH, Kim NH. Early prediction factors of poor outcome in Guillain–Barré syndrome. *Soonchunhyang Med Sci*. 2016;22(2):79–82. doi:10.15746/sms.16.018
48. Khedr EM, Mohamed MZ, Shehab MMM. The early clinical and laboratory predictors of GBS outcome: Hospital-based study, Assiut University, Upper Egypt. *Egypt J Neurol Psychiatry Neurosurg*. 2023;59(1):45. doi:10.1186/s41983-023-00646-2
49. Ishaque T, Islam MB, Ara G, et al. High mortality from Guillain–Barré syndrome in Bangladesh. *J Peripher Nerv Syst*. 2017;22(2):121–126. doi:10.1111/jns.12215
50. Shangab M, Al Kaylani M. Clinical predictors for mechanical ventilation and prognosis in patients with Guillain–Barré syndrome: A 10-year experience. *Neurol Sci*. 2021;42(12):5305–5309. doi:10.1007/s10072-021-05251-w
51. Verma R, Chaudhari TS, Raut TP, Garg RK. Clinico-electrophysiological profile and predictors of functional outcome in Guillain–Barré syndrome (GBS). *J Neurol Sci*. 2013;335(1–2):105–111. doi:10.1016/j.jns.2013.09.002
52. Paul BS, Bhatia R, Prasad K, Padma MV, Tripathi M, Singh MB. Clinical predictors of mechanical ventilation in Guillain–Barré syndrome. *Neurol India*. 2012;60(2):150. doi:10.4103/0028-3886.96383
53. Beghi E. The prognosis and main prognostic indicators of Guillain–Barré syndrome: A multicentre prospective study of 297 patients. *Brain*. 1996;119(6):2053–2061. doi:10.1093/brain/119.6.2053
54. Walgaard C, Lingsma HF, Ruts L, Van Doorn PA, Steyerberg EW, Jacobs BC. Early recognition of poor prognosis in Guillain–Barré syndrome. *Neurology*. 2011;76(11):968–975. doi:10.1212/WNL.0b013e3182104407
55. Kobori S, Kubo T, Otani M, et al. Coexisting infectious diseases on admission as a risk factor for mechanical ventilation in patients with Guillain–Barré syndrome. *J Epidemiol*. 2017;27(7):311–316. doi:10.1016/j.je.2016.07.003
56. Di X, Wang J, Li L, Liu L. Establishment of a single-center-based early prognostic scoring system for Guillain–Barré syndrome. *BMC Neurol*. 2023;23(1):97. doi:10.1186/s12883-023-03143-4
57. Nasiri J, Ghazavi M, Yaghini O, Chaldavi M. Clinical features and outcome of Guillain–Barré syndrome in children. *Iran J Child Neurol*. 2018;12(2):49–57. PMID:29696046. PMCID:PMC5904738.
58. Alloush T, Fahmy NA, Fouad MM, Albaroudy HO, Hamdy M, Salem HH. Prediction of outcome in patients with Guillain–Barré syndrome: An Egyptian study. *Neurosci Med*. 2019;10(3):232–246. doi:10.4236/NM.2019.103018
59. Wang Y, Shang P, Xin M, Bai J, Zhou C, Zhang HL. The usefulness of chief complaints to predict severity, ventilator dependence, treatment option, and short-term outcome of patients with Guillain–Barré syndrome: A retrospective study. *BMC Neurol*. 2017;17(1):200. doi:10.1186/s12883-017-0982-3
60. Kaida K, Morita D, Kanzaki M, et al. Anti-ganglioside complex antibodies associated with severe disability in GBS. *J Neuroimmunol*. 2007;182(1–2):212–218. doi:10.1016/j.jneuroim.2006.09.013
61. Lardone RD, Yuki N, Odaka M, Daniotti JL, Irazoqui FJ, Nores GA. Anti-GM1 IgG antibodies in Guillain–Barré syndrome: Fine specificity is associated with disease severity. *J Neurol Neurosurg Psychiatry*. 2010;81(6):629–633. doi:10.1136/jnnp.2009.183665
62. Koga M, Yuki N, Hirata K, Morimatsu M, Mori M, Kuwabara S. Anti-GM1 antibody IgG subclass: A clinical recovery predictor in Guillain–Barré syndrome. *Neurology*. 2003;60(9):1514–1518. doi:10.1212/01.WNL.0000061615.77865.83
63. Bech E, Ørntoft TF, Andersen LP, Skinhøj P, Jakobsen J. IgM anti-GM1 antibodies in the Guillain–Barré syndrome: A serological predictor of the clinical course. *J Neuroimmunol*. 1997;72(1):59–66. doi:10.1016/S0165-5728(96)00145-2
64. Wu LY, Zhou Y, Qin C, Hu BL. The effect of TNF-alpha, FcγR and CD1 polymorphisms on Guillain–Barré syndrome risk: Evidences from a meta-analysis. *J Neuroimmunol*. 2012;243(1–2):18–24. doi:10.1016/j.jneuroim.2011.12.003
65. Safa A, Azimi T, Sayad A, Taheri M, Ghafouri-Fard S. A review of the role of genetic factors in Guillain–Barré syndrome. *J Mol Neurosci*. 2021;71(5):902–920. doi:10.1007/s12031-020-01720-7
66. Tunç A. Early predictors of functional disability in Guillain–Barré syndrome. *Acta Neurol Belg*. 2019;119(4):555–559. doi:10.1007/s13760-019-01133-3
67. Sipilä JOT, Kauko T, Soilu-Hänninen M. Admission sodium level and prognosis in adult Guillain–Barré syndrome. *Int J Neurosci*. 2017;127(4):344–349. doi:10.3109/00207454.2016.1163551
68. Saifudheen K, Jose J, Gafoor VA, Musthafa M. Guillain-Barré syndrome and SIADH. *Neurology*. 2011;76(8):701–704. doi:10.1212/WNL.0b013e31820d8b40
69. Wang Y, Liu J. Hyponatremia is a predictor for poor outcome in Guillain–Barré syndrome. *Neurol Res*. 2015;37(4):347–351. doi:10.1179/1743132814Y.0000000455
70. Rumalla K, Reddy AY, Letchuman V, Mittal MK. Hyponatremia in Guillain–Barré syndrome. *J Clin Neuromuscul Dis*. 2017;18(4):207–217. doi:10.1097/CND.0000000000000157
71. Ozdemir HH. Analysis of the albumin level, neutrophil-lymphocyte ratio, and platelet-lymphocyte ratio in Guillain–Barré syndrome. *Arq Neuropsiquiatr*. 2016;74(9):718–722. doi:10.1590/0004-282X20160132
72. Jahan I, Ahmed R, Ahmed J, et al. Neutrophil-lymphocyte ratio in Guillain–Barré syndrome: A prognostic biomarker of severe disease and mechanical ventilation in Bangladesh. *J Peripher Nerv Syst*. 2023;28(1):47–57. doi:10.1111/jns.12531
73. Sun S, Wen Y, Li S, Huang Z, Zhu J, Li Y. Neutrophil-to-lymphocyte ratio is a risk indicator of Guillain–Barré syndrome and is associated with severity and short-term prognosis. *Heliyon*. 2023;9(3):e14321. doi:10.1016/j.heliyon.2023.e14321
74. Ning P, Yang B, Yang X, et al. Lymphocyte-based ratios for predicting respiratory failure in Guillain–Barré syndrome. *J Neuroimmunol*. 2021;353:577504. doi:10.1016/j.jneuroim.2021.577504
75. Ning P, Yang B, Yang X, et al. Clinical value of C-reactive protein/albumin ratio in Guillain–Barré syndrome. *Neurol Sci*. 2021;42(8):3275–3283. doi:10.1007/s10072-020-04930-4
76. Sahin S, Cinar N, Karsidag S. Are cerebrospinal fluid protein levels and plasma neutrophil/lymphocyte ratio associated with prognosis of Guillain–Barré syndrome? *Neurol Int*. 2017;9(2):7032. doi:10.4081/ni.2017.7032
77. Gonzalez-Quevedo A, Carriera Fernandez R, O'Farrill Lestayo Z, Luis Suarez I, Mustelier Becquer R, Luis Gonzalez RS. An appraisal of blood-cerebrospinal fluid barrier dysfunction during the course of Guillain–Barré syndrome. *Neurol India*. 2009;57(3):288. doi:10.4103/0028-3886.53282
78. Bourque PR, Brooks J, Warman-Chardon J, Breiner A. Cerebrospinal fluid total protein in Guillain–Barré syndrome variants: Correlations with clinical category, severity, and electrophysiology. *J Neurol*. 2020;267(3):746–751. doi:10.1007/s00415-019-09634-0
79. Bae JS, Kim YJ, Kim JK. Diabetes mellitus exacerbates the clinical and electrophysiological features of Guillain–Barré syndrome. *Eur J Neurol*. 2016;23(3):439–446. doi:10.1111/ene.12885
80. Wang Y, Li G, Yang S, et al. Fasting glucose levels correlate with disease severity of Guillain–Barré syndrome. *PLoS One*. 2015;10(12):e0145075. doi:10.1371/journal.pone.0145075
81. Peric S, Bozovic I, Bjelica B, et al. Diabetes mellitus may affect short-term outcome of Guillain–Barré syndrome. *J Peripher Nerv Syst*. 2017;22(2):127–130. doi:10.1111/jns.12206
82. Gao Y, Zhang HL, Xin M, et al. Serum folate correlates with severity of Guillain–Barré syndrome and predicts disease progression. *Biomed Res Int*. 2018;2018:5703279. doi:10.1155/2018/5703279
83. Petzold A, Hinds N, Murray NF, et al. CSF neurofilament levels: A potential prognostic marker in Guillain–Barré syndrome. *Neurology*. 2006;67(6):1071–1073. doi:10.1212/01.wnl.0000237334.69665.92
84. Axelsson M, Sjögren M, Andersen O, Blennow K, Zetterberg H, Lycke J. Neurofilament light protein levels in cerebrospinal fluid predict long-term disability of Guillain–Barré syndrome: A pilot study. *Acta Neurol Scand*. 2018;138(2):143–150. doi:10.1111/ane.12927
85. Martín-Aguilar L, Camps-Renom P, Lleixà C, et al. Serum neurofilament light chain predicts long-term prognosis in Guillain–Barré syndrome patients. *J Neurol Neurosurg Psychiatry*. 2021;92(1):70–77. doi:10.1136/jnnp-2020-323899
86. López-Hernández JC, Jorge De Saráchaga A, Briseño-Godínez ME, et al. Deltoid muscle strength and autonomic dysfunction as independent risk factors for invasive mechanical ventilation in patients with Guillain–Barré syndrome. *Int J Neurosci*. 2023;133(12):1403–1410. doi:10.1080/00207454.2022.2082963

87. Sundar U, Abraham E, Gharat A, Yeolekar ME, Trivedi T, Dwivedi N. Neuromuscular respiratory failure in Guillain–Barré syndrome: Evaluation of clinical and electrodiagnostic predictors. *J Assoc Physicians India*. 2005;53:764–768. PMID:16334619.
88. Miller RG, Peterson GW, Daube JR, Albers JW. Prognostic value of electrodiagnosis in Guillain–Barré syndrome. *Muscle Nerve*. 1988;11(7): 769–774. doi:10.1002/mus.880110714
89. Ruts L, Van Doorn PA, Lombardi R, et al. Unmyelinated and myelinated skin nerve damage in Guillain–Barré syndrome: Correlation with pain and recovery. *Pain*. 2012;153(2):399–409. doi:10.1016/j.pain.2011.10.037
90. Grimm A, Décard BF, Schramm A, et al. Ultrasound and electrophysiologic findings in patients with Guillain–Barré syndrome at disease onset and over a period of six months. *Clin Neurophysiol*. 2016; 127(2):1657–1663. doi:10.1016/j.clinph.2015.06.032
91. França Jr MC, Deus-Silva L, Castro RD, et al. Guillain-Barré syndrome in the elderly: Clinical, electrophysiological, therapeutic and outcome features. *Arq Neuropsiquiatr*. 2005;63(3B):772–775. doi:10.1590/S0004-282X2005000500010
92. Wang Y, Lang W, Zhang Y, Ma X, Zhou C, Zhang HL. Long-term prognosis of Guillain–Barré syndrome not determined by treatment options? *Oncotarget*. 2017;8(45):79991–80001. doi:10.18632/oncotarget.20620
93. Rajabally YA, Uncini A. Outcome and its predictors in Guillain–Barré syndrome. *J Neurol Neurosurg Psychiatry*. 2012;83(7):711–718. doi:10.1136/jnnp-2011-301882
94. Kleyweg RP, Van Der Meché FGA, Schmitz PIM. Interobserver agreement in the assessment of muscle strength and functional abilities in Guillain–Barré syndrome. *Muscle Nerve*. 1991;14(11):1103–1109. doi:10.1002/mus.880141111
95. Hughes RAC, Newsom-Davis JM, Perkin GD, Pierce JM. Controlled trial prednisolone in acute polyneuropathy. *Lancet*. 1978;312(8093): 750–753. doi:10.1016/S0140-6736(78)92644-2
96. Walgaard C, Lingsma HF, Ruts L, et al. Prediction of respiratory insufficiency in Guillain–Barré syndrome. *Ann Neurol*. 2010;67(6):781–787. doi:10.1002/ana.21976
97. Luijten LWG, Doets AY, Arends S, et al. Modified Erasmus GBS Respiratory Insufficiency Score: A simplified clinical tool to predict the risk of mechanical ventilation in Guillain–Barré syndrome. *J Neurol Neurosurg Psychiatry*. 2023;94(4):300–308. doi:10.1136/jnnp-2022-329937
98. Doets AY, Lingsma HF, Walgaard C, et al. Predicting outcome in Guillain–Barré syndrome: International validation of the Modified Erasmus GBS Outcome Score. *Neurology*. 2022;98(5):e518–e532. doi:10.1212/WNL.0000000000013139
99. Van Koningsveld R, Steyerberg EW, Hughes RA, Swan AV, Van Doorn PA, Jacobs BC. A clinical prognostic scoring system for Guillain–Barré syndrome. *Lancet Neurol*. 2007;6(7):589–594. doi:10.1016/S1474-4422(07)70130-8
100. Min YG, Ju W, Seo JW, et al. Serum C3 complement levels predict prognosis and monitor disease activity in Guillain–Barré syndrome. *J Neurol Sci*. 2023;444:120512. doi:10.1016/j.jns.2022.120512
101. Ortiz Corredor F, Mieth Alviar KW. Prognostic factors for walking in childhood Guillain–Barré syndrome [in Spanish]. *Rev Neurol*. 2003;36(12):1113. doi:10.33588/rn.3612.2003056
102. Kroczka S, Świerczyńska, Kaciński M. Kliniczne i neurofizjologiczne następstwa zespołu Guillain-Barre. *Przegl Lek*. 2011;68(11):1098–1103. https://ruj.uj.edu.pl/server/api/core/bitstreams/859b996a-0270-4b82-a90b-244232beda4e/content. Accessed May 4, 2024.
103. Cheng B, Chang W, Chen J, et al. Long-term prognosis for Guillain–Barré syndrome: Evaluation of prognostic factors and clinical experience of automated double filtration plasmapheresis. *J Clin Apher*. 2003;18(4):175–180. doi:10.1002/jca.10066
104. Liu S, Dong C, Ubogu EE. Immunotherapy of Guillain–Barré syndrome. *Hum Vaccin Immunother*. 2018;14(11):2568–2579. doi:10.1080/21645515.2018.1493415
105. Shahrizaila N, Lehmann HC, Kuwabara S. Guillain–Barré syndrome. *Lancet*. 2021;397(10280):1214–1228. doi:10.1016/S0140-6736(21)00517-1